ABSTRACT

Title of dissertation: GENERAL THEORY
OF NONUNIFORM FLUIDS:
FROM HARD SPHERES TO IONIC FLUIDS

Yng-gwei Chen, Doctor of Philosophy, 2004

Dissertation directed by: John D. Weeks
Department of Physics and
Department of Chemistry and Biochemistry
Institute for Physical Science and Technology

The exclusion effects of repulsive intermolecular potential cores are often modeled by hard sphere fluids, for which an accurate *Hydrostatic Linear Response* (HLR) equation was previous developed by Katsov in 2001 for computing the density response to general external fields. In this dissertation the HLR equation is combined with various thermodynamic integration pathways to investigate the solvation free energy of cavity insertion which characterizes the entropic cost of solvating molecules in a fluid. A *Shifted Linear Response* (SLR) equation is developed to build in the exact limits of external fields varying in very small ranges and fluids confined in

narrow spaces, where the HLR fails qualitatively. The SLR is derived from an expansion truncated at linear order about a reference density, and an *Insensitivity Criterion* (IC) is proposed for determining an optimal reference density.

The slow $1/r$ decay of the Coulomb potential is characteristically long-ranged, but it also becomes strong at short distances. The structure of ionic systems exhibits an intricate interplay between the short and long length scales of their molecular potentials. A strategy is proposed for separating the Coulomb interaction between *general* charge distributions into a short-ranged piece $u_0(r)$ and a slowly varying piece $u_1(r)$. In the strong coupling states of the ionic systems that we have studied, *mimic systems* with only the short-ranged part $u_0(r)$ are found to show very similar correlation functions. The slow decays of ion-ion and ion-dipole interactions give rise to unique long-wavelength constraints on ionic fluid structure. *Local Molecular Field Theory* (LMF), which maps an external field in the full system to a mimic system in the presence of a renormalized field, can correct the mimic correlations by embodying contributions from $u_1(r)$. The LMF has been applied to both uniform and nonuniform model ionic systems, and accurate results for bulk correlation functions, internal energy and the density distribution in a confined system are obtained. For a system of counterions confined by charged walls, the LMF and the mimic system have especially helped shed light on many phenomena that had previously lacked coherent physical interpretations and consistent approximations.

GENERAL THEORY OF NONUNIFORM FLUIDS: FROM HARD SPHERES TO IONIC FLUIDS

by

Yng-gwei Chen

Dissertation submitted to the Faculty of the Graduate School of the
University of Maryland, College Park in partial fulfillment
of the requirements for the degree of
Doctor of Philosophy
2004

Advisory Committee:

Professor John D. Weeks, Chair/Advisor
Professor Michael E. Fisher
Professor J. Robert Dorfman
Professor Devarajan Thirumalai, Dean's Representative
Professor Theodore R. Kirkpatrick

Dedication

To yop, who has accompanied me through

all the harshest and sweetest

ACKNOWLEDGMENTS

First, I would like to thank my advisor, Professor John D. Weeks, who has been incredibly supportive to me in the past years. Nothing in this thesis, and much more beyond this thesis, could have been possible without his encouragement and guidance.

I also feel grateful to both Professor Michael E. Fisher and Professor J. Robert Dorfman. Their truly enlightening courses had inspired me to work on statistical mechanics. Thanks are also due to Professor Devarajan Thirumalai and Professor Theodore R. Kirkpatrick for serving in the committee and reviewing this dissertation.

Finally, I would like to express my gratitude to all the wonderful friends that I am so lucky to have around. You all have lightened up various spots of my memory with your warmth and friendship.

TABLE OF CONTENTS

LIST OF FIGURES

LIST OF TABLES

Chapter 1

Introduction

1.1 Overview

Based on the framework of statistical mechanics, this dissertation will focus on developing systematic and physical theories for understanding the equilibrium properties of both uniform and inhomogeneous fluids. Depending on the spatial length scales of the molecular interactions, different treatments may be required for handling the distinctive physics involved. The attempt to understand systems with only short-ranged repulsive interactions and also those further complicated by long-ranged Coulomb interactions comprises two major parts of this research. In particular, the understanding and accurate treatment of long-ranged interactions is often closely intertwined with the considerations required for the shorter-ranged correlation. A consistent and successful theoretical framework to bridge and also to clarify the interplay between interactions of different length scales had previously been absent. In this thesis, theories have been developed to specifically tackle such challenges. To single out the most essential physics and to examine these ideas in clear and

controlled detail, the theories have also been applied to various standard model systems. It is hoped that the experience thus obtained can be further applied to more sophisticated and experimentally realistic systems. Theoretical analysis, numerical solutions and computer simulations have all been employed in this research.

Short-Ranged and Repulsive Interactions At the microscopic length scale, the molecular interactions in most physical systems possess effective short-ranged repulsive cores. These repulsive cores lead to highly nontrivial packing of the fluid particles so that the correlation function of a dense fluid often exhibits characteristic oscillations [24]. A fluid consisting only of hard spheres, simple as it is as a model to represent such packing effects, still presents considerable theoretical difficulties. Moreover, a hard sphere fluid of *properly* chosen diameter has also proven useful as a starting point for perturbation theories treating more general and softer repulsive cores. Theories for computing the singlet density response of a hard sphere fluid in the presence of a general external field have been devised. The *hydrostatic linear response* (HLR) equation, based on the ideas of a *hydrostatic shift* of the chemical potential and the local field, and *linear response* to nonuniform fields, was first proposed for this purpose by Katsov and Weeks [40] and had proven to be computationally efficient and encouragingly accurate, especially for slowly varying external fields and hard-wall like potentials. In this dissertation, various thermodynamic integration pathways are combined with the HLR equation and shown to yield accurate results for predicting solvation free energies. However, there are still

two important limiting cases that the HLR fails to capture. One is for external fields that are nonzero only in a very tiny region; the other is for external fields that confine the fluid to a very small region, like a narrow slit. To remedy these deficiencies of the HLR theory, a new and more general equation, *shifted linear response* (SLR) equation, has been subsequently developed. The SLR equation has the HLR as a limit and provides a unifying view for the two seemingly opposite limits that the HLR fails to reproduce.

Long-ranged and Ionic Interactions In recent years, much interest and many efforts have been drawn to the understanding of biological systems**.** In living cells, electronic charges, either in intercellular electrolytes or those generally distributed on various macromolecules such as proteins and DNAs, are a ubiquitous presence. The ability to treat Coulomb interactions is thus deemed crucial for studying a wide range of biophysical phenomena. Coulomb interactions, because of their very long-ranged $1/r$ decay, have posed significant challenges to theoretical statistical mechanics and computer simulations particularly. In this thesis, *local molecular field theory* (LMF) [74], which has close connections with conventional theories such as Poisson Boltzmann (PB) or Debye Huckel (DH) [2, 50] approximations, has been applied to various model ionic systems. The LMF shows greatly improved accuracy over all ionic strength regimes and reproduce the weak coupling limit exactly. On the contrary, the DH or the PB approximation, though exact for weak coupling, fail very quickly once away from this limit. The present theory is based

on new physical insights into the traditional "mean-field-like" theories, separating out long-wavelength perturbation potentials based on a very general recipe. This separation of potential reveals underlying *mimic* systems which have much shorter-ranged molecular interactions. For uniform fluids, the correlation functions of mimic systems can be strikingly close to those of the full ionic systems to which they correspond. When computing the density response of an ionic system to an external field, the LMF maps the external field to a new renormalized field in the mimic system that induces the same density response as the full field would in the ionic system. And, again, the nonuniform mimic system's correlation functions can agree very well with those of the full Coulomb system. This dissertation will present applications of the LMF theory to the structural and thermodynamic properties of both uniform and inhomogeneous model ionic systems. Our theory can also be connected to the Ewald summation method [16, 1] and other ways of treating long-ranged interactions in computer simulations [1].

1.2 Outline of the Dissertation

This dissertation consists of two major parts. The first part, in chapters 1 and 2, concerns the treatment of the response of hard sphere fluids to general external fields. In Chapter 1, the HLR equation is combined with different thermodynamic integration pathways to compute the solvation free energies and surface tensions of

[1] For a survey for other algorithms, such as *fast multipole method*, *particle-mesh* (PM) and *particle-mesh/particle-particle* (P^3M), see reference [16].

spherical cavities of various sizes. The varying accuracy of the different pathways and their comparison with other theories based on Gaussian fluctuations [11] are explained. Chapter 2 addresses the *tiny field* and *narrow slit* (confining fields) limiting cases that the HLR fails to recover. The exact density response of a hard sphere fluid to such fields are derived. A density expansion that expands the fluids' nonuniformity locally about a possibly different bulk system at each point of the r-space, as first proposed by J. K. Percus [59], is truncated at the linear order to produce the *shifted linear response equation* (SLR). With a properly chosen reference density, the SLR equation is shown to be exact at both limits in which the HLR fails. The SLR theory is also exact in the hydrostatic limit and reduces to the HLR theory. A new *insensitivity criterion* (IC) is proposed for determining a proper reference density for the use of the SLR. Applications of the IC to various external fields are presented and discussed in comparison with the HLR, PY, and computer simulation results.

The second part of the dissertation, ranging from Chapter 3 to 5, presents the development of the *local molecular theory* [74] and its applications to model ionic systems. Chapter 3 focuses on two single-component ionic systems, *one-component plasma* (OCP) and the *one-component charged hard spheres* (OCCHS). A controlled separation of the Coulombic potential is proposed to reveal a *family* of mimic systems for both systems. The molecular interactions of the mimic systems are strictly short-ranged, free of the $1/r$ decay of the full Coulombic interaction. It is shown in

this chapter that in dense states, the correlation functions of these mimic systems are extremely close to those of the OCP and OCCHS. Taking advantage of the similarity of the structure factors between the full system and its mimic counterparts, a simple and very accurate approximation can be derived to correct the internal energy of the mimic system. At low density states, the mimic system's correlation functions no longer resemble those of the full system, and the LMF can be used to correct the differences. However, at sufficiently low densities, the LMF theory is especially simple, since the response to an external field can be accurately approximated using a simple Boltzmann factor. This leads to our mimic Poisson Boltzmann (MPB) approximation, which reduces to the standard PB approximation as the density approaches zero. We find the MPB approximation has a much wider range of validity. An important sum rule, the Stillinger-Lovett second moment condition [69] that governs the small k behavior of the ionic structure factor can also be satisfied by scaling of the LMF equation.

Chapter 4 further generalizes the separation of Coulomb interaction to arbitrary charge distributions that may be carried by molecules. This derivation lays the foundation for applying LMF theory to multi-component ionic systems and in particular to systems involving dipolar interactions. A multipole expansion of the Coulomb potential between charged entities is designed by substituting a *damped* Green's function for the ordinary $1/r$ Green's function of Poisson's equation [38]. The expansion is constructed so that contributions arise only from long wavelengths;

it converges rapidly even for short molecular distances. The perturbation potential for the LMF comprises only the lowest order nonvanishing multipole moment that can be unambiguously extracted from the expansion. The LMF equation is specifically generalized to be expressed in terms of general multipole moments, and the sum rules involving monopoles and dipoles can be seen to emerge readily from the equation. The general separation of Coulomb potential is controlled by an important length scale parameter, and the minimum working choice of this parameter is also discussed. A binary ionic mixture model, *size asymmetric primitive model* (SAPM) is investigated at the end of Chapter 3. The mimic system defined through such a potential separation also shows striking structural similarity to the full system at strong coupling states. At low density but strong coupling states, the correlation functions of the mimic system even exhibits the features that characterize ion clustering in a regime where some traditional integral equation approaches fail to converge.

Chapter 5, in contrast to the applications to bulk correlations in the preceding chapters, presents a qualitative analysis of the LMF to an explicit nonuniform system. The system considered is a one-component plasma confined by two charged planar walls. The PB approximation is exact for the weak coupling states, but fails qualitatively to recover the strong coupling limit. The PB theory always predicts an effective repulsive pressure between the walls, thus is unable to explain both computer simulations and experimental observations [20, 52, 53, 54, 71] that show

effective wall attraction at strong coupling states. Here, the LMF is shown to be exact in both weak and strong coupling limits of such a system. Moreover, we show that its approximation by the MPB holds in both limits, so a simple and general analytic approach is available. The different regimes are characterized by the interplay between a single coupling parameter ξ and the wall separation $\tilde{d}$ are categorized and examined in detail. This system has a complex $\xi - \tilde{d}$ phase diagram, but the LMF is capable of treating and accounting for *all* the possible regimes of this model. The LMF provides a clear physically compelling explanation of the somewhat mysterious effective attraction between the walls [2], and it offers also important insights into more general qualitative issues that traditional approaches cannot provide, such as how two strong coupling walls can separate into two independent, strong coupling walls at large distances. Although such decoupling of the walls can be understood physically, theoretical treatments for the transition into such a regime are lacking, as is any understanding of an intriguing re-entrant repulsion at large separations.

[2]The numerical solution of the MPB is more recently carried out by C. Kaur and has also shown impressive quantitative agreement with simulation results.

Chapter 2

Different Thermodynamic Pathways to the Solvation Free Energy of a Spherical Cavity in a Hard Sphere Fluid

This chapter is heavily based on a published paper by Chen, Y.-G. and Weeks, J. D., *Journal of Chemical Physics*, 118 (17): 7944-7953, 2003.

2.1 Introduction

The solvation free energy determines how readily a solute can be dissolved in a given solvent fluid. This plays an important role in many chemically and biologically important processes, perhaps most notably in hydrophobic interactions in water. A significant part of the solvation free energy arises from the required expulsion of solvent molecules from the region occupied by the harshly repulsive molecular core of the solute. These very strong "excluded volume" interactions can significantly perturb the local density around the solute and cause simple approaches based on gradient expansions to fail.

These effects can be seen most clearly in the simple model system treated in this chapter. We will calculate the excess or solvation free energy associated with

the insertion of a spherical cavity with radius R_v into a hard sphere fluid, whose molecules have diameter σ. By definition, the centers of the solvent molecules are completely excluded from the region of the cavity, which thus acts like a hard core external field.

This system has many interesting limits. When the exclusion field or cavity radius R_v equals σ, then the cavity acts like another solvent particle and the solvation free energy is directly related to the chemical potential of the solvent. As the cavity radius tends to infinity it effectively turns into a hard wall and the relevant thermodynamic quantity is the surface free energy or surface tension associated with a hard wall in a hard sphere fluid. A cavity with radius $R_v = \sigma/2$ acts like a hard core "point solute" of zero diameter. Even shorter-ranged hard core fields or *"tiny cavities"* with $R_v \leq \sigma/2$ are also of interest, since the induced structure and solvation free energy of a tiny cavity can be calculated exactly. This limit can thus serve as a nontrivial check on approximate methods.

The most commonly used method today for such problems is weighted density functional theory (DFT) [15]. Here one attempts to describe the free energy directly as a functional of some kind of smoothed or weighted average of the nonuniform and often rapidly varying singlet density. This has the advantage that the free energy is obtained directly and by construction the associated fluid structure (obtained by functionally differentiating the free energy) is consistent with the approximate free energy. However the choice of appropriate weighting functions is by no means obvi-

ous and a number of different and often highly formal schemes have been proposed.

We focus instead in this chapter on making direct use of structural information about the nonuniform solvent fluid to obtain the solvation free energy. We believe this allows physical intuition to play a more central role and we can take advantage of the recent development of a generally very accurate theory relating the structure of a nonuniform hard sphere fluid to the associated external field [40].

As we will see below, the free energy can then be calculated by integration, starting from an initially known state (e.g., the uniform fluid) and determining the free energy changes as the solute-solvent interaction (the hard core external field) is "turned on", or alternatively, as the density is changed from the initial to the final state. There exist many possible routes from the initial to the final state, and we will generally refer to them as *thermodynamic pathways*. If exact results are used for the intermediate values of the structure and associated fields, then all these different pathways will give the same (exact) result for the free energy.

In practice, of course, approximations will have to be made and the different pathways will generally yield different results. This is sometimes referred to as the "thermodynamic inconsistency" of structurally based methods [15]. But this can be viewed more positively as giving one the freedom to choose particular pathways that could be relatively insensitive to the errors that exist in the structural theory, and we will try to use this flexibility to obtain the most accurate results. Moreover, there is an inherent smoothing of the structural information in the integration used to obtain

the free energy. The differences in free energy predicted by different pathways will also give us some indication about the overall quality of the theory.

This approach generally requires the density profiles and associated fields of all the intermediate states along the various pathways, and thus a fast and accurate method for determining these quantities is crucial for computation efficiency. We will use here the generally accurate *hydrostatic linear response* (HLR) equation [40] proposed by Katsov and Weeks. A different physically motivated derivation of the HLR equation is given below.

We will also examine the alternative free energy predictions that arise from a theory closely related to the HLR equation, the *Gaussian field model* (GFM) developed by Chandler [11]. For a solute with a hard core the GFM proposes an approximate partition function from which the associated density response can be derived. In the particular case where a rigid cavity is inserted into a hard sphere fluid, the HLR and the GFM approaches turn out to make identical predictions for the induced structure. Thus structurally based routes to the free energy involving only hard core fields will give the same results. In addition, one can use the approximate GFM partition function to evaluate the solvation free energy directly. However, as we will show later, the latter approach tends to produce less accurate results. This deficiency shows up even more strongly in the tiny cavity limit where the structural predictions of the HLR and the GFM are *exact*, and several pathways giving the exact free energy can be found. This illustrates the advantage of consid-

ering a variety of thermodynamic pathways that can make best use of the available structural information.

2.2 Density Response to an External Field

2.2.1 The Hydrostatic Linear Response (HLR) Equation

We describe the system using a grand canonical ensemble, and thus want to determine the excess grand free energy arising from insertion of a spherical cavity or hard core external field of radius R_v. To derive the HLR equation [40] we start with the basic linear response equation [24] for a nonuniform hard sphere system in a *general* external field $\phi(\mathbf{r})$, with chemical potential μ^B, inverse temperature $\beta = (k_B T)^{-1}$ and associated density $\rho(\mathbf{r};\ \mu^B, [\phi]) \equiv \rho(\mathbf{r})$:

$$-\beta\delta\phi(\mathbf{r}_1) = \int d\mathbf{r}_2\, \chi^{-1}(\mathbf{r}_1, \mathbf{r}_2; [\rho])\delta\rho(\mathbf{r}_2). \tag{2.1}$$

This relates *small* perturbations in the density and field through the (inverse) linear response function

$$\chi^{-1}(\mathbf{r}_1, \mathbf{r}_2; [\rho]) \equiv \delta(\mathbf{r}_1 - \mathbf{r}_2)/\rho(\mathbf{r}_1) - c(\mathbf{r}_1, \mathbf{r}_2; [\rho]). \tag{2.2}$$

Here $c(\mathbf{r}_1, \mathbf{r}_2; [\rho])$ is the direct correlation function of the nonuniform hard sphere system. The notation $[\rho]$ indicates that these correlation functions are nonlocal functionals of the density $\rho(\mathbf{r})$.

Since we want to focus on the effects of the perturbing field, we have used the *inverse* form of linear response theory [63] in Eq.(2.1), where the field appears

explicitly only on the left hand side, evaluated at $\mathbf{r}_1$. This provides many advantages in dealing with large field perturbations, as will soon become apparent. In most cases we will consider perturbations about a *uniform* system with chemical potential μ and density $\rho(\mu) \equiv \rho(\mathbf{r};\ \mu, [\phi = 0])$. When using this simplified notation $\rho(\mu)$ should not be confused with $\rho(\mathbf{r}) \equiv \rho(\mathbf{r};\ \mu^B, [\phi])$. Similarly, we will let $\mu(\rho)$ denote the chemical potential of the uniform fluid as a function of density ρ. In a uniform system the direct correlation function c will take the simple form $c(r_{12}; \rho)$, where $r_{12} \equiv |\mathbf{r}_1 - \mathbf{r}_2|$.

But how can we use Eq.(2.1) to describe the density response to a *large* field perturbation such as the hard core field of interest here? This linear relation between a (possibly infinite) external field perturbation on the left hand side and the finite induced density change on the right must certainly fail for values of $\mathbf{r}_1$ where the field is very large. Conversely, Eq.(2.1) should be most accurate for those values of $\mathbf{r}_1$ where the field is small — in particular where the field *vanishes* — and then through the integration over all $\mathbf{r}_2$ it relates density changes in regions where the field vanishes to density changes in the regions where the field is nonzero.

To treat large fields, we note that for any given $\mathbf{r}_1$ we can locally impose the optimal condition that the field perturbation vanishes by introducing a *shifted* chemical potential

$$\mu^{\mathbf{r}_1} \equiv \mu^B - \phi(\mathbf{r}_1), \tag{2.3}$$

and a *shifted* external field

$$\phi^{\mathbf{r}_1}(\mathbf{r}) \equiv \phi(\mathbf{r}) - \phi(\mathbf{r}_1). \tag{2.4}$$

Since there is an arbitrary zero of energy and a constant external field acts like a shift of the chemical potential in the grand ensemble, we make no physical changes if we shift both functions by the same amount. In particular $\rho(\mathbf{r};\ \mu^B, [\phi]) = \rho(\mathbf{r};\ \mu^{\mathbf{r}_1}, [\phi^{\mathbf{r}_1}])$.

The superscript $\mathbf{r}_1$ in $\mu^{\mathbf{r}_1}$ indicates a particular value of the chemical potential, which from Eq.(2.3) depends parametrically on $\mathbf{r}_1$ through the local value of the field. When $\phi(\mathbf{r}_1)$ vanishes, then $\mu^{\mathbf{r}_1}$ reduces to μ^B. We define $\rho^{\mathbf{r}_1}$, the *hydrostatic density*, by

$$\rho^{\mathbf{r}_1} \equiv \rho(\mathbf{r};\ \mu^{\mathbf{r}_1}, [0]) = \rho(\mu^{\mathbf{r}_1}). \tag{2.5}$$

Thus $\rho^{\mathbf{r}_1}$ is the density of the *uniform* fluid in zero field at the shifted chemical potential $\mu^{\mathbf{r}_1}$; equivalently $\rho^{\mathbf{r}_1}$ satisfies

$$\mu(\rho^{\mathbf{r}_1}) = \mu^{\mathbf{r}_1} = \mu^B - \phi(\mathbf{r}_1). \tag{2.6}$$

Thus far, we have have merely introduced an equivalent (and apparently more complicated!) way of describing the system in terms of a shifted field and a shifted chemical potential. However this perspective immediately suggests a very simple first approximation to the density response to a *slowly varying* external field. Since $\phi^{\mathbf{r}_1}(\mathbf{r})$ by construction vanishes for $\mathbf{r} = \mathbf{r}_1$, if $\phi^{\mathbf{r}_1}(\mathbf{r})$ is sufficiently slowly varying, then the region around $\mathbf{r}_1$ within a correlation length is essentially in zero field. In

that case the uniform hydrostatic density $\rho^{\mathbf{r}_1}$ is clearly a good approximation to $\rho(\mathbf{r}_1)$, the exact induced density at $\mathbf{r}_1$. Moreover, when the field is more rapidly varying, it is natural to introduce a second and even more accurate approximation to the density response.

The hydrostatic density $\rho^{\mathbf{r}_1}$ takes account only of the local value of the field at $\mathbf{r}_1$ by a shift of the chemical potential. The HLR equation improves on this "local field" approximation by using *linear response theory* to determine the density change from the hydrostatic density induced by nonlocal values of the shifted field $\phi^{\mathbf{r}_1}(\mathbf{r})$. Thus starting from the uniform density $\rho^{\mathbf{r}_1}$, we assume a linear response to the shifted field, replacing $\chi^{-1}(\mathbf{r}_1, \mathbf{r}_2; [\rho])$ by $\chi^{-1}(r_{12}; \rho^{\mathbf{r}_1})$ in Eq.(2.1) and setting $\delta\phi(\mathbf{r}) = \phi^{\mathbf{r}_1}(\mathbf{r})$ and $\delta\rho(\mathbf{r}_2) = \rho(\mathbf{r}_2) - \rho^{\mathbf{r}_1}$. Then the left side of Eq.(2.1) vanishes (giving the optimal linear response condition), and we have

$$0 = \int d\mathbf{r}_2 \, \chi^{-1}(r_{12}; \rho^{\mathbf{r}_1})[\rho(\mathbf{r}_2) - \rho^{\mathbf{r}_1}], \tag{2.7}$$

which can be rewritten exactly using Eq.(2.2) as

$$\rho(\mathbf{r}_1) = \rho^{\mathbf{r}_1} + \rho^{\mathbf{r}_1} \int d\mathbf{r}_2 \, c(r_{12}; \rho^{\mathbf{r}_1})[\rho(\mathbf{r}_2) - \rho^{\mathbf{r}_1}]. \tag{2.8}$$

This is our final result, which we refer to as the HLR equation. We view this as an integral equation relating the hydrostatic density $\rho^{\mathbf{r}_1}$ to the full density $\rho(\mathbf{r})$ and solve it self-consistently for all $\mathbf{r}_1$. When $\phi(\mathbf{r}_1)$ is known, we can immediately determine $\rho^{\mathbf{r}_1}$ at each $\mathbf{r}_1$ from the local relation in Eq.(2.6), and then solve Eq.(2.8) by iteration for all $\mathbf{r}_1$ to determine the full density response $\rho(\mathbf{r})$. Conversely, for a

given equilibrium density distribution $\rho(\mathbf{r})$ we can use HLR equation to determine the associated field $\phi(\mathbf{r})$. This inverse solution of Eq.(2.8) is particularly easy to carry out, since we can determine the local field at each $\mathbf{r}_1$ separately, without iteration. Accurate results have been obtained for many test cases with strong repulsive or attractive fields [40, 42].

This requires in particular expressions for $\mu(\rho)$ and for the direct correlation function $c(r_{12};\rho)$ of the *uniform* hard sphere fluid. In this chapter we will use the Percus-Yevick (PY) [60] approximation for $c(r_{12};\rho)$. This same function also arises from a self-consistent solution of the HLR equation, where the density response to a hard core field with $R_v = \sigma$ (equivalent to fixing a solvent particle at the origin) is related to the uniform fluid pair correlation function. Thus this self-consistent use of the HLR equation provides a physically suggestive way of deriving the PY result for $c(r_{12};\rho)$ [40]. The PY $c(r_{12};\rho)$ has a very simple analytical form and proves sufficiently accurate for our purposes here. Even better results can be found if one uses the very accurate expressions for the bulk $c(r_{12};\rho)$ and $\mu(\rho)$ as given by the GMSA theory [73] as inputs to the HLR equation.

2.2.2 Relation to the PY Approximation for a Hard Core Solute

A spherical cavity acts like a hard core external field ϕ that excludes the centers of all solvent molecules from the cavity region. We take the center of the cavity as the origin of our coordinate system, so that all distances are measured relative to

the cavity center. Note that both the hydrostatic density $\rho^{\mathbf{r}_1}$ from Eq.(2.5) and the full density response $\rho(\mathbf{r}_1)$ from Eq.(2.8) vanish whenever $\mathbf{r}_1$ is located in the cavity. This exact "hard core condition" comes out naturally from the theory, and does not have to be imposed by hand as in the GFM or the GMSA approaches.

To make contact with the PY approximation, recall that the *cavity-solvent direct correlation function* $C(\mathbf{r}_1; \rho^B, R_v)$ for this system exactly satisfies

$$C(\mathbf{r}_1; \rho^B, R_v) = \int d\mathbf{r}_2 \chi^{-1}(r_{12}; \rho^B)[\rho(\mathbf{r}_2) - \rho^B]. \tag{2.9}$$

Thus $C(\mathbf{r}_1)$ is the function that replaces $-\beta\delta\phi(\mathbf{r}_1)$ so that the linear response equation (2.1) gives exact results when the full density change relative to the bulk is used on the right hand side. When this is compared to the HLR equation (2.7) for $\mathbf{r}_1$ *outside* the cavity region (where $\rho^{\mathbf{r}_1} = \rho^B$ and $\phi = 0$) we see that the HLR equation predicts that $C(\mathbf{r}_1)$ vanishes. Thus for the HLR equation $\rho(\mathbf{r}_1)$ vanishes inside the cavity region and $C(\mathbf{r}_1)$ vanishes outside. This is the same as the PY approximation for the hard core cavity-solvent system [40, 74].

If R_v is greater than $\sigma/2$, with σ the solvent hard core diameter, then an equivalent exclusion is achieved by replacing the hard core external field by a hard core solute particle with (additive) diameter

$$\sigma_v \equiv 2R_v - \sigma. \tag{2.10}$$

From this it follows that if the PY approximation for the bulk c or χ^{-1} is used, the density $\rho(\mathbf{r})$ predicted by the HLR equation is identical to that given by the PY

equation for the solute-solvent pair correlation function for a binary hard sphere mixture in the limit that the concentration of the solute species goes to zero [27]. Since an exact analytical solution of the PY equation for a binary HS mixture at arbitrary concentrations is known [45], we can take advantage of these results when computing the excess grand free energy.

This equality of solutions of the HLR equation and the PY mixture equation holds only for hard core cavity fields with radius $R_v \geq \sigma/2$ or $\sigma_v \geq 0$. As discussed below in Sec. 2.5, for *tiny cavities* with $R_v \leq \sigma/2$ the HLR equation can be solved directly and gives *exact* results for the density response if exact bulk correlation functions are used, and very accurate results when the PY approximation for the bulk c is used. However, the corresponding PY mixture solutions in this range of R_v (arrived at formally by taking σ_v in Eq.(2.10) to be *negative*) are much less accurate. This inaccuracy arises from using the PY mixture solutions for negative σ_v. The *direct* solution of the PY cavity-solute equation for a tiny cavity, where a given approximation for the bulk c is used along with the PY approximation that $C(\mathbf{r}_1)$ vanishes outside the cavity and $\rho(\mathbf{r}_1)$ vanishes inside, gives the same accurate results as the HLR equation. However, for more general external fields, the HLR equation is quite distinct from the PY approximation, and is generally more accurate; it has given good results for a wide range of fields [40, 42, 74]. This additional flexibility of the HLR equation will be required later in this chapter when we discuss alternate density routes to the free energy.

2.3 Thermodynamic Pathways to the Free Energy

In this section we discuss three different exact thermodynamic pathways for obtaining the excess free energy of inserting a cavity into a hard sphere fluid. The first two are well known, and the third describes a new density route that may have some computational advantages in other applications. We use the HLR equation to provide the needed structural information in all cases. We believe our calculation here represents the first use of a density route to obtain the excess free energy for this system. We then describe a simple but less accurate route to the free energy based on use of the partition function for the GFM.

2.3.1 Compressibility Route

In this route the excess free energy is determined by varying the chemical potential of the system while the external field $\phi(\mathbf{r})$ producing the cavity with radius R_v remains constant. In the grand canonical ensemble the average number of particles $\langle N \rangle$ is given by

$$\frac{\partial \Omega}{\partial \mu} = -\langle N \rangle, \tag{2.11}$$

where $\Omega(\mu, [\phi])$ is the grand free energy. We can then calculate the free energy difference between the final state of interest and the trivial ideal gas state of zero density with $\mu = -\infty$ and $\Omega = 0$ by integration:

$$\Omega(\mu^B, [\phi]) = -\int_{-\infty}^{\mu^B} d\mu \langle N \rangle = -\int_{-\infty}^{\mu^B} d\mu \int d\mathbf{r} \rho(\mathbf{r}; \mu, [\phi]). \tag{2.12}$$

Then $\Delta\Omega_v \equiv \Omega(\mu^B,[\phi]) - \Omega(\mu^B,[0])$, the desired excess grand free energy of the nonuniform fluid relative to the uniform bulk state, is given by

$$\Delta\Omega_v = -\int_{-\infty}^{\mu^B} d\mu \int d\mathbf{r}_1 \{\rho(\mathbf{r}_1;\mu,[\phi]) - \rho(\mu)\}. \tag{2.13}$$

As before, $\rho(\mu)$ gives the density of the uniform hard sphere solvent fluid as a function of the chemical potential.

Since $\rho(\mathbf{r};\mu,[\phi])$ vanishes inside the cavity, Eq.(2.13) shows there is a term in the excess free energy proportional to the cavity volume v given by

$$v\int_{-\infty}^{\mu^B} d\mu\rho(\mu) = v\int_0^{\rho^B} d\rho\frac{d\mu}{d\rho}\rho = vp^B, \tag{2.14}$$

on using the thermodynamic relation $\rho(\partial\mu/\partial\rho)_T = (\partial p/\partial\rho)_T$. This exact leading order term for large v is determined when using the compressibility route so that p^B is the uniform fluid pressure calculated by the compressibility route [33].

The term in curly brackets in Eq.(2.13) can be rewritten in a more convenient form for calculations by using the inverse relation to Eq.(2.9) for a general chemical potential μ:

$$\rho(\mathbf{r}_1;\mu,[\phi]) - \rho(\mu) = \int d\mathbf{r}_2 \chi(r_{12};\mu) C(\mathbf{r}_2;\rho(\mu),R_v), \tag{2.15}$$

where $\chi(r_{12};\mu) \equiv \rho\delta(\mathbf{r}_1-\mathbf{r}_2) + \rho^2[g(r_{12})-1]$ is the usual linear response function of the uniform solvent fluid and $g(r)$ is the radial distribution function. Substituting into Eq.(2.13) and carrying out the integration over $\mathbf{r}_1$, we have the formally exact

result [1]

$$\begin{aligned}\beta\Delta\Omega_v &= -\beta\int_{-\infty}^{\mu^B} d\mu\hat{\chi}(0,\mu)\int d\mathbf{r}_2 C(\mathbf{r}_2;\rho(\mu),R_v)\\ &= -\int_0^{\rho^B} d\rho\ \hat{C}(0;\rho,R_v).\end{aligned} \tag{2.16}$$

Here $\hat{\chi}(0,\mu)$ is the $k=0$ value of the Fourier transform of χ, with a similar definition for $\hat{C}(0;\rho,R_v)$. In the last equality we used the uniform fluid compressibility relation $\beta\hat{\chi}(0,\mu) = d\rho(\mu)/d\mu$ to change variables to an integration over density. We will explicitly solve the HLR equation for $R_v \leq \sigma/2$ in Sec. 2.5 below, and from the equivalence between the HLR equation and PY mixture equation for $R_v \geq \sigma/2$, we can use the exact solution of the PY mixture equation to obtain $\hat{C}$ at larger R_v. Thus we can analytically carry out the integration in Eq.(2.16) for all R_v.

2.3.2 Virial Route

We now consider a different thermodynamic pathway, which was first used in scaled particle theory [65, 26]. Here we keep the chemical potential fixed at μ^B and vary the *range* of the external hard core field by a scaling parameter λ, defining $\phi_\lambda(\mathbf{r}) \equiv \phi(\mathbf{r}/\lambda)$. For the hard core cavity field of interest here, as λ is varied from 0 to 1 the

[1] Equation (2.16) is a special case of the general exact result from potential distribution theory [82] that the excess free energy arising from inserting a single solute molecule at some position $\mathbf{r}_0$ in a (generally nonuniform) solvent fluid is equal to the one-body direct correlation $c^{(1)}(\mathbf{r}_0)$ of the solute [30]. In the present case the solute is the spherical cavity and the fluid in the absence of the solute is uniform. Integrating the functional derivative relation between the one-body and the two-body (solute-solvent) direct correlation functions [24] for a uniform density change then gives Eq.(2.16).

radius of the exclusion zone then varies from 0 to R_v. Since the density is generally related to the external field in the grand ensemble by

$$\frac{\delta\Omega}{\delta\phi(\mathbf{r})} = \rho(\mathbf{r}), \tag{2.17}$$

the desired free energy difference is given by integration:

$$\beta\Delta\Omega_v = \int_0^1 d\lambda \int d\mathbf{r}\rho_\lambda(\mathbf{r})\frac{\partial\beta\phi_\lambda(\mathbf{r})}{\partial\lambda}. \tag{2.18}$$

Here $\rho_\lambda(\mathbf{r}) \equiv \rho(\mathbf{r};\mu^B,[\phi_\lambda])$. This formula is quite general and holds for any λ-dependent potential that vanishes for $\lambda = 0$. By exploiting special properties of the scaled hard core potential (the derivative of the Boltzmann factor of a hard core potential is a delta function) it is easy to show that Eq.(2.18) can be exactly rewritten as

$$\beta\Delta\Omega_v = 4\pi R_v^3 \int_0^1 d\lambda\lambda^2\rho_\lambda(\lambda R_v). \tag{2.19}$$

Here $\rho_\lambda(\lambda R_v)$ is the *contact density* at the surface of the scaled exclusion zone with radius λR_v. As in the compressibility route, we can analytically carry out the integration in the virial route to obtain solvation free energies for cavities for all R_v. The equivalent PY solution for binary hard sphere mixtures is used for the contact densities for all λR_v's larger than $\sigma/2$, while the explicit solution of the HLR equation is used for the λR_v's smaller than $\sigma/2$.

2.3.3 Density Routes

In addition to these particular pathways, we can also imagine *directly changing* the equilibrium density from ρ^B to $\rho(\mathbf{r})$ over some convenient pathway specified by a

coupling parameter λ, while taking account of the associated changes in Ω and $\phi(\mathbf{r})$. Integrating Eq.(2.18) by parts to make $\rho_\lambda(\mathbf{r})$ explicitly the controlling variable, we have exactly

$$\beta\Delta\Omega_v = \int d\mathbf{r}\rho(\mathbf{r})\phi(\mathbf{r}) - \int_0^1 d\lambda \int d\mathbf{r}\, \phi_\lambda(\mathbf{r})\frac{\partial\rho_\lambda(\mathbf{r})}{\partial\lambda}. \tag{2.20}$$

Here $\phi_\lambda(\mathbf{r})$ is the external field consistent with the specified density profile, so that $\rho(\mathbf{r};\mu^B,[\phi_\lambda]) = \rho_\lambda(\mathbf{r})$. For a given density field $\rho_\lambda(\mathbf{r})$, the HLR equation (2.8) can be solved inversely to obtain the associated hydrostatic density field $\rho_\lambda^{\mathbf{r}}$. Using Eq.(2.6), $\phi_\lambda(\mathbf{r})$ at each $\mathbf{r}$ is locally related to $\rho_\lambda^{\mathbf{r}}$ through $\mu(\rho)$. Here we used the accurate Carnahan-Starling expression [7] for $\mu(\rho)$.

Most workers have considered a simple *linear* density path where

$$\rho_\lambda(\mathbf{r}) = \rho^B + \lambda[\rho(\mathbf{r}) - \rho^B]. \tag{2.21}$$

This has some theoretical advantages since $\partial\rho_\lambda(\mathbf{r})/\partial\lambda$ is independent of λ and has been successfully used in numerical calculations of the surface tension of the liquid-vapor interface [42]. However, when $\phi(\mathbf{r})$ has a hard core (or is strongly repulsive), then the region near $\lambda = 1$ in the λ-integration in Eq.(2.20) must be treated carefully, since for $\mathbf{r}$ in the hard core region $\partial\rho_\lambda(\mathbf{r})/\partial\lambda$ is constant, while $\phi_\lambda(\mathbf{r})$ must tend to infinity as $\lambda \to 1$. Although the singularity in the potential is integrable (for a hard core potential the divergent term in $\beta\phi_\lambda$ goes as $-\ln(1-\lambda)$ and could be treated separately), in any case large contributions to the integral arise from a relatively small interval near $\lambda = 1$. This could cause problems in a numerical integration.

To illustrate the computational advantages and flexibility that different pathways can provide, we introduce here a new density route that removes this possible difficulty. We consider a path that is linear in the *square root of the density*:

$$\rho_\lambda^{1/2}(\mathbf{r}) \equiv (\rho^B)^{1/2} + \lambda[\rho^{1/2}(\mathbf{r}) - (\rho^B)^{1/2}], \tag{2.22}$$

where $\rho_\lambda^{1/2}(\mathbf{r}) = \sqrt{\rho_\lambda(\mathbf{r})}$, etc. For this pathway we have

$$\frac{\partial \rho_\lambda(\mathbf{r})}{\partial \lambda} = 2\rho_\lambda^{1/2}(\mathbf{r}) \frac{\partial \rho_\lambda^{1/2}(\mathbf{r})}{\partial \lambda}. \tag{2.23}$$

Both factors on the right side of Eq.(2.23) are easy to determine from Eq.(2.22). The numerical integration in Eq.(2.20) can now be carried out straightforwardly since the $\rho_\lambda^{1/2}(\mathbf{r})$ factor in Eq.(2.23) will cause $\partial\rho_\lambda(\mathbf{r})/\partial\lambda$ to tend to zero exponentially fast wherever $\phi_\lambda(\mathbf{r})$ becomes large. Results using this path are reported below. Other paths implementing this idea exist and we have not tried to make an optimal choice.

2.3.4 Gaussian Field Model

Finally we consider an alternative approach, the Gaussian field model (GFM) [11], that for hard core fields has many common elements with the HLR method. The GFM describes density fluctuations in a uniform fluid with average density ρ by an effective quadratic Hamiltonian

$$\mathcal{H}^B = \frac{k_B T}{2} \int d\mathbf{r}_1 \int d\mathbf{r}_2 \delta\check{\rho}(\mathbf{r}_1) \chi^{-1}(\mathbf{r}_{12}; \rho) \delta\check{\rho}(\mathbf{r}_2), \tag{2.24}$$

where $\delta\check{\rho}(\mathbf{r}) = \check{\rho}(\mathbf{r}) - \rho$ with $\check{\rho}(\mathbf{r})$ the microscopic density. The partition function for a system in an external field $\phi(\mathbf{r}) = \phi_0(\mathbf{r}) + \phi_1(\mathbf{r})$, with ϕ_0 a hard core field producing

a cavity of radius R_v and ϕ_1 a weaker perturbation, is then assumed to be given by [11]

$$\begin{aligned}\Xi_v &= \int \mathcal{D}\check{\rho}(\mathbf{r}) \left\{\prod_{\mathbf{r}\in v} \delta[\check{\rho}(\mathbf{r})]\right\} \\ &\quad \times \exp[-\beta\mathcal{H}^B + \beta \int dr \check{\rho}(\mathbf{r})\phi_1(\mathbf{r})]. \end{aligned} \tag{2.25}$$

The product of delta functions imposes the constraint that the density vanish inside the cavity. Inserting a Fourier representation for the δ-functions and formally integrating $\check{\rho}(\mathbf{r})$ from $-\infty$ to ∞ yields a Gaussian approximation for the partition function, as discussed below.

Moreover, using the same approximations, by functionally differentiating Ξ_v with respect to the field, one obtains the nonuniform singlet density in the GFM. In the case of a pure hard core field with $\phi_1 = 0$, the density response to a cavity with radius R_v is given by

$$\rho(\mathbf{r}_1) = \rho^B - \rho^B \int_v d\mathbf{r}_2 \int_v d\mathbf{r}_3 \chi(r_{12};\mu^B)\chi_{in}^{-1}(\mathbf{r}_2,\mathbf{r}_3). \tag{2.26}$$

The integrations are restricted to the cavity region, as indicated by the subscript v on the integral symbols. Here χ_{in}^{-1} is the inverse of the restricted linear response function $\chi_{in}(r_{12};\mu^B)$, which equals $\chi(r_{12};\mu^B)$ if both $\mathbf{r}_1$ and $\mathbf{r}_2$ are in the cavity region and equals zero otherwise. Thus χ_{in}^{-1} is nonzero only inside the cavity and satisfies

$$\int_v d\mathbf{r}_2 \chi(r_{12};\mu^B)\chi_{in}^{-1}(\mathbf{r}_2,\mathbf{r}_3) = \delta(\mathbf{r}_1 - \mathbf{r}_3), \tag{2.27}$$

when both $\mathbf{r}_1$ and $\mathbf{r}_3$ are in the cavity region. Comparing Eq.(2.26) to Eq.(2.15), one can identify the cavity-solvent direct correlation function in the GFM as

$$C(\mathbf{r}_2) = -\rho^B \int_v d\mathbf{r}_3 \chi_{in}^{-1}(\mathbf{r}_2, \mathbf{r}_3). \tag{2.28}$$

By properties of χ_{in}^{-1}, the GFM $C(\mathbf{r})$ vanishes outside the cavity region and $\rho(\mathbf{r})$ in Eq.(2.26) vanishes inside. Thus the GFM gives exactly the same solution for the density response to a hard core external field as the PY or the HLR equations. (In the more general case where there is an additional perturbation potential ϕ_1, the various approaches differ. The GFM can be shown to treat the softer tail using the mean spherical approximation, which is different from and generally less accurate than the hydrostatic shift used in the HLR equation.)

Thus for cavities or hard core solutes all structurally based routes to the excess free energy will give the same results when using the GFM or the HLR equation. In addition, the GFM partition function also provides a direct and very simple route to the free energy [11]. However this route is inherently approximate because Eq.(2.25) is not really a free energy functional for the whole configuration space, but rather a restricted one describing only the space outside of the specified cavity region. This functional may legitimately describe subsequent *small* perturbations of ϕ_1 outside of the cavity, but it does not contain enough information about the functional dependence on the cavity volume in the first place. Moreover the approximations made in evaluating the GFM partition function do not build in the fact that in grand canonical ensemble, the thermodynamic properties should depend on $\mu - \phi$ rather

than on μ and ϕ individually. Thus it is also not consistent with the free energy prediction from the compressibility route, which integrates over states at different chemical potentials but with a fixed hard core always present.

Evaluating the Gaussian integrals in Eq.(2.25), the excess grand free energy arising from a cavity with radius R_v is given by

$$\begin{aligned} \beta\Delta\Omega_v &= -\log \Xi_v/\Xi^B \\ &= -\frac{1}{2}\rho^B \hat{C}(0;\rho^B,R_v) + \log\left(\det \chi_{in}\right). \end{aligned} \tag{2.29}$$

Here Ξ_v denotes the partition function with no particles in the cavity region and Ξ^B is the uniform bulk partition function. The term involving $\hat{C}$ in Eq.(2.29) arises from the Gaussian integration of $\check{\rho}$ in Eq.(2.25) and Eq.(2.28). When compared with the exact Eq.(2.16) from the compressibility route, we see the GFM effectively approximates $\hat{C}(0;\rho,R_v)$ for intermediate density values by $\left(\rho/\rho^B\right)\hat{C}(0;\rho^B,R_v)$. This free energy contribution has a form similar to a harmonic oscillator with $\left(\rho/\rho^B\right)\hat{C}(0;\rho^B,R_v)$ analogous to the restoring force. The second term is a result of the reduction of the configuration space.

An alternate perspective considers the average probability $P_v(N)$ of finding N particles in the volume v with radius R_v. The probability of inserting a cavity is thus $P_v(0)$. Then a formally exact expression for the excess free energy $\beta\Delta\Omega_v$ is

$$\beta\Delta\Omega_v = -\log P_v(0) = -\log \frac{\Xi_v[0]}{\sum_{N=0}^{N_{max}} \Xi_v[N]}. \tag{2.30}$$

Here $\Xi_v[N]$ is the constrained partition function when N particles are in the specified

volume. This formula has been successfully used in the information theory approach developed by Hummer, Pratt and coworkers [35].

If the GFM is used to approximate the partition functions in Eq.(2.30) by replacing the product of δ-functions in Eq.(2.25) by the single average constraint $\delta[\int_v d\mathbf{r}\hat{\rho}(\mathbf{r}) - N]$, one arrives at a Gaussian approximation [35, 49] for $\Xi_v[N]$. This "discrete" approximation for $\beta\Delta\Omega_v$ based on this use of the GFM is

$$\beta\Delta\Omega_v = -\log \frac{e^{-\bar{N}^2/2\chi_v}}{\sum_{N=0}^{N_{max}} e^{-(N-\bar{N})^2/2\chi_v}} \tag{2.31}$$

where

$$\chi_v \equiv \int_v d\mathbf{r}_1 \int_v d\mathbf{r}_2 \chi(|\mathbf{r}_1 - \mathbf{r}_2|), \tag{2.32}$$

and $\bar{N} = \rho^B v$.

We determined the solvation free energy $\beta\Delta\Omega_v$ for the GFM using both the continuum version, Eq.(2.29), and the discrete version, Eq.(2.31). For the uniform χ we used the PY result. To estimate $\log\det\chi_{in}$ we expanded χ_{in} in the volume v using two orthogonal basis functions. A single constant basis function was used in Ref. [49]. This is exact for tiny cavities with $R_v \leq \sigma/2$, as can be seen using Eq.(2.44) below. We chose one basis function to be constant. The other was taken to be $j_0(R_v r/\pi)$, the zeroth order spherical Bessel function with its first node fixed at $r = R_v$, but made orthogonal to the first (constant) basis function. The second basis function is thus a linear combination of $j_0(R_v r/\pi)$ and a constant. This was introduced to test the accuracy of the one basis function approximation previously used and hopefully will give improved results for larger R_v.

2.4 Results for Larger Cavities with $R_v > \sigma/2$

We now discuss the solvation free energies given by the various pathways for a cavity with $R_v > \sigma/2$, equivalent to a physically realizable hard core solute particle with diameter $\sigma_v > 0$. (Results for tiny cavities with $R_v \leq \sigma/2$ are discussed in Sec. 2.5 below.) We use the simplest version of the theory, where the PY approximation is used for the uniform fluid correlation functions. Fig. (2.1) give the solvation free energy $\beta\Delta\Omega_v$ from the different pathways as a function of the packing fraction $\eta = \pi\rho^B\sigma^3/6$ for $R_v/\sigma = 1,\ 1.5,\ 1.75$, where the results can be compared to computer simulations [13] of Crooks and Chandler. Note that the volume of a spherical cavity with $R_v = 1.75\sigma$ is over 42 times greater than that of a solvent particle. For $R_v = \sigma$ the results also give the excess chemical potential as a function of density for the uniform hard sphere fluid.

As discussed above, we can obtain analytical expressions for $\Delta\Omega_v$ for both the compressibility and virial routes. The compressibility route gives

$$\begin{aligned}\beta\Delta\Omega_v &= \frac{\eta(-2+7\eta-11\eta^2)}{2(1-\eta)^3} - \log(1-\eta) + \frac{18\eta^3}{(1-\eta)^3}\frac{R_v}{\sigma} \\ &\quad -\frac{18\eta^2(1+\eta)}{(1-\eta)^3}\frac{{R_v}^2}{\sigma^2} + \frac{8\eta(1+\eta+\eta^2)}{(1-\eta)^3}\frac{{R_v}^3}{\sigma^3},\end{aligned} \tag{2.33}$$

and the virial route gives

$$\begin{aligned}\beta\Delta\Omega_v &= \frac{\eta(-2+7\eta-5\eta^2)}{2(1-\eta)^3} - \log(1-\eta) \\ &\quad -\frac{18\eta^2(1-\eta)}{(1-\eta)^3}\frac{{R_v}^2}{\sigma^2} + \frac{8\eta(1+\eta-2\eta^2)}{(1-\eta)^3}\frac{{R_v}^3}{\sigma^3}.\end{aligned} \tag{2.34}$$

Results for the density route and for the GFM are computed numerically.

In this range of R_v there is good agreement except at the highest densities between the compressibility, virial and density routes, with best results overall arising from the compressibility route. The direct GFM predictions in Fig. (2.2) from the partition function are less satisfactory. Both the discrete and the continuum versions of the GFM give results that approach zero incorrectly as $\rho^B \to 0$, and the continuum values are consistently too large at high density while the discrete values are too small. The discrete version of the GFM uses a Gaussian approximation for the constrained partition functions and gives less accurate results than could be obtained from a fit to accurate values of $\langle N \rangle$ and $\langle N^2 \rangle$ as in the information theory approach [35].

As $R_v \to \infty$, the surface of the cavity approaches that of a planar wall. As shown in Eq.(2.14) there is a diverging term in the excess free energy given by the cavity volume $v = 4\pi R_v^3/3$ times the bulk pressure p^B, and the more interesting quantity to calculate is the surface term γ_v, given by

$$\beta\gamma_v = \frac{\beta\Delta\Omega_v - \beta p^B v}{4\pi R_v^2}. \tag{2.35}$$

The surface tension of the planar wall is then γ_∞. In the present case, both the compressibility and the virial routes give analytical expressions for $\beta\Delta\Omega_v$ which depend on R_v as a polynomial: $a_0 + a_1 R_v/\sigma + a_2 R_v^2/\sigma^2 + a_3 R_v^3/\sigma^3$. The coefficient a_3 thus gives another route to the bulk pressure on taking the wall limit. The p^B used in Eq.(2.35) has to agree with the prediction from the a_3 so that γ_∞ is finite. As discussed earlier, the compressibility $\beta\Delta\Omega_v$ yields the same bulk pressure as given

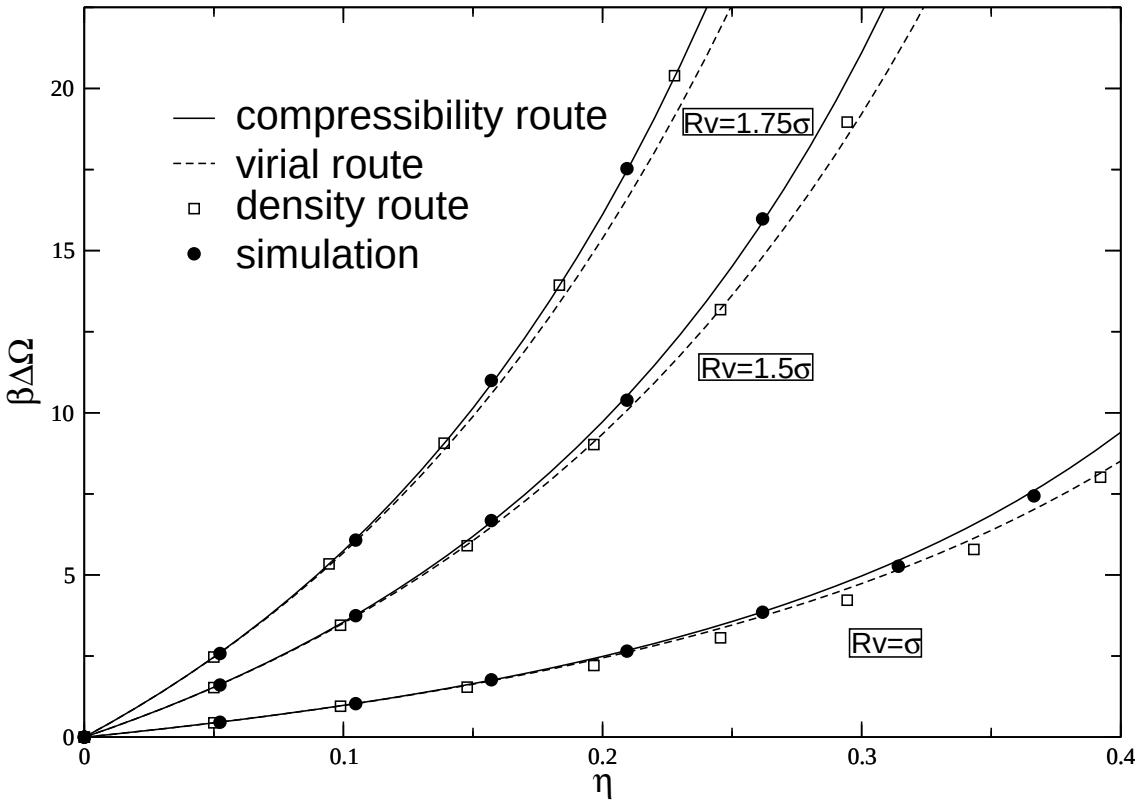

Figure 2.1: The excess free energy predicted by the three thermodynamic routes for cavity radii $R_v = \sigma$, 1.5σ and 1.75σ, compared with simulation data. η is the packing fraction and is equal to $\pi\rho^B\sigma^3/6$.

by the accurate uniform fluid PY compressibility equation of state. The virial route does not automatically build in this consistency, and the pressure predicted from the coefficient a_3 is less accurate than the uniform fluid PY virial equation of state.

The coefficient of the quadratic term then gives the surface tension $\beta\gamma_\infty = a_2/4\pi\sigma^2$. Using the compressibility route we find

$$-4\pi\beta\gamma_\infty\sigma^2 = \frac{18\eta^2(1+\eta)}{(1-\eta)^3}, \tag{2.36}$$

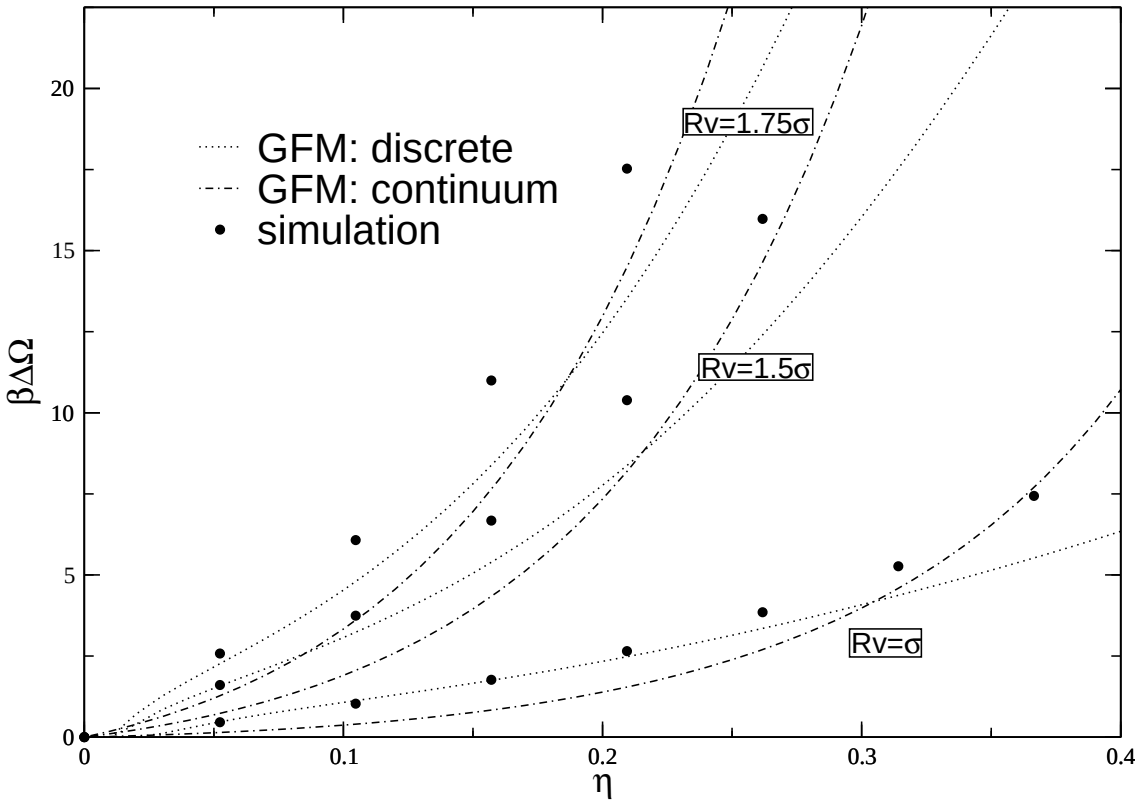

Figure 2.2: The excess free energy predictions by both the discrete and the continuum versions of the GFM, plotted for the same R_v values and on the same scale as in Fig. 2.1.

while the virial route gives

$$-4\pi\beta\gamma_\infty\sigma^2 = \frac{18\eta^2(1-\eta)}{(1-\eta)^3}. \tag{2.37}$$

The γ_∞ obtained by the compressibility route coincides with that given by scaled particle theory [65, 26, 34]. We obtained γ_∞ numerically for the density route.

These results can be compared to the quasi-exact formula [28]

$$-4\pi\beta\gamma_\infty\sigma^2 = \frac{18\eta^2(1+\frac{44}{35}\eta-\frac{4}{5}\eta^2)}{(1-\eta)^3}, \tag{2.38}$$

which fits simulation data [34] and imposes the known first and second surface virial

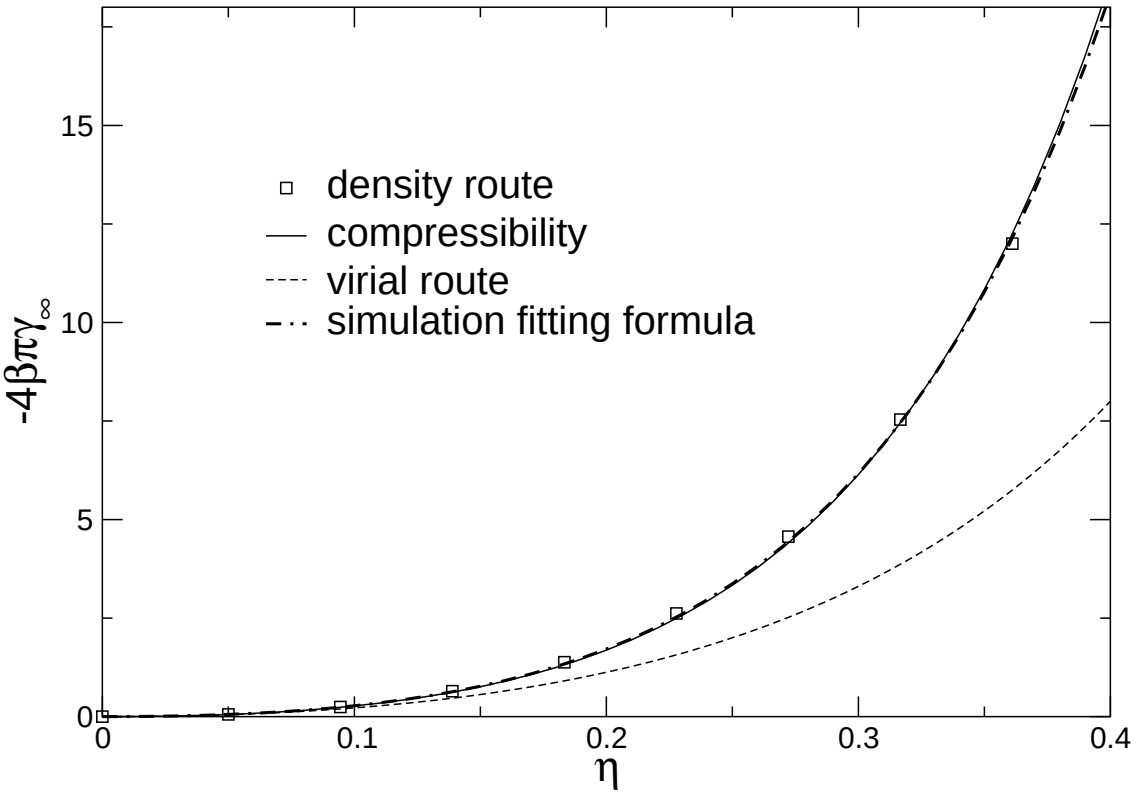

Figure 2.3: Surface tension predicted by the thermodynamic routes compared with the simulation fitting formula.

coefficients [4]. As shown in Fig. (2.3) the compressibility and density routes give excellent results, while the virial route is much less satisfactory.

This can be understood since the virial route uses only the contact densities at the fixed bulk density. The HLR equation is least accurate for the contact density at high bulk density and for large R_v, while the density response away from the solute is more accurate. On the other hand, the compressibility and density routes make use of the density response at all distances and over a range of densities from low density to the final $\rho(\mathbf{r})$ where the HLR equation is more accurate.

2.5 A Special Regime: "Tiny" Cavities

2.5.1 Exact Results

The density response to a *tiny cavity* with $R_v \leq \sigma/2$ is especially simple, since the center of at most one hard core solvent particle can lie anywhere within such a region [65, 26]. This fact allows one to determine *exactly* both the density response to a tiny cavity and the solvation free energy. Here we will compare these exact results to the predictions of the HLR and GFM approaches

As in Eq.(2.30), the solvation free energy is directly related to the average probability that no particles are in the cavity region, namely,

$$e^{-\beta\Delta\Omega_v} = P_v(0), \tag{2.39}$$

where $P_v(N)$ is the probability of finding N particles simultaneously in the region with volume $v = 4\pi R_v^3/3$. When $R_v \leq \sigma/2$, the region can hold no more than one solvent particle, so that

$$P_v(0) + P_v(1) = 1, \tag{2.40}$$

and

$$\rho^B v = \langle N \rangle_v = P_v(1). \tag{2.41}$$

Substituting these into Eq.(2.39) we thus find the *exact* result [65, 26]

$$\beta\Delta\Omega_v = -\log(1 - \rho^B v). \tag{2.42}$$

This argument can be extended to show that the *exact* density response to a

tiny cavity is [64]:

$$\rho(\mathbf{r}) = \frac{\rho^B[1 - \int_v d\mathbf{r}'\rho^B g(|\mathbf{r}' - \mathbf{r}|)]}{(1 - \rho^B v)} \tag{2.43}$$

for $\mathbf{r}$ outside v, with $\rho(\mathbf{r}) = 0$ for $\mathbf{r}$ inside. Here $g(r)$ is the exact radial distribution function for the uniform solvent fluid. Note that the contact density $\rho(R_v) = \rho^B/(1-\rho^B v)$ is exactly determined independent of the details of $g(r)$, since the corresponding $g(|\mathbf{r}' - \mathbf{r}|)$ in Eq.(2.43) vanishes for all $\mathbf{r}'$ inside v. This result is valid as long as the inserted region v can hold no more than one solvent particle, so Eq.(2.43) also holds for solvents with a hard core pair potential plus a softer tail.

2.5.2 Structural Predictions of the GFM and HLR Methods

Now let us examine the GFM result in Eq.(2.26) for the case of a density response to a tiny cavity. Since $g(|\mathbf{r}_1 - \mathbf{r}_2|) = 0$ when both $\mathbf{r}_1$ and $\mathbf{r}_2$ are in v, then $\chi_{in}(\mathbf{r}_1, \mathbf{r}_2) = \rho^B\delta(\mathbf{r}_1 - \mathbf{r}_2) - (\rho^B)^2$ inside v. It is easy to see from Eq.(2.27) that the inverse function χ_{in}^{-1} then has the simple form [39]

$$\chi_{in}^{-1}(\mathbf{r}_1, \mathbf{r}_2) = \frac{\delta(\mathbf{r}_1 - \mathbf{r}_2)}{\rho^B} + \frac{1}{1 - \rho^B v}. \tag{2.44}$$

When Eq.(2.44) is inserted into Eq.(2.26) to obtain the GFM density response to a tiny cavity, we recover the *exact* expression for $\rho(\mathbf{r})$ given in Eq.(2.43), provided that the exact uniform fluid $g(r)$ or $c(r)$ is used. If approximate (say PY) results are used to describe the uniform fluid response functions then strictly speaking the GFM and HLR predictions for $\rho(\mathbf{r})$ will not be exact for all $\mathbf{r}$. However, the contact density $\rho(R_v)$ is exact in any case, since, as noted earlier, this requires only that

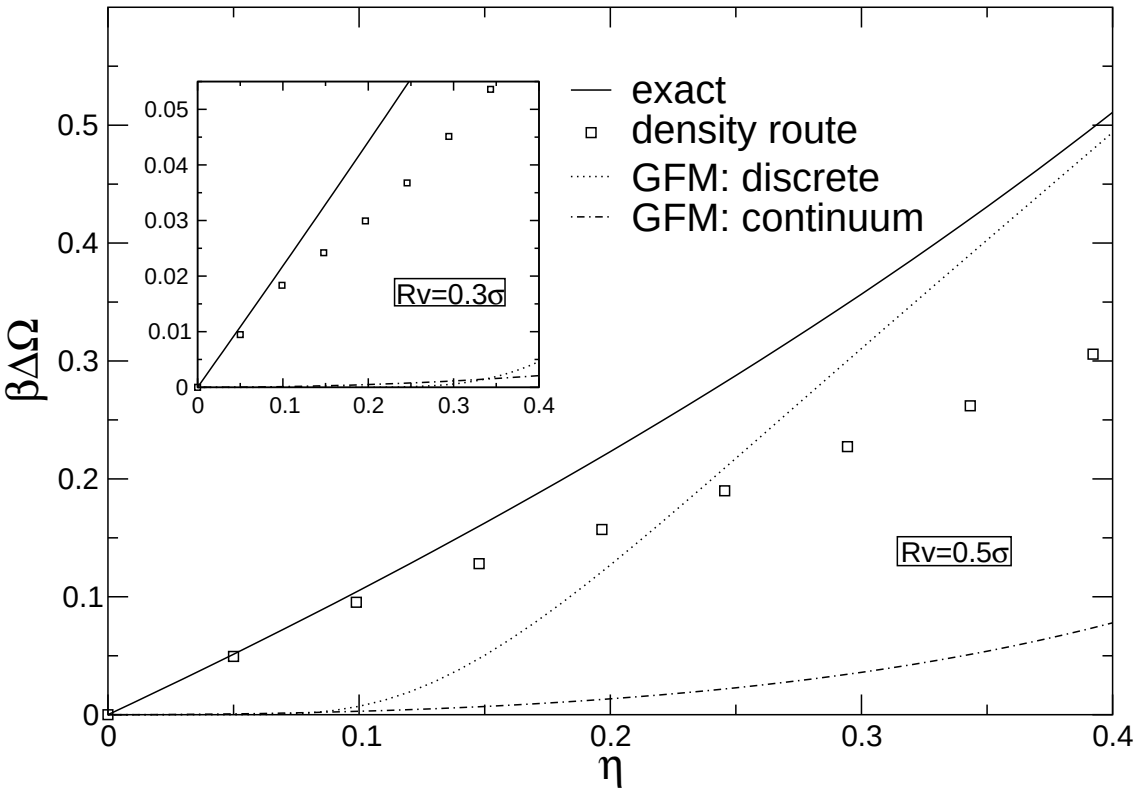

Figure 2.4: The compressibility and virial routes are exact for the tiny cavity regime. The density route is plotted along with the GFM results to compare with the exact free energy predictions for $R_v = 0.3\sigma$ and 0.5σ.

the approximate $g(r)$ vanish inside the cavity region. Because of the equivalence between the structural predictions of the GFM and the HLR equation, these same conclusions hold for the HLR equation. In particular, the density response outside a tiny cavity is *exactly* described by linear response theory about the uniform bulk system.

2.5.3 Solvation Free Energy from Thermodynamic Pathways

Moreover, these theories give the *exact* result of Eq.(2.42) for the solvation free energy $\beta\Delta\Omega_v$, independent of possible errors in $g(r)$, for all structurally based thermodynamic pathways that use only tiny hard core fields. In particular, the virial route in Eq.(2.19) gives exact results for $\beta\Delta\Omega_v$ since this requires only the (exact) contact values $\rho_\lambda(\lambda R_v)$. The compressibility route as written in Eq.(2.16) requires $C(\mathbf{r}_1)$, which from Eq.(2.28) depends only on the exact χ_{in}^{-1} in Eq.(2.44). Both results require only that the bulk $g(r)$ vanish for $r < \sigma$, and are unaffected by any errors at larger r. This is in accord with our general supposition that particular thermodynamic pathways can be relatively insensitive to errors in the structural theory.

However the choice of pathway is important. Thus the density routes do not give $\beta\Delta\Omega_v$ exactly even in the tiny cavity regime. This is because as $\rho_\lambda(\mathbf{r})$ is varied, the corresponding $\phi_\lambda(\mathbf{r})$ in general is not a pure hard core field and spreads outside the cavity region. Neither the GFM nor the HLR theories can treat these softer and longer-ranged fields exactly even if exact uniform fluid correlation functions are used.

2.5.4 Solvation Free Energy from the GFM Partition Function

The $\beta\Delta\Omega_v$ obtained directly by taking the logarithm of the partition function in Eq.(2.29) can be expressed analytically for tiny cavities as

$$\beta\Delta\Omega_v = \frac{1}{2}\log\left(1-\rho^B v\right) + \frac{1}{2}\frac{\rho^B v}{1-\rho^B v}. \tag{2.45}$$

As $v \to 0$, this goes as $(\rho^B v)^2/4$, while the exact result from Eq.(2.42) goes as $\rho^B v$. This quadratic term arises from the assumption of Gaussian fluctuations, which breaks down in this limit. The alternate discrete version from Eq.(2.31) reduces to

$$\beta\Delta\Omega_v = -\log\frac{e^{-\bar{N}\,/\,[2(1-\bar{N})]}}{e^{-\bar{N}\,/\,[2(1-\bar{N})]} + e^{-(1-\bar{N})/[2\bar{N}]}}, \tag{2.46}$$

where $\bar{N} \equiv \rho^B v$. This has the peculiar behavior as $v \to 0$ that all derivatives vanish, and so is significantly in error in this regime. See Fig. 2.4 for comparison with the exact answer.

2.6 Conclusion

We have discussed several different thermodynamic routes that can be used to determine the solvation free energy for inserting both small and large cavities into a hard sphere fluid. Generally accurate results are found by using the HLR equation to relate the densities and associated fields over the intermediate states of the different pathways. We also considered the GFM and showed that it gives results equivalent to the HLR equation for the density response induced by a rigid cavity. However

the GFM cannot describe the softer external potentials and intermediate densities needed for the density routes and for more general thermodynamic pathways. Direct use of the approximate partition function of the GFM to determine the solvation the free energy of a cavity also gives less accurate results.

Best results using the HLR equation for the solvation free energy of a cavity are found from the compressibility and density routes. This can be understood since most states along these routes require the density response at intermediate densities and distances away from the cavity where the HLR equation is most accurate. The HLR equation can also be used for more general solutes with different shapes or longer ranged attractive interactions and in applications where other pathways may be more useful. Combined with an appropriate pathway it represents a versatile and computationally efficient method for determining both the structure and the thermodynamics of nonuniform fluids.

Chapter 3

Shifted Linear Truncation Theory for Hard Sphere Fluids

A paper adapted from this chapter, "*Structure of nonuniform hard sphere fluids from shifted linear truncations of functional expansion*" by Chen, Y.-G. and Weeks, J. D., has been submitted to *Journal of Physical Chemistry* (in press).

3.1 Introduction

The HLR approximation, as demonstrated in the previous chapter, is a generally accurate and computational efficient method for determining the density response of hard sphere fluids to general external fields. However, the HLR equation can become qualitatively incorrect when the fluid is extremely confined. In this chapter, a new conceptual framework for developing more accurate theories of nonuniform hard sphere fluids is proposed. Both the HLR and PY approximations can be derived from this framework. This enables us to better understand the validity of these approximations and why they fail to be accurate in some cases, and provides possible clues about how the deficiencies could be remedied. In the following sections, several limiting cases of this framework will be examined and a criterion for its practical

application is developed. This is an on-going research project and future work along these lines is planned.

3.2 Exact Expansions for the Density Response to an External Field

The potential distribution theorem of Widom [82] relates the density response $\rho(\mathbf{r})$ of a single component hard sphere fluid in an external field $\phi(\mathbf{r})$ to the probability $P(\mathbf{r};[\rho])$ of inserting a fluid particle at the position $\mathbf{r}$ in the nonuniform fluid:

$$\rho(\mathbf{r}) = \Lambda^{-3} e^{\beta[\mu-\phi(\mathbf{r})]} P(\mathbf{r};[\rho]). \tag{3.1}$$

The direct interaction from the external field is excluded in determining $P(\mathbf{r};[\rho])$. Equivalently, $P(\mathbf{r};[\rho])$ is the probability that a cavity whose radius is equal or greater than the diameter d of the hard sphere exists at the particular point $\mathbf{r}$, since only then can the hard sphere be inserted. Here μ is the chemical potential, Λ the thermal de Broglie wavelength, and $[\rho]$ specifies explicitly the functional dependence on the density profile. $P(\mathbf{r};[\rho])$ can be formally reexpressed in terms of the *one-body direct correlation function* [15, 24]$c^{(1)}(\mathbf{r};[\rho])$ as

$$P(\mathbf{r};[\rho]) = e^{c^{(1)}(\mathbf{r};[\rho])}. \tag{3.2}$$

By expanding $P(\mathbf{r}_1;[\rho])$ at a given $\mathbf{r}_1$ in a functional Taylor series about a *uniform* fluid state at some density $\tilde{\rho}$, Percus derived the following expansion for

the nonuniform density [59]

$$\begin{aligned}\rho(\mathbf{r}_1) &= \Lambda^{-3}e^{\beta[\mu-\phi(\mathbf{r}_1)]+c^{(1)}(\tilde{\rho})}\{1+\int d\mathbf{r}_2\, c^{(2)}(r_{12};\tilde{\rho})(\rho(\mathbf{r}_2)-\tilde{\rho}) \\ &\quad + \int d\mathbf{r}_2 \int d\mathbf{r}_3\, [c^{(2)}(r_{12};\tilde{\rho})c^{(2)}(r_{13};\tilde{\rho}) + c^{(3)}(\mathbf{r}_1,\mathbf{r}_2,\mathbf{r}_3;\tilde{\rho})](\rho(\mathbf{r}_2)-\tilde{\rho})(\rho(\mathbf{r}_3)-\tilde{\rho})+...\}\end{aligned} \tag{3.3}$$

The $c^{(n)}(\mathbf{r}_1,\mathbf{r}_2,...,\mathbf{r}_n)$ are defined by successive functional derivatives of $c^{(1)}(\mathbf{r})$ with respect to the singlet density, i.e.,

$$c^{(n)}(\mathbf{r}_1,\mathbf{r}_2,...,\mathbf{r}_n) = \frac{\delta c^{(n-1)}(\mathbf{r}_1,\mathbf{r}_2,...,\mathbf{r}_{n-1})}{\delta\rho(\mathbf{r}_n)}. \tag{3.4}$$

Since we expand about a uniform bulk state, $c^{(2)}(\mathbf{r}_1,\mathbf{r}_2;[\rho]) = c^{(2)}(r_{12};\tilde{\rho})$, where $r_{12} = |\mathbf{r}_2-\mathbf{r}_1|$, due to translational invariance. Although the density $\rho(\mathbf{r})$ can have discontinuities caused by the discontinuities in the external field $\phi(\mathbf{r})$, representing, e.g., a hard wall or a spherical cavity, $P(\mathbf{r};[\rho])$ is always continuous and smooth [59, 60, 24] even across any discontinuities in $\phi(\mathbf{r})$. The expansion of Eq.(3.3) is thus designed to take advantage of this smoothness of $P(\mathbf{r};[\rho])$. The hope is that with proper choice of $\tilde{\rho}$ the expansion can be truncated at some low order and a relatively simple theory for $\rho(\mathbf{r})$ will result.

Percus considered several other expansions as well [59], some of which might seem more promising. For example by directly expanding $c^{(1)}(\mathbf{r}_1;[\rho])$ in Eq.(3.2) in a Taylor series, we are guaranteed that the resulting approximation for the density after a truncation is always nonnegative, an exact and desirable property not always produced by truncations of Eq.(3.3). However there is a well defined limit where the

expansion in Eq.(3.3) truncates *exactly*, in contrast to the corresponding expansion for $c^{(1)}$. Moreover we will show that both the HLR and the PY equations can be derived from Eq.(3.3). This suggests that it offers a versatile starting point for further research.

3.3 Confined Fields and the PY Approximation

One limit where the expansion in Eq.(3.3) is particularly useful is when the external field ϕ is nonzero only in a region much smaller than the correlation length of the fluid. The analyticity of $P(\mathbf{r};[\rho])$ then ensures that its values in the tiny region where ϕ is nonzero can be accurately determined by making use of *low order extrapolation* of its values *outside*, i.e., where ϕ vanishes. For such locally confined fields, it seems clear that the expansion in Eq.(3.3) should be about $\tilde{\rho} = \rho^B$, the bulk density. This is related to the chemical potential μ from Eq.(3.1) and Eq.(3.2) by

$$\rho^B = \Lambda^{-3} e^{\beta\mu} e^{c^{(1)}(\rho^B)}. \tag{3.5}$$

It seems plausible that expansion only to *linear order* in Eq.(3.3) could give an accurate description of the fluid's density response to a very confined field:

$$\rho(\mathbf{r}_1) = \Lambda^{-3} e^{\beta[\mu-\phi(\mathbf{r}_1)]+c^{(1)}(\rho^B)}[1 + \int d\mathbf{r}_2\, c^{(2)}(r_{12};\rho^B)(\rho(\mathbf{r}_2)-\rho^B)]. \tag{3.6}$$

This qualitative argument will be made more precise below. Using Eq.(3.5), this equation can be rewritten as

$$\rho(\mathbf{r}_1) = \rho^B e^{-\beta\phi(\mathbf{r}_1)}[1 + \int d\mathbf{r}_2\, c^{(2)}(r_{12};\rho^B)(\rho(\mathbf{r}_2)-\rho^B)]. \tag{3.7}$$

If the direct correlation function $c^{(2)}(r_{12};\rho^B)$ of the uniform bulk fluid is known, Eq.(3.7) can be solved for the density $\rho(\mathbf{r})$ induced by the external field $\phi(\mathbf{r})$.

Equation (3.7) is the *PY approximation* [59, 60] for nonuniform fluids. We show below that it gives exact results for *any* sufficiently localized $\phi(\mathbf{r})$, as suggested by the extrapolation argument. Moreover, as discussed in the previous chapter of this thesis, the PY approximation is known to give reasonably accurate results for the density response to larger spherical cavities, where $\phi(\mathbf{r})$ is infinitely repulsive inside a spherical region of radius R, but zero elsewhere, including the hard wall limit. For such potentials the exact result $\rho(\mathbf{r}) = 0$ is trivially obtained from Eq.(3.7) in regions where $\phi(\mathbf{r})$ is infinite because of the Boltzmann factor $e^{-\beta\phi(\mathbf{r})}$.

Despite this success, the linear extrapolation using the bulk fluid in Eq.(3.7) would be expected to give poor results for external fields that remain finite and vary over extended regions, especially in negative regions of the field where errors in the truncated series can be greatly magnified by the Boltzmann factor $e^{-\beta\phi(\mathbf{r})}$. These are limits where the PY approximation is known to be very inaccurate.

3.4 Exact Shifting Property in the Grand Ensemble

When the linear truncation is inaccurate, it may seem difficult to make further progress, since the higher order terms in Eq.(3.3) are too complicated to use in practical calculations. However, as mentioned by Percus [59], one does *not* always have to expand Eq.(3.3) about the bulk density defined by Eq.(3.5), nor does one

have to expand about the same bulk state for each $\mathbf{r}$ value of $\rho(\mathbf{r})$. We can use this additional flexibility to greatly extend the accuracy of different linear truncations of Eq.(3.3).

As discussed in detail in the last chapter of this thesis, it is the combination $\mu - \phi(\mathbf{r})$ that determines the density profile in the grand canonical ensemble, and not μ and $\phi(\mathbf{r})$ separately. When both the chemical potential and the external field are shifted by the same constant, the system's properties should remain unchanged. This exact *shifting property* of the grand ensemble will play a key role in what follows.

In particular, a uniform system with chemical potential μ and a constant field $\phi^c = c$ everywhere is thus equivalent to a bulk system in zero field with shifted chemical potential $\tilde{\mu}^c = \mu - c$ [24]. The basic idea leading to the HLR equation discussed in the last chapter is that the response to non-constant but slowly varying fields is naturally and accurately approximated in terms of a uniform fluid at a chemical potential similarly shifted by the *local* value of the external field. Both the HLR equation and the new approximate theory we will develop below are consistent with the shifting property and thus predict the same density profile $\rho(\mathbf{r})$ for all systems related by a uniform shift of the external field and the chemical potential.

To exploit this shifting property of the grand canonical ensemble in Eq.(3.3) we consider a general shifted chemical potential

$$\tilde{\mu}^{\mathbf{r}_1} = \mu - a^{\mathbf{r}_1} \tag{3.8}$$

and a shifted external field

$$\tilde{\phi}^{\mathbf{r}_1}(\mathbf{r}) = \phi(\mathbf{r}) - a^{\mathbf{r}_1}, \tag{3.9}$$

both of which are shifted from the original μ and $\phi(\mathbf{r})$ by a constant $a^{\mathbf{r}_1}$ that in principle can depend on the point $\mathbf{r}_1$ about which the expansion is carried out. The superscript $\mathbf{r}_1$ in $\tilde{\mu}^{\mathbf{r}_1}$, $\tilde{\phi}^{\mathbf{r}_1}$, $a^{\mathbf{r}_1}$ indicated this parametric dependence on $\mathbf{r}_1$. The shifted chemical potential $\tilde{\mu}^{\mathbf{r}_1}$ defines at each $\mathbf{r}_1$ an associated bulk system with a uniform density

$$\tilde{\rho}^{\mathbf{r}_1} \equiv \rho(\tilde{\mu}^{\mathbf{r}_1}), \tag{3.10}$$

whose correlation functions are used in the expansion. Equation (3.3) thus becomes

$$\begin{aligned}
\rho(\mathbf{r}_1) \;=\; & \Lambda^{-3} e^{\beta[\tilde{\mu}^{\mathbf{r}_1} - \tilde{\phi}^{\mathbf{r}_1}(\mathbf{r}_1)] + c^{(1)}(\tilde{\rho}^{\mathbf{r}_1})} \{1 + \int d\mathbf{r}_2\, c^{(2)}(r_{12}; \tilde{\rho}^{\mathbf{r}_1})(\rho(\mathbf{r}_2) - \tilde{\rho}^{\mathbf{r}_1}) \\
& + \int d\mathbf{r}_2 \int d\mathbf{r}_3\, [c^{(2)}(r_{12}; \tilde{\rho}^{\mathbf{r}_1}) c^{(2)}(r_{13}; \tilde{\rho}^{\mathbf{r}_1}) \\
& + c^{(3)}(\mathbf{r}_1, \mathbf{r}_2, \mathbf{r}_3; \tilde{\rho}^{\mathbf{r}_1})](\rho(\mathbf{r}_2) - \tilde{\rho}^{\mathbf{r}_1})(\rho(\mathbf{r}_3) - \tilde{\rho}^{\mathbf{r}_1}) + ...\}
\end{aligned} \tag{3.11}$$

In principle, if we could accurately evaluate *all* terms in the Taylor series, the same exact result for $\rho(\mathbf{r}_1)$ would be found for any choice of $a^{\mathbf{r}_1}$ (subject to the convergence of the series) due to the shifting property. But this is hopelessly complicated in general and approximate values for $\rho(\mathbf{r}_1)$ from truncations of the series do depend on the choice of the $a^{\mathbf{r}_1}$.

3.5 Shifted Linear Truncations

Our strategy is to try to choose the $a^{\mathbf{r}_1}$ or the $\tilde{\rho}^{\mathbf{r}_1}$ at *each* $\mathbf{r}_1$ in such a way that a self consistent solution for $\rho(\mathbf{r}_1)$ based on a simple low order truncation of the

series in Eq.(3.3) can give accurate results. In particular, we suppose that the $a^{\mathbf{r}_1}$ can be chosen by some argument to be specified later so that the expansion can be truncated at linear order to a good approximation. We thus arrive at a very general starting point, which we refer to as the *shifted linear response* (SLR) equation:

$$\begin{aligned}\rho(\mathbf{r}_1) &= \Lambda^{-3} e^{\beta[\tilde{\mu}^{\mathbf{r}_1} - \tilde{\phi}^{\mathbf{r}_1}(\mathbf{r}_1)] + c^{(1)}(\tilde{\rho}^{\mathbf{r}_1})} \{1 + \int d\mathbf{r}_2\, c^{(2)}(r_{12}; \tilde{\rho}^{\mathbf{r}_1})(\rho(\mathbf{r}_2) - \tilde{\rho}^{\mathbf{r}_1})\} \\ &= \tilde{\rho}^{\mathbf{r}_1} e^{-\beta\tilde{\phi}^{\mathbf{r}_1}(\mathbf{r}_1)} \{1 + \int d\mathbf{r}_2\, c^{(2)}(r_{12}; \tilde{\rho}^{\mathbf{r}_1})(\rho(\mathbf{r}_2) - \tilde{\rho}^{\mathbf{r}_1})\} \qquad (3.12)\end{aligned}$$

Specific choices of the $a^{\mathbf{r}_1}$ or $\tilde{\rho}^{\mathbf{r}_1}$ will lead to different approximations for $\rho(\mathbf{r}_1)$. The PY approximation arises from the choice $a^{\mathbf{r}_1} = 0$ or $\tilde{\rho}^{\mathbf{r}_1} = \rho^B$. As we argued above this choice should give very accurate results for sufficiently localized fields. However, when the external field is extended but slowly varying, a different choice of $a^{\mathbf{r}_1}$ is clearly more appropriate. As shown in the previous chapter, the HLR equation is very accurate in such cases. This uses the *hydrostatic shift,* where the external field is locally shifted at each $\mathbf{r}_1$ to be zero. This corresponds to the choice

$$a^{\mathbf{r}_1} = \phi(\mathbf{r}_1), \qquad (3.13)$$

in Eq.(3.12) so that $\tilde{\phi}^{\mathbf{r}_1}(\mathbf{r}_1) = 0$ and $\tilde{\rho}^{\mathbf{r}_1} = \rho^{\mathbf{r}_1} \equiv \rho(\mu - \phi(\mathbf{r}_1))$. When the hydrostatic shift is employed, the SLR equation (3.12) reduces exactly to the HLR equation.

Thus the expansion Eq.(3.11) provides an alternative derivation of the HLR equation in addition to the previous argument using linear response with the hydrostatic shift (also see reference [40]). More important, it provides the additional flexibility needed to suggest improvements of the HLR equation. With proper choice

of $a^{\mathbf{r}}$, Eq.(3.12) can be used to describe and bridge several limits that both the PY and the HLR equations fail to capture. These limiting cases will be addressed in the following.

3.5.1 "Tiny" Fields

Consider first a very localized field $\phi(\mathbf{r})$ that is non-vanishing only within a spherical volume V^{ϕ} of radius $d/2$, with d the hard sphere diameter:

$$\begin{aligned} \phi(\mathbf{r}) &\neq 0, \, |\mathbf{r}| < \frac{d}{2} \\ &= 0, \text{ otherwise.} \end{aligned} \tag{3.14}$$

This volume is so small that it can simultaneously accommodate the centers of at most *one* hard sphere particle. We call localized fields that are nonzero only in such a tiny region *tiny fields*. A special case of "tiny fields" is a *tiny cavity*, where ϕ is infinite in V^{ϕ}. The density response of a hard sphere fluid to any tiny field can be determined exactly, as we now show.

We start with the grand partition function $\Xi[\phi]$ when a general external field ϕ is present in the fluid:

$$\begin{aligned} \Xi[\phi] &= \sum_{N=0}^{\infty} \frac{z^N}{N!} Z_N[\phi] \\ &= \sum_{N=0}^{\infty} \frac{z^N}{N!} \int d\mathbf{r}_1 ... \mathbf{r}_N e^{-\beta \sum_{n=1}^{N} \phi(\mathbf{r}_i) - \beta V_N(\mathbf{r}_1, \mathbf{r}_2, ..., \mathbf{r}_N)}. \end{aligned} \tag{3.15}$$

Here $Z_N[\phi]$ is the canonical partition in the presence of the field, $Z_N[0]$ refers to

that of a bulk fluid, i.e., when the external field is zero, and $z \equiv \exp(\beta\mu)/\Lambda^3$. $V_N(\mathbf{r}_1, \mathbf{r}_2, ..., \mathbf{r}_N)$ is the intermolecular interaction potential between the N fluid particles. Introducing the Mayer f-function for the external field

$$f^\phi(\mathbf{r}) \equiv e^{-\beta\phi(\mathbf{r})} - 1, \tag{3.16}$$

Eq.(3.15) can be rewritten in terms of an expansion about the uniform fluid with $\phi = 0$:

$$\begin{aligned}
\Xi[\phi] &= \sum_{N=0}^{\infty} \frac{z^N}{N!} \sum_{n=0}^{N} \int d\mathbf{r}_1 d\mathbf{r}_2 ... d\mathbf{r}_n \frac{N!}{(N-n)!n!} f^\phi(\mathbf{r}_1) f^\phi(\mathbf{r}_2) ... f^\phi(\mathbf{r}_n) \\
&\quad \int d\mathbf{r}_{n+1}, ..., d\mathbf{r}_N e^{-\beta V_N(\mathbf{r}_1, ..., \mathbf{r}_N)} \qquad (3.17) \\
&= \sum_{n=0}^{\infty} \frac{1}{n!} \int d\mathbf{r}_1 d\mathbf{r}_2 ... d\mathbf{r}_n f^\phi(\mathbf{r}_1) f^\phi(\mathbf{r}_2) ... f^\phi(\mathbf{r}_n) \\
&\quad \sum_{N \geq n}^{\infty} \frac{z^N}{(N-n)!} \int d\mathbf{r}_{n+1}, ..., d\mathbf{r}_N e^{-\beta V_N(\mathbf{r}_1, ..., \mathbf{r}_N)} \qquad (3.18) \\
&= \Xi[0] \sum_{n=0}^{\infty} \frac{1}{n!} \int d\mathbf{r}_1 d\mathbf{r}_2 ... d\mathbf{r}_n f^\phi(\mathbf{r}_1) f^\phi(\mathbf{r}_2) ... f^\phi(\mathbf{r}_n) \rho^{(n)}(\mathbf{r}_1, ..., \mathbf{r}_n; [0]) \\
& \qquad (3.19)
\end{aligned}$$

Here $\rho^{(n)}(\mathbf{r}_1, ..., \mathbf{r}_n; [0])$ is the n-particle distribution function in the uniform grand canonical ensemble with chemical potential μ.

For general extended fields this formal expansion does not converge rapidly. However it can be very useful when the field is confined to a small localized region of space since $f^\phi(\mathbf{r})$ is nonzero only where ϕ is nonzero. In particular for tiny fields the expansion Eq.(3.19) must truncate *exactly* due to the vanishing of the $\rho^{(n)}(\mathbf{r}_1, ..., \mathbf{r}_n, [0])$ when more than one hard particle is simultaneously within the

volume V^ϕ. By functional differentiation of Eq.(3.19) we can also find an expression for $\rho(\mathbf{r};[\phi])$ that similarly truncates. Thus we have exactly for tiny fields

$$\Xi[\phi] = \Xi[0][1 + \int d\mathbf{r}_1 \rho^B f^\phi(\mathbf{r}_1)], \tag{3.20}$$

and

$$\rho(\mathbf{r}_1;[\phi]) = \frac{\rho^B e^{-\beta\phi(\mathbf{r}_1)}}{1 + \int d\mathbf{r}_2 \rho^B f^\phi(\mathbf{r}_2)}[1 + \int d\mathbf{r}_2 \rho^B g^{(2)}(|\mathbf{r}_1 - \mathbf{r}_2|;\rho^B) f^\phi(\mathbf{r}_2)]. \tag{3.21}$$

This exact result for the density response to a tiny field ϕ was originally derived in a different way by Reiss and coworkers [64]. Here $g^{(2)}(|\mathbf{r}_1 - \mathbf{r}_2|;\rho^B)$ is the exact radial distribution in the uniform hard sphere fluid. This same formula clearly holds for a more general model with longer ranged pair interactions outside the hard core if the appropriate $g^{(2)}$ is used.

As might be expected by the appearance of ρ^B in this equation, one can show (see appendix B for details) that the PY approximation Eq.(3.7) is consistent with this exact result for *any* tiny field. In accord with the qualitative argument above, the linear extrapolation from the bulk into the tiny region is *exact* in this case. This desirable feature of the PY approximation for nonuniform fluids does not seen to be known in the literature. This corresponds in the SLR equation to the choice $a^{\mathbf{r}} = 0$, i.e., $\tilde{\rho}^{\mathbf{r}} = \rho^B$ and shows that the series indeed truncates exactly in this special case.

However, a closely related limit highlights a general problem with the PY approximation. Consider a field $\phi^c(\mathbf{r})$ that is a non-zero constant c outside a tiny region V^ϕ and any value $\phi(\mathbf{r})$ inside. This can immediately be shifted to be the type

for which Eq.(3.20) and Eq.(3.21) hold by making the choice $a^r = c$. For such a field ϕ^c we then have

$$\rho(\mathbf{r}_1;[\phi]) = \frac{\tilde{\rho}^c e^{-\beta\tilde{\phi}^c(\mathbf{r}_1)}}{1+\int d\mathbf{r}_2\tilde{\rho}^c\tilde{f}^c(\mathbf{r}_2)}[1+\int d\mathbf{r}_2\tilde{\rho}^c g^{(2)}(|\mathbf{r}_1-\mathbf{r}_2|;\tilde{\rho}^c)\tilde{f}^c(\mathbf{r}_2)]. \tag{3.22}$$

Here $\tilde{\rho}^c = \rho(\mu - c)$ and $\tilde{f}^c$ is defined as in Eq.(3.16) with the shifted tiny field $\tilde{\phi}^c(\mathbf{r}) = \phi^c(\mathbf{r}) - c$.

For a perturbation that varies significantly only in a very local region (compared with the correlation length of the particles), a particle situated in the perturbed region, though directly affected by the field, should screen the perturbation from the rest of the fluid particles. The fluid's response thus essentially remains that of the uniform fluid outside the local region. The shifted field represents such a localized perturbation. Thus choosing the density $\tilde{\rho}^c$ to be that of the bulk environment i.e., $\rho(\mu - c)$, will truncate Eq.(3.19) at low order, leading to Eq.(3.22). And again, the choice $a^{\mathbf{r}} = c$ in the SLR equation (3.12) gives this exact result.

In this essentially equivalent case however, the PY approximation, which always uses the *unshifted* ρ^B, will give an incorrect result, even though it can exactly describe the tiny field limit when $c = 0$. Unlike the SLR equation, the PY approximation does not build in the exact shifting feature of the grand canonical ensemble. This can cause significant errors for extended slowly varying fields.

However, the HLR approximation uses the hydrostatic shift Eq.(3.13) and thus will correctly describe the shifted bulk density $\tilde{\rho}^c$ in this case. Moreover it is exact for *tiny cavities* [39](tiny fields that are infinitely repulsive inside V^ϕ) since any

finite value for $a^{\mathbf{r}}$ inside the cavity would still give the correct zero density. However the HLR equation is *not* exact for more general finite tiny fields. The HLR local density $\rho^{\mathbf{r}}$ would follow the variations in ϕ inside the tiny region, contrary to the exact result with a constant $\tilde{\rho}^c$ everywhere. Rapidly varying tiny fields can generate noticeable errors in the HLR approximation, as will be shown in a later section where computational results are reported.

3.5.2 Narrow Slits

Another application that may at first seem to be very different from the tiny field case is when an extended external field confines the fluid to a region of reduced dimensions. For example, consider a hard sphere fluid confined between two planar hard walls forming a narrow slit. We can get exact results for this case from Eq. (3.19) by exploiting the shifting property of the grand ensemble. The confining field can be taken to be the limit of piecewise constant potentials defined so that

$$\begin{aligned} \phi^c(z) &= 0, \;\; 0 < z < L_s \\ &= c, \;\; \text{otherwise}, \end{aligned} \tag{3.23}$$

in the limit where $c \to \infty$. In this limit the fluid's density will be zero except in the narrow region between the walls. Here L_s is the effective width of the slit as seen by the centers of the fluid particles.

If we formally introduce the *uniform* shift $a^z = c$ we have

$$\begin{aligned} \tilde{\phi}^c(z) &= -c,\ 0 < z < L_s \\ &= 0, \text{ otherwise} \end{aligned} \tag{3.24}$$

and the shifted external field $\tilde{\phi}^c(z)$ is non-zero only in the narrow slit region, similar to a tiny field. However, the shifted slit field is not strictly a tiny field as defined in the previous section where the expansion exactly truncates, because even when $L_s \to 0$, many particles in principle can still be found in the slit, aligned in a two-dimensional layer along the walls of the slit. But once this shift has been made, the expansion in Eq.(3.19) and Eq.(3.22) converges rapidly for small L_s since the contribution from the integration over the $\tilde{f}^c$ tends to zero. The shifted chemical potential $\tilde{\mu}^c = \mu - c$ tends to $-\infty$, corresponding to an expansion about the ideal gas limit where the shifted bulk density $\tilde{\rho}^c$ tends to zero and $c^{(1)}(\tilde{\rho}^c) = 0$.

Inside the slit where $\tilde{\mu}^c - \tilde{\phi}^c(\mathbf{r}_1) = \mu - \phi^c(\mathbf{r}_1) = \mu$, we have a finite limiting density as $L_s \to 0$ given by

$$\tilde{\rho}^c e^{-\beta\tilde{\phi}^c(\mathbf{r}_1)} = \Lambda^{-3} e^{\beta[\tilde{\mu}^c - \tilde{\phi}^c(\mathbf{r}_1)] + c^{(1)}(\tilde{\rho}^c)} = \Lambda^{-3} e^{\beta\mu}. \tag{3.25}$$

Equation (3.22) then gives the first two terms in an exact (but non-truncating) virial-like expansion valid for narrow slits. Higher order terms can be determined straightforwardly from Eq.(3.19). In agreement with previous work [31], there is a

constant limiting lowest order density profile in the narrow slit given by

$$\begin{aligned} \rho(z) &= \Lambda^{-3} e^{\beta\mu},\ 0 < z < L_s \\ &= 0,\ \text{otherwise.} \end{aligned} \tag{3.26}$$

For a value of μ corresponding to a dense uniform hard sphere fluid, this yields a very large limiting value for the reduced density in the slit $\rho^{3D} d^3 \equiv \Lambda^{-3} e^{\beta\mu} d^3 \gg 1$. However the density of fluid particles per unit area of the wall $\rho^{2D} d^2 \equiv \Lambda^{-3} e^{\beta\mu} d^2 L_s$ tends to zero as $L_s \to 0$. Thus particles in the narrow slit are very far apart laterally and an expansion about the ideal gas limit is physically appropriate.

Clearly the SLR equation can reproduce these exact limiting results if the proper choice $a^z = c$ for all z (where $c \to \infty$) is made. However, the PY approximation uses $a^z = 0$ everywhere in the SLR equation, while the HLR equation assumes $a^z = c$ outside the slit but $a^z = 0$ inside, and hence they both give incorrect results in the limit $L_s \to 0$. Both theories correctly predict zero density outside the slit, since for any choice of a^z, the factor $\tilde{\rho}^{z_1} e^{-\beta \tilde{\phi}^{z_1}(z_1)}$ in Eq.(3.12) immediately makes $\rho(z_1)$ zero outside the slit. However, inside the slit both the PY and the HLR equations take $\tilde{\rho}^{z_1} = \rho^B$ and thus expand about the bulk reference state, which gives a very poor description of the dilute 2D gas in the slit. The PY and the HLR solution are equivalent for this system. As $L_s \to 0$ they predict a limiting density much lower than given by Eq.(3.26). These problems arise only at small separations of the order or smaller that of the hard sphere diameter d. At larger separations and in the one wall limit both theories give much more satisfactory results [29], as that

can be observed in Fig.(3.8).

3.6 A New Criterion for the Shifted Linear Response (SLR) Equation

The above discussion has shown the versatility of the SLR equation and its ability to give exact limiting results in several specific cases with proper choice of the $\tilde{\rho}^z$. It has also shown that inaccuracies arise in some cases from the prescribed local choices made by the PY and HLR equations. Thus we need to have a more general and systematic way of arriving at better choices for $\tilde{\rho}^z$ in the SLR equation. To that end we first look more closely at the reasons why the HLR choice fails in some cases.

3.6.1 Limitations of the HLR Equation

The expansion Eq.(3.11) provides an alternative derivation for the HLR equation in addition to the linear response and hydrostatic shift arguments used in the previous chapter. It can be observed that the HLR approximation always shifts the external field such that the field value is locally zero at the point of interest, and expands the density about that of the local uniform system at the shifted chemical potential. Unlike the PY approximation, the HLR thus builds in the invariance of a grand canonical ensemble when both the chemical potential and the external field are shifted by a constant. It is an excellent approximation when the external field is slowly varying, truncating the expansion of Eq.(3.11) about the hydrostatic density

Eq.(3.10) efficiently. Moreover it gives the same results as the PY approximation for hard core fields. In general the HLR approximation is much more accurate and more useful than the PY approximation for a wide range of external fields.

However, HLR's choice of $\tilde{\rho}^{\mathbf{r}} = \rho(\mu - \phi(\mathbf{r}))$ depends on the external field too locally in cases where the external fields varies significantly in local regions much smaller than the correlation length of the fluid. In such cases, the proper density $\tilde{\rho}^{\mathbf{r}}$ to expand about is often not the hydrostatic density $\rho(\mu - \phi(\mathbf{r}))$, but a nonlocal extrapolation using the density of the surroundings, as illustrated by the tiny field and narrow slit examples discussed above. To improve the HLR approximation using the SLR equation (3.12), one needs a new way to choose $\tilde{\rho}^{\mathbf{r}}$ that can account for this extrapolation of the local uniform system in such cases, while not spoiling the good results of the HLR equation in most other applications. We describe below our first attempt to develop such a criterion.

3.6.2 The Insensitivity Criterion

If all orders are exactly retained in the expansion (3.11), it should be invariant with respect to a simultaneous shift of the chemical potential μ and the external field ϕ. Thus Eq.(3.11) should hold for all choices of $\tilde{\rho}^{\mathbf{r}}$. However only certain choices of $\tilde{\rho}^{\mathbf{r}}$ can efficiently truncate the series at low orders. One possible criterion for truncation

is to choose a $\tilde{\rho}^{\mathbf{r}}$ that minimizes the contribution from the quadratic term

$$\begin{aligned}\mathbf{Q}(\mathbf{r}_1) \equiv & \int d\mathbf{r}_2 \int d\mathbf{r}_3 c^{(2)}(r_{12};\tilde{\rho}^{\mathbf{r}_1})c^{(2)}(r_{13};\tilde{\rho}^{\mathbf{r}_1}) \\ & +c^{(3)}(\mathbf{r}_1,\mathbf{r}_2,\mathbf{r}_3;\tilde{\rho}^{\mathbf{r}_1}))(\rho(\mathbf{r}_2)-\tilde{\rho}^{\mathbf{r}_1})(\rho(\mathbf{r}_3)-\tilde{\rho}^{\mathbf{r}_1}) \end{aligned} \tag{3.27}$$

in Eq.(3.11). However, unlike $c^{(2)}(r_{12};\rho)$, $c^{(3)}(\mathbf{r}_1,\mathbf{r}_2,\mathbf{r}_3;\rho)$ is often not available analytically [60, 45] (and accurately) and the 6-dimension integral of $\mathbf{Q}(\mathbf{r})$ is very computational demanding.

To circumvent the difficulty of dealing with the $\mathbf{Q}(\mathbf{r})$ directly, a reasonable alternative is to consider how the predictions of the SLR equation change as $\tilde{\rho}^{\mathbf{r}}$ is varied. Since the SLR equation is a truncation of the exact series in Eq.(3.11), it is certainly not invariant with respect to variation of *any* $\tilde{\rho}^{\mathbf{r}}$. However if the truncation is accurate for some particular choice of $\tilde{\rho}^{\mathbf{r}}$, in effect the higher order terms in the series have then been taken into account. Thus the SLR equation should be relatively *insensitive* to small variations about the particular $\tilde{\rho}^{\mathbf{r}}$ that makes the higher order corrections to the SLR equation small. This condition need not be exact, even in the case of a tiny field where the series truncates exactly, but it seems likely that it could produce reasonable choices for $\tilde{\rho}^{\mathbf{r}}$ in many cases.

This leads to the following self-consistent condition for the density given by the SLR equation (3.12):

$$\delta\rho(\mathbf{r}_1)/\delta\tilde{\rho}^{\mathbf{r}_2} = 0,\ \forall \mathbf{r}_1,\mathbf{r}_2, \tag{3.28}$$

expressing the insensitivity of the density with respect to variations in $\tilde{\rho}^{\mathbf{r}}$. Differentiating both sides of the SLR equation (3.12) and collecting the terms given by

$\delta\rho(\mathbf{r}_1)/\delta\tilde{\rho}^{\mathbf{r}_2}$ (for more details of the derivation, see appendix C), the insensitivity criterion in Eq.(3.28) can be written as:

$$\tilde{\rho}^{\mathbf{r}_1} = \frac{\int d\mathbf{r}_2 W(|\mathbf{r}_1 - \mathbf{r}_2|; \tilde{\rho}^{\mathbf{r}_1})\rho(\mathbf{r}_2)}{\int d\mathbf{r}_2 W(|\mathbf{r}_1 - \mathbf{r}_2|; \tilde{\rho}^{\mathbf{r}_1})}. \tag{3.29}$$

where

$$W(|\mathbf{r}_1 - \mathbf{r}_2|; \rho) \equiv \dot{c}^{(1)}(\rho)c^{(2)}(|\mathbf{r}_1 - \mathbf{r}_2|; \rho) + \dot{c}^{(2)}(|\mathbf{r}_1 - \mathbf{r}_2|; \rho) \tag{3.30}$$

and

$$\dot{c}^{(1)}(\rho) \equiv dc^{(1)}(\rho)/d\rho; \quad \dot{c}^{(2)}(|\mathbf{r}_1 - \mathbf{r}_2|; \rho) \equiv dc^{(2)}(|\mathbf{r}_1 - \mathbf{r}_2|; \rho)/d\rho. \tag{3.31}$$

Because the function $W(|\mathbf{r}_1 - \mathbf{r}_2|; \rho)$ in Eq.(3.30) has range of $c^{(2)}(|\mathbf{r}_1 - \mathbf{r}_2|; \rho)$, Eq.(3.29) shows that $\tilde{\rho}^{\mathbf{r}_1}$ can be interpreted as the full density $\rho(\mathbf{r})$ averaged over the range of the fluid's correlation length around the point $\mathbf{r}_1$, using a self-consistent *weighting function* W that itself depends on $\tilde{\rho}^{\mathbf{r}_1}$. We will refer to the resulting $\tilde{\rho}^{\mathbf{r}}$ as the *smoothed reference density* in what follows. Some versions of weighted density functional theory [51, 15] have used similar weighted densities, though the detailed implementation and justification is rather different.

Equation (3.29) derived from the insensitivity criterion (IC) can then be solved with the SLR equation to determine both the full density $\rho(\mathbf{r})$ and the smoothed density $\tilde{\rho}^{\mathbf{r}}$. We refer to these coupled equations as the *IC equations*. The IC equations can be solved numerically by iteration.

3.6.3 Results in Limiting Cases

We first verify that the IC equations can give accurate results in limiting cases where the proper choice of $\tilde{\rho}^{\mathbf{r}}$ is known. In the hydrostatic limit where the external field is very slowly varying, $\rho(\mathbf{r})$ must reduce to the hydrostatic density $\rho^{\mathbf{r}} = \rho(\mu - \phi(\mathbf{r}))$, as given by the HLR equation. In this same limit $\rho(\mathbf{r}_2)$ in the IC equation (3.29) can be approximated by $\rho(\mathbf{r}_1)$ and taken outside the integral. This gives $\tilde{\rho}^{\mathbf{r}} = \rho(\mathbf{r})$ and hence $\tilde{\rho}^{\mathbf{r}} = \rho^{\mathbf{r}}$. The IC equations thus reduce to the HLR equation for slowly varying fields and recover the hydrostatic limit correctly. However, because of the averaging in Eq.(3.29), in other limits the IC choice of $\tilde{\rho}^{\mathbf{r}}$ is less local than the HLR choice $\rho^{\mathbf{r}}$ and tends to smear out the nonuniformity caused by external perturbations in small regions.

For the narrow slit limit discussed above, the $\tilde{\rho}^{\mathbf{r}}$ given by Eq.(3.29) correctly approaches zero as $L \to 0$, since the Boltzmann factor $e^{-\beta\phi(\mathbf{r})}$ ensures that $\rho(\mathbf{r})$ is zero inside the walls. Thus the IC equations are *exact* in the narrow slit limit as $L_s \to 0$ and correct the poor predictions of both the HLR and PY equations.

For tiny fields, the IC choice in Eq.(3.29) strictly reproduces the exact bulk density choice $\tilde{\rho}^{\mathbf{r}} = \rho(\mu - \phi(\infty))$ only in the limit where $V^{\phi} \to 0$, and is not exact for general tiny fields. However $\tilde{\rho}^{\mathbf{r}}$ is generally very close to that of the bulk density because the tiny field volume V^{ϕ} has little weight in the averaging. Thus the IC equations can be expected to agree reasonably well with exact results for general tiny fields, as will be shown in the next section.

3.7 Results

We first consider the density response of a hard sphere fluid at a moderate packing fraction $\eta = 0.3$ to a series of spherical model potentials of varying ranges and different signs. In particular we studied repulsive (attractive) step functions of height $3k_BT$ ($-3k_BT$) and different ranges and "triangular" fields that start with the same height at the origin and vary linearly in r to the cutoff. Hard sphere cavities with the same cutoffs were also studied. Numerical solutions of the IC, HLR, and PY equations are presented, together with results of Monte Carlo simulations for the fluid's density response. The PY bulk direct correlation function $c^{(2)}(r_{12};\rho)$, which is very accurate at these densities, was used in the theoretical calculations. The Carnahan-Starling equation [7] of state was used for computing the density $\tilde{\rho}^{\mathbf{r}} = \rho(\mu - a^{\mathbf{r}})$ of the locally shifted uniform system.

3.7.1 "Tiny" Fields

For tiny fields, all results should be compared to the PY approximation, which is exact for such fields (subject only to the small errors in the PY bulk direct correlation function). As can be seen in Fig.(3.1) and Fig. (3.2), the HLR equation is exact only for tiny *cavities*. For finite tiny fields, its major errors occur in the tiny region where the field is nonvanishing. The density response predicted by the HLR equation often exhibits a negative region where the external field varies most rapidly. The IC approximation, on the other hand, in general agrees with the PY

approximation much better in the tiny field region and in particular eliminates the negative densities given by HLR. However the IC is not exact for tiny fields, and tends to overestimate the contact densities.

3.7.2 Extended Fields

For more extended fields, none of the approximations are exact, so Monte Carlo simulations were carried out to test the various theories. As shown in Fig.(3.3) and Fig.(3.4), as the range of the "step" and the "triangle" potentials becomes wider, the HLR approximation becomes more accurate. However, it still exhibits negative densities in its solution for both repulsive and attractive step potentials, especially for the narrower steps. For the same width of the potentials, the HLR equation does better in predicting the response to the triangle potentials than to the step potentials. This agrees with the expectation that the HLR equation should be more accurate when the external field is more slowly varying.

The PY approximation, on the contrary, becomes less accurate when the field's width increases, as is seen in Fig.(3.3). This is because the PY expansion about the bulk density and extrapolation into the region where the external field is non-vanishing becomes less and less justified when the range of the potential increases. This problem of the PY approximation is much more acute for attractive potential, when its errors are magnified by the large Boltzmann factor (Eq.(3.7)), and the results are so poor that we do not show them in Fig.(3.4). Indeed, the PY approximation for nonuniform fluid is hardly ever applied in practice except for strongly

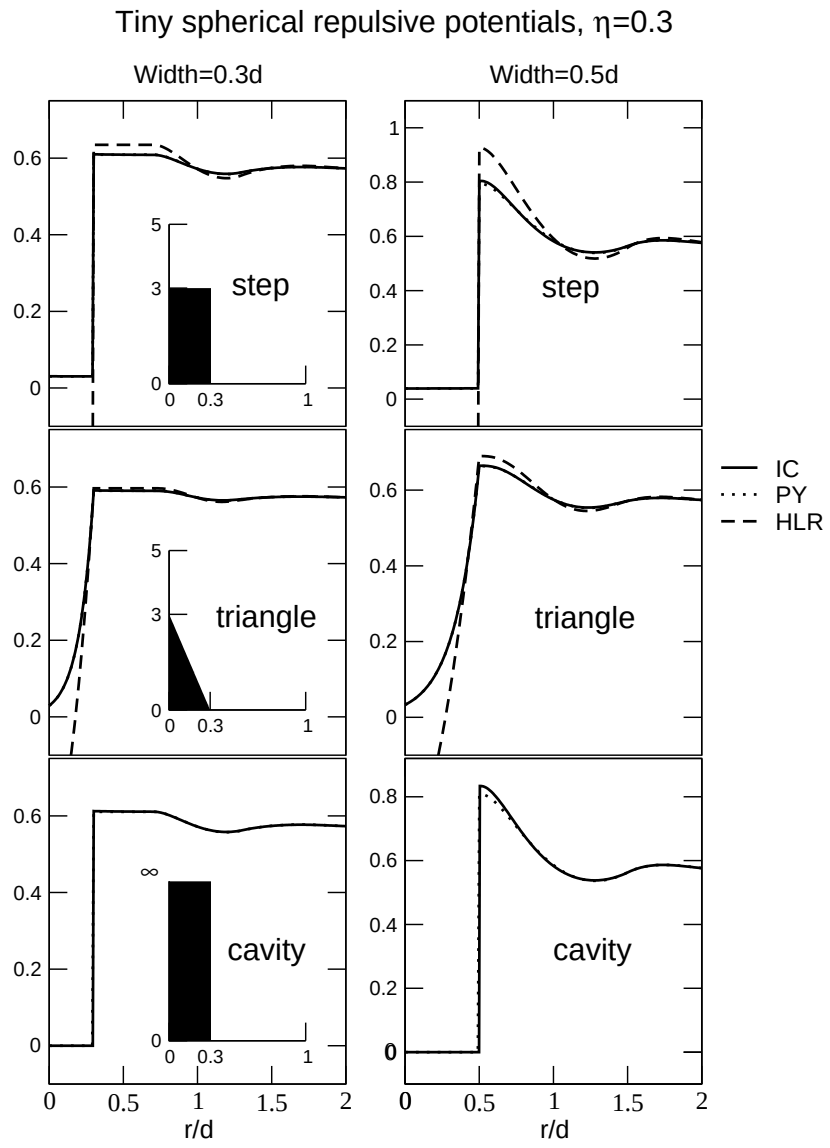
Tiny spherical repulsive potentials, η=0.3
Width=0.3d
Width=0.5d
step
triangle
cavity
IC
PY
HLR
r/d
r/d

Figure 3.1: The density response to tiny repulsive external fields of different widths W is plotted. The curves are the predictions by the IC, PY and HLR approximations. The PY approximation is exact for the density values inside the non-zero field region. All the external fields are spherical. "Step" denotes a spherical step function where $\beta\phi(r) = 3, \forall r < W$ and $\beta\phi(r) = 0,$ otherwise. "Triangle" refers to the potential $\beta\phi(r) = 3 - 3r/W$ that has the same height as the step potentials but decays linearly to zero at $r = W$ with $\beta\phi(r) = 0,$ otherwise. "Cavity" refers to the hard core potential $\beta\phi(r) = \infty, \forall r < W$ and $\beta\phi(r) = 0,$ otherwise. The form of the potentials $\beta\phi(r)$ are illustrated in the insets. For the cavity potentials, the PY and HLR approximations give identical density solutions. The bulk fluid's packing fraction $\eta \equiv \pi\rho^B d^3/6$ is $\eta = 0.3$.

repulsive potentials, where the value $\tilde{\rho}^{\mathbf{r}}$ value is essentially irrelevant.

The IC approximation is able again to correct the negative densities given by HLR and, most notably, to capture the highly nontrivial density profile inside both positive and negative step potentials due to the packing of the hard spheres. However, for spherical cavities, although it is known that the PY (and HLR) approximation consistently predicts a contact density lower than the exact value, the IC noticeably over-corrects the contact densities. This has a deleterious effect on the rest of the profile, especially near the cavity region.

The density response given by the HLR and IC equations for two deep *attractive parabolic bowl potentials* are plotted in Fig.(3.5) for a hard sphere fluid with packing fraction $\eta = 0.25656$. Fig.(3.6) shows the potentials on the left and the reference densities $\rho^{\mathbf{r}}$ and $\tilde{\rho}^{\mathbf{r}}$ for the HLR and IC equations on the right. For the

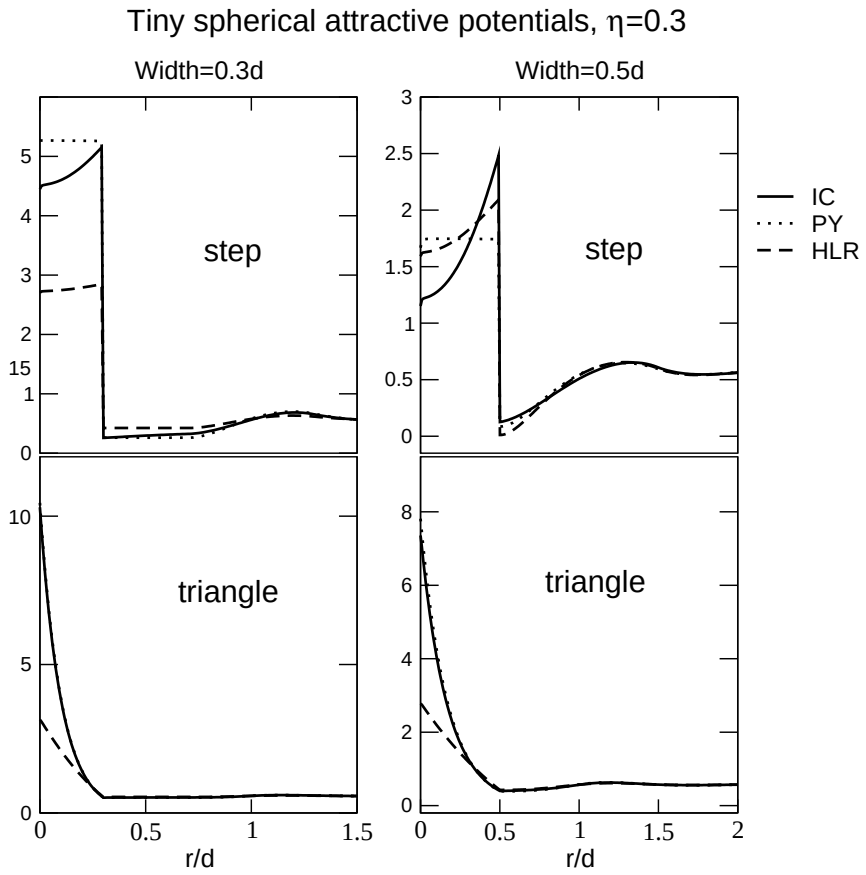

Figure 3.2: The curves plotted here follow the same legend conventions used in Fig.(3.1) and are computed at the same bulk packing fraction $\eta = 0.3$. The external fields calculated here are all tiny spherical attractive potentials. Step and triangle potentials are defined as in Fig.(3.1), except that the sign of the potential is negative.

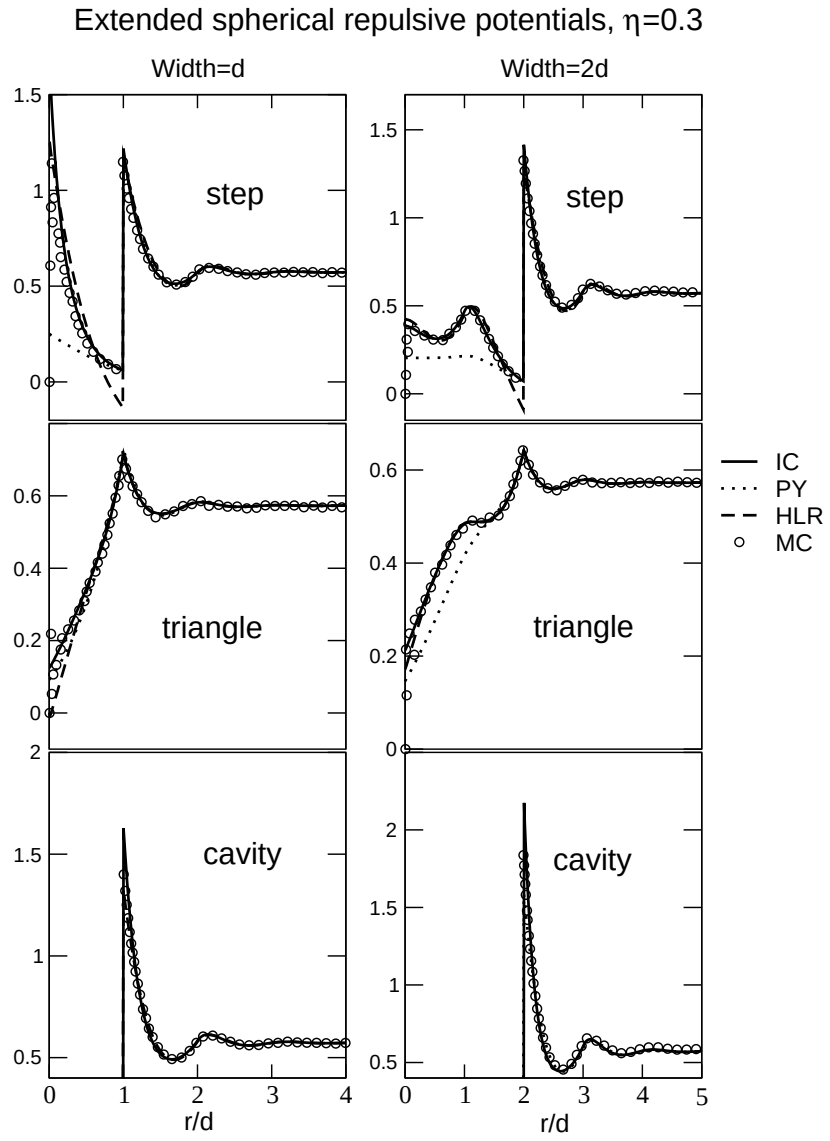

Figure 3.3: Density response to extended spherical repulsive potentials of varying widths. Conventions and bulk packing fraction are those of Fig.(3.1) and Fig.(3.2).

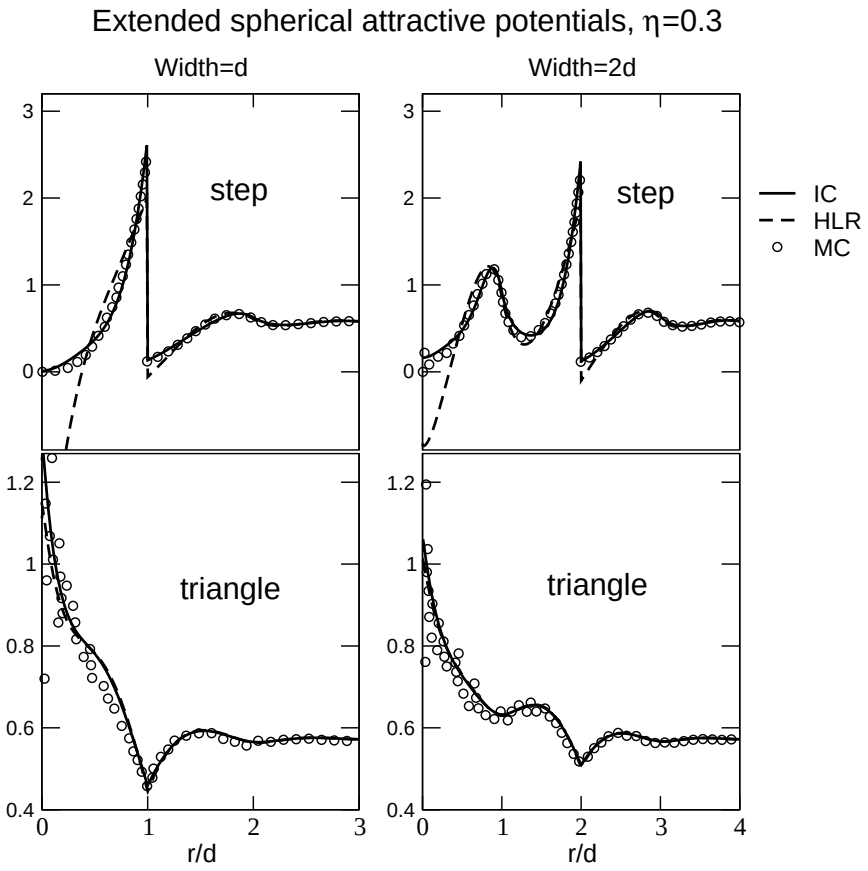

Figure 3.4: Density response to extended spherical attractive potentials of varying widths. Conventions and bulk packing fraction are those of Fig.(3.1) and Fig.(3.2).

shallower bowl potential (see the left graphs of Fig.(3.6)), both the IC and HLR approximations agree well with the Monte Carlo simulations. The reference density $\tilde{\rho}^{\mathbf{r}}$ of the IC approximation is very close to that of the hydrostatic density $\rho^{\mathbf{r}}$, as can be seen in the right graph of Fig.(3.6), except that $\tilde{\rho}^{\mathbf{r}}$ varies smoothly near the edge of the bowl, while the hydrostatic density has a discontinuous derivative.

For the deeper bowl potential, both approximations deviate noticeably from the simulation data, but nonetheless capture the nontrivial oscillatory density profile inside the bowl. In particular, both reproduce the density *minimum* at the center of the bowl, where the external field is actually most attractive, due to nonlocal effects from packing of the hard spheres. However, the HLR density becomes negative at the bottom of the bowl, while the IC density remains positive, though somewhat lower than the MC result. The reference density $\tilde{\rho}^{\mathbf{r}}$ for the IC method for the deeper bowl potential has more oscillations than that of the shallow bowl potential, and exhibits a maximum at the center, which is the key for keeping its predicted full density positive. Once outside the bowl, all approximations agree well with the MC result.

Fig.(3.7) plots the density response solutions to a soft continuous repulsive potential of the form $\beta\phi(r) = A\mathrm{erf}(r/\sigma)/r$. This is a potential that will be very relevant for the ionic systems we study in later chapters. Here all the approximate results agree quite well with the simulations, except that the HLR equation again shows a narrow negative density region for the more rapidly varying potential (left

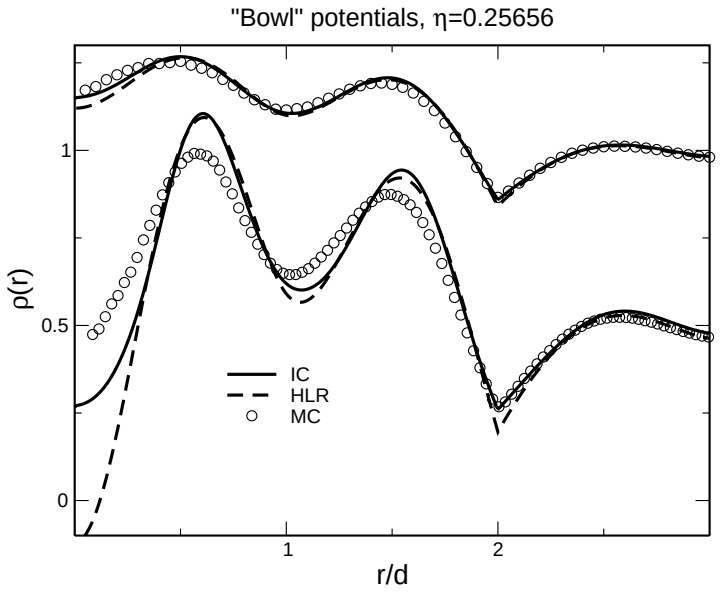

Figure 3.5: Density responses to attractive parabolic bowl potentials. Here $\eta = 0.25656$. The HLR solution and Monte Carlo simulation of the same potentials had also been computed by Katsov and Weeks, see reference [40].

graphs of Fig.(3.7)).

Finally, in Fig.(3.8), the density response to a planar hard wall determined using the IC and HLR approximations is compared to the results of the generalized mean spherical approximation (GMSA) [73]. The GMSA fits the contact density at the wall to the bulk equation of state using an exact sum rule, and is known to be very accurate for such systems. Thus it can be used as a benchmark for the other approximations. As shown in the previous chapter, the HLR approximation agrees very well with the GMSA except for its consistent underestimate of the contact density.

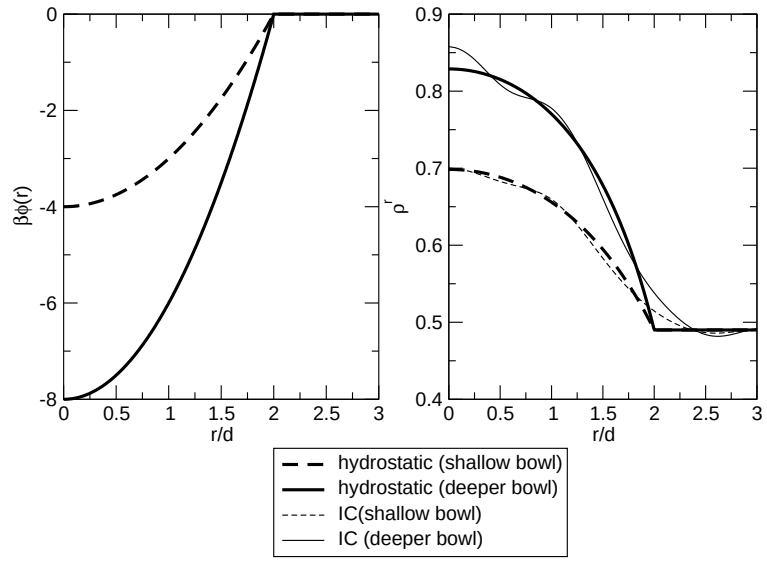

Figure 3.6: The left graph gives the bowl potentials $\beta\phi(r) = A(r^2 - 4)$, with $A = 1$ for the shallow bowl, $A = 2$ for the deeper bowl. The right graph compares the hydrostatic densities $\rho^{\mathbf{r}}$ of the external fields to the $\tilde{\rho}^{\mathbf{r}}$ given by the IC equations.

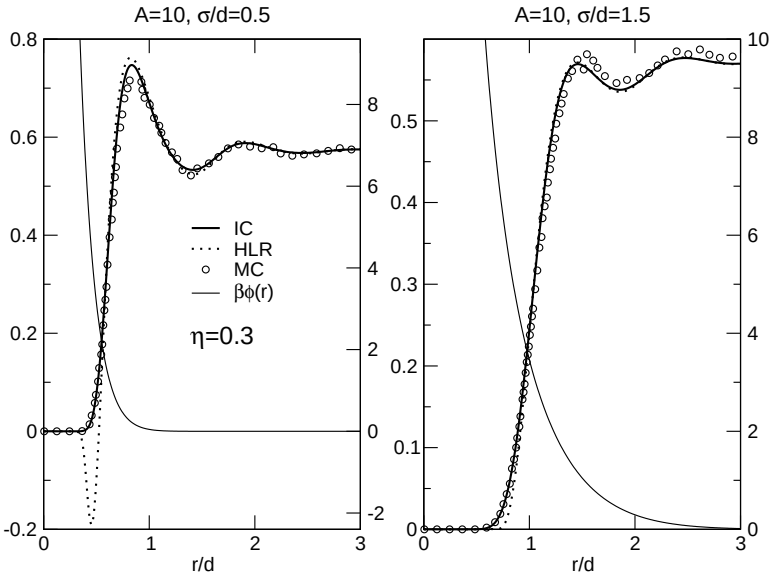

Figure 3.7: he density response to two external fields of the form $A\mathrm{erfc}(r/\sigma)/r$. Note that the right y-axis refers to the density curves while the left y-axis labels $\beta\phi(r)$. Here $\eta = 0.3$.

The IC method is now significantly less satisfactory than it was in the other cases. The main problem arises from a severe overestimate of the contact density, which goes on to spoil the rest of the density profile. The state shown is at a moderate packing fraction $\eta = 0.314$ and the errors get even worse at higher densities. This problem is similar to that seen for the cavity potentials presented before.

The IC method can also be used in an inverse way to determine what $\tilde{\rho}^{\mathbf{r}}$ is needed to obtain a given density $\rho(\mathbf{r})$ as a solution to the SLR equation. We determined the $\tilde{\rho}^{\mathbf{r}}$ associated with the accurate GMSA $\rho(\mathbf{r})$ in this way, and it can be seen that this GMSA $\tilde{\rho}^{\mathbf{r}}$ dips below the bulk density (used in the relatively accurate HLR equation) near the wall. The IC $\tilde{\rho}^{\mathbf{r}}$ shows a similar deviation, but has more oscillations and dips a little too low near the wall, which causes the high contact density it predicts.

This example shows that small changes in $\tilde{\rho}^{\mathbf{r}}$ near the wall can have large effects on the predicted density profile near the wall in the SLR equation. The fact that the HLR choice, clearly appropriate for slowly varying fields, continues to give reasonably good results for single hard walls and hard cavities seems fortuitous, as illustrated by the errors HLR produces for rapidly varying but finite potentials. The IC method, which gives very good results in most other limits, correctly predicts the lowering of $\tilde{\rho}^{\mathbf{r}}$ near the hard wall but overestimates its magnitude.

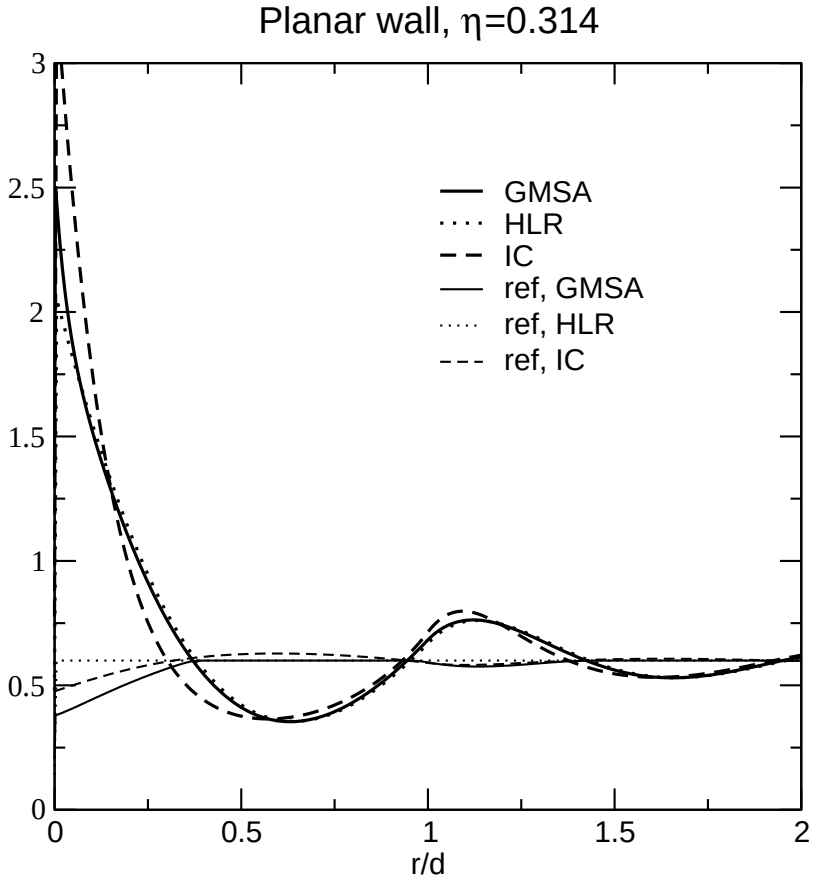

Figure 3.8: Density response to one planar hard wall positioned at $z = 0$. The bulk packing fraction is $\eta = 3.14$. The "ref" curves give the $\tilde{\rho}^z$ used with the different approximations. The $\tilde{\rho}^z$ for the GMSA approximation [73] is obtained by using GMSA's $\rho(z)$ in IC equation and solving inversely for the corresponding $\tilde{\rho}^z$.

3.8 Conclusion

The SLR equation provides a versatile framework for computing the density response of hard sphere fluids to general external fields. By satisfying the exact shifting property of the grand ensemble, it is possible to accommodate exactly two important limits using this framework: slowly varying external fields (hydrostatic limit) and the opposite limit where fields can be very rapidly varying but only perturb the fluid in tiny or narrow regions. Errors in specific predictions arising from the linear truncation in the SLR equation can be minimized by choosing locally at every point in space a different uniform system with density $\tilde{\rho}^{\mathbf{r}}$ to expand about.

In principle there could be different prescriptions for how this could best be achieved in particular applications and for specific properties. In most cases the simple local HLR choice is quite sufficient. However this has problems for rapidly varying but finite fields and the SLR equation, which reduces to the HLR equation for slowly varying fields, offers additional flexibility. A general idea often used in other expansions in liquid state theory is to choose a reference density $\tilde{\rho}^{\mathbf{r}}$ that at least minimizes the next order correction to the SLR equation. However, this is very complicated, and there will still be unknown contributions from the higher order terms.

Here as a first attempt, we have devised an *insensitivity criterion* (IC), based on the idea that the SLR equation should be insensitive to small variations of $\tilde{\rho}^{\mathbf{r}}$. This property would be exactly satisfied if all terms in the expansion were taken

into account, and by imposing it self-consistently on the SLR equation we hope to generate a truncation where the contribution from higher order terms are indeed small. The resulting IC method is very successful in correcting the negative density regions that the HLR often exhibits for rapidly varying finite fields, and although not exact, the IC method also shows considerable improvement over HLR for the tiny field cases. Moreover, the IC method is exact for narrow slits as the slit width $L_s \to 0$, while the HLR and PY approximations have very significant errors in this limit.

However, the IC method tends to overestimate the contact value of the density response to simple hard core cavities of all sizes, and this damages the accuracy of the rest of the density profile. In practice this is not a significant limitation, since these cases are reasonably well treated by the HLR and PY approximations, even though they noticeable underestimate the contact density. Other specific conditions for hard core potentials, such as the sum rule used in the GMSA approximation, could be taken into account to improve the IC method in this limit. But it seems conceptually worthwhile to see if $\tilde{\rho}^{\mathbf{r}}$ can be chosen more generally within the SLR framework so that accurate results naturally arise in this limit as well. To that end we believe it would be profitable to further study the tiny field limit, where similar problems are encountered, to gain additional insights for optimal use of the SLR equation.

Chapter 4

Connecting Systems with Short and Long Ranged Interactions: Local Molecular Field Theory for Ionic Fluids

This chapter is heavily based on a paper "Connecting systems with short and long ranged interactions: local molecular field theory for ionic fluids" by Chen, Y.-G. and Weeks, J. D., submitted to *Journal of Physical Chemistry* (in press).

4.1 Introduction

The local molecular field (LMF) theory had been successfully applied to nonuniform simple fluids [43, 41, 78, 79, 80, 74]. In this chapter, a new theory for the structure and thermodynamics of ionic fluids based on a generalization of the LMF theory is described. A basic step in the LMF theory is the replacement of longer ranged and slowly varying parts of the intermolecular interactions by an appropriately chosen effective single particle potential. The structure and thermodynamics of the resulting reference system with shorter ranged intermolecular interactions in the presence of the effective field is then related to that of the original system of interest.

This strategy seems particularly appropriate for ionic systems since at long

distances the Coulomb interaction is weak and very slowly varying, and systems with short ranged interactions are significantly easier to treat by theory or simulations. However Coulomb interactions can be very strong and rapidly varying at short distances. A key question that is addressed is how to divide the Coulomb interaction into "short" and "long" ranged parts so that the LMF theory can give accurate results. Its answer allows for the first *controlled* use of the LMF approximation, and exceptionally accurate results are found, even better than those found earlier for fluids with short ranged interactions.

Although the most physically interesting applications of these ideas are probably to nonuniform mixtures of size and charge asymmetric ions, in this initial discussion we consider a uniform *one-component charged hard sphere system* (OCCHS) where almost all the ideas in the LMF theory can be seen in their simplest form [24]. The OCCHS is made up of (say positively) charged "ions" comprised of hard spheres with a diameter $d \geq 0$ with centrally embedded positive point charges in the presence of a uniform neutralizing background. The only nontrivial correlations are between the positive ions and for most purposes we can think of this as a one-component system with very long ranged repulsive interactions. A special case is the *one-component plasma* (OCP) where there is no hard core ($d = 0$). Nothing in the theory makes essential use of the simplifications in the OCCHS. Generalizations to nonuniform and asymmetric models are straightforward in most cases, and equally good results have been found.

4.2 Local Molecular Field Equation (LMF)

4.2.1 Nonuniform Systems

Let us discuss the qualitative ideas leading to the LMF equation. These will be further developed and made more precise in our discussion of the OCCHS. The simplest application of LMF theory relates the structure and thermodynamics of a nonuniform system of interest with a spherically symmetric pair potential $w(r)$ in an external field whose value at any point $\mathbf{r}_1$ is $\phi(\mathbf{r}_1)$ to those of a *reference system* with a shorter ranged pair interaction $u_0(r)$ in a renormalized effective field $\phi_R(\mathbf{r}_1)$. ϕ_R is supposed to be chosen to take account of the averaged effects of the *perturbation potential* $u_1(r)$, where

$$w(r) = u_0(r) + u_1(r). \tag{4.1}$$

This separation of the intermolecular interaction w into two parts can be done in an infinite number of ways, and any choice of u_1 defines a possible associated reference system. However the averaging procedure leading to the simple LMF theory can be expected to give very accurate results only for certain properly chosen *slowly varying* u_1.

Fig.(4.1) gives examples of separations of the repulsive Coulomb potential we will use in this chapter, parameterized by an important length scale σ. As explained in detail in Section 4.4, when σ is chosen larger than some state-dependent minimum size $\sigma_{\min}$, the Coulomb perturbation u_1 is sufficiently slowly varying that the LMF theory can give very accurate results. This is the crucial step in developing a simple

and accurate theory for ionic systems.

We will refer to the resulting special reference systems with properly chosen σ as "mimic systems." In realistic models of ionic solutions there are always strong short ranged repulsive core interactions that must be dealt with in any quantitative theory or simulation. The mimic system simply treats the short ranged rapidly varying part of the Coulomb potential as an additional core-like contribution that generates a modified core interaction. As we will see, many properties of the full long ranged system can be very accurately described using those of the short ranged mimic system.

For simple fluids with short ranged interactions the LMF approach has proved most useful when w can be divided into a slowly varying perturbation $u_1(r)$ describing the relatively weak and longer ranged attractive interactions and a short ranged rapidly varying core potential u_0, which accounts for the local excluded volume correlations of the particles [75]. A separation with these qualitative features suffices to motivate the derivation of the basic LMF equation that follows.

For any given $\phi(\mathbf{r})$ an associated $\phi_R(\mathbf{r})$ could always found in principle so that the nonuniform singlet density $\rho_0(\mathbf{r};[\phi_R])$ in the reference system (denoted by the subscript 0) equals that in the full system $\rho(\mathbf{r};[\phi])$. Of course the latter is not known in advance and its determination is one of the main goals of the theory. However, if a $u_1(r)$ can be chosen to be slowly varying over the range of excluded volume correlations induced by the short ranged potential $u_0(r)$, then we can make

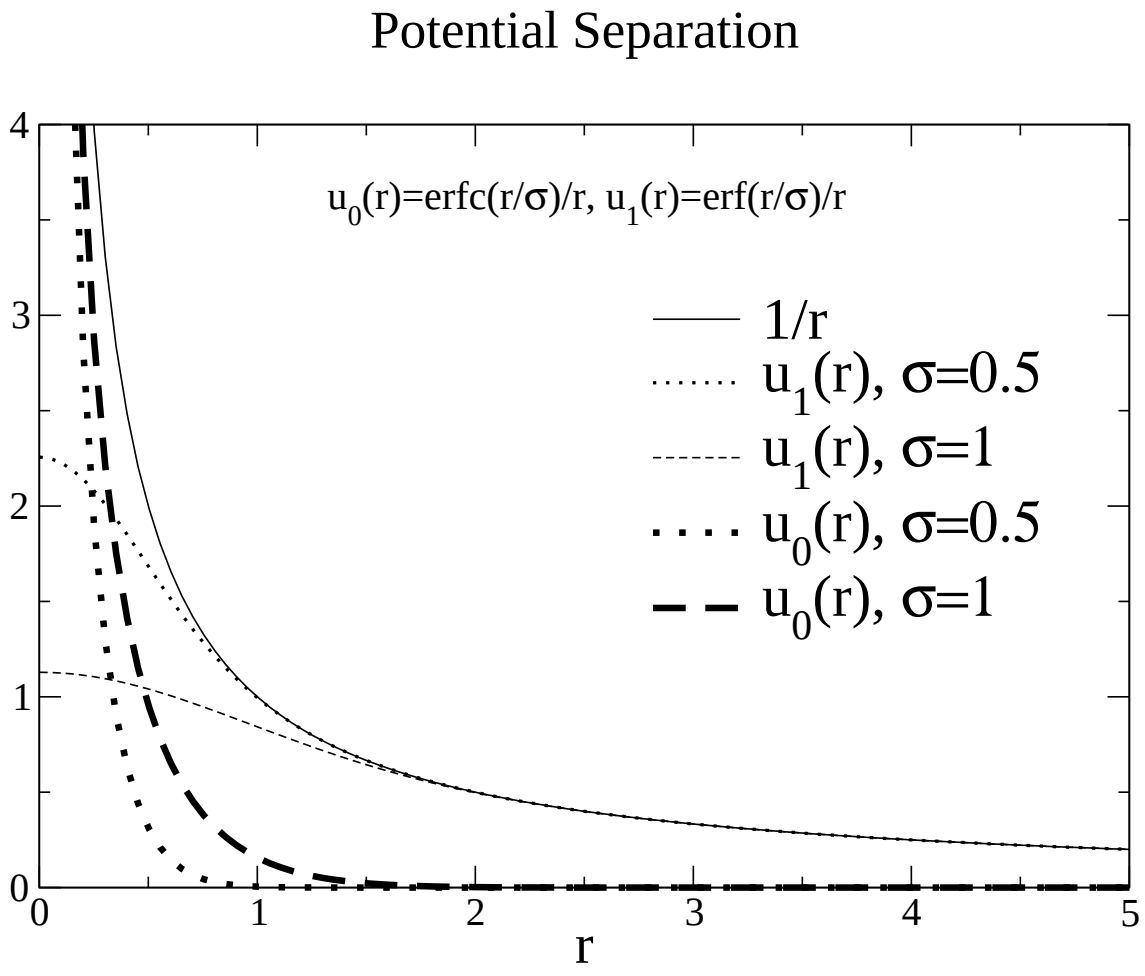

Figure 4.1: The separation of the $1/r$ potential into a short ranged piece $u_0(r) = \text{erfc}(r/\sigma)/r$ and a long ranged piece $u_1(r) = \text{erf}(r/\sigma)/r$. A bigger σ corresponds to a longer ranged mimic system $u_0(r)$, and a more slowly varying $u_1(r)$. Here two relevant σ values are shown for comparison.

some physically motivated approximations to derive a self-consistent equation to determine the associated ϕ_R.

At high densities we expect that short ranged correlations in both systems are controlled by packing effects from the identical repulsive cores, and it seems plausible that ϕ_R can be chosen so that both the singlet densities and the conditional singlet densities in the reference and full systems resemble each other. That is, when

$$\rho_0(\mathbf{r};[\phi_R]) = \rho(\mathbf{r};[\phi]), \tag{4.2}$$

we also expect that

$$\rho_0(\mathbf{r}_1|\mathbf{r}_2;[\phi_R]) \simeq \rho(\mathbf{r}_1|\mathbf{r}_2;[\phi]) \tag{4.3}$$

holds to a good approximation. Here $\rho_0(\mathbf{r}_1|\mathbf{r}_2;[\phi_R])$ is the (conditional) density at $\mathbf{r}_1$ given that a particle is fixed at $\mathbf{r}_2$, directly related to the nonuniform pair correlation function. With this assumption we can derive an equation for ϕ_R that also turns out to give exact results at very low densities, where pair correlations are not important.

As discussed previously [79], by subtracting the balance of forces as described by the exact Yvon-Born-Green hierarchy [24] for the full and reference systems we find a relation between the associated forces

$$-\nabla_1[\phi_R(\mathbf{r}_1) - \phi(\mathbf{r}_1)] = -\int d\mathbf{r}_2 \rho_0(\mathbf{r}_2|\mathbf{r}_1;[\phi_R])\nabla_1 u_1(r_{12}). \tag{4.4}$$

Moreover, if $u_1(r_{12})$ is very slowly varying over the range of short ranged pair correlations, then $\nabla_1 u_1(r_{12})$ essentially vanishes in the range of integration where $\rho_0(\mathbf{r}_2|\mathbf{r}_1;[\phi_R])$ differs significantly from $\rho_0(\mathbf{r}_2;[\phi_R])$ in Eq.(4.4). Then we can replace

the former by the latter, and take the gradient outside the integral and integrate eq 4.4.

In making this replacement we have ignored correlations between the particles at $\mathbf{r}_1$ and $\mathbf{r}_2$, and in most contexts this would represent a crude and generally inaccurate approximation. However for *slowly varying* u_1 we see that this particular use of the (mean field) approximation can be very accurate, even at high density. Choosing the constant of integration so that the bulk densities in zero field satisfy $\rho^B = \rho_0^B$ we arrive at the simple *local molecular field* (LMF) equation [43, 74] for the effective field ϕ_R:

$$\phi_R(\mathbf{r}_1) = \phi(\mathbf{r}_1) + \int d\mathbf{r}_2[\rho_0(\mathbf{r}_2;[\phi_R]) - \rho_0^B]u_1(\mathbf{r}_{12}), \tag{4.5}$$

which is the starting point for our work on nonuniform fluids with both short and long ranged interactions.

To solve this self consistent equation we need to determine the nonuniform density $\rho_0(\mathbf{r}_2;[\phi_R])$ in the presence of the effective field ϕ_R. The LMF approach does not specify or require a particular way to do this. However since the intermolecular interactions and the effective field have shorter ranges in the reference system, both theory and simulations of the nonuniform structure are usually easier to carry out than in the full system. Equation 4.2 then provides the fundamental link between structure in the nonuniform reference and full systems, and from this thermodynamic functions can be determined.

The name "local molecular field" is suggested by the direct analogy to the

spatially varying effective field introduced in the usual mean or molecular field theory for a nonuniform Ising model [5, 77]. However, while the latter theory is usually viewed as a crude approximation, the derivation sketched above suggests that if a proper choice of a slowly-varying u_1 is made, then accurate results should be found from a self-consistent solution of the LMF equation in many cases, provided that an accurate treatment of the density response $\rho_0(\mathbf{r};[\phi_R])$ to a given ϕ_R is used. In this chapter we use the exact Eq.(4.8) below at low densities and results of computer simulations at higher densities, so whatever errors remain arise only from the LMF approximation itself.

4.2.2 Uniform Systems

LMF theory is equally useful for uniform fluids. [72, 80] In particular eq 6.14 is consistent with the physical idea that in a *dense* uniform fluid with $\phi = 0$ the forces associated with the slowly varying u_1 from oppositely situated particles essentially *cancel* in most relevant configurations [83, 75]. Moreover, any residual effects are strongly damped by the small compressibility at high density, so we expect that the radial distribution functions will satisfy

$$g_0(r) \simeq g(r), \tag{4.6}$$

as predicted by Eq.(4.3) and Eq.(6.14) for $\phi = \phi_R = 0$. For example, Eq.(4.6) holds to a rather good approximation at high density in the uniform Lennard-Jones (LJ) fluid provided that the WCA separation [12, 75, 76] with its relatively slowly varying

u_1 is used, showing the consistency of the physical picture.

This perfect cancellation argument can at best give reasonable results only for uniform fluids at high density. However, LMF theory can be applied to a general nonuniform fluid, and by taking such a perspective and using only the basic Eq.(4.2), we can significantly improve on the predictions of Eq.(4.6) for pair correlations in uniform fluids. [72, 80]

Corrections to Eq.(4.6) can be found by considering the particular external field arising from a fluid particle fixed at the origin, $\phi(\mathbf{r}) = w(r)$. The induced density now gives

$$\rho(r;[w]) = \rho^B g(r). \tag{4.7}$$

This exact equation [58] relating the nonuniform singlet density induced by a fixed particle to the radial distribution function $g(r)$ in the uniform fluid plays a key role in the theory below. There are now net unbalanced forces arising from the fixed particle and eq 6.14 predicts a nonzero ϕ_R, which can be used in Eq.(4.2) to give a more accurate approximation for $\rho(r;[w])$ and hence $g(r)$.

For the uniform LJ fluid this approach accurately determines the small corrections to Eq.(4.6) at high density [72, 80]. Moreover at very low densities where Eq.(4.6) would be very inaccurate, Eq.(6.14) gives $\phi_R(\mathbf{r}) = \phi(r) = w(r)$ and we obtain the *exact* low density limit [24] for $g(r) = \exp[-\beta w(r)]$ by using Eq.(4.2) and the exact low density limit of the reference system in the field ϕ_R:

$$\rho_0(\mathbf{r};[\phi_R]) = \rho^B e^{-\beta\phi_R(\mathbf{r})}. \tag{4.8}$$

Here $\beta = (k_B T)^{-1}$.

Similar accurate results for the nonuniform LJ fluid have been found for more general external fields representing hard core solutes of various sizes, for the liquid-vapor interface, and for drying transitions [43, 41]. Thus LMF theory has provided a qualitatively and often quantitatively accurate description of structure, thermodynamics, and phase transitions in fluids with short ranged interactions [74].

4.3 One-Component Charged Hard Spheres (OCCHS)

In this chapter we focus on the uniform OCCHS, where there are N positive ions in a volume V with a uniform neutralizing background that also penetrates the ions. The pair potential $w(r)$ for the ions in the OCCHS is usually written as

$$w(r) = w_d(r) + w_q(r), \tag{4.9}$$

the sum of a hard sphere potential

$$w_d(r) \equiv \begin{cases} \infty, \ r \leq d \\ 0, \ r > d \end{cases} \tag{4.10}$$

and the pair potential $w_q(r)$ arising from point charges of magnitude q, where

$$w_q(r) \equiv \frac{q^2}{\epsilon r}. \tag{4.11}$$

The separation in Eq.(4.9) is a special case of eq 4.1 and more general separations of w will prove useful in the LMF theory developed below. In Eq.(4.11) the solvent is crudely represented by a uniform static dielectric constant ϵ. In the limit $d = 0$, the OCCHS reduces to the OCP.

It is convenient to introduce a characteristic length describing the typical distance between neighboring particles. A standard choice is the *ion sphere radius* a chosen so that

$$\frac{4\pi}{3}\rho^B a^3 = 1 \tag{4.12}$$

The nearest neighbor spacing is about $1.6a$ when the ions are arranged in a simple cubic lattice.

Thermodynamic properties in the OCCHS can then be characterized using two dimensionless parameters, the *ionic strength*

$$\Gamma \equiv \frac{\beta q^2}{\epsilon a}, \tag{4.13}$$

which compares the bare Coulomb interaction energy between two ions separated by the characteristic distance a to $k_B T$, and the *hard sphere packing fraction*

$$\eta \equiv \pi\rho^B d^3/6. \tag{4.14}$$

Note that $d/a = 2\eta^{1/3}$. In the OCP $d = \eta = 0$ and thermodynamic properties depend only on the single dimensionless parameter Γ.

Pair correlations between the ions in the uniform fluid are most conveniently described in terms of the density change induced by fixing a particle at the origin:

$$\Delta\rho(r;[w]) \equiv \rho(r;[w]) - \rho^B = \rho^B h(r), \tag{4.15}$$

where $\rho^B = N/V$ and $h(r) \equiv g(r) - 1$ is the pair correlation function in the uniform fluid.

The unique consequences of the long ranged interaction in the OCCHS are most easily seen by taking the Fourier transform of Eq.(4.15) and defining the dimensionless *structure factor*

$$S(k) \equiv 1 + \Delta\hat{\rho}(k;[w]) = 1 + \rho^B \hat{h}(k), \tag{4.16}$$

where the caret denotes a Fourier transform. As argued generally in the seminal work of Stillinger and Lovett [69] (SL), there should be complete screening at long wavelengths of any induced charge distribution in a conducting ionic fluid. This constrains the behavior at small wavevectors of the charge-charge correlation function. For the OCCHS the only nontrivial correlations are between the positive ions and the results of SL reduce to the requirement that $S(k)$ has the *universal* form

$$S(k) = 0 + k^2/k_D^2 + \mathrm{O}(k^4), \tag{4.17}$$

independent of any details of the short ranged core potential w_d or any other short ranged interactions that might exist. Here k_D is the *Debye wavevector*, defined by

$$k_D^2 \equiv 4\pi\beta q^2 \rho^B/\epsilon = 3\Gamma/a^2. \tag{4.18}$$

The exact vanishing of $S(k)$ at $k = 0$ arises from electrical neutrality (the "zeroth" moment condition) and the fixed coefficient of the quadratic term is an example of the famous SL *second moment condition* [69, 55]. This behavior is distinctly different than that found in any fluid with short ranged interactions, where $S_0(k)$ at $k = 0$ is finite, proportional to the compressibility, and the coefficient of k^2 depends on the details of the intermolecular interactions.

Thermodynamic properties can be found by integration of the correlation functions. In particular, accounting for the background by taking the appropriate limits of the standard result for a two component system [56], the excess internal energy (over the ideal gas) of the uniform OCCHS can be exactly written as

$$\frac{\beta E^{ex}}{N} = \frac{\beta \rho^B}{2} \int d\mathbf{r} \frac{q^2}{\epsilon r} h(r). \tag{4.19}$$

4.4 LMF Theory for OCCHS

4.4.1 Gaussian Charge Distribution

We want to use the general LMF equation to describe the ion correlation functions in the uniform OCCHS. It is clear from the derivation in section 4.2 that a proper separation of the interaction potential $w = u_0 + u_1$ is required for this self-consistent approach to be accurate. At first glance it may seem natural to use the separation on the right side of Eq.(4.9), where u_0 is taken to be the hard core potential w_d and u_1 is the full point charge interaction w_q in Eq.(4.11). However at short distances outside the hard core the Coulomb potential can be strong and rapidly varying and such interactions cannot be accurately treated by the averaging used in Eq.(6.14).

Indeed in the OCP with no hard core there are arbitrarily large and rapidly varying interactions as $r \to 0$. This limit makes it clear that we should try to separate the point charge Coulomb pair interaction $w_q(r)$ itself into a slowly varying part $w_{q1}(r)$, which we will take as a particularly appropriate $u_1(r)$ to use in the LMF theory, and then combine the remainder $w_{q0}(r) \equiv w_q(r) - u_1(r)$ with $w_d(r)$ (and

more generally with any other short ranged core interactions that exist) to give the associated $u_0(r)$.

This strategy differs from that used in many density functional and integral equation methods, where one first chooses a mathematically convenient or especially simple *reference potential* $\tilde{u}_0(r)$ and then treats the remainder $w(r) - \tilde{u}_0(r)$ as a perturbation, taking advantage of the particular form of the reference system in whatever approximate theories are used. However, for Coulomb systems at least, the existing theories often have large and uncontrolled errors with the usual choices of $\tilde{u}_0$. We believe our approach of choosing a slowly varying u_1 for use in the LMF theory offers many conceptual and computational advantages, and it connects directly to similar physically motivated work on fluids with short ranged interactions.

To that end we interpret the $1/r$ term in w_q as the electrostatic potential of a unit point charge in vacuum. The same slowly varying asymptotic behavior would come from any other normalized charge distribution and the "smearing" of the point charge would produce a less rapidly varying potential at small r. This suggests using a properly chosen charge distribution to determine $w_{q1}(r)$ or $u_1(r)$.

Consider in particular as in the Ewald sum method [24, 16] a normalized unit *Gaussian charge distribution*

$$P_\sigma(r) = \pi^{-3/2}\sigma^{-3}\exp[-(r/\sigma)^2], \tag{4.20}$$

where σ indicates the length scale of the smearing. The particular advantages of this choice will soon become apparent. Our use of a Gaussian charge distribution

to determine a slowly varying part of the Coulomb pair interaction is simpler than in the Ewald sum method, which considers periodic images of ion configurations with embedded screening (negative) and compensating (positive) Gaussian charge distributions. [16]

The electrostatic potential $v_\sigma(r)$ arising from Eq.(4.20) satisfies Poisson's equation $\nabla^2 v_\sigma(r) = -4\pi P_\sigma(r)$, which is easily solved by Fourier transform to give

$$\hat{v}_\sigma(k) = \frac{4\pi}{k^2} \exp[-\tfrac{1}{4}(k\sigma)^2], \tag{4.21}$$

or in r-space,

$$v_\sigma(r) = \frac{1}{r} \operatorname{erf}(r/\sigma), \tag{4.22}$$

where erf is the usual error function [16]. The point charge model corresponds to the limit $\sigma = 0$.

Thus we can write

$$\frac{1}{r} = \frac{1}{r}\operatorname{erfc}(r/\sigma) + \frac{1}{r} \operatorname{erf}(r/\sigma), \tag{4.23}$$

and use this identity to extract from the dimensionless Coulomb pair interaction $\beta w_q(r)$ a σ-dependent perturbation piece $\beta u_1(r)$:

$$\beta u_1(r) = \frac{\beta q^2}{\epsilon} v_\sigma(r) = \frac{\beta q^2}{\epsilon r} \operatorname{erf}(r/\sigma). \tag{4.24}$$

This perturbation remains finite as $r \to 0$, with $\beta u_1(0) = 2\pi^{-1/2}\beta q^2/(\epsilon\sigma)$.

As illustrated in Fig.(4.1), with appropriate choices of σ we can produce a very slowly varying $u_1(r)$, which from Eq.(4.21) also decays very rapidly in k-space.

As argued in section 4.2, these are the qualitative features that would be most appropriate for a perturbation u_1 to give accurate results from LMF theory. The choice of σ in the Gaussian charge distribution permits a *controlled use* of the LMF approximation, and as shown below, with proper choices of σ the LMF theory can give exceptionally accurate results.

Any particular choice of σ in Eq.(4.24) then fixes the associated reference system interaction as [1]

$$\beta u_0(r) = \beta u_d(r) + \frac{\beta q^2}{\epsilon r}\mathrm{erfc}(r/\sigma). \tag{4.25}$$

The Coulomb part $w_{q0}(r)$ of the reference interaction decays very rapidly for $r > \sigma$. For large r we have

$$\beta w_{q0}(r) \equiv \frac{\beta q^2}{\epsilon r}\mathrm{erfc}(r/\sigma) \sim \frac{\beta\sigma q^2}{\sqrt{\pi}\epsilon r^2}\exp[-(r/\sigma)^2]. \tag{4.26}$$

We call the special reference systems that result from optimal choices of σ as discussed in section 4.4.4 below *mimic systems*, since at high density the local structure in the uniform mimic system as exhibited in $g_0(r)$ very accurately approximates the $g(r)$ of the full system as in Eq.(4.6). This again illustrates the consistency and accuracy of the LMF approach when an appropriate mimic system is used.

Equation 4.24 can also be interpreted physically as the Coulomb energy arising from two ions each with a rigid Gaussian charge distribution, Eq.(4.20), with a

[1] This choice of a reference system for the OCP was first suggested in reference [10] However they considered too small σ to observe mimic system behavior and used integral equation methods rather than the LMF theory to try to correct for the long ranged interactions.

width $\tilde{\sigma} = \sigma/\sqrt{2}$. More generally, in ionic solutions we can always replace point charges on the ions by rigid charge distributions without changing any physics if we appropriately modify the core interactions as in Eq.(4.25). This can be very useful because the rapidly varying short ranged parts of the Coulomb interaction can often be more accurately treated by the same specialized methods used for the other strong core interactions, which must be present in any realistic model of ionic solutions.

4.4.2 Scaled LMF Equation for the OCCHS

We now apply the general LMF Eq.(6.14) to the OCCHS in the special case where the external field $\phi(\mathbf{r}) = w(r)$ is that resulting from an ion fixed at the origin, given by Eq.(4.9). This choice allows us to describe uniform fluids, as discussed in Section 4.2.2. We take advantage of spherical symmetry and use the Gaussian charge separation of $w(r)$ given in Eq.(4.24) and Eq.(4.25).

The LMF Eq.(6.14) can be naturally rewritten in terms of the more slowly varying "perturbation part" of the effective field

$$\phi_{R1}(r) \equiv \phi_R(r) - u_0(r). \tag{4.27}$$

If the perfect cancellation argument were exact, then $\phi_R(r) = u_0(r)$, or $\phi_{R1}(r) = 0$, corresponding to a fixed mimic particle at the origin, and the resulting induced density in the mimic system would be $\Delta\rho_0(r;[u_0]) = \rho^B h_0(r)$, with $h_0(r)$ the pair correlation function in the uniform mimic system. The LMF equation corrects

this approximation by determining a finite short ranged effective field perturbation $\phi_{R1}(r)$, which we can picture as arising from a modified solute particle at the origin, [72, 80] that takes better account of the locally averaged effects of the slowly varying interactions u_1.

Taking Fourier transforms, and introducing for reasons that will soon become apparent a multiplicative parameter α that scales the amplitude of $\hat{\phi}_{R1}$, a scaled version of the LMF equation can be written as

$$\beta\rho^B\hat{\phi}_{R1}(k) = \frac{\alpha k_D^2}{k^2}\exp[-\tfrac{1}{4}(k\sigma)^2]S_R(k), \tag{4.28}$$

where

$$S_R(k) \equiv 1 + \Delta\hat{\rho}_0(k;[\phi_R]) \tag{4.29}$$

For now we simply note that the original unscaled LMF equation has $\alpha = 1$, and view α as a parameter at our disposal. A similar scaling of the LMF equation for systems with short ranged interactions was discussed earlier [43].

Before giving quantitative results in sections 4.5 and 4.6 below, let us discuss some qualitative features of a self-consistent solution of Eq.(4.28). Such a solution would determine a short ranged effective field, implying a $\hat{\phi}_{R1}(k)$ that is finite as $k \to 0$, along with the associated $\Delta\hat{\rho}_0(k;[\phi_R])$. By the fundamental assumption of LMF theory in Eq.(4.2), the latter is the LMF approximation to the full $\Delta\hat{\rho}(k;[w])$ in the OCCHS. In particular $S_R(k)$ in Eq.(4.29) is the LMF approximation to $S(k)$ in Eq.(4.16), and when no confusion will result, we will simply write $S(k)$. $S_R(k)$ should be carefully distinguished from $S_0(k) \equiv 1 + \Delta\hat{\rho}_0(k;[u_0])$, which equals the

structure factor in the *uniform* mimic system with $\phi_{R1} = 0$.

4.4.3 Choice of LMF Scaling Parameter α

In order that $\hat{\phi}_{R1}(k)$ remain finite as $k \to 0$ in Eq.(4.28), it is clear that with any choice of α, the associated $S_R(0)$ must vanish identically. In practice it is not easy to ensure this in a self consistent iterative solution of Eq.(4.28), and we give in the Appendix in Eq.(D.3) an alternate but equivalent version that is numerically more stable.) Thus the LMF theory gives an approximate structure factor $S_R(k)$ that always obeys the exact neutrality condition. Its expansion at small k has the general form

$$S_R(k) = 0 + B(\alpha)k^2 + \mathrm{O}(k^4), \tag{4.30}$$

resembling Eq.(4.17), but the coefficient $B(\alpha)$ of k^2 depends on α and does not necessarily obey the exact second moment condition. However, by substituting Eq.(4.30) into Eq.(4.28), we see that the exact result $B(\alpha) = k_D^{-2}$ is found if α is chosen self consistently so that [2]

$$\beta\rho^B\hat{\phi}_{R1}(0) = \alpha. \tag{4.31}$$

Thus by proper choice of α, we can guarantee that the approximate structure factor $S_R(k)$ also obeys the exact second moment condition. We show below in section 4.5 that with optimal choices of the key parameter σ, even the unscaled LMF

[2]This criterion can equivalently be reexpressed in terms of the normalization of the electrostatic potential [55].

theory with $\alpha = 1$ often gives very good numerical results. However it is conceptually important to realize that the LMF approach can be naturally generalized as in Eq.(4.28) so that the exact second moment condition is satisfied, and this adds essentially no numerical costs to the self consistent solution. We use Eq.(4.28) along with Eq.(4.31) in most of the work reported below, and usually refer to this generalized approach as the LMF theory. If we want to emphasize that the second moment condition is satisfied, we will refer to the LMF2 theory, and distinguish this from the original unscaled version, which we will call the LMF0 theory.

4.4.4 Choice of Mimic Interaction Core Size σ

The ability to choose a σ larger than some $\sigma_{\min}$ allows for a consistent application of LMF theory to ionic fluids, ensuring that the LMF approximation is used only for slowly varying parts of the Coulomb interactions. The choice of $\sigma_{\min}$ determines an effective Coulomb core size from the core component $w_{q0}(r)$ of the Coulomb interaction. This may be larger or smaller than the "physical" core size d, which can be varied independently in the OCCHS.

For strong coupling with $\Gamma \gg 1$, we expect considerable cancellation of the very strong forces from ions at distances larger than the nearest neighbor spacing a. Thus the effective core size $\sigma_{\min}/a$ should be of order unity and essentially independent of Γ at large Γ.

However, for weak couplings with $\Gamma \ll 1$ we would expect that any choice of $\sigma \gtrsim \sigma_{\min}$ with $\sigma_{\min} \simeq \Gamma a$ will be sufficient for the LMF equation to give good

results. This (conservative) choice of $\sigma_{\min}$ corresponds to the Bjerrum length [24]. Only on length scales $\sigma_{\min}$ much less that the average neighbor separation a will even the bare Coulomb interactions between ions exceed k_BT, which would characterize an effective Coulomb core size. A more detailed argument [3] suggests that we can take even smaller σ, including $\sigma = 0$, for $\Gamma \ll 1$ and still get accurate results from the LMF theory. We will see below that these qualitative considerations hold true generally.

In particular, by choosing σ large enough we can guarantee that $\beta\rho^B\hat{\phi}_{R1}(k)$ is nonzero only at small wavevectors, since the Gaussian factor in Eq.(4.28) causes rapid decay for $k\sigma \gtrsim 2$. The Gaussian charge distribution produces this very efficient localization of $\beta\rho^B\hat{\phi}_{R1}(k)$ to small wavevectors, and is much superior in this regard to most other smooth distributions.

This property is very important at high density and strong coupling where $S_R(k)$ can have significant structure at $ka \simeq 2\pi$, where a roughly measures the typical distance between nearest neighbor particles. At those larger wavevectors that characterize short ranged structure in r-space, $\beta\rho^B\hat{\phi}_{R1}(k)$ essentially vanishes

[3] Using the Debye-Hückel approximation for the OCP $S_R^{DH}(k) = k^2/(k^2 + k_D^2)$ and Eq.(4.18) in Eq.(4.28) (consistent with $\alpha = 1$) we have $\beta\rho^B\hat{\phi}^D_{R1}(k) = 3\Gamma e^{-\frac{1}{4}(k\sigma)^2}/[(ka)^2 + 3\Gamma]$. The exact $S_R(k)$ has the same form at small k (in accord with the SL moment conditions) and generally very different behavior at wavevectors larger than $k_a \equiv 1/a$ that characterize local structure in r-space. In order to achieve mimic system behavior with $S_R(k) \simeq S_0(k)$ at larger wavevectors we require $\beta\rho^B\hat{\phi}_{R1}(k) \ll 1$ for all such wavevectors. Since $S_R(k)$ is generally of order unity, it should suffice to choose σ so that $\beta\rho^B\hat{\phi}^D_{R1}(k_a) = 3\Gamma e^{-\frac{1}{4}(\sigma/a)^2}/[1 + 3\Gamma] \ll 1$. For large Γ we require σ of order a, but for small $\Gamma \ll 1$ even $\sigma = 0$ will still satisfy this rough criterion.

for any choice of $\sigma \geq \sigma_{\min} \simeq a$. Thus for such wavevectors we have $S_R(k) \simeq S_0(k)$ from a crude linear response argument. Differences in these functions should show up only at small k, where $S_R(k)$ will satisfy the SL moment conditions while $S_0(k)$ remains finite as $k \to 0$. However at high densities the compressibility in the mimic system is small, so that the absolute differences between $S_R(k)$ and $S_0(k)$ remain small even at small wavevectors, as will be illustrated in Fig.(4.9) below.

On taking inverse transforms we then expect that $h_0(r) \simeq h(r)$ holds true to a very good approximation at high densities, as was qualitatively suggested by the cancellation argument leading to eq 4.6. Thus we predict a *family* of uniform mimic systems for different $\sigma \geq \sigma_{\min}$, all of which should give essentially the same short ranged structure at high density that closely approximates that of the full ionic system. This is a dramatic example showing that the inverse problem of uniquely determining the intermolecular potential from $h_0(r)$ can be ill-conditioned.

A "molecular-sized" choice of $\sigma \simeq \sigma_{\min}$ for the mimic system is considerably smaller than the typical choices made in Ewald sum methods, where σ is usually taken to be proportional to the simulation system size [16]. Larger σ values will give equally good results, provided that the resulting mimic system is described accurately. However generally there is little to gain from such choices, since the LMF theory is already consistent for $\sigma \simeq \sigma_{\min}$, and it may be more difficult to treat the longer ranged interactions in mimic systems with larger σ. Thus optimal choices for σ are generally near $\sigma_{\min}$.

At lower densities and weak coupling there is little structure in $S_R(k)$ and $S_0(k)$ at larger wavevectors, and we can choose a much smaller $\sigma_{\min}$ as argued above and still make consistent use of the LMF approximation. Very accurate results for $S_R(k)$ are again found from a self-consistent solution of Eq.(4.28), but the long wavelength perturbations from $\beta\rho^B\hat{\phi}_{R1}(k)$ are not damped by low compressibility in the mimic system, and $h_0(r)$ can differ noticeably from $h(r)$. As $\Gamma \to 0$, our theory reduces correctly to the exact Debye-Hückel (DH) limit [24].

4.5 Results at Low Density: Mimic Poisson-Boltzmann (MPB) Approximation

At low enough bulk densities, the mimic system's response to $\phi_R(r)$ can be described using the simple ideal gas Boltzmann factor as in Eq.(4.8), so that

$$\Delta\rho_0(\mathbf{r};[\phi_R]) = \rho^B[e^{-\beta\phi_R(\mathbf{r})} - 1]. \tag{4.32}$$

This also represents the LMF prediction for the full system's $\rho^B h(r)$, and requires only that second and higher order virial corrections to the *mimic system's* pair correlation function can be ignored. When Eq.(4.32) is substituted in the LMF equation 4.28, a closed equation for $\phi_R(\mathbf{r})$ results. A self consistent solution is readily found by iteration, using the equivalent but numerically more stable version of the LMF equation in Eq.(D.3).

Equation 4.32 is the same structural approximation that is used in the Poisson-Boltzmann (PB) theory [24]. Indeed if we set $\alpha = 1$ and $\sigma = 0$ in the LMF equation

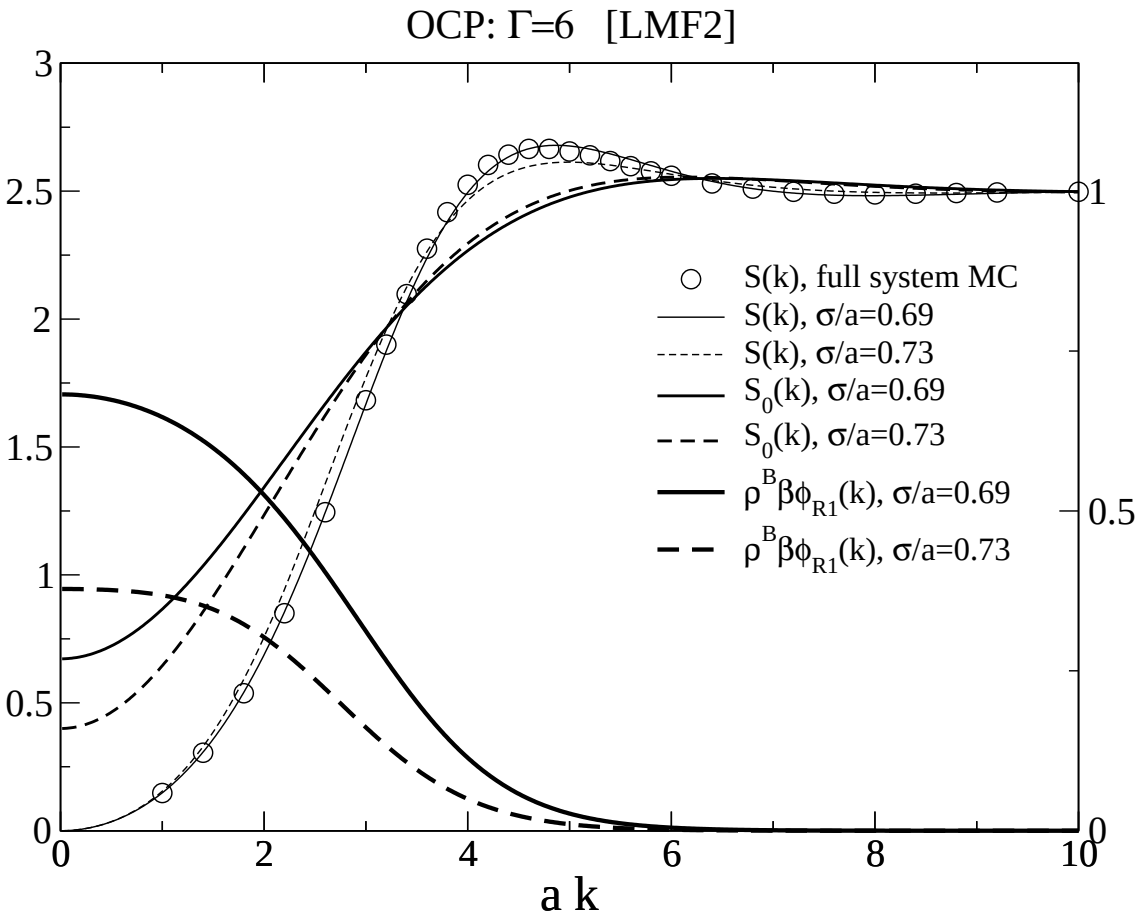

Figure 4.2: $S_R(k) = S(k)$ at moderate coupling for the OCP computed using the MPB theory with different σ's and compared to $S_0(k)$ for the uniform mimic system. Also shown are the associated $\rho\beta\hat{\phi}_{R1}$, which use the scale on the left y-axis. When $\rho\beta\hat{\phi}_{R1}$ is taken into account using the MPB theory, both choices of σ give very similar $S(k)$ that compare well with simulation data for the full system [17].

4.28 combined with Eq.(4.32), the results reduce *exactly* to those of the standard PB theory. The PB theory thus results from taking the full Coulomb interaction of Eq.(4.11) as the perturbation u_1 in the LMF equation and using the Boltzmann approximation for the density response.

We refer to the low density limit of our theory, where Eq.(4.32) is used in Eq.(4.28), as the *mimic Poisson-Boltzmann* (MPB) theory. The MPB theory differs from the PB theory only by the choice of σ yielding a consistent mimic system along with a choice of α that ensures that the second moment condition is exactly satisfied. As we will see, these simple modifications greatly improve the accuracy and range of validity of the MPB theory.

4.5.1 MPB Theory for One-Component Plasma (OCP)

Consider first the OCP, where there is no length scale in the potential to suggest an intrinsic core size. A qualitative discussion of the choice of the effective size $\sigma_{\min}$ was given above. In practice it is easy to determine $\sigma_{\min}$ by solving Eq.(4.28) using successively larger values of σ. For $\sigma < \sigma_{\min}$ the results vary strongly with σ and are generally very inaccurate. But for all $\sigma > \sigma_{\min}$ the LMF theory is consistent and should give very similar predictions for the full system's structure as exhibited in $S_R(k)$, even though the effective fields $\beta\rho^B\hat{\phi}_{R1}(k)$ and the uniform mimic systems' structure factors $S_0(k)$ can still vary strongly with σ. This is illustrated in Fig.(4.2) for the state with $\Gamma = 6$, where the convergence of the results for $\sigma/a = 0.69$ and $\sigma/a = 0.73$ is shown.

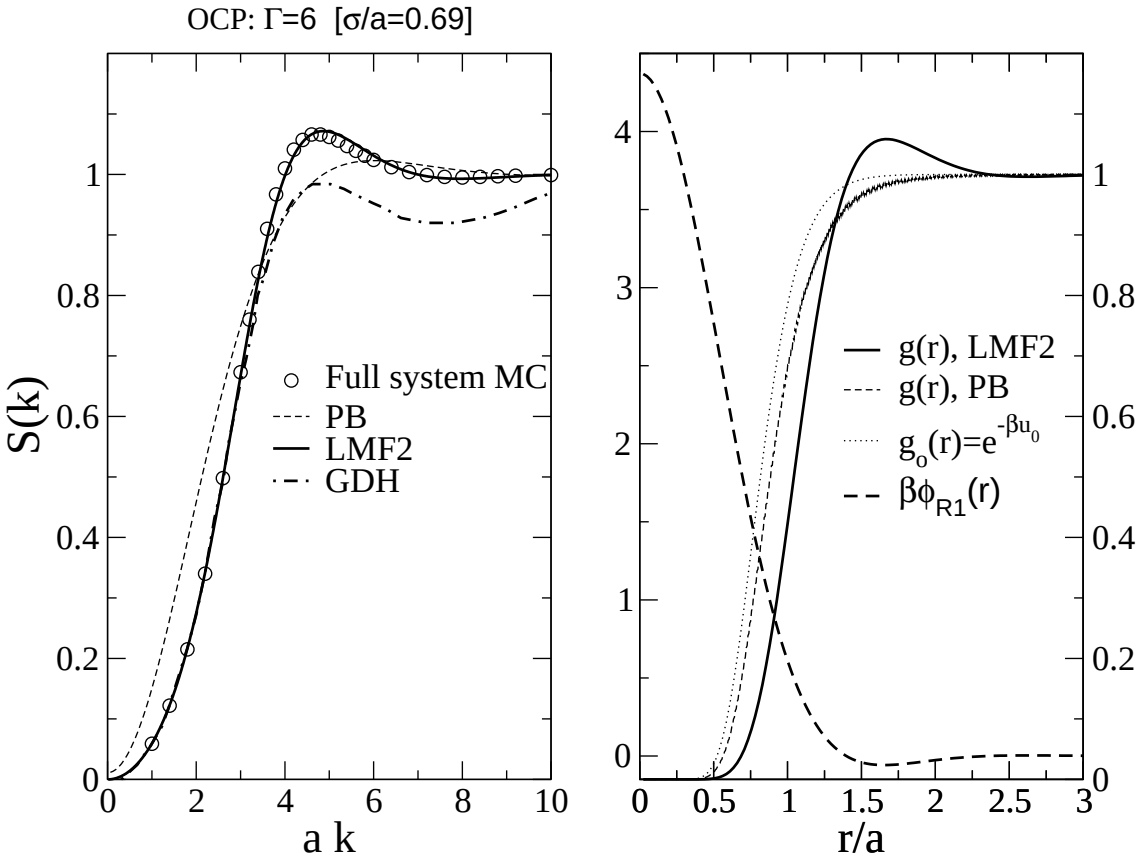

Figure 4.3: Moderate coupling OCP structure computed using the MPB theory. In the left graph, the LMF2 $S(k)$ is compared with the result of the generalized Debye-Hückel theory [70] (GDH), and the usual PB theory. The right graph makes the same comparison for $g(r)$ and also shows the effective field perturbation $\beta\phi_{R1}(r)$, which uses the scale on the left y-axis. Both the LMF2 and GDH solutions satisfy the second moment condition while PB does not. The GDH result is expressed as an expansion and computed up to its $l = 6$ term [70].

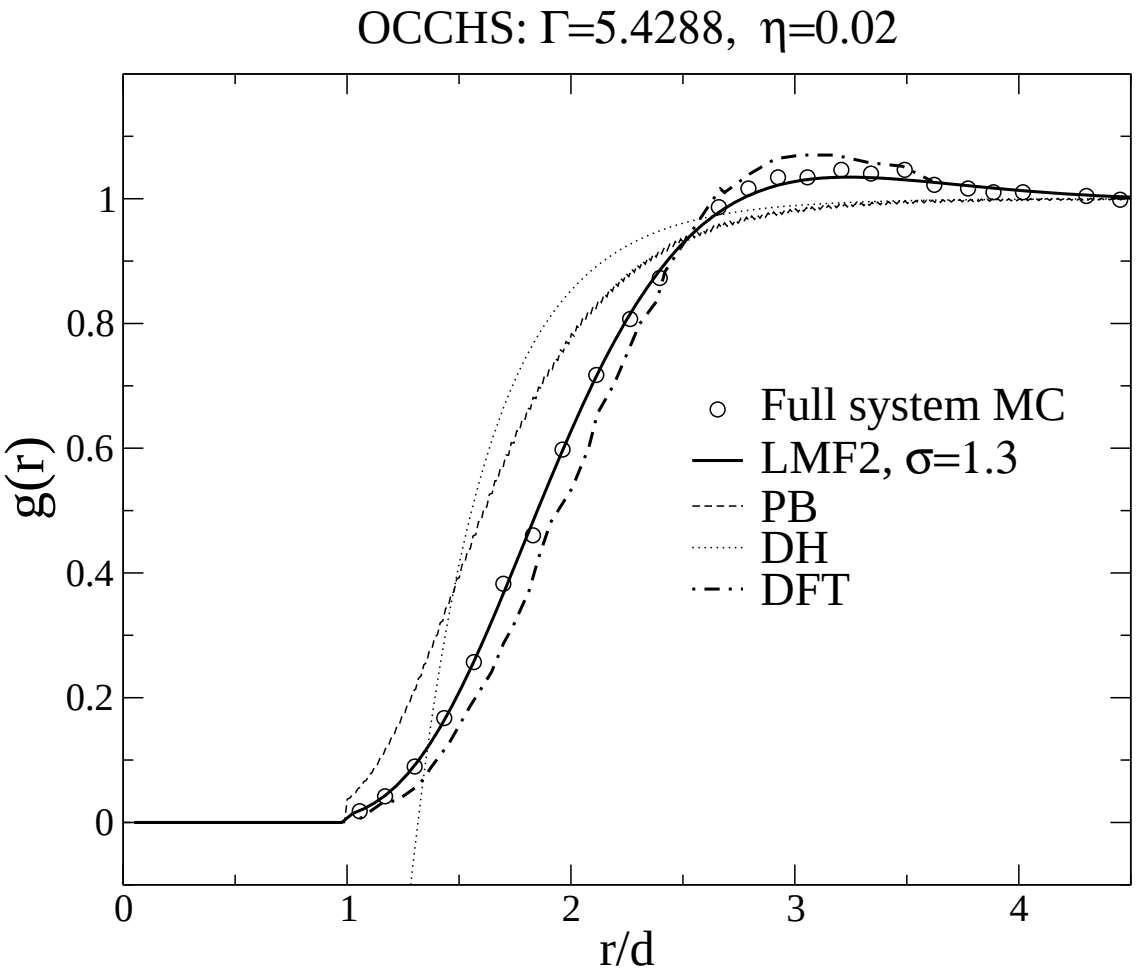

Figure 4.4: Low density OCCHS structure. The LMF2 $g(r)$ from the MPB theory is compared with the result of density functional theory [57] (DFT) and the PB and DH approximations. Though constrained to be zero inside the hard core by a boundary condition, the DH $g(r)$ has a negative region near $r = d$, where $u_0(r)$ is also rapidly rising, with a value of -1.62 at contact. The PB and DH theories fail to capture qualitatively the onset of oscillation in $g(r)$ at this moderate coupling strength.

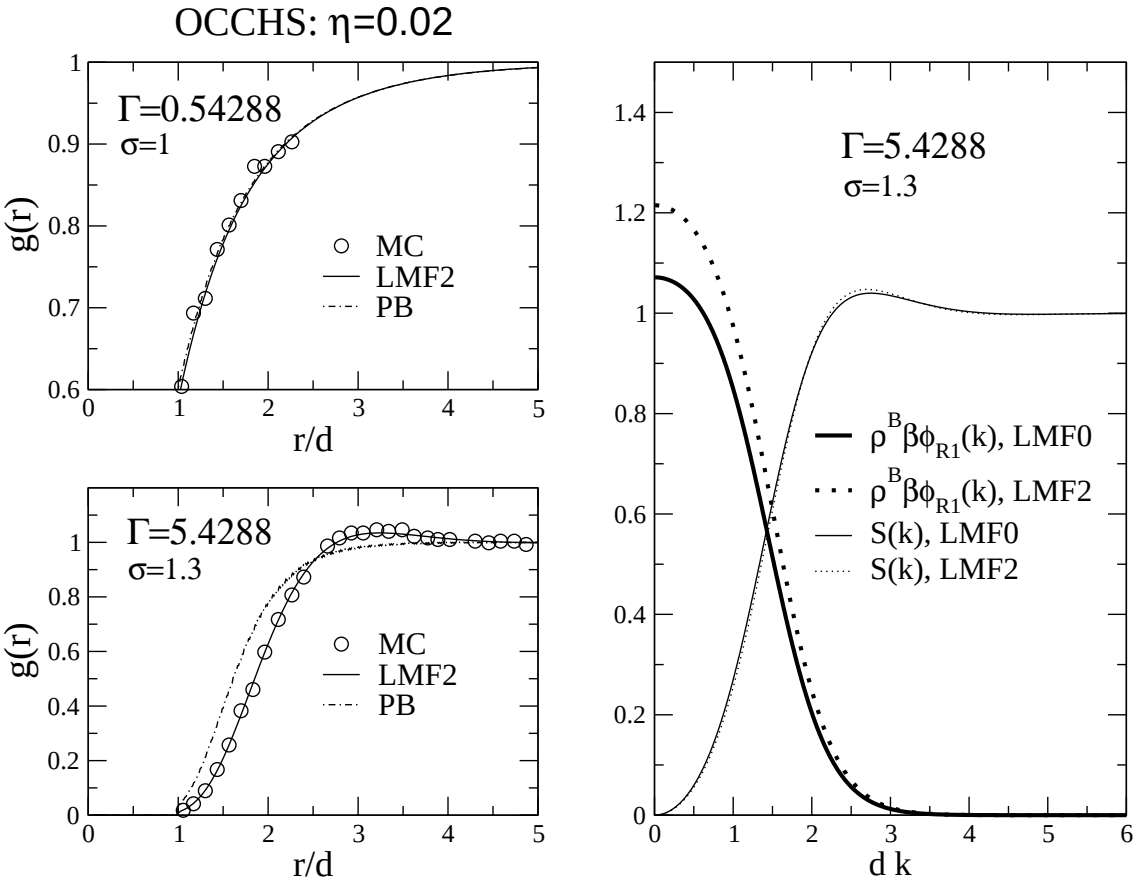

Figure 4.5: The upper and lower left graphs show the MPB and PB approximations for the OCCHS $g(r)$ compared to MC data [57] for the full system for weak and moderate ionic strengths. The PB approximation is satisfactory only at weak couplings. The right graph shows that varying α so that the second moment condition is satisfied in the MPB theory changes the amplitude of $\beta\rho\hat{\phi}_{R1}(0)$ but in this case the effects on $S(k)$ are hardly visible on the scale of the graph.

The LMF equation itself would continue to give (even more) accurate results for larger σ if an accurate theory for the structure $\Delta\rho_0(\mathbf{r};[\phi_R])$ induced by a given ϕ_R is used. However the simple Boltzmann approximation used in Eq.(4.32) for this quantity must fail at higher densities where there are significant correlations between mimic system particles. This sets a $\sigma_{\max}$ above which the results of the MPB theory become inaccurate, very roughly estimated by $\rho^B\sigma^3_{\max} \lesssim 0.1$ as for hard sphere fluids.

As Γ increases, eventually the $\sigma_{\min}$ needed for the accuracy of the LMF approximation exceeds this $\sigma_{\max}$ and the MPB theory fails. The internal consistency or inconsistency as σ is varied is very evident from the MPB theory itself. In practice we find very good and consistent results for all $\Gamma \lesssim 6$ and the slight differences in the $S(k)$ curves in Fig.(4.2) and deteriorating results at larger σ indicate that we are near the upper limit of Γ where the MPB theory can be trusted. This represents a surprisingly strong coupling, since the lowest order Boltzmann approximation for the structure in eq 4.32 is used, and shows the virtues of choosing a mimic system.

As shown in Fig.(4.3), the results of the MPB theory for $\Gamma = 6$ are in very good agreement with computer simulations [17], and compare very favorably to those of the usual (nonlinear) PB theory or the generalized Debye-Hückel (GDH) theory developed by Levin and coworkers [70]. Note that the MPB theory, unlike the usual PB approximation, can predict oscillations in both $S(k)$ and $g(r)$ from the self consistent determination of $\phi_{R1}(r)$ despite using only the lowest structural

approximation, Eq.(4.32).

4.5.2 MPB theory for OCCHS

We now turn to the OCCHS. This has more complex structure because of possible competition between correlations induced by the hard cores and the soft repulsive Coulomb interactions. We follow the usual convention where lengths are measured in terms of the hard core diameter d.

In Fig.(4.4) we compare the results of the MPB theory to MC simulations, to results of a density functional treatment, and to the PB and DH theories for a low density state with $\eta = 0.02$ but with a moderate ionic strength $\Gamma = 5.43$. The MPB theory gives excellent results with a molecular-sized $\sigma = 1.3d$, noticeably better than those of the considerably more complicated density functional theory [57].

The right panel in Fig.(4.5) illustrates the role of α for this state, and shows that the self consistent choice of $\alpha = 1.2$ can ensure that the exact second moment condition is satisfied, though on the scale of the graph the differences between the $S_R(k)$ with $\alpha = 1$ are hardly visible. The left panels show that for much weaker coupling with $\Gamma = 0.54$ even the usual PB approximation (with $\sigma = 0$) gives good results, indicating that at weak coupling the choice of σ is not so important. However, unlike the MPB theory, the PB approximation can satisfy the second moment condition exactly only in the limit $\Gamma \to 0$, where it reduces to the DH approximation [24].

4.6 Results at High Density and Strong Coupling

4.6.1 Structure in Mimic and Full Systems

At high densities we expect that the local structure in r-space of even the *uniform* mimic system, where all corrections from ϕ_{R1} are ignored, will closely resemble that of the full system as suggested in Eq.(4.6). This is illustrated in Fig.(4.6) for the OCCHS for high density states with moderately strong couplings. Canonical Monte Carlo simulations are carried out to obtain the uniform mimic system's correlation function $g_0(r)$, and these are compared [4] to previous simulations for the full system [25], where Ewald sum methods were used to account for the long ranged interactions. Because of the short ranged interactions u_0 in the mimic system, our simulations are completely straightforward and no Ewald sums or other special treatment of the periodic boundary conditions are required. Again a molecular-sized choice of $\sigma = d$ of order the nearest neighbor spacing suffices.

Also shown on the same graphs are the bare ion potential $\beta w(r)$ and the mimic potential $\beta u_0(r)$. Despite the much smaller amplitude of the latter and its much shorter range, the mimic $g_0(r)$ has a striking resemblance to the full system's $g(r)$,

[4] The $S_0(k)$ at larger wavevectors can be accurately determined by a Fourier transform of the simulated $g_0(r)$, but at small wavevectors we directly sampled the ensemble average

$$\frac{1}{N} < \hat{\rho}_{\mathbf{k}} \hat{\rho}_{-\mathbf{k}} > = \frac{1}{N} < \sum_{i \neq j}^{N} \sum e^{-i\mathbf{k}\cdot(\mathbf{r}_i - \mathbf{r}_j)} > + 1.$$

We used $N = 250$ and 432 particles for the OCP and up to 686 particles for the high density OCCHS.

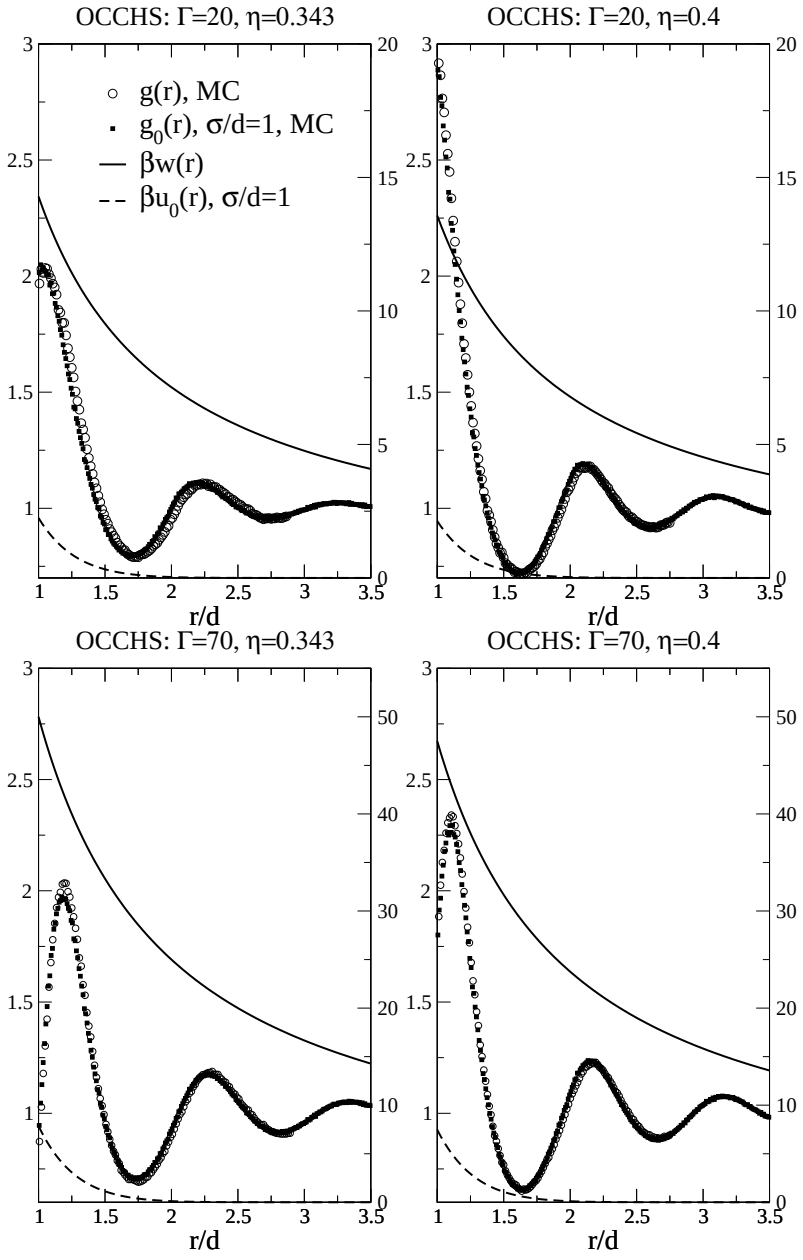

Figure 4.6: OCCHS correlation functions $g(r)$ at stronger coupling strengths Γ and large packing fractions η for the full and mimic systems as determined by MC simulations. Note the maximum in $g(r)$ away from contact for $\Gamma = 70$, indicating the strength of the Coulomb repulsions. Also shown are $\beta w(r)$, the full potential of the ionic fluid, and the mimic potential $\beta u_0(r)$, both of which use the scale on the right y-axis. There is a hard core interaction for $r < d$.

and the differences are hardly visible on the scale of the graph.

At the strongest couplings, the correlation functions at both densities have a first peak shifted away from contact with the embedded hard sphere. Such a correlation function is very different from the correlation function of a hard sphere fluid, which has its maximum at contact, and shows that the strong short ranged parts of the Coulomb interactions can compete with packing effects from hard cores even at high density. This also emphasizes the importance of having the softer piece $w_{q0}(r) = q^2\mathrm{erfc}(r/\sigma)/\epsilon r$ outside the hard core in our mimic system potential $\beta u_0(r)$ in Eq.(4.25) in order to reproduce correlation functions in the OCCHS, especially for strong coupling states.

There have been several previous empirical attempts to fit correlation functions for Coulomb systems at high density using effective short ranged systems. The DH limit might suggest that a generalized Yukawa fluid could be useful, [14] but the results were not very accurate and there was no systematic way to determine parameters for the effective potentials.

Most relevant to our work are ion reaction field (RF) methods, where an effective finite-ranged interaction $w_{q0}^{RF}(r)$ was originally determined from the electrostatic potential of a positive point charge surrounded by a neutralizing uniform spherical charge distribution with a radius r_c [36]. Good results for correlation functions were found using the RF method in several applications at high density, though some spurious oscillations were seen near the cutoff r_c. These were attributed to

the discontinuity of the second and higher order derivatives of $w_{q0}^{RF}(r)$ at r_c and better results were found using a smoother "charge cloud" distribution that had discontinuities only in fourth and higher order derivatives at the cutoff [37].

Our w_{q0} in Eq.(4.26) can be similarly interpreted in terms of the potential arising from a positive point charge surrounded by a neutralizing Gaussian charge distribution. All derivatives of w_{q0} are continuous because of the smooth cutoff, and by construction the associated perturbation w_{q1} decays very rapidly in k-space. It is the latter property that fundamentally leads to mimic system behavior with a proper choice of σ. Our work thus provides a conceptual framework for understanding why RF methods can work as well as they do in some cases and how results can be significantly improved, especially at lower densities or in nonuniform environments by using the LMF theory.

Fig.(4.7) gives a more detailed comparison of the structure of the high density/strong coupling state with $\Gamma = 70$ and $\eta = 0.4$ to that of two different mimic systems with $\sigma = d$ and $\sigma = 1.5d$. Despite the fact that the (repulsive) potential of the latter is always greater than or equal to that of the former, both mimic systems have very similar correlation functions that agree very well with that of the full system, which can be viewed as the limit $\sigma = \infty$. Thus for high density states all mimic systems with $\sigma > \sigma_{\min}$ have essentially the same short-ranged structure in r-space.

Fig.(4.8) gives similar results for the OCP at very strong coupling strengths

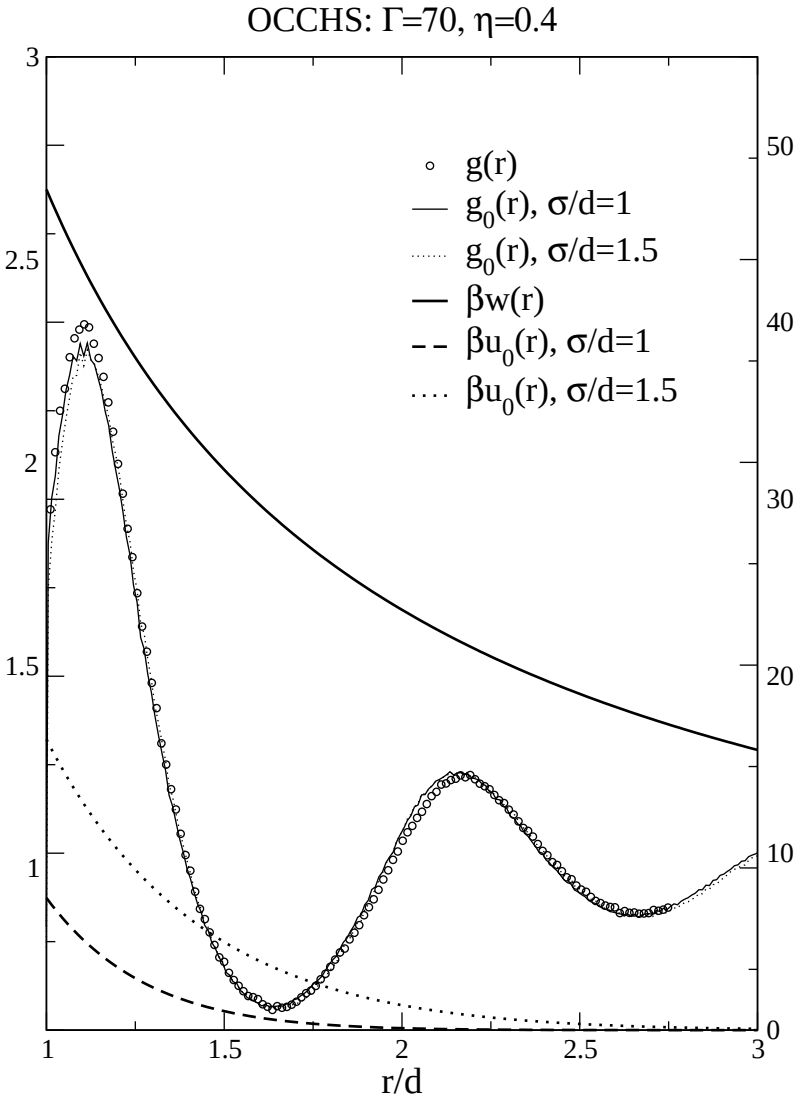

Figure 4.7: Illustration of mimic system behavior. OCCHS correlation function for the state $\Gamma = 70$ and $\eta = 0.4$ compared to those of two different mimic systems with different σ values. Also shown are $\beta w(r)$, the full potential of the ionic fluid, and the mimic potentials $\beta u_0(r)$, all of which use the scale on the right y-axis.

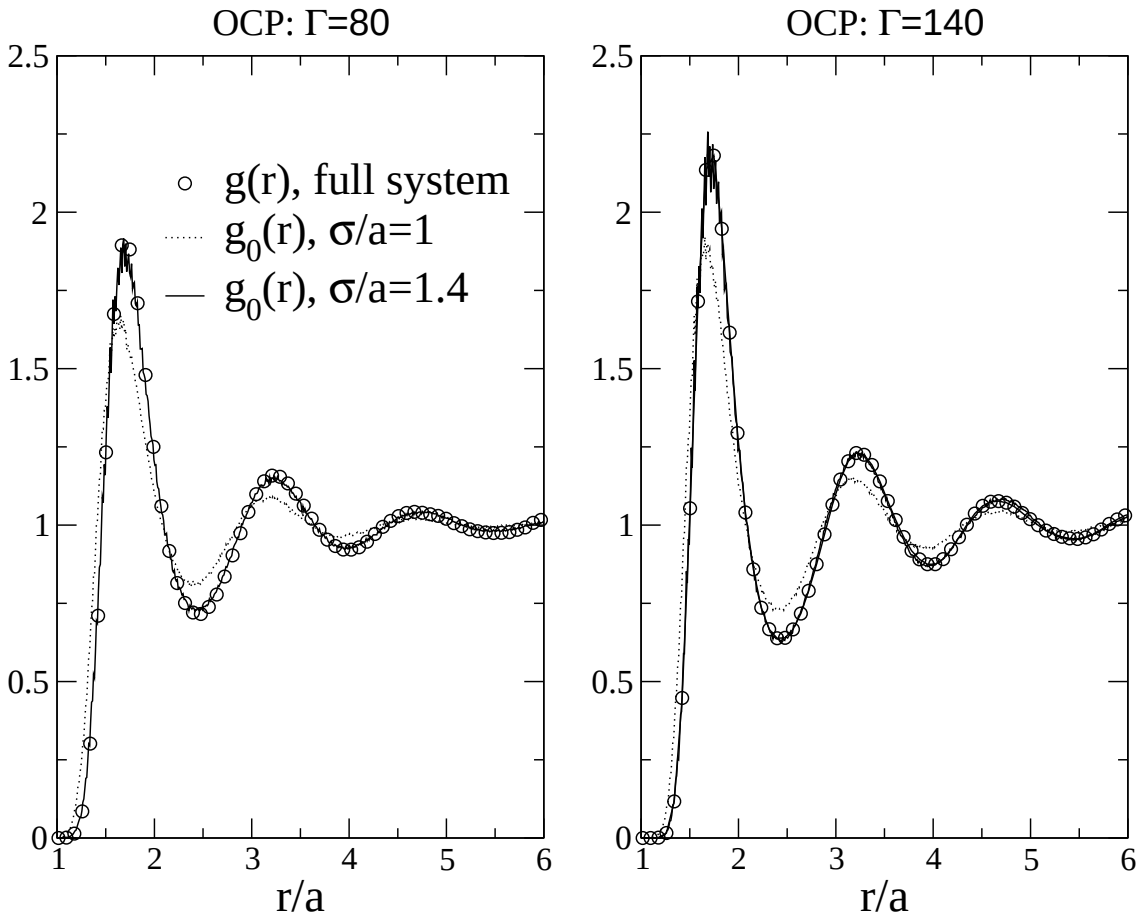

Figure 4.8: High coupling strength OCP correlations for the full and mimic systems. For $\sigma = 1.4a$, $g_0(r)$ is essentially indistinguishable from the full system's $g(r)$. However a smaller $\sigma = a$ fails to mimic the full system's correlations. Note that around $\Gamma \simeq 170$ the OCP starts to freeze [68]. Our simulations indicate that the mimic system with $\sigma = 1.4a$ also freezes at around the same Γ.

$\Gamma = 80$ and $\Gamma = 140$. We find excellent agreement with simulations of the full system [68] using a mimic system with $\sigma/a = 1.4$. As we would expect, for small enough σ the good agreement fails, as illustrated by results for $\sigma/a = 1$.

Fig.(4.9) compares the mimic structure factor $S_0(k)$ and a simple estimate for $S_R(k) = S(k)$ based on a linear response treatment [46] of the effects of $\beta\rho^B\hat{\phi}_{R1}(k)$. Only at very small k as revealed in the inset can any differences be seen. The linear response treatment turns out give an $S_R(k)$ that satisfies exactly both the zeroth and second moment conditions with $\alpha = 1$, and the results converge to $S_0(k)$ at larger k controlled by the factor $\exp[-\frac{1}{4}(k\sigma)^2]$ arising from our choice of a mimic system. These features would be found in any more exact treatment and suffice at high densities to give a very accurate estimate of $S_R(k)$. This also suggests that the results from other approximate theories may be improved by use of a good mimic system. Indeed, as already shown in Fig.(4.6), the simplest possible theory where the effects from ϕ_{R1} are ignored completely, already gives excellent results for short ranged correlations in r-space.

4.6.2 Internal Energy at High Density

With accurate approximations for $S(k)$ and $h(r)$ in hand, it is straightforward to calculate thermodynamic properties by integration. The simplest of these is the internal energy, given by Eq.(4.19). One can always solve the LMF equation to obtain $h(r)$ and use this integral to compute the internal energy of an ionic system, and we would expect very accurate results. Here we show that because of the great

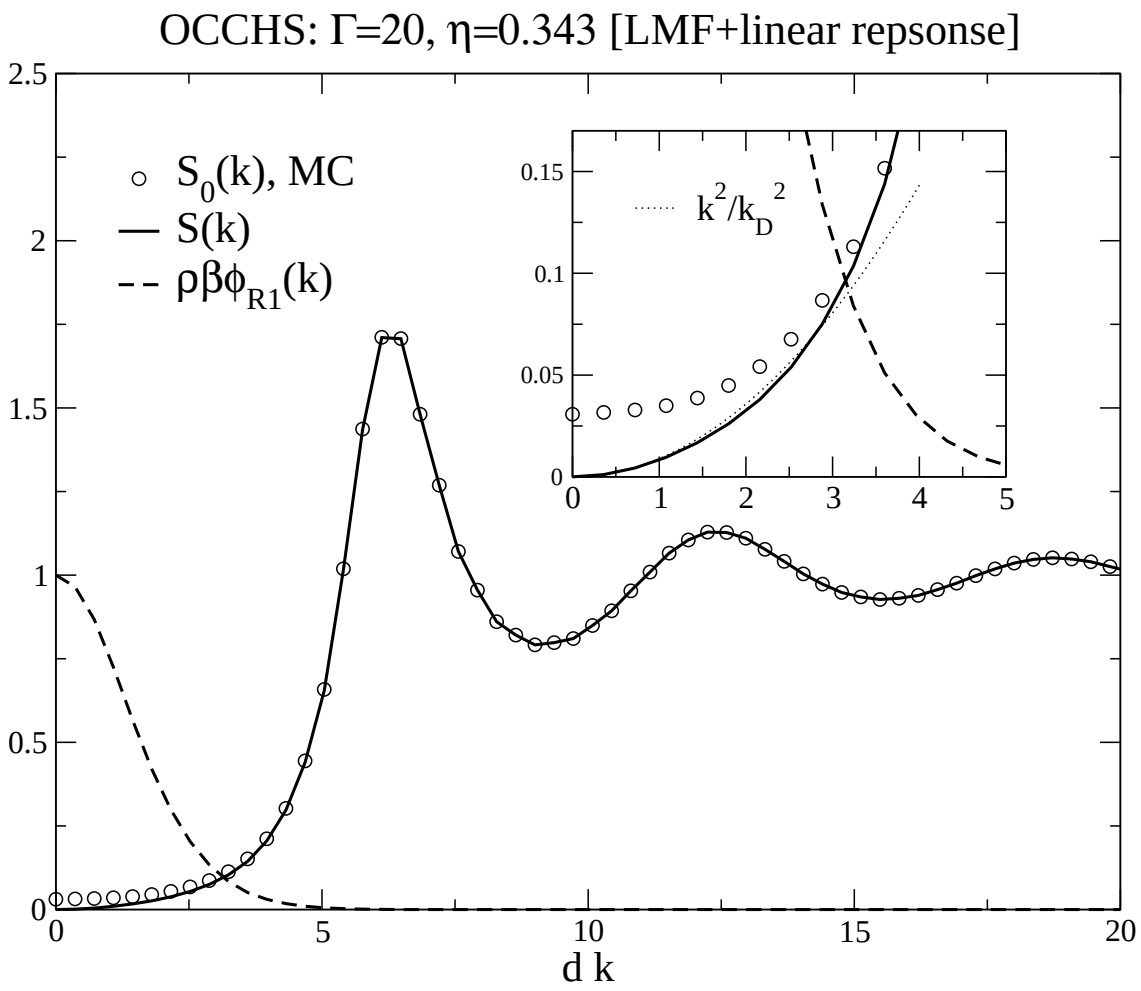

Figure 4.9: Linear response theory is used to approximate the change in $S_R(k) = S(k)$ in the mimic system induced by the the perturbation $\hat{\phi}_{R1}(k)$. With $\alpha = 1$, the linear response theory for $S(k)$ satisfies both SL moment conditions. The inset is a blown-up view of the structure factor at small k where the differences in $S_0(k)$ and $S(k)$ can be seen.

similarity of the local structure of the mimic and full systems in r- and k-space at *high density*, we can obtain an accurate estimate of the energy in terms of the mimic system's energy and a simple analytic correction without explicitly solving the LMF equation.

Equation 4.19 can be rewritten in k-space and the Coulomb interaction separated into mimic and perturbation parts, so that

$$\begin{aligned}\frac{\beta E^{ex}}{N} &= \frac{1}{2}\frac{1}{(2\pi)^3}\int d\mathbf{k}\frac{4\pi\beta q^2}{\epsilon k^2}[1-e^{-\frac{1}{4}(k\sigma)^2}]\rho^B\hat{h}(k) \\ &\quad +\frac{1}{2}\frac{1}{(2\pi)^3}\int d\mathbf{k}\frac{4\pi\beta q^2}{\epsilon k^2}e^{-\frac{1}{4}(k\sigma)^2}\rho^B\hat{h}(k). \end{aligned} \tag{4.33}$$

In the first term of Eq.(4.33), because $\rho^B\hat{h}_0(k)$ differs from $\rho^B\hat{h}(k)$ only at small k, where the factor $1-e^{-\frac{1}{4}(k\sigma)^2}$also approaches zero, we can replace the latter by the former with little error. In the second term, $e^{-\frac{1}{4}(k\sigma)^2}$ decays very quickly at higher k, so only the small-k features of $\rho^B\hat{h}(k) \simeq -1+k^2/k_D^2$ from the SL moment conditions are needed to have an accurate estimate of the integration.

The first term then gives the internal energy of the mimic system

$$\frac{\beta E_0^{ex}}{N} = \frac{1}{2}\int d\mathbf{r}u_0(r)\rho^B h_0(r), \tag{4.34}$$

(with a background contribution $-\pi\beta q^2\sigma^2\rho^B/\epsilon$ arising from the use of h_0 in the integral rather than g_0), while the second term corrects the mimic system's energy and can be integrated analytically to give

$$\frac{\beta E_1^{ex}}{N} = \frac{\beta q^2}{\epsilon\sqrt{\pi}\sigma}\left(-1+\frac{2}{(k_D\sigma)^2}\right). \tag{4.35}$$

Γ	η	σ/a	σ/d	Full MC	Theory [Eq.(4.36)]	$\beta E_0^{ex}/N$
20	-	1.4	-	-16.67	-16.59	-8.66
20	0.343	1.4	1	-17.17	-17.12	-9.20
20	0.4	1.4736	1	-17.33	-17.27	-9.73
70	-	1.4	-	-60.81	-60.72	-32.65
70	0.343	1.4	1	-61.09	-61.02	-32.94
70	0.4	1.4736	1	-61.32	-61.24	-34.56
80	-	1.4	-	-69.69	-69.64	-37.54
125	-	1.4	-	-109.73	-109.74	-59.50
140	-	1.4	-	-123.09	-123.13	-66.85
160	-	1.4	-	-141.72*	-141.57*	-77.23

Table 4.1: Excess internal energy $\beta E^{ex}/N$. The full MC data are taken from references [25] and [68]. At $\Gamma = 160$, both the full and the mimic systems are near solidification, and the results depend on initial conditions.

Thus the internal energy can be estimated as

$$\frac{\beta E^{ex}}{N} \simeq \frac{\beta E_0^{ex}}{N} + \frac{\beta E_1^{ex}}{N}. \tag{4.36}$$

Results for this approximation are compared to MC results in Table 4.1 for a variety of high density/strong coupling states. The Gaussian charge distribution is the key to the accuracy of eq 4.36, both because of its fast decay in k-space and its use in revealing an excellent mimic system for the full ionic system.

Note that at high densities or ionic strengths, the Debye wave vector k_D in Eq.(4.18) can be very large, making neutrality the major contribution to $\beta E_1^{ex}/N \simeq -\beta q^2/(\epsilon\sqrt{\pi}\sigma)$. Though the physical interpretation of this term is very different, its limiting value is the same as the self-interaction correction in the Ewald sum method

[16]. A similar correction was used in ion RF methods [36].

At high density where the compressibility χ_T of the mimic system is very small, we can obtain a good estimate of the internal energy by simply replacing $h(r)$ by $h_0(r)$ in Eq.(4.19), where because of the background subtraction, a finite result is found for any short ranged $h_0(r)$. Separating the Coulomb interaction as in Eq.(4.33), and using only the $k = 0$ result $\rho^B \hat{h}_0(0) = -1 + k_B T \rho \chi_T$ in the second integral we find analogous to Eq.(4.35):

$$\frac{\beta E_1^{ex}}{N} \simeq \frac{\beta q^2}{\epsilon \sqrt{\pi} \sigma} \left(-1 + k_B T \rho \chi_T\right), \tag{4.37}$$

which agrees with Eq.(4.35) in the relevant limit of large k_D and small χ_T.

4.7 Final Remarks

It is straightforward to apply these idea to charge and size asymmetric primitive models (see Sec.5.5, in the next chapter) or to "simple molten salt" models [24] with softer repulsive cores. The LMF approximation has been used to look at the OCP near a charged hard wall [44] (also see chapter 6). Here very accurate results are found both in the weak and strong coupling limits, and the more complicated pair level theory recently introduced [6] is not required. Details will be presented elsewhere, and only few general remarks are made here.

For size asymmetric primitive models, it has been found that the simplest choice of a single σ parameter for all species gives excellent results. This can be understood as a consequence of Stillinger and Lovett's fundamental insight that for

general ionic mixtures universal consequences of the long ranged Coulomb interactions can be seen in the small wavevector behavior of the charge-charge correlation function. By using the smeared charge distributions implied by a proper choice of σ, we arrive at a smeared charge-charge correlation function that has significant structure only at small wave vectors. The LMF theory can then reproduce the exact long wavelength behavior found by SL, and the slowly varying smeared Coulomb perturbations have little effect on the shorter wavelength correlations induced by the modified ion cores in the mimic system, just as illustrated here for the OCCHS.

The main complication that arises for such mixtures is that the resulting mimic systems will have short ranged attractive as well as repulsive interactions, but this is required if we want the mimic system's structure to resemble that of the full Coulomb system. However, the LMF theory can then to a very good approximation take care of the "universal" long ranged parts of the Coulomb interactions, which cause major conceptual and computational problems in most approaches, while leaving a nonuniversal, but surprisingly short ranged problem to be treated by whatever means are available. Simulations are straightforward and some recent theoretical developments for treating systems with strong but short ranged interactions look very promising [62]. The ideas presented here offer a powerful general perspective, and are actively pursuing their consequences for static and dynamic properties of fluids with both short and long ranged interactions.

Chapter 5

Potential Separation of Coulombic Interaction

In the previous chapter, the potential separation and the associated mimic system used with the LMF have been studied for one-component systems. Here in this chapter, a potential separation strategy is derived for more general charged systems. Dipolar systems hopefully can be also studied using the same conceptual framework. Application to a binary, asymmetric primitive model is also presented.

5.1 Interaction Between Two Rigid Charge Distributions

Suppose there are two charge distributions $q_i(\mathbf{r})$ and $q_j(\mathbf{r})$ carried by two particles belonging to species i and j. Each distribution is described by its own *body-frame*. Now suppose both distributions start with their body-frame overlapped, and the $q_j(\mathbf{r})$ is displaced from $q_i(\mathbf{r})$ by a vector $\mathbf{R}$ so $q_j(\mathbf{r})$ becomes $q_j(\mathbf{r}-\mathbf{R})$ in the coordinate system of $q_i(\mathbf{r})$. There are also angular coordinates expressing the orientation of the molecule body frames, which we do not explicitly show here. Now the electronic potential energy between the two charge distributions, one centered at $\mathbf{r} = 0$, the

other centered at $\mathbf{r} = \mathbf{R}$ depends on the $\mathbf{R}$ and is given by

$$w_{q.ij}(\mathbf{R}) = \int d\mathbf{r} \int d\mathbf{r}' q_i(\mathbf{r}) q_j(\mathbf{r} - \mathbf{R}) \frac{1}{\epsilon |\mathbf{r} - \mathbf{r}'|}, \tag{5.1}$$

which can be also expressed as a $\mathbf{k}$-space integral

$$w_{q,ij}(\mathbf{R}) = \frac{1}{(2\pi)^3} \int d\mathbf{k} \hat{q}_i(-\mathbf{k}) \hat{q}_j(\mathbf{k}) e^{-i\mathbf{k}\cdot\mathbf{R}} \frac{4\pi}{\epsilon k^2}. \tag{5.2}$$

The caret denotes the Fourier transform of the decorated function herein. Note that the discussion in this chapter will be limited to the cases where the dielectric constant ϵ is a constant through out the space, thus no image charges need to be considered. At large $\mathbf{R}$'s, only the small k components of the $\hat{q}_i(\mathbf{k})$ and $\hat{q}_j(\mathbf{k})$ have significant contribution to the integral; higher k components are eliminated by the strong oscillation of the factor $e^{-i\mathbf{k}\cdot\mathbf{R}}$. Thus, at large $\mathbf{R}$'s, $w_{q,ij}(\mathbf{R})$ can be expanded near $k = 0$ and the series is expected to converge rapidly[1]. However, at small $\mathbf{R}$'s, the $e^{-i\mathbf{k}\cdot\mathbf{R}}$ by itself can no longer truncate the high k components of the integrand, particularly if $\hat{q}_i(-\mathbf{k})$ and $\hat{q}_j(\mathbf{k})$ decay slowly in the $\mathbf{k}$ space. Although $w_{q,ij}(\mathbf{R})$ in general (depending on how localized $q_i(\mathbf{r})$ and $q_j(\mathbf{r})$ are) is long-ranged and becomes quite slowly varying for $\mathbf{R} \to \infty$, at small separations, the $w_{q,ij}(\mathbf{R})$ can also become very rapid varying from the high-k components in the integration.

For the use of LMF, a perturbative potential $u_{1,ij}(\mathbf{R})$ that remains smooth as two molecules are brought to close distances is crucial for the accuracy of the theory. To result in a smooth and better behaved $u_{1,ij}(\mathbf{R})$, the rapid varying, short-ranged

[1]This is the idea behind the multipole expansion [38] of electric potential.

part of $w_{q,ij}(\mathbf{R})$ at small $\mathbf{R}$'s can actually be combined with the other short-ranged, non-Coulombic core interaction $w_{s,ij}(\mathbf{R})$[2]. As discussed in the previous chapter, replacing the Green's function of the Poisson's equation, $1/r$, by $\mathrm{erf}(\frac{r}{\sigma})/r$ and define

$$w_{q1,ij}(\mathbf{R}) = \int d\mathbf{r} \int d\mathbf{r}' q_i(\mathbf{r}) q_j(\mathbf{r}-\mathbf{R}) \frac{\mathrm{erf}(\frac{|\mathbf{r}-\mathbf{r}'|}{\sigma})}{\epsilon|\mathbf{r}-\mathbf{r}'|} \tag{5.3}$$

$$= \frac{1}{(2\pi)^3} \int d\mathbf{k} \hat{q}_i(-\mathbf{k}) \hat{q}_j(\mathbf{k}) e^{-i\mathbf{k}\cdot\mathbf{R}} e^{-\frac{1}{4}(k\sigma)^2} \frac{4\pi}{\epsilon k^2}. \tag{5.4}$$

$\mathrm{erf}(\frac{r}{\sigma})/r$ decays asymptotically as $1/r$ and approaches smoothly to a finite value (for finite σ) at $r = 0$. So the $w_{q1,ij}(\mathbf{R})$ defined through Eq.(5.3) is also slowly varying at all r's. The remainder $w_{q0,ij}(\mathbf{R})$ of $w_{q,ij}(\mathbf{R})$ is

$$w_{q0,ij}(\mathbf{R}) = \int d\mathbf{r} \int d\mathbf{r}' q_i(\mathbf{r}) q_j(\mathbf{r}-\mathbf{R}) \frac{\mathrm{erfc}(\frac{|\mathbf{r}-\mathbf{r}'|}{\sigma})}{\epsilon|\mathbf{r}-\mathbf{r}'|},$$

which is much shorter-ranged and decays much faster than the $w_{q1,ij}(\mathbf{R})$. Because of the Gaussian function's rapid decay in the k-space, it can be seen from Eq.(5.4) that a long-wavelength expansion of the $w_{q1,ij}(\mathbf{R})$ should converge must more rapidly not just for large $\mathbf{R}$'s, but *for all* $\mathbf{R}$'s! All short-wavelength details of the charge distribution, for $k\sigma \geq 1$, are essentially *irrelevant* to $w_{q1,ij}(\mathbf{R})$. $w_{q1,ij}(\mathbf{R})$ retains the asymptotic decay of the $w_{q,ij}(\mathbf{R})$ but behaves much more smoothly at small $\mathbf{R}$'s. $w_{q1,ij}(\mathbf{R})$ thus is a much more ideal starting point for choosing the perturbative potential $u_{1,ij}(\mathbf{R})$ for treating the Coulomb interaction with the LMF theory.

[2]Here only pair-wise interaction is considered for the $w_{d,ij}$.

5.2 Asymptotic and Multipole Moment Expansion

When molecules carry net charges or dipoles, their pair interactions can be very long-ranged, and such slow decay of the interactions often causes theoretical difficulty and are computational very costly. On the other hand, the LMF can treat the averaged effect of these long-ranged component as an effective renormalized field in a mimic system with much shorter-ranged interaction. Systems with typical short-ranged interactions are often much easier to manage theoretically and offers insights for such systems to be developed as a separate and specialized task, without the complication arising from the long ranged interactions. To investigate the asymptotic part of Coulomb interaction $w_{q,ij}(\mathbf{R})$ between $q_i(\mathbf{r})$ and $q_j(\mathbf{r})$, the charge distributions i, j can be expanded in a Taylor series at long wavelengths, i.e.,

$$\hat{q}_i(\mathbf{k}) = \sum_n \frac{1}{n!}\mathbf{k}^n \cdot \nabla_{\mathbf{k}}^n \hat{q}_i(0) \tag{5.5}$$

$$(\mathbf{k}^n)_{\mu_1\mu_2\ldots\mu_n} \equiv k_{\mu_1}k_{\mu_2}\ldots k_{\mu_n} \tag{5.6}$$

$$(\nabla_{\mathbf{k}}^n)_{\mu_1\mu_2\ldots\mu_n} \equiv \frac{\partial^n}{\partial k_{\mu_1}\partial k_{\mu_2}\ldots\partial k_{\mu_n}}. \tag{5.7}$$

The μ_i subscripts denote the three components k_x, k_y, k_z of a vector $\mathbf{k}$. Eq.(5.4) can then expanded as the following

$$\begin{aligned} w_{q1,ij}(\mathbf{R}) &= \sum_{n_i,n_j} \frac{1}{n_i!n_j!} \nabla_{\mathbf{k}}^{n_i} \hat{q}_i(0) \nabla_{\mathbf{k}}^{n_j} \hat{q}_j(0) \\ &\quad \cdot \frac{1}{(2\pi)^3} \int d\mathbf{k} (-\mathbf{k}^{n_i}) \mathbf{k}^{n_j} \frac{4\pi}{\epsilon k^2} e^{-\frac{1}{4}(k\sigma)^2} e^{-i\mathbf{k}\cdot\mathbf{R}} \qquad (5.8) \\ &= \sum_{n_i,n_j} \frac{1}{n_i!n_j!} \nabla_{\mathbf{k}}^{n_i} \hat{q}_i(0) \nabla_{\mathbf{k}}^{n_j} \hat{q}_j(0) \cdot (-i\nabla)_{\mathbf{r}}^{n_i} (i\nabla)_{\mathbf{r}}^{n_j} \qquad (5.9) \\ &\quad \cdot \frac{1}{(2\pi)^3} \int d\mathbf{k} \frac{4\pi}{\epsilon k^2} e^{-\frac{1}{4}(k\sigma)^2} e^{-i\mathbf{k}\cdot\mathbf{R}} \qquad (5.10) \\ &= \sum_{n_i,n_j} \frac{1}{n_i!n_j!} \nabla_{\mathbf{k}}^{n_i} \hat{q}_i(0) \nabla_{\mathbf{k}}^{n_j} \hat{q}_j(0) \cdot (-i\nabla)_{\mathbf{r}}^{n_i} (i\nabla)_{\mathbf{r}}^{n_j} (\frac{\mathrm{erf}(\frac{r}{\sigma})}{\epsilon r}) \qquad (5.11) \\ &= \sum_{n_i,n_j} \frac{1}{n_i!n_j!} [\nabla_{\mathbf{k}}^{n_i} \hat{q}_i(0) \cdot (-i\nabla)_{\mathbf{r}}^{n_i}] [\nabla_{\mathbf{k}}^{n_j} \hat{q}_j(0) \cdot (i\nabla)_{\mathbf{r}}^{n_j}] (\frac{\mathrm{erf}(\frac{r}{\sigma})}{\epsilon r}) \qquad (5.12) \end{aligned}$$

The $\mathbf{k}$-space gradient of a charge distribution measures the multipole moments of distributions as

$$\begin{aligned} \nabla_{\mathbf{k}}^{n} \hat{q}_i(0) &= (-i)^n \int d\mathbf{r} q_i(\mathbf{r}) \mathbf{r}^n \\ &\equiv (-i)^n \mathbf{M}_i(n), \qquad (5.13) \end{aligned}$$

so Eq.(5.8) can be written as

$$w_{q1,ij}(\mathbf{r}) = \sum_{n_i,n_j} \frac{1}{n_i!n_j!} [\mathbf{M}_i(n_i) \cdot (-\nabla)_{\mathbf{r}}^{n_i}] [\mathbf{M}_j(n_j) \cdot \nabla_{\mathbf{r}}^{n_j}] (\frac{\mathrm{erf}(\frac{r}{\sigma})}{\epsilon r}). \qquad (5.14)$$

Note that the $\mathbf{M}_i(n)$ is a rank-n tensor, and is directly related to the nth multipole moment of charge distribution $q_i(\mathbf{r})$. The lowest n terms are especially familiar:

$$\mathbf{M}_i(0) = \int d\mathbf{r} q_i(\mathbf{r}), \text{ monopole} \tag{5.15}$$

$$\mathbf{M}_i(1) = \int d\mathbf{r}\mathbf{r} q_i(\mathbf{r}), \text{ dipople} \tag{5.16}$$

$$\mathbf{M}_i(2) = \int d\mathbf{r}\mathbf{r}\mathbf{r} q_i(\mathbf{r}), \text{ quadrupole.} \tag{5.17}$$

Note that the $\mathbf{M}_i(2)$ is not the conventional traceless quadrupole moment [38]. With the $\text{erf}(\frac{r}{\sigma})/r$ replaced by $1/r$ or when $\sigma \to 0$, Eq.(5.14) becomes that of the ordinary multipole expansion of $w_{q,ij}(\mathbf{R})$ [38]. However, unlike the later, for finite σ's, the expansion Eq.(5.14) of $w_{q1,ij}(\mathbf{R})$ converges much faster, i.e., it takes much fewer terms to reliably estimate $w_{q,ij}(\mathbf{R})$ at small $\mathbf{R}$'s than would be the case with $w_{q,ij}(\mathbf{R})$. Also, $\text{erf}(\frac{r}{\sigma})/r$ is smooth and finite even near the origin, and so are its successive gradients. These features of Eq.(5.14) have very significant implications for advanced simulation methods of ionic interaction such as the *fast multipole method* (FMM) [18] and various *particle-mesh* (PM) schemes[3]. The FMM approximates the Coulomb interaction between distant charge clusters by a multipole expansion[4] which is the $\sigma \to 0$ limit of Eq.(5.14). With an elaborate algorithm for summing the multipole moments, the computation complexity of the FMM in principle can achieve an $O(N)$ scaling with the number of particles N. However, the $O(N)$ scaling is plagued by a huge prefactor – p^4, where p is the number of multipole moments used, and it

[3]For a survey, see e.g., reference [16].

[4]The "local expansion" used in FMM actually corresponds to expanding $q_j(\mathbf{r})$ near its body frame's origin.

is often observed that it takes a very big N for the FMM to break even with the prefactor and become more efficient than Ewald summation (which is "said" to scale as $O(N^{3/2})$ [16, 1]). However, the need to use many multipole moments is most likely due to the use of the usual multipole expansion of Eq.(5.1,5.2) even at small $\mathbf{R}$'s. Unlike $w_{q1,ij}(\mathbf{R})$, $w_{q,ij}(\mathbf{R})$ can be rapidly varying at small $\mathbf{R}$'s such that straightforward multipole expansion converges poorly at small $\mathbf{R}$'s. In fact, since all realistic molecules at short distances interact also with potentials of non-Coulombic origin, which are excluded from the FMM algorithm and treated as they would be in ordinary systems with only short-ranged interactions, the rapid varying part of the Coulomb interaction should be *routinely* combined with other core interactions, instead of being treated by an asymptotic expansion! As is evident from Eq.(5.4), the multipole expansion of $w_{q1,ij}(\mathbf{R})$ can converge much faster than that of $w_{q,ij}(\mathbf{R})$ and $w_{q1,ij}(\mathbf{R})$ is much smoother at small $\mathbf{R}$'s than $w_{q,ij}(\mathbf{R})$. If the FMM algorithm is used only for approximating the $w_{q1,ij}(\mathbf{R})$, the number of multipole moments needed could be significantly reduced and the $O(N)$ scaling would be much less compromised by the accompanying prefactor. The $w_{q0,ij}(\mathbf{R})$ could then just be combined with other core interactions. There are also "particle-mesh" algorithms (PM, PME, SPME)[5], which solve Poisson's equation on a mesh for the electronic interaction and scale as $O(N \log N)$. Because of the interpolation schemes employed for assigning charges on mesh points, the major limitation of these algorithms is that they are most efficient

[5]See a survey in reference [16], appendix **B**.

when particle densities are rather uniform but can deteriorate to much a slower $O(N^2)$ scaling for highly nonuniform particle densities. Again, if Poisson's equation is solved for the $w_{q1,ij}(\mathbf{R})$, i.e., charge distribution $\hat{q}(\mathbf{k})$ smeared as $\hat{q}(\mathbf{k})e^{-\frac{1}{8}(k\sigma)^2}$, then the algorithms would be much less sensitive to the nonuniformity of $\hat{q}(\mathbf{k})$ and avoid the degrading of efficiency. Similar ideas involving splitting the $1/r$ Coulomb potential into a short-ranged and a long-ranged piece have also been explored for the improvement of PM [16].

5.3 Treating the Leading Asymptotic Effects of the Coulomb Interaction with the LMF Theory

In the last section, a multipole expansion of $w_{q1,ij}(\mathbf{R})$ is derived for using a *damped* (in the k-space) Green's function $\mathrm{erf}(\frac{r}{\sigma})/r$ in place of $1/r$, as a result $w_{q1,ij}(\mathbf{R})$ is also smooth at small $\mathbf{R}$'s. However, the multipole moments of a charge distribution in general depend on the choice of origin of the associated body frame, with the exception of the lowest order nonvanishing multipole moment. This means that only the leading asymptotic derived from Eq.(5.14) is *unambiguous* with respect to the chosen origin of the body frame. The trickiest to handle are charge distributions whose lowest order multipoles are monopoles or dipoles, since they cause interactions that decay very slowly as $1/r$ or $1/r^2$, thus are particularly demanding for computer simulations or theoretical treatments. On the other hand, the LMF is particularly useful for treating the averaged effect of such long-ranged potentials. To treat the

leading order, slowest decaying part of interactions between charge carriers with the LMF, the perturbative potential $u_{1,ij}(\mathbf{r})$ for the LMF can be defined using only *the lowest nonvanishing multipole moments* of charge distributions $q_i(\mathbf{r})$ and $q_j(\mathbf{r})$

$$u_{1,ij}(\mathbf{r}) \equiv \frac{1}{n_i^*!n_j^*!}[\mathbf{M}_i(n_i^*)\cdot(-\nabla)_{\mathbf{r}}^{n_i^*}][\mathbf{M}_j(n_j^*)\cdot\nabla_{\mathbf{r}}^{n_j^*}](\frac{\mathrm{erf}(\frac{r}{\sigma})}{\epsilon r}), \tag{5.18}$$

$$\hat{u}_{1,ij}(\mathbf{k}) = \frac{i^{(n_i^*+n_j^*)}}{n_i^*!n_j^*!}[\mathbf{M}_i(n_i^*)\cdot(-\mathbf{k})^{n_i^*}][\mathbf{M}_j^*(n_j^*)\cdot\mathbf{k}^{n_j^*}]\frac{4\pi e^{-\frac{1}{4}(k\sigma)^2}}{\epsilon k^2}. \tag{5.19}$$

n_i^* denotes the order of the lowest nonvanishing multipole moment of the charge distribution on particle i . So if both i and j particles carry net charges, then

$$u_{1,ij}(\mathbf{r}) = \frac{q_i q_j \mathrm{erf}(\frac{r}{\sigma})}{\epsilon r}, \tag{5.20}$$

which are the case of *primitive models*. Dipolar-monopole, dipole-dipole interaction (on induced dipoles) as they are in *civilized models*[6] or even more elaborate models for water molecules, can be treated with the LMF with the perturbative potentials

$$u_{1,ij}(\mathbf{r}) = q_i(\mathbf{p}_j\cdot\nabla)(\frac{\mathrm{erf}(\frac{r}{\sigma})}{\epsilon r}),\ \text{monopole } q_i \text{ with dipole } \mathbf{p}_j \tag{5.21}$$

$$u_{1,ij}(\mathbf{r}) = (\mathbf{p}_i\cdot\nabla)(\mathbf{p}_j\cdot\nabla)(\frac{\mathrm{erf}(\frac{r}{\sigma})}{\epsilon r}),\ \text{dipoles } \mathbf{p}_i,\ \mathbf{p}_j, \tag{5.22}$$

and a mimc system with interactions

$$u_{0,ij}(\mathbf{r}) = w_{ij}(\mathbf{r}) - u_{1,ij}(\mathbf{r}). \tag{5.23}$$

Note that especially for molecules modeled as carrying partial charge sites (such as water molecules), one would like to choose the body frame of the molecules such

[6]Point dipoles are assigned at the centers of hard sphere particles.

that higher order multipoles are as small as possible[7]. For example, for a molecule with a net charge, i.e., a nonvanishing monopole, the origin of the molecule's body frame can always be preferably chosen such that the dipole moment vanishes[8]. In fact, molecules are often modeled as carrying "point multipoles", which is to say that all higher order moments are zero. However, such description of course are subject to a particular choice of origin that overlaps with where the point multipole is assigned. In fact, if the origin of the molecule is deliberately shifted, artificial and non-zero higher multipoles will be generated as well! So if considering a case of salt dissolved in water, then the monopole-monopole (ion v.s. ion), monopole-dipole (ion v.s. water) and dipole-dipole (water v.s. water) interactions[9] can be treated through the LMF theory with a mimic system free of such long ranged asymptotic decay. What's more, the LMF equation will ensure that important sum rules like neutrality, dipole moment conservation are also built in (as will be addressed in the next section).

Ewald summation methods have also been generalized to charged system models that deal with the effect of higher order multipole moments [1]. In the case that point multipole moments are assigned to molecules, the r-space part

[7]The generalized "norm" of a rank-n tensor $\mathbf{T}_n$ can be defined by $\|\mathbf{T}_n\| \equiv \max(\mathbf{T}_n \cdot \mathbf{u}^n), \forall \mathbf{u}$. $\mathbf{u}$ is the vector in the vector space that the tensor $\mathbf{T}_n$ operates on. A choice of body frame origin that minimizes $\mathbf{M}(n^* + 1)$ (second to the lowest multipole moment) is thus preferred.

[8]In general it is not always possible to make multipoles (higher order than dipole) to vanish by shifting the origin of the body frame.

[9]Note that the dipole-dipole interaction between ions and waters need not be considered, because the dipole should be made zero by choosing the "right" origin of body frame.

of the Ewald sum method actually corresponds to summing short-ranged potentials as those in Eq.(5.18). However, when particles are modeled as carrying partial charge sites, Ewald summation method sums over the monopole-monopole $u_{0,(i,a)(j,b)}(r) = q_{(i,a)}q_{(j,b)}\mathrm{erfc}(r/\sigma)/\epsilon r$ terms for each site (i, j refer to molecule labels and a, b refer to site labels) in r-space, instead of the lowest total multipole moment interaction between i, j molecules. The separation of potential proposed in this chapter particularly differs from that of Ewald summation in this latter case. In fact, the Ewald summation's r-space short-ranged potential between two charged molecules often carries many more multipole moments than just the lowest order ones of the LMF $u_{0,ij}(\mathbf{r})$.

Finally, the $w_{1,ij}(\mathbf{r})$ and $u_{1,ij}(\mathbf{r})$ are defined with a certain relative orientation of i, j molecules. If a particular body frame is chosen, $u_{1,ij}$ will also carry the Euler angles of the body frame rotation. That is, $u_{1,ij} = u_{1,ij}(\mathbf{r}, \Omega)$, so $\mathbf{r}$ is the vector pointing from the origin of the i particle to that of the j's, and Ω represents the rotation of the j's body frame with respect to the i's. The Ω goes into the definition of Eq.(5.18) by rotating the $\mathbf{M}_j(n)$'s by Ω, i.e., $\mathbf{M}_j = \mathbf{M}_j(n, \Omega)$. Since the phase space should also involve nontrivial contributions from the rotation degrees of freedom of the molecules (if they are not spherically symmetric), the generalized LMF equation for such systems should also take into the averaged effect of molecular rotations, and would be written as

$$\phi_{R,i}(\mathbf{r}_1, \Omega_1) = \phi_i(\mathbf{r}_1, \Omega_1) + \int d\mathbf{r}_2 d\Omega_2 \sum_j \rho_j(\mathbf{r}_2, \Omega_2) u_{1,ij}(\mathbf{r}_{12}, \Omega_{12}). \tag{5.24}$$

Note that the angular integration in Eq.(5.24) in normalized such that $\int d\Omega = 1$.

5.4 Determining σ

For the application of the LMF for general charge distributions, the question of how one should choose the σ parameter still remains. The bigger the σ is, the smoother the $u_{1,ij}(\mathbf{r})$'s will be. In general, one would like to have a reference system such that its structure differs from that of the full system only at wave vectors that are smaller than a certain wave vector κ. κ is supposed to characterize the length scale of the short-ranged "core" interaction and structure of the full system. To study more specifically how this criterion leads to the choice of σ, consider a special case of using the LMF to compute the pair correlation functions of a bulk ionic fluid. Because the correlation function between i,j species is the same as the density response of the j species to an i particle fixed at the origin, to apply the LMF for the bulk correlation functions, all involved species should take turns being fixed at the origin. Each pair response, between the fixed ith species and the responding jth, is associated with an LMF equation

$$\phi_{R,ij}(\mathbf{r}_1, \Omega_1) \;=\; w_{ij}(\mathbf{r}_1, \Omega_{12}) + \int d\mathbf{r}_2 d\Omega_3 \sum_h \delta\rho(\mathbf{r}_2, \Omega_2) u_{1,hj}(\mathbf{r}_{21}, \Omega_{12}) \quad (5.25)$$

$\delta\rho_{ih}(\mathbf{r}_2, \Omega_2) \equiv \rho_{ih}(\mathbf{r}_2, \Omega_2) - \rho_h,\ \rho_h = \rho x_h.$ $\rho_{ih}(\mathbf{r}, \Omega) = \rho_h^B g_{ih}(\mathbf{r}, \Omega)$ is the density of the hth species at $\mathbf{r}$ and with orientation Ω with respect to the particle of ith species fixed at the and x_j is the mole fraction of species j. $\phi_{R,ij}(\mathbf{r}_1, \Omega_1)$ is the local molecular field seen by the jth species' reference particle when an ith particle is fixed

at the origin. The $\phi_{R,ij}$ can be also divided into a short-ranged piece $\phi_{R0,ij} = u_{0,ij}$ and a long-ranged $\phi_{R1,ij} defined by$

$$\phi_{R1,ij}(\mathbf{r}_1, \Omega_1) \equiv u_{1,ij}(\mathbf{r}_1, \Omega_1) + \int d\mathbf{r}_2 d\Omega_2 \sum_h \delta\rho_{ih}(\mathbf{r}_2, \Omega_2) u_{1,hj}(\mathbf{r}_{21}, \Omega_{12}). \quad (5.26)$$

Using Eq.(5.19), one can perform Fourier transform with respect to the $\mathbf{r}_1$ dependence of Eq.(5.26)

$$\begin{aligned}
\hat{\phi}_{R1,ij}(\mathbf{k}, \Omega_1) &= \hat{u}_{1,ij}(\mathbf{k}, \Omega_1) + \int d\Omega_2 \sum_h \delta\hat{\rho}_{ih}(\mathbf{k}, \Omega_2) \hat{u}_{1,hj}(\mathbf{k}, \Omega_{12}) && (5.27)\\
&= \frac{4\pi e^{-\frac{1}{4}(k\sigma)^2}}{\epsilon k^2} \frac{i^{(n_i^* + n_j^*)}}{n_i^*! n_j^*!} (\mathbf{M}_i^* \cdot (-\mathbf{k})^{n_i^*}) (\mathbf{M}_j^* \cdot \mathbf{k}^{n_j^*}) \\
&\quad + \int d\Omega_2 \sum_h \frac{4\pi e^{-\frac{1}{4}(k\sigma)^2}}{\epsilon k^2} \delta\hat{\rho}_{ih}(\mathbf{k}, \Omega_2) \frac{i^{(n_h^* + n_j^*)}}{n_h^*! n_j^*!} (\mathbf{M}_h^* \cdot (-\mathbf{k})^{n_h^*}) (\mathbf{M}_j^* \cdot \mathbf{k}^{n_j^*}) \\
&= \frac{i^{n_j^*}}{n_j^*!} (\mathbf{M}_j^* \cdot \mathbf{k}^{n_j^*}) \hat{\psi}_i(\mathbf{k}) && (5.28)\\
\hat{\psi}_i(\mathbf{k}) &\equiv \frac{4\pi e^{-\frac{1}{4}(k\sigma)^2}}{\epsilon k^2} \left\{ \frac{i^{n_i^*}}{n_i^*!} (\mathbf{M}_i^* \cdot (-\mathbf{k})^{n_i^*}) \right. \\
&\quad \left. + \int d\Omega_2 \sum_h \frac{i^{n_h^*}}{n_h^*!} (\mathbf{M}_h^* \cdot (-\mathbf{k})^{n_h^*}) \delta\hat{\rho}_{ih}(\mathbf{k}, \Omega_2) \right\} && (5.29)
\end{aligned}$$

$\psi_i(\mathbf{r})$ is the electric potential contributed by the i particle at the origin and the rest of the fluid particles. $\psi_i(\mathbf{r})$ also bears the angular dependence implicitly in the $\mathbf{M}_i^*$. From Eq.(5.28), when the $u_{1,ij}(\mathbf{r})$ involves monopole and dipole interactions, in order for $\hat{\phi}_{R1,ij}(0, \Omega_1)$ to be finite, the summation of the $\hat{\rho}_{ij}(\mathbf{k}, \Omega)$'s has to to remove the $1/k^2$ and $\mathbf{k}/k^2$ divergence in the equation Eq.(5.28), and this in fact implies that the LMF solution will satisfy the sum rules for *neutrality and dipole moment*

conservation [9]. Further more, consider a field $\hat{\Psi}(\mathbf{k})$ defined as

$$\hat{\Psi}(\mathbf{k}) \equiv \int d\Omega_1 \sum_i x_i \frac{i^{n_i^*}}{n_i^*} (\mathbf{M}_i^* \cdot (-\mathbf{k})^{n_i^*}) \rho\beta \hat{\psi}_i(\mathbf{k}, \Omega_1) \tag{5.30}$$

$$= \frac{4\pi\rho\beta e^{-\frac{1}{4}(k\sigma)^2}}{\epsilon k^2} \left\{ \int d\Omega_1 \sum_i x_i \frac{i^{n_i^*} i^{n_i^*}}{n_i^* n_i^*} (\mathbf{M}_i^* \cdot (-\mathbf{k})^{n_i^*})(\mathbf{M}_i^* \cdot (-\mathbf{k})^{n_i^*}) \right.$$

$$+ \int d\Omega_1 d\Omega_2 \sum_{i,j} \frac{i^{(n_i^*+n_j^*)}}{n_i^*! n_j^*!} (\mathbf{M}_i^* \cdot (-\mathbf{k})^{n_i^*})(\mathbf{M}_j^* \cdot (-\mathbf{k})^{n_j^*})$$

$$\left. \rho x_i x_j \hat{h}_{ij}(\mathbf{k}, \Omega_1, \Omega_2) \right\} \tag{5.31}$$

$$= \int d\Omega_1 d\Omega_2 \sum_{i,j} \frac{4\pi\beta\rho e^{-\frac{1}{4}(k\sigma)^2}}{\epsilon k^2} \frac{(-i)^{(n_i^*+n_j^*)}}{n_i^*! n_j^*!} \mathbf{k}^{n_i^*+n_j^*}$$

$$\cdot \hat{\mathbf{S}}_{\mathbf{M}_i^* \mathbf{M}_j^*}(\mathbf{k}, \Omega_1, \Omega_2) \tag{5.32}$$

$$\hat{\mathbf{S}}_{\mathbf{M}_i^* \mathbf{M}_j^*}(\mathbf{k}, \Omega_1, \Omega_2) \equiv \mathbf{M}_i^* \mathbf{M}_j^* \hat{S}_{ij}(\mathbf{k}, \Omega_{12}), \tag{5.33}$$

$$= \mathbf{M}_i^* \mathbf{M}_j^* \left(x_i \delta_{n_i n_j} \delta(\Omega_{12}) + \rho x_i x_j \hat{h}_{ij}(\mathbf{k}, \Omega_{12}) \right), \tag{5.34}$$

x_i is the molar fraction of species i. Note that $\hat{\mathbf{S}}_{\mathbf{M}_i^* \mathbf{M}_j^*}$ is a tensor of rank $n_i^* + n_j^*$. The explicit angular dependence of Ω_1 is specified in Eq.(5.30) since the angles of the molecule i at the origin will also be averaged over in the integration of Ω_1. $\Psi(\mathbf{R})$ given in $\mathbf{k}$-space in Eq.(5.30) is the potential energy between two particles separated by $\mathbf{R}$, averaged over the species (thus also "type" of charge distributions) and angular degrees of freedom. In a ion-dipole mixture, e.g.,

$$\hat{\Psi}(\mathbf{k}) = \frac{4\pi\beta\rho e^{-\frac{1}{4}(k\sigma)^2}}{\epsilon k^2} \left(\hat{S}_{QQ}(\mathbf{k}) + \mathbf{k} \cdot \hat{\mathbf{S}}_{QD}(\mathbf{k}) + \mathbf{k}\mathbf{k} \cdot \hat{\mathbf{S}}_{DD}(\mathbf{k}) \right), \tag{5.35}$$

$$\hat{\mathbf{S}}_{QD}(\mathbf{k}) \equiv \int d\Omega_1 \int d\Omega_2 \sum_i^{\text{ion}} \sum_j^{\text{dipole}} q_i \mathbf{p}_j \hat{S}_{ij}(\mathbf{k}, \Omega_{12}), \tag{5.36}$$

$$\hat{\mathbf{S}}_{DD}(\mathbf{k}) \equiv \int d\Omega_1 \int d\Omega_2 \sum_{i,j}^{\text{dipole}} \mathbf{p}_i \mathbf{p}_j \hat{S}_{ij}(\mathbf{k}, \Omega_{12}). \tag{5.37}$$

Note that in the expansion of $\hat{\Psi}$, the structure factors weighted by different multipoles accompany different interactions of $1/k^2$, $\mathbf{k}/k^2$, $\mathbf{k}^2/k^2$,...,etc, as seen in Eq.(5.35). For primitive models of spherical ions only, for which orientation information is irrelevant,

$$\hat{\Psi}(k) = \frac{4\pi\beta\rho e^{-\frac{1}{4}(k\sigma)^2}}{\epsilon k^2}\hat{S}_{QQ}(k), \tag{5.38}$$

$$\hat{S}_{QQ}(k) = \sum_{i,j}\sum q_i q_j \hat{S}_{i,j}(k). \tag{5.39}$$

The Stillinger-Lovett second moment condition [69] is equivalent to the normalization of $\hat{\Psi}(0) = 1$ of Eq.(5.38). More generally, the second moment condition can be generalized to any systems in which mobile ions (or dipoles) are involved, and it can be expressed as the normalization of the ion-ion and ion-dipole parts of the $\hat{\Psi}$

$$\lim_{k\to 0} \frac{4\pi\beta\rho e^{-\frac{1}{4}(k\sigma)^2}}{\epsilon k^2}\left(\hat{S}_{QQ}(\mathbf{k}) + \mathbf{k}\cdot\hat{\mathbf{S}}_{QD}(\mathbf{k})\right) = 1. \tag{5.40}$$

Eq.(5.40) had been also derived for the primitive model (ion mixtures) and the civilized model (ion-dipole mixtures)[10].

$\hat{\Psi}(\mathbf{k})$ characterizes the small $\mathbf{k}$ corrections that the LMF theory should subsequently predict to modify the reference system's structure. Thus $\hat{\Psi}(\mathbf{k})$ is expected to be small for all $k > \kappa$ by a properly chosen σ, κ is the wave vector that characterizes the *effective core* size of the molecules. This implies the following criteria for

[10]See reference [9]. Their results are further simplified by the fact that primitive model ions are spherically symmetric. And note that $\hat{S}_{QQ}$ in general should have the vector dependence as in Eq.(5.40) since the ions can have non-spherical shapes.

the choice of σ:

$$\hat{\Psi}_0(\mathbf{k})|_{\mathbf{k}=\vec{\kappa}} < 1, \text{ i.e.,} \tag{5.41}$$

$$\frac{4\pi\beta\rho e^{-\frac{1}{4}(\kappa\sigma)^2}}{\epsilon\kappa^2}\sum_{A,B}\vec{\kappa}^{(n_A^*+n_B^*)}\cdot\mathbf{M}_A^*\mathbf{M}_B^*\hat{\mathbf{S}}_{0,AB}(\vec{\kappa}) < 1 \tag{5.42}$$

$$\sum_{i_A}^{N_A}\sum_{j_B}^{N_B}\mathbf{M}_{i_A}^*\mathbf{M}_{j_B}^*\hat{S}_{0,i_Aj_B}(\mathbf{k},\Omega_{12}) \equiv \hat{\mathbf{S}}_{0,AB}(\mathbf{k}), \tag{5.43}$$

$\hat{S}_{0,ij}(\mathbf{k},\Omega_{12})$ is the partial structure factor of the reference system and the capital A, B subscripts denote the types of the lowest multipoles. The $\sum_i^{N_A}$ of Eq.(5.43) sums over all the species whose lowest multipoles are type A, so for example, $\hat{\mathbf{S}}_{QD}(\mathbf{k})$ would sum all ion (Q) or dipole (D) species. If the $u_{1,ij}(\mathbf{r},\Omega)$ are turned on from the reference system so the full molecular interaction $w_{ij}(\mathbf{r},\Omega)$ is recovered, the $\hat{\Psi}_0(\mathbf{k})$ then estimates the yet-to-be-screened potential that will further perturb the system's structure until the structure of the full system is obtained. At high densities and when under strong coupling conditions, the $\beta u_{1,ij}(\mathbf{R})$ is often much greater than unity when reaching a_{ij} (the average spacing of ij pair), meaning that the ij pairs interaction goes beyond a_{ij} and much cancellation of the intermolecular forces from more distant neighbors is expected. So at high densities the $1/\kappa$ should be taken to be about the typical spacing a of the particles[11], and κ is also supposed to be where the $\hat{\mathbf{S}}_{AB}(\mathbf{k})$'s start exhibiting oscillations.

At low densities, $\beta u_{1,ij}(\mathbf{r},\Omega) \ll 1$ at $r = a_{ij}$, $1/\kappa$ could then be about some

[11]There are still subtleties regarding the fact that when the molecules are very asymmetric(size and concentration), there is the problem of what it means by the averaged particle spacing, and which one (or even how to average) to choose.

average "bare" core size of the $\beta u_{1,ij}(\mathbf{R},\Omega)$'s, denoted as l_{ij}. l_{ij} typically measures where $u_{1,ij}(\mathbf{R},\Omega)$ reaches kT . As such, we should require $\kappa l < 1$ (l referring to all pairs of l_{ij}). In such regimes, the particle correlations are mostly determined by l_{ij}, thus σ chosen to be smooth across each of the core sizes would be a *conservative* estimate to ensure the LMF's accuracy. However, when $\rho \to 0$, $\hat{S}_{ij}(\mathbf{k},\Omega_{12}) \to x_i\delta_{ij}$ so Eq.(5.42) becomes

$$\frac{4\pi\beta\rho e^{-\frac{1}{4}(\kappa\sigma)^2}}{\epsilon\kappa^2}\sum_A x_A(\vec{\kappa}^{n_A^*}\cdot\mathbf{M}_A^*)^2 \quad < \quad 1 \tag{5.44}$$

$$\sim \frac{4\pi\beta\rho e^{-\frac{1}{4}(\kappa\sigma)^2}}{\epsilon\kappa^2}\sum_A x_A(\kappa^{n_A^*}\|\mathbf{M}_A^*\|)^2 \quad < \quad 1, \tag{5.45}$$

κ has also angular degree of freedom. If $4\pi\beta\rho/\epsilon$ is small enough, even without the damping of $e^{-1/4(k\sigma)^2}$, i.e., setting $\sigma = 0$, Eq.(5.44) could still hold for $\kappa \sim 1/l$. This in fact is the limit where the usual Poisson-Boltzmann approximation can apply. For the simpler example of one-component plasma or primitive model, Eq.(5.45) becomes

$$\frac{4\pi\beta\rho e^{-\frac{1}{4}(\kappa\sigma)^2}q^2}{\epsilon\kappa^2} \qquad < \qquad 1 \tag{5.46}$$

$$\Rightarrow (\frac{k_D}{\kappa})^2 \quad e^{-\frac{1}{4}(\kappa\sigma)^2} < \quad 1. \tag{5.47}$$

Once the system enters the weak coupling regime that $\beta q^2/\epsilon a \ll 1$, which also implies that $k_D a \ll 1$ and $k_D l \ll 1$, then Eq.(5.47) holds even with $\sigma = 0$.

The discussions above only serve as qualitative criteria for choosing σ, they are by no means strictly quantitative, particularly for very asymmetric molecules. However, it is crucial to recognize that the σ is *not* a "fitting" parameter. While

these criteria estimate the smallest working σ (σ_{min}) for the use of the LMF, one can always increase the σ value until the LMF solution starts being invariant with respect to the increase of the σ (with the condition that the reference system can be treated accurately). The analysis here is meant to demonstrate that $\sigma_m in$ remains a molecular scale length scale, for all coupling ranges.

5.5 Application on a Size-Asymmetric Primitive Model

5.5.1 Model Description

A model of great current interest is the size-asymmetric primitive model (SAPM) of ionic solutions, where one considers oppositely charged hard spheres of different sizes in a dielectric continuum. The different hard sphere diameters crudely account for the different sizes of real cations and anions, and there is an interesting and not well-understood dependence of the critical temperature and critical density in this model as the size ratio is varied. We consider in particular the equimolar system studied by Weis and Levesque (WL) [81], where the diameter ratio $d_1/d_2 = 0.4$, with d_2 the negative ion diameter, and symmetric charges $|q_1| = |q_2| = q$. Thus $w_{s,ij}(r) = \infty$ for $r \leq d_{ij}$, where $d_{ij} = (d_i + d_j)/2$, and is zero otherwise, and $w_{q,ij}(r) = q_i q_j/\epsilon r$.

Let us denote the general dimensionless measure of the strength of the Coulomb interactions by the *ionic strength* $\Gamma_a \equiv \beta q^2/(\epsilon a)$, the ratio of the *Bjerrum length* $l_B \equiv \beta q^2/\epsilon$ (which is also called the reduced temperature β^* used by WL) to some characteristic nearest neighbor spacing a. WL take $a = d_2$ and thus characterize the

states by $\Gamma_{d_2} = l_B/d_2$ (called q^{*2} in their notation), and a reduced density $\rho^* = \rho^B d_2^3$, where $\rho^B = (N_1 + N_2)/V$ is the total bulk number density of both ions. According to the potential separation strategy introduced in the previous sections, the $w_{q,ij}(r)$ of the SAPM can be divided into

$$\begin{aligned} u_{0,ij}(r) &= q_i q_j \mathrm{erfc}(r/\sigma)/r, \forall r \in d_{ij} \\ &= \infty, \text{otherwise}, \end{aligned}$$

and $u_{1,ij}(r) = q_i q_j \mathrm{erf}(r/\sigma)/r$. The structure of the SAPM in condensed or liquid-vapor coexistence states are the result of the competition between the Coulomb interaction and the packing arrangement of the embedded hard cores. At strong coupling states, this competition, no matter which factor dominates, produces elaborate and distinctive features in the ion correlations. At a high density liquid state of the SAPM, when the Coulomb interaction extends and remains strong beyond the average spacing a of the ions, then $\Gamma_a > 1$. However, most of the Coulomb interaction that extends outside the a would cancel, causing the bulk structure of the SAPM to be very similar to a fluid with much shorter ranged molecular interaction. This cancellation of the long forces remains effective for $r > a$ only. When $\sigma \sim a$ is chosen, because the $u_{1,ij}(r)$ is then ensured to be slowly varying across the range of the a, turning off the $u_{1,ij}(r)$ as is done in the mimic system should not alter significantly the structure of the fluid.

5.5.2 Correlations of the Mimic System

Monte Carlo simulations for the mimic system are carried out for two high density states to compare with WL's simulation results for the SAPM. Both states are at the same reduced temperature $\beta^* = 16$, but one is at a higher density ($\rho^* = 1.4$) than the other ($\rho^* = 0.8$) . The ions' averaged spacing is about the order of d_2. From Fig.(5.1) and Fig.(5.2), at $\sigma = 1.2d_2$ one can observe that *all* the partial correlation functions of the mimic system and the full SAPM are strikingly similar. Note that the correlation functions of the SAPM exhibits *charge oscillation* that is characteristic of strong coupling and dense electrolytes. The correlations between the repulsive pairs "++" and "−−" obviously oscillate out of phase with respect to that of the "+−" pair correlation. Clearly, such "charge" oscillation is not unique or solely dictated by the Coulomb interaction, since the mimic system captures this feature almost perfectly. Moreover, these partial correlations are also very different from the oscillatory profiles of a high density hard sphere mixture, as is evident from the very high contact density of the $g_{12}(r)$, for which the attractive tail outside of the hard core is responsible. This also shows that the embedded hard cores can *not* be a good mimic system for the SAPM.

At much lower densities, however, if the SAPM remains at a strong coupling state, i.e., $\Gamma_a > 1$, there is still significant force cancellation at distances greater than a. However, because the ionic fluid is much more compressible at a low density state, turning on the perturbation potential $u_{1,ij}(r)$ from the mimic system would have

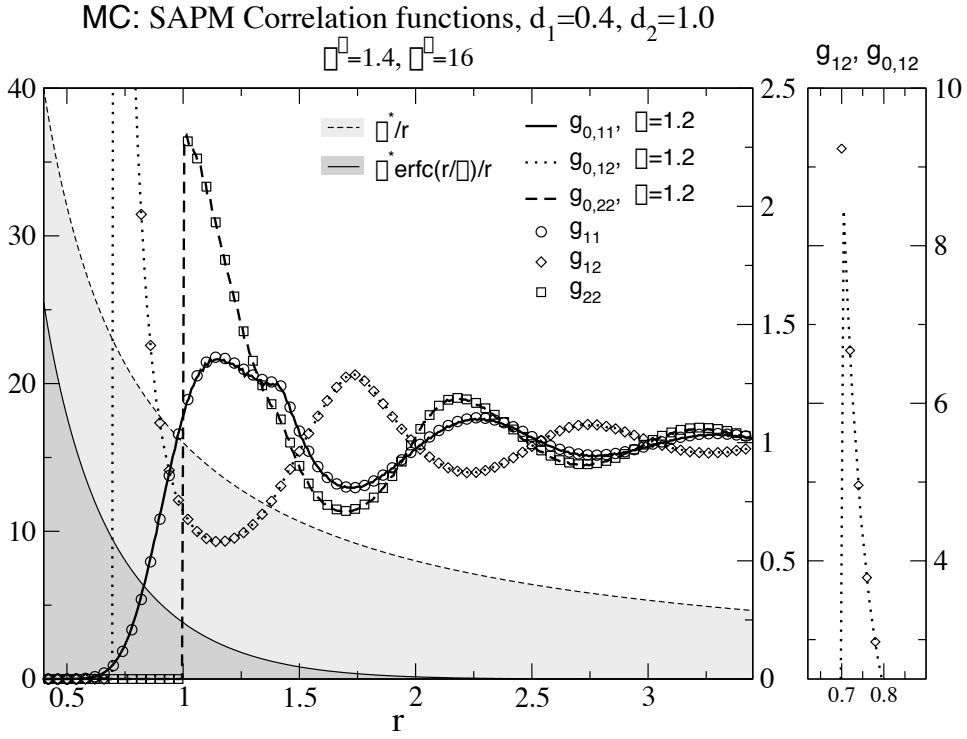

Figure 5.1: The system presented in this graph is at $\rho^* = 1.4$, $\beta^* = 16$. Partial correlation functions of the SAPM, $(g_{ij}(r))$, and of the mimic system, $(g_{0,ij}(r))$, are obtained by Monte Carlo simulations. The SAPM data are taken from reference [81], by the courtesy of J. J. Weis. The full Coulomb interaction $\beta q^2/\epsilon r$ is plotted in comparison with the mimic system's interaction $u_{0,ij}(r)$, using the left axis. The correlation functions are plotted using the right axis. The second graph gives an enlarged view near the peaks of the $g_{0,12}(r)$ and $g_{ij}(r)$: both have high contact values. Note that all length scales are in unit of d_2, which is the hard sphere diameter of species 2.

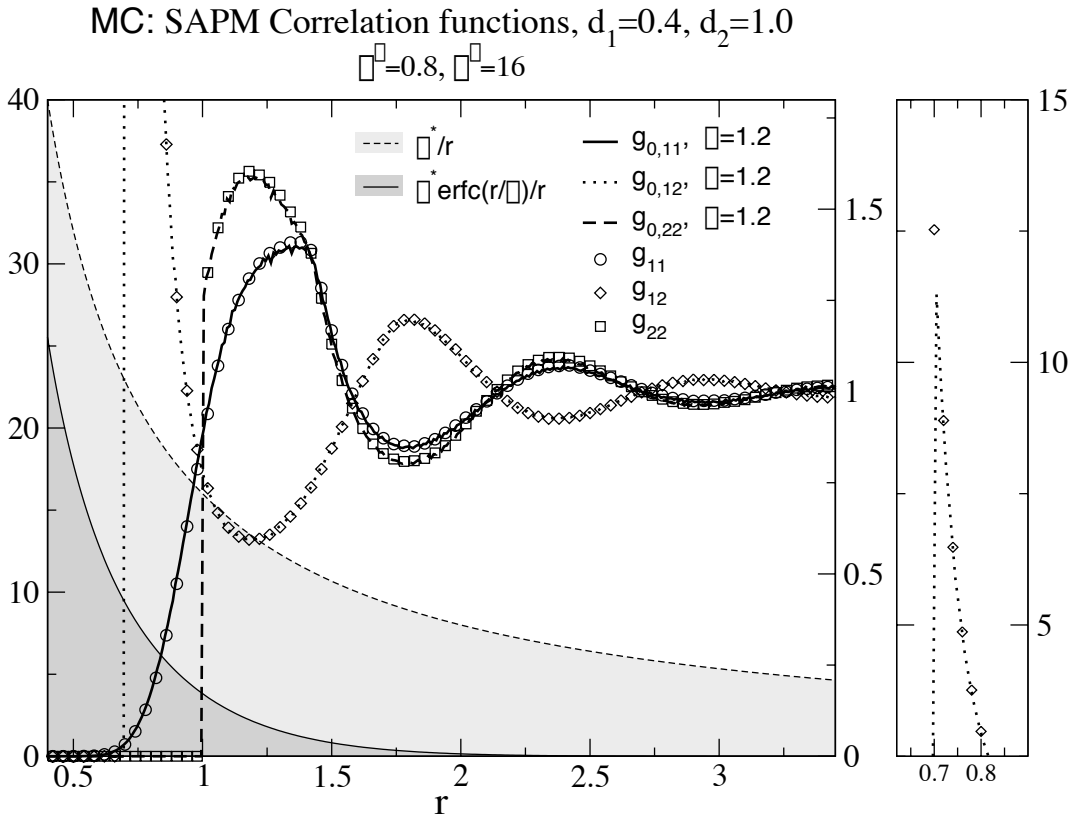

Figure 5.2: Similar to Fig.(5.1), but at another state $\rho^* = 0.8\,\beta^* = 16$.

more influence on the fluid's structure than the high density state just presented. Moreover, because at low densities the ions are further apart, the configuration of the ions no larger have to compromise with the close packing of the hard cores. As such, the SAPM exhibits qualitatively different behavior compared with that seen at high density liquid states.

Monte Carlo simulation results for the mimic system of the SAPM at two strong coupling gas state ($\rho^* = 0.04, \beta^* = 4$ and $\rho^* = 0.04, \beta^* = 9$) are presented in Fig.(5.3) and Fig.(5.4). The a for this state can be roughly estimated by the radius of ionic sphere – $a \sim (4\pi/3\rho^B)^{-1/3} = 1.8d_2$, so $\Gamma_a > 1$ for both states, and the $\sigma_{min} \sim a$ is expected to be sufficient for choosing the mimic system. However, the two states show qualitatively different features in their correlations functions. The lower temperature state in Fig.(5.4) exhibits pronounced peaks at a separation of $r = 1.4d_2$ in like-charge pairs ("++" and "−−") correlation functions, while the partial correlation functions remain monotonic at the high temperature state of Fig.(5.3). At the same low density $\rho^* = 0.04$, the fluid's correlation would have already been well described by the Boltzmann factor of the $w_{d,ij}(r)$ if the hard spheres did not carry the charges. With $\sigma = 2.5d_2$, the mimic systems of both gas states have correlations very similar to those of the SAPM, although the agreement is not as good as it is for high density states, where corrections even at small wave vectors are damped by the low compressibility in the mimic system. high density states. Most notable is that the mimic system can also exhibit first peaks similar

to those of the full system, as seen in Fig.(5.4). Such first peaks of the correlation functions between like-charge pairs are characteristic of triplet, linear clusters of the ions, including "+-+" or "-+-". The peak position thus is the distance between the like charge ions, $d_1 + d_2 = 1.4d_2$ of the linear ion clusters. In principle, the ions can form still longer and bigger clusters, which would be reflected by subsequent peaks of the correlation functions at larger r's . Such higher order ion clusters are especially enhanced by stronger ionic strength. At the state of Fig.(5.4), the ionic strength is not enough for longer clusters to hold against fluctuations, so the correlation functions remain rather structureless after the first peak. On the other hand, $\sigma = 1.2d_2$, which is sufficient to give excellent results for the high density state in Fig.(5.1), is too small at this state to serve as a mimic system and its correlations deviates in magnitude from the SAPM significantly. Still, even for $\sigma = 1.2d_2$, the reference correlations show pairing peaks between "++", "−−" pairs at the same separation of r.

The clustering of the ions has probably been the most challenging phenomenon for theoretical treatments of such systems. It is particularly crucial for the study of critical phenomenon and vapor-liquid coexistence [67, 66, 47, 3]. The Poisson Boltzmann approximation is unable to predict any clustering, neither is it capable of treating the high density states. Integral equation theories such as HNC have been more successful for primitive models high density states [12], but, as WL has

[12]For example, see the HNC result for SAPM computed by WL.

commented, the HNC fails to predict ion clustering and even has no solution when $\rho^* = 0.04, \beta^* = 7.14$. The zeroth order approximation of the LMF theory, $g_{0,ij}(r) \approx g_{ij}(r)$, already builds in the most important feature of ion aggregation in the mimic system. If necessary, particularly for the long-wavelength behavior $g_{ij}(r)$, further improvements can be obtained from the molecular fields $\phi_{R,ij}(r)$ through the LMF equations

$$\phi_{R,ij}(r) = w_{ij}(r) + \int d\mathbf{r}' \sum_h (\rho_{0,ih}(\mathbf{r}'; [\phi_R]) - \rho_h^B) u_{1,hj}(|\mathbf{r} - \mathbf{r}'|), \tag{5.48}$$

which is a special case of the more general expression of Eq.(5.25). Although a theoretical treatment for the mimic system has yet to be developed, and so far we have only resorted to computer simulations, it is nonetheless short-ranged and thus much more manageable in terms of theoretical approximations and qualitative arguments and is computationally much more efficient. The LMF theory provides a self-consistent and very natural framework to decouple the interplay between the long-range interaction from the more complex short-ranged correlation.

5.6 Conclusion

In this chapter, the separation of long-ranged Coulomb interaction and the associated reference system interaction is derived for general charge distributions. The decoupling of the long ranged interaction between charged entities from a mimic system of only short-ranged interaction is systematically controlled by a single parameter σ. The high wave vector components of the molecular potential are truncated by

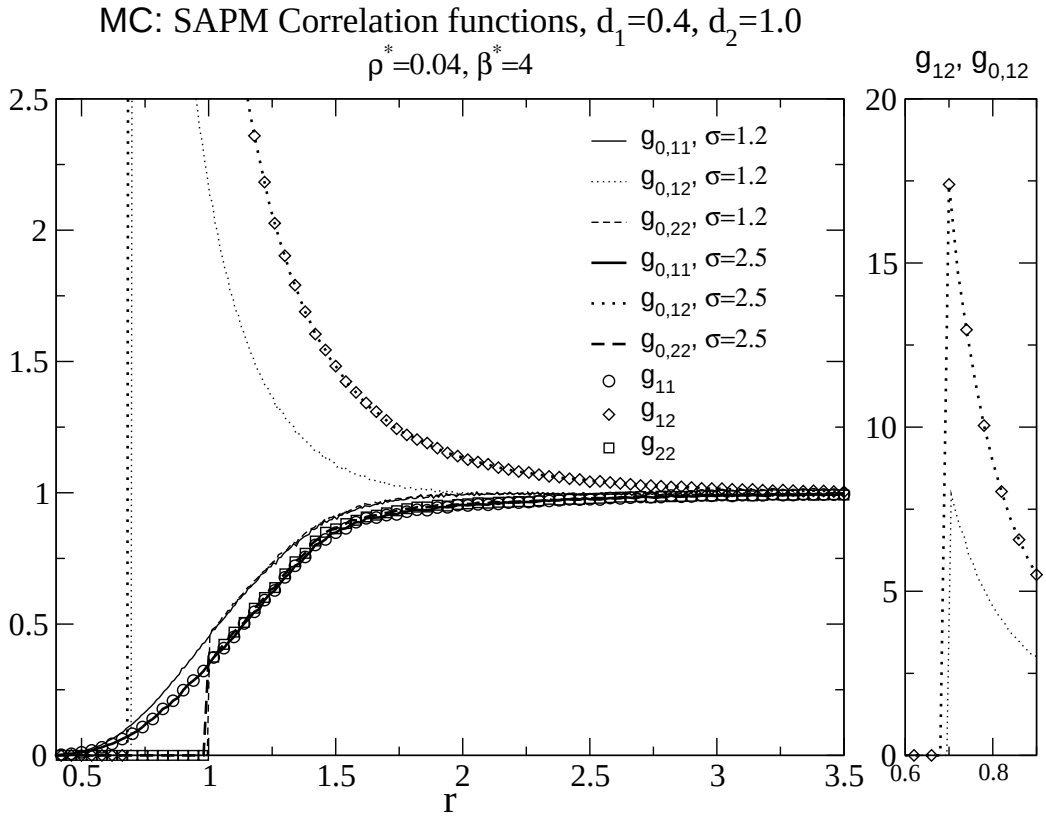

Figure 5.3: Low density gas state SAPM at $\rho^* = 0.04, \beta^* = 4$. Follow the same convention as Fig.(5.1), except that now the correlation functions use the left axis.

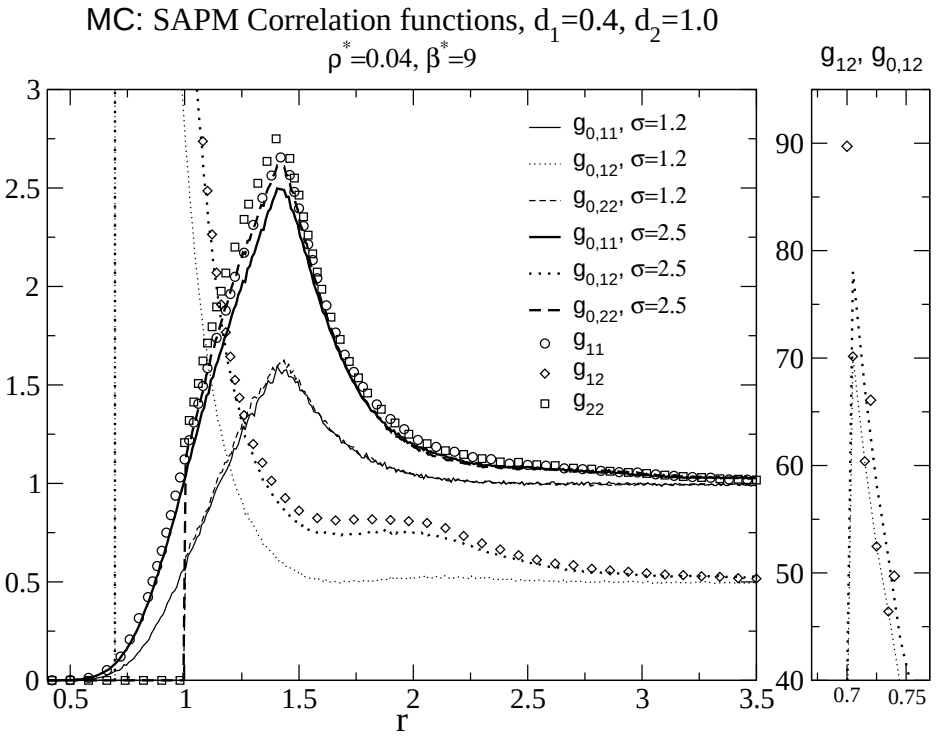

Figure 5.4: Low density gas state SAPM at $\rho^* = 0.04, \beta^* = 9$. Follow the same convention as Fig.(5.1), except that now the correlation functions use the left axis.

a rapidly decaying Gaussian function, whose width is characterized by a parameter σ. The value of σ thus determines the range of the wavelengths to be separated and treated by the LMF. The multipole expansion for Coulomb interactions converges much faster if the Green's function $1/r$, which propagates the interaction between two charge distributions, is replaced by a damped Green's function $\mathrm{erfc}(r/\sigma)/r$. The perturbative potential $u_{1,ij}(\mathbf{R}, \Omega)$ retains only the contribution of the lowest order nonvanishing multipole moments, which are independent of the choice of the body-frame carrying the charge distributions, but the origin of the body-frame should preferably be chosen to minimize the higher order moments. With such a strategy of potential separation derived in this chapter, the LMF can be applied to dipolar systems as well. These ideas are also relevant for computer simulation methods such as fast multipole method and particle-mesh algorithms [16].

These approaches have been tested in the SAPM. The mimic system for SAPM is defined by a single parameter σ. The $u_{0,ij}(r)$ of the mimic system and the size of σ are determined according to the derivation for general charge distributions. By properly choosing σ, mimic systems correlations resemble strikingly the correlation functions of SAPM at strong coupling states, at both low and high densities. Most notably, the mimic system is able to exhibit the characteristic ion pairing peaks observed in the correlations of a low density, strong coupling SAPM. The mimic system, incorporated with the LMF, may provide a very natural way of building in the ion clustering phenomenon which are crucial for the study of the critical point

and liquid-vapor coexistence of electrolyte models.

Chapter 6

Charged Planar Walls and Counterions

It has been observed that like-charged ions can exhibit effective attractions [61, 19, 71, 22, 21]. This came as a surprise since the standard Poisson-Boltzmann approximation (PB) [2], which had been and still is often employed in the study of ion distribution in the presence of external fields, always predicts repulsions. The failure of PB appears twofold. When the ions considered do not vary dramatically in core sizes or valences, such as simple electrolytes, PB can be applied to solve for the bulk correlation functions of the system of interest, but it fails to pick up the "ion-pairing" or even higher order clustering that occurs at low density and for strongly coupled electrolytes (low temperature or large charges) [67, 66, 47, 81, 48]. If the considered charged entities are extremely asymmetric and some species are much more dilute, which is often the case in colloidal suspensions, where macroions are sparsely immersed with much smaller counterions or coions, the macroions are often modeled as external fields of extended dimensions and held in a certain configuration. The counterion distribution in the presence of the held "macroion-fields" is then studied as a function of the configuration of the macroions, and the information

regarding the effective interaction between the macroions can then be extracted from the counterion distribution [8, 21, 23, 54, 22]. Macroion-macroion correlation however is mostly ignored in this kind of setup. The PB approximation for such systems always predicts repulsion between macroions at all macroion separations and ionic strengths. While in the bulk electrolyte models, the PB approximation ignores ion correlations of all pairs when estimating the potentials of mean force, in the second set of models just mentioned, the PB is forced to take into account the macroion-microion correlations explicitly but drops that of macroion-macroion due to the nature of the models.

In previous chapters, the LMF equation has been applied to bulk ionic correlations with the use of short-ranged mimic systems for the ionic system of interest. At low densities and low temperature, "mimic ion-pairing" and increasingly higher order clustering similar to that of ionic systems can be found. The LMF theory can be used to correct the long-wavelength part of the mimic system structure, and the use of a proper mimic system provides a very natural way to build in clustering for describing the full ionic system. For model setups that treat macroion as frozen external fields, the LMF theory can also be shown to naturally bridge the weak coupling regime (which PB can describe) and the strong coupling regime related to the intricate like-charge attraction (where PB fails qualitatively).

In the following we will examine in particular how LMF theory can be applied for two particularly simplified model systems and how the LMF can be simplified

in some important limits.

6.1 A Single Charged Wall with Counterions

6.1.1 Model Description and the Reduced Scales

The first model considered is a globally neutral system comprised of one planar, charged wall and a single species of counterions with no hard cores, as in the OCP. The charged wall is supposed to model the much larger-sized macroions in the case where all macroions are very far apart from each other. This model is simplified to exclude coions so as to focus on the charge density distribution near a macroion. The investigation of this model serves as a introduction of our general approach and prepares for the more complicated two-charged-wall model that will be discussed in the later part of this chapter. Suppose that the wall located at $z = 0$ carries a positive surface charge density $-\lambda e_0$, while the counterions with negative charge qe_0 are restricted to the $z > 0$ half space. Here e_0 is the unit charge, all charge carriers and the background are supposed to have the same dielectric constant ϵ so no additional polarization of the involved medium needs to be considered. The counterions interact with a Coulomb potential $q^2e_0^2/\epsilon r$, so that their interaction strength/range is characterized by

$$l_Q = \beta q^2 e_0^2/\epsilon = q^2 l_B. \tag{6.1}$$

$l_B = \beta e_0^2/\epsilon$ is the Bjerrum length and $r = l_Q$ is the distance where the counterion interaction energy falls to kT. The charged wall creates a constant electric field

$E_w = 2\pi\lambda e_0/\epsilon$ pointing outward from the wall. The E_w can be easily obtained from Gauss' law

$$\oint_\Omega dS\, \mathbf{E}\cdot\hat{\mathbf{n}} = 4\pi Q/\epsilon, \tag{6.2}$$

where Q is the net charge within the volume enclosed by the surface area Ω. The charged wall field E_w then gives rise to an electric potential

$$\phi_w(z) = \frac{-2\pi\lambda e_0}{\epsilon}|z|, \tag{6.3}$$

measured from the wall to z. In fact, $-2\pi/\epsilon(|z-z_0|-|z_0|)$ is the Green's function of Poisson's equation in this planar geometry

$$\frac{\partial^2\phi(z)}{\partial z^2} = -\frac{4\pi}{\epsilon}\delta(z-z_0), \tag{6.4}$$

if $z=0$ is the chosen *zero of potential*, i.e., $\phi(z=0)=0$. This convention will be used throughout the discussion about this single-charged-wall system. The potential energy cost to displace a counterion from the charged wall to a perpendicular distance z away is thus $2\pi\lambda q e_0^2/\epsilon|z|$. The strength and thus the "depth" of the attractive well from the wall felt by a counterion can then be characterized by the Gouy-Chapman length l_G

$$l_G = \frac{\epsilon}{2\pi\beta\lambda q e_0^2} = \frac{q}{2\pi l_Q \lambda}. \tag{6.5}$$

Note that l_G is the distance from the wall at which the attractive potential energy between the wall and a counterion reaches kT, and it can serve as a measure of the "width" of the attractive potential well that the counterions feel. If lengths

are measured in unit of l_G, the electric contribution of this system's Hamiltonian (measured in kT) is

$$\beta\mathcal{H}_{el} = \sum_i \frac{2\pi\beta\lambda q e_0^2}{\epsilon} z_i + \sum_{i,j} \frac{\beta q^2 e_0^2}{\epsilon|\mathbf{r}_i - \mathbf{r}_j|} \tag{6.6}$$

$$= \sum_i \frac{z_i}{l_G} + \sum_{i,j} \frac{l_Q}{|\mathbf{r}_i - \mathbf{r}_j|}, \forall\{z_i\} > 0 \tag{6.7}$$

and can be expressed in terms of only dimensionless reduced quantities as

$$\beta\mathcal{H}_{el} = \sum_i \tilde{z}_i + \sum_{i,j} \frac{\xi}{|\tilde{\mathbf{r}}_i - \tilde{\mathbf{r}}_j|}, \tag{6.8}$$

$$\xi \equiv \frac{l_Q}{l_G} = \frac{2\pi\lambda q^3 {e_0}^2}{\epsilon^2 k^2 T^2}, \tag{6.9}$$

$$\tilde{\mathbf{r}} \equiv \frac{\mathbf{r}}{l_G}. \tag{6.10}$$

Eq.(6.8) embodies the underlying scaling property of $\beta\mathcal{H}_{el}$, which depends only on ξ. The wall surface charge density also be written in dimensionless variables as $l_G^2\lambda = q/2\pi\xi$.

6.1.2 The LMF Equation

Suppose the counterion interaction is $w(r)$: the LMF equation can be applied to this system with the separation of the potential in the form

$$w(r) = u_0(r) + u_1(r) \tag{6.11}$$

$$u_0(r) = \frac{q^2 e_0^2 \mathrm{erfc}(\frac{r}{\sigma})}{\epsilon r}, \tag{6.12}$$

$$u_1(r) = \frac{q^2 e_0^2 \mathrm{erf}(\frac{r}{\sigma})}{\epsilon r}, \tag{6.13}$$

where $u_0(r)$ defines the mimic potential of the counterions, as in the case of the OCP model. The LMF equation can also be expressed in terms of a set of dimensionless

quantities as

$$\tilde{\phi}_R(\tilde{z}) = \tilde{z} + \int d\tilde{\mathbf{r}}_0 \tilde{\rho}(\tilde{z}_0) \frac{\xi \mathrm{erf}(\frac{|\tilde{\mathbf{r}}-\tilde{\mathbf{r}}_0|}{\tilde{\sigma}})}{|\tilde{\mathbf{r}}-\tilde{\mathbf{r}}_0|}, \forall \tilde{z} > 0 \quad (6.14)$$

$$= \infty, \text{ otherwise,} \quad (6.15)$$

with $\tilde{\sigma} \equiv \sigma/l_G$, $\tilde{\rho}(\tilde{z}) \equiv l_G^3 \rho(\tilde{z} l_G)$ and $\tilde{\phi}_R(\tilde{z}) \equiv \beta \phi_R(\tilde{z} l_G)$. Note that the counterion density $\tilde{\rho}(\tilde{z})$ is not subtracted by a finite bulk density in Eq.(6.14), because the zero of potential of this system, unlike the usual case in the bulk fluid, is not set at infinity, but rather at $\tilde{z} = 0$. Also because the linear attractive potential from the wall forms an essentially infinitely deep well, this system does not have a bulk region. The chemical potential or fugacity of the mimic counterions has to be determined self-consistently with the LMF equation such that the counterion density satisfies the neutrality condition of the total system, i.e.,

$$\frac{-q}{2\pi\xi} + \int d\tilde{z} \tilde{\rho}(\tilde{z}) q = 0 \quad (6.16)$$

$$\Rightarrow \int d\tilde{z} 2\pi\xi \tilde{\rho}(\tilde{z}) = 1. \quad (6.17)$$

While $\tilde{\rho}(\tilde{z})$ is the dimensionless particle density of the counterions, $\tilde{n}(\tilde{z}) \equiv 2\pi\xi\tilde{\rho}(\tilde{z})$ thus is the charge density relative to that of the wall surface charge (absolute value, sign not considered). Eq.(6.14) can be integrated over the planar degrees of freedom

as

$$\tilde{\phi}_R(\tilde{z}) = \tilde{z} + \int d\tilde{z}_0 \tilde{\rho}(\tilde{z}_0)\tilde{u}_1(\tilde{z}_0,\tilde{z}), \tag{6.18}$$

$$= \tilde{z} + \int d\tilde{z}_0 \tilde{n}(\tilde{z}_0)\tilde{G}(\tilde{z}_0,\tilde{z}), \tag{6.19}$$

$$\tilde{u}_1(\tilde{z}_0,\tilde{z}) = 2\pi\xi\tilde{G}(\tilde{z}_0,\tilde{z}), \tag{6.20}$$

$$\tilde{G}(\tilde{z}_0,\tilde{z}) \equiv -|\tilde{z}-\tilde{z}_0|\mathrm{erf}(\frac{|\tilde{z}-\tilde{z}_0|}{\tilde{\sigma}}) - \frac{\tilde{\sigma}}{\sqrt{\pi}}e^{-(\frac{\tilde{z}-\tilde{z}_0}{\tilde{\sigma}})^2} + |\tilde{z}_0|\mathrm{erf}(\frac{|\tilde{z}_0|}{\tilde{\sigma}}) + \frac{\tilde{\sigma}}{\sqrt{\pi}}e^{-(\frac{\tilde{z}_0}{\tilde{\sigma}})^2}. \tag{6.21}$$

Note again that the *zero of potential* is consistently chosen at $\tilde{z} = 0$ for all the potentials of interest, and this choice removes the infinities resulting from the direct integration of $\tilde{u}_1(\tilde{\mathbf{r}}_0,\tilde{\mathbf{r}})$ over the planar degrees of freedom. Moreover, the counterion distribution should not depend on such a choice. Any other choice only results in a constant shift in both the $\tilde{\phi}_R(\tilde{z})$ and the chemical potential solution of the mimic system. Note that $\tilde{G}(\tilde{z}_0,\tilde{z})$ is the Green's function of a dimensionless Poisson's equation [38] with a normalized Gaussian planar charge distribution $\frac{\tilde{\sigma}}{\sqrt{\pi}}e^{-(\frac{\tilde{z}-\tilde{z}_0}{\tilde{\sigma}})^2}$centered at $\tilde{z}_0$, i.e, the solution of

$$\frac{\partial^2\tilde{G}(\tilde{z}_0,\tilde{z})}{\partial\tilde{z}^2} = -2(\frac{\tilde{\sigma}}{\sqrt{\pi}})e^{-(\frac{\tilde{z}-\tilde{z}_0}{\tilde{\sigma}})^2}. \tag{6.22}$$

The integral form of Eq.(6.18) can thus also be recast in the form of Poisson's equation as if each counterion carries a "smeared" surface charged density cloud instead of a point as charge

$$\frac{\partial^2\tilde{\phi}_R(\tilde{z})}{\partial\tilde{z}^2} = -2\tilde{n}^*(\tilde{z}), \tag{6.23}$$

$$\tilde{n}^*(\tilde{z}) \equiv \int dz_0\tilde{n}(\tilde{z}_0)\frac{\tilde{\sigma}}{\sqrt{\pi}}e^{-(\frac{\tilde{z}-\tilde{z}_0}{\tilde{\sigma}})^2}. \tag{6.24}$$

Eq.(6.23) is then subjected to the boundary condition that $\tilde{n}(\tilde{z}) = 0, \forall \tilde{z} < 0$ and $\dot{\tilde{\phi}}_R(\infty) = 0$ (which can be seen to be equivalent to the neutrality of the system by Gauss' theorem). As the $\tilde{G}(\tilde{z}_0, \tilde{z})$ in Fig.(6.1) shows, with increasing $\tilde{\sigma}$, the $\tilde{G}(\tilde{z}_0, \tilde{z})$ becomes increasingly slowly varying within a distance $\tilde{\sigma}$ from the position of the charge source and only rises up linearly at larger separations from the charge source, i.e., $\tilde{u}_1(\tilde{z}_0, \tilde{z}) \to -|\tilde{z} - \tilde{z}_0|$ up to a constant.

6.1.3 The Nonuniform Mimic System

Since the external field $\tilde{\phi}(\tilde{z})$ has a Coulomb component, then separating out its long-ranged part, denoted by $\tilde{\phi}_1(\tilde{z})$, naturally leaves a short-range part of the external field $\tilde{\phi}_0(\tilde{z})$. $\tilde{\phi}_1(\tilde{z})$ can be given by the "damped" Green's function $\tilde{G}(\tilde{z}_0, \tilde{z})$ defined by Eq.(6.22), i.e., $\tilde{\phi}_1(\tilde{z}) = -\tilde{G}(0, \tilde{z})$. For our discussion of counterions confined by a charged wall, this separation is defined by

$$\tilde{\phi}_0(\tilde{z}) \equiv |\tilde{z}| - \left(|\tilde{z}| \mathrm{erf}(\frac{|\tilde{z}|}{\tilde{\sigma}}) + \frac{\tilde{\sigma}}{\sqrt{\pi}} e^{-(\frac{\tilde{z}}{\tilde{\sigma}})^2} - \frac{\tilde{\sigma}}{\sqrt{\pi}} \right), \forall \tilde{z} > 0 \tag{6.25}$$

$$\Rightarrow \tilde{\phi}_0(\tilde{z}) = \begin{cases} |\tilde{z}| \mathrm{erfc}(\frac{|\tilde{z}|}{\tilde{\sigma}}) - \frac{\tilde{\sigma}}{\sqrt{\pi}} e^{-(\frac{\tilde{z}}{\tilde{\sigma}})^2} + \frac{\tilde{\sigma}}{\sqrt{\pi}}, \forall \tilde{z} > 0 \\ \infty, \forall \tilde{z} < 0. \end{cases} \tag{6.26}$$

The $\tilde{\phi}_0(\tilde{z})$ quickly approaches a constant once $\tilde{z} > \tilde{\sigma}$, so its corresponding force is weak once outside a range $\tilde{\sigma}$ from the wall. The $\tilde{\phi}_1(\tilde{z})$ combined with the integration over the counterion interactions gives rise to a correction $\tilde{\phi}_{R1}(\tilde{z})$ to the $\tilde{\phi}_0(\tilde{z})$, namely,

$$\tilde{\phi}_{R1}(\tilde{z}) \equiv \int d\tilde{z}_0 [-\delta(\tilde{z}_0) + \tilde{n}(\tilde{z}_0)] \tilde{u}_1(\tilde{z}_0, \tilde{z}), \tag{6.27}$$

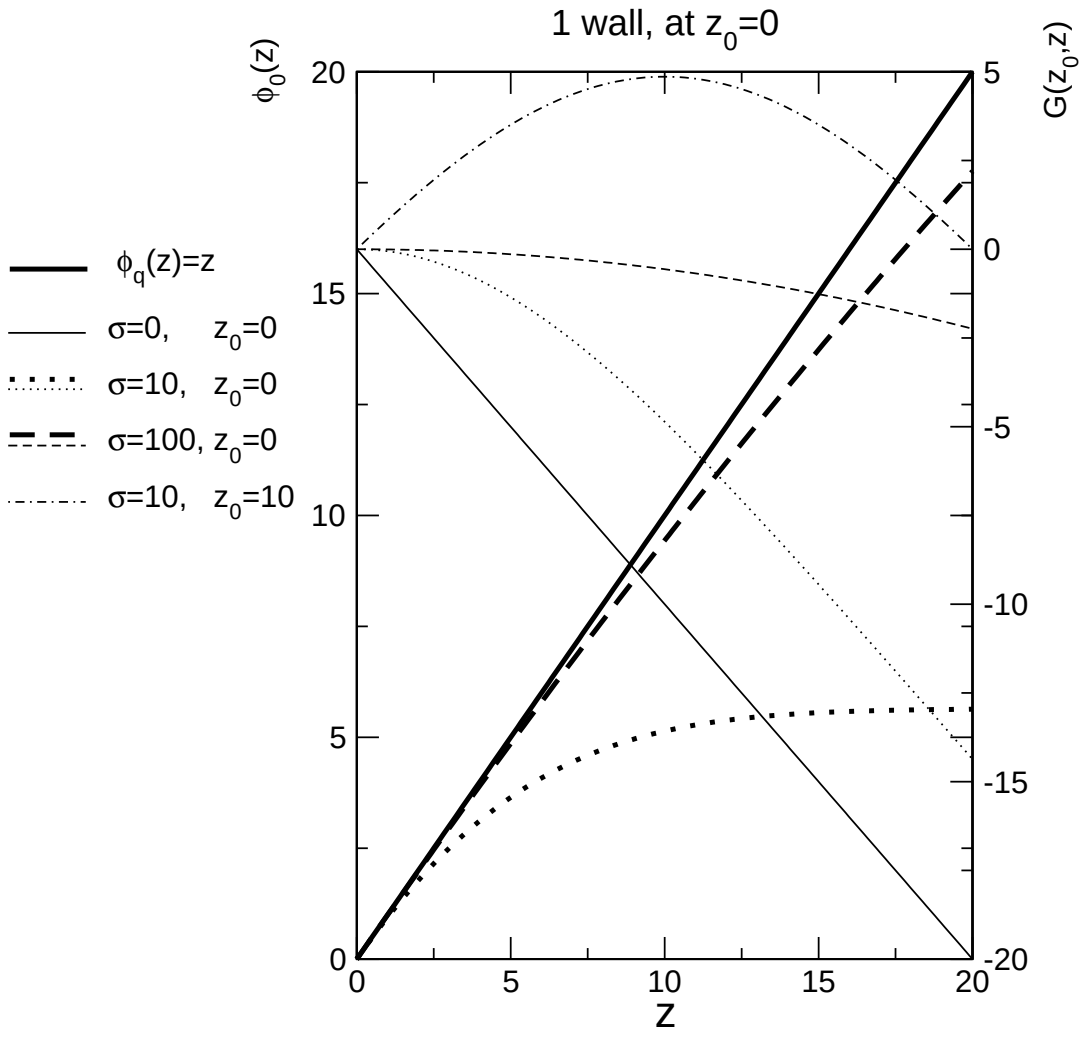

Figure 6.1: The functions $\tilde{\phi}_0(\tilde{z})$ and $\tilde{G}(\tilde{z}_0, \tilde{z})$ for different $\tilde{\sigma}$'s are plotted for the single wall system. Except for the $\tilde{\phi}_q(\tilde{z}) = \tilde{z}$, the other two thick lines are $\tilde{\phi}_0(\tilde{z})$'s, using the left y-axis. The thin lines are $\tilde{G}(\tilde{z}_0, \tilde{z})$, using the right y-axis. $\tilde{G}(\tilde{z}_0, \tilde{z})$ is plotted with respect to $\tilde{z}$, at $\tilde{z}_0 = 0$ and $\tilde{z}_0 = 10$. Note that the superscript tilde is omitted in this and all the following figures.

so that $\tilde{\phi_R}(\tilde{z}) = \tilde{\phi}_0(\tilde{z}) + \tilde{\phi}_{R1}(\tilde{z})$. The $-\delta(\tilde{z}_0)$ in the integrand of Eq.(6.27) is the surface charge density located at $\tilde{z} = 0$ and with a sign opposite to that of the counterions. The neutrality condition of the system, Eq.(6.16), ensures that $d\tilde{\phi}_{R1}(\tilde{z})/d\tilde{z} \equiv \dot{\tilde{\phi}}_{R1}(\tilde{z})$ is local and vanishes at $\tilde{z} = \infty$, which means that the mean force $-\dot{\tilde{\phi}}_R(\tilde{z})$ should also decay to zero, unlike the constant electric field produced by a bare charged wall. Moreover, because $\tilde{u}_1(0, \tilde{z}) \sim 0$ is both weak and slowly varying within a distance $\tilde{\sigma}$ near the wall, $\tilde{\phi}_{R1}(\tilde{z})$ should contribute little correction to the $\tilde{\phi}_0(\tilde{z})$ for $0 < \tilde{z} < \sigma$, and thus only for larger $\tilde{z}$'s does the correction become especially important in determining the asymptotic behavior of the $\tilde{n}(\tilde{z})$. With a $\tilde{\sigma}$ sufficiently big, the distribution of the mimic counterions in the presence of $\tilde{\phi}_0$ thus can be expected to resemble that of the full LMF solution of $\tilde{n}(\tilde{z})$ *at short distances* from the wall, provided that the chemical potential is properly chosen, as will be discussed later. The $\tilde{\phi}_0$ is thus referred to as the *mimic external field*, and the system of mimic particles in the presence of $\tilde{\phi}_0$ is the *nonuniform mimic system*. This is actually similar to the previously discussed cases for correlation functions of bulk fluids. The density profile induced in the mimic system by fixing a mimic particle at the origin is very similar to that of the full ionic system, so here the $\phi_0(\mathbf{r})$ is just the $u_0(\mathbf{r})$.

In addition to this interpretation of ϕ_0 as the remaining interaction after the long ranged and slowly varying part of the ionic interaction is separated out, ϕ_0 can be also understood very simply using a unique feature associated with ionic

systems. From the LMF equation, one would be able to estimate the $\phi_R(\mathbf{r})$ if the $\rho(\mathbf{r})$ could be roughly approximated in advance. In general, one does not know $\rho(\mathbf{r})$ until the LMF equation is solved self-consistently. However, if the external field is charged, the charge density in response to the external field must satisfy an important constraint – it has to neutralize the external charges. For this single charged wall system, the counterion density is thus constrained by Eq.(6.16). So ϕ_0 effectively arises from approximating $\tilde{n}(\tilde{z})$ by $\delta(\tilde{z})$ in the LMF equation, while the $\tilde{\phi}_{R1}(\tilde{z})$ by Eq.(6.27) is the remainder that eventually will need to be accounted for, in particular for the asymptotic properties of the counterion distribution, if the full LMF equation is solved. When using the LMF for treating other shorter-ranged molecular potentials [49, 74], such as that of Lennard Jones potential, one does not have constraints similar to the neutrality condition. As such, the ϕ_0 associated with a general ϕ cannot be so easily estimated in advance.

6.1.4 Choice of σ

In Eq.(6.18), σ must still be chosen properly, and an approximation for the mimic system response to $\phi_R(z)$, is needed in order to solve Eq.(6.18) self-consistently. To pick a proper σ, let's first examine the important length scales that characterize the counterions' spacing and the range of wall-counterion and counterion-counterion interactions. Because the attractive potential is increasingly strong as a counterion is pulled away from the wall, most of the counterions will be concentrated within the range of the Gouy-Chapman length from the wall. The Gouy-Chapman length

l_G is unity in reduced units, so if $\tilde{a}_{3D}$ denotes the average spacing of the counterions in 3 dimensions, then $1/\tilde{a}_{3D}^3 \sim \tilde{\rho}$. Because of the neutrality of the whole system, as demanded by Eq.(6.16), $q/\tilde{a_{3D}}^3 \sim q/2\pi\xi$ suggests that

$$\tilde{a}_{3D} \sim \xi^{\frac{1}{3}}. \tag{6.28}$$

On the x-y plane, the lateral average spacing projected on the x-y plane of the counterions, $\tilde{a}_{\parallel}$, is dictated also by neutrality that $q/\tilde{a}_{\parallel}^2 \sim \frac{q}{2\pi\xi}$, i.e.,

$$\tilde{a}_{\parallel} \sim \xi^{\frac{1}{2}}. \tag{6.29}$$

Also Eq.(6.9) shows that ξ measures the strength and range of the counterion-counterion interaction. So the relative scales of ξ, $\tilde{a}_{3D}$ and $\tilde{a}_{\parallel}$ at weak coupling ($\xi \ll 1$) or strong coupling limit ($\xi \gg 1$) are as follows:

$$\begin{cases} \xi \ll 1 \quad \Longrightarrow \quad \xi \ll \tilde{a}_{\parallel} \ll \tilde{a}_{3D} \ll 1 \\ \xi \gg 1 \quad \Longrightarrow \quad \xi \gg \tilde{a}_{\parallel} \gg \tilde{a}_{3D} \gg 1 \end{cases}. \tag{6.30}$$

In the weak coupling limit where $\xi \ll 1$, the 3D spacing $\tilde{a}_{3D}$ is much smaller than the Gouy-Chapman length. Also, ξ, which indicates the range of the counterion-counterion interaction, is much smaller than $\tilde{a}_{3D}$. This means that in this limit, there are many counterions within the Gouy-Chapman length from the wall that significantly screen the electric potential from the wall. However, these particles are also far apart and and even nearest neighbors feel only weak interaction from each other. The counterions thus can move rather freely in all three dimensions, and the counterions are only weakly confined by the wall's attraction. The counterions' typical

distribution in a weak coupling state is illustrated in Fig.(6.2), and it can be seen that because many layers of counterions can stack perpendicular to the wall, the lateral spacing $\tilde{a}_{\|}$ is much smaller than $\tilde{a}_{3D}$.

In the opposite, strong coupling limit of $\xi \gg 1$, $\tilde{a}_{\|} \gg \tilde{a}_{3D} \gg 1$ indicates that the counterions are bound very tightly to the wall, forming a very thin and strongly correlated 2D layer as shown in the Fig.(6.2). In this limit, the counterion-counterion interaction range ξ is much greater than that of the counterions' lateral spacing $\tilde{a}_{\|}$, which now characterizes the typical spacing of the counterions [54]. Counterions are hardly allowed to have position fluctuations perpendicular to the wall, so any of them essentially finds no neighbors stacked next to it along the $\tilde{z}$ direction. However, the particles are strongly correlated in the x-y plane, their lateral spacing $\tilde{a}_{\|}$ is much greater than the Gouy-Chapman length so that their mutual forces comparably result in very little net $\tilde{z}$-component. Along the lateral direction, the counterions appear to be "crowded" and their interactions significantly overlap. The forces coming from beyond the range of $\tilde{a}_{\|}$ thus to a good extent get canceled, leaving the effective core range of the counterions to be of the order of $\tilde{a}_{\|}$.

In order for the LMF equation to be accurate, σ needs to be chosen to ensure that the $u_1(\mathbf{r})$ is slowly varying across the counterions' core range. For $\xi < 1$, the counterion interaction core range is simply ξ, so $\tilde{\sigma} > \xi$ should suffice. For $\xi > 1$, because of force cancellation, the effective core size is determined by $\tilde{a}_{\|}$, so $\tilde{\sigma} > \tilde{a}_{\|} \sim \xi^{1/2}$ is required. Such a choice for $\tilde{\sigma}$ is a conservative estimate and it

may be actually more than needed. For example, when $\xi < 1$, and $\tilde{a}_{\|} < 1$, each counterion sees only few neighbors that hardly contribute significant mean forces to it, so even if the u_1 is not smoothed, the error of mean potential estimate could still be negligible.

Hence forward $\tilde{a}$ will refer to the relevant length scale which characterizes the *typical spacing* of the counterions. $\tilde{a}$ depends on the state of the system, $\tilde{a} \sim \tilde{a}_{\|}$ for $\xi \gg 1$, while $\tilde{a} \sim \tilde{a}_{3D}$ for $\xi \ll 1$. As a conservative estimate, $\tilde{a}$ can be always chosen to be the larger of $\tilde{a}_{3D}$ and $\tilde{a}_{\|}$, and the minimum working $\tilde{\sigma}$, $\tilde{\sigma}_{min}$, is about $\tilde{\sigma} \sim \xi$, when $\tilde{a} > \xi$ (which means counterions on average feel only weak interaction with each other), but $\tilde{\sigma}_{min} \sim \tilde{a}$ for $\tilde{a} < \xi$ (counterions' interaction extends beyond the averaged spacing $\tilde{a}$ and are forced to explore their strongly repulsive cores which cause significant short-ranged correlation among the counterions).

6.1.5 Approximation for Mimic System's Response to the Molecular Field

To solve the LMF equation Eq.(6.18), one needs to decide a proper chemical potential for the mimic system and also how the mimic system would respond to the molecular field, i.e., a theory for $\tilde{\rho}_0(\tilde{z}; \tilde{\mu}_0, [\tilde{\phi}_R])$, since the LMF equation approximates that $\tilde{\rho}_0(\tilde{z}; \tilde{\mu}_0, [\tilde{\phi}_R]) \approx \tilde{\rho}(\tilde{z}; \mu(\xi), [\phi])$. Here, the chemical potential of the full system is given implicitly by the coupling parameter ξ, which constrains the total surface particle density of the counterions.

When $\xi < 1$, as discussed above, $\tilde{\sigma}$ can be chosen as $\tilde{\sigma} \sim \xi$. The counterions

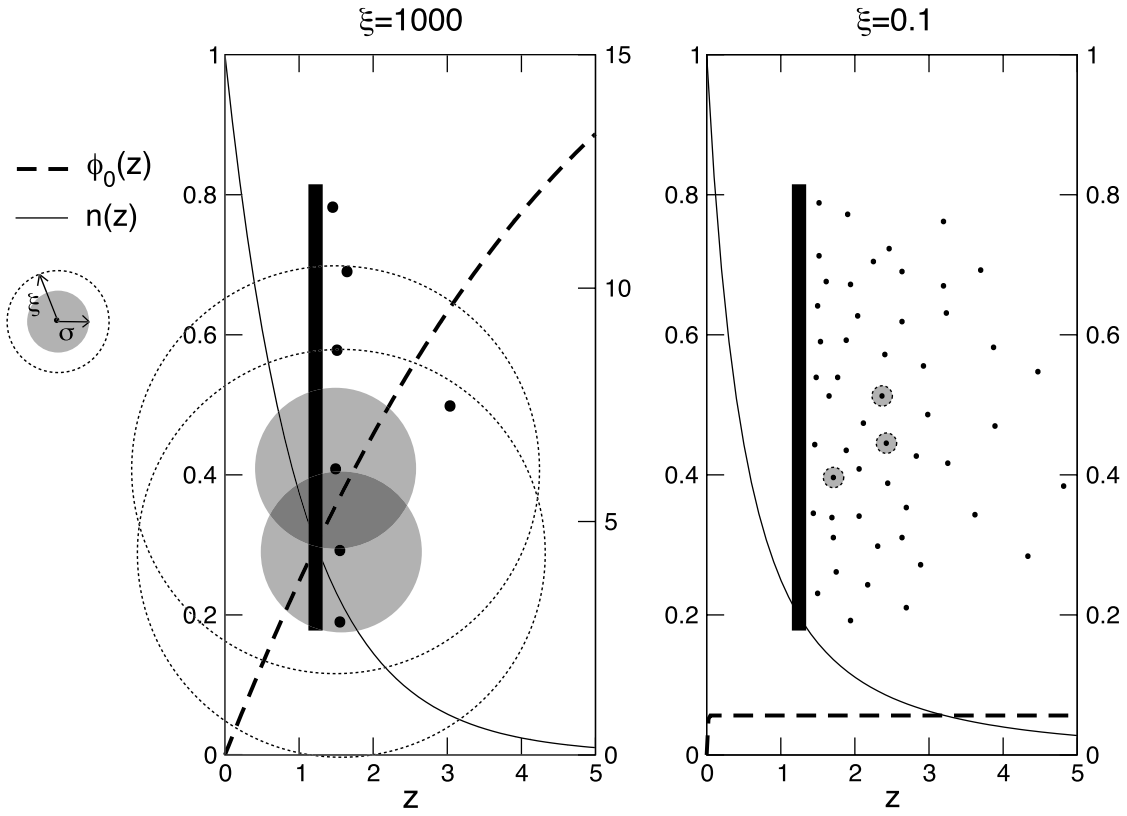

Figure 6.2: The $\tilde{\phi}_0(\tilde{z})$ of the one wall system is plotted for a strong coupling ($\xi = 1000$) and a weak coupling ($\xi = 0.1$) state. The $\tilde{n}(\tilde{z})$ of $\xi = 1000$ is estimated by $\tilde{n}(\tilde{z}) \sim \exp(-\tilde{\phi}_0(\tilde{z}))$ and the PB solution $1/(\tilde{z}+1)^2$ is plotted for $\xi = 0.1$. The counterion distributions for the two states are also schematically presented. The gray circles characterize the radii $\tilde{\sigma}$ of the mimic systems, and $\tilde{\sigma} = \xi^{1/2}$ for $\xi = 1000$ and $\tilde{\sigma} = \xi$ for $\xi = 0.1$. The dotted circles are the length of ξ.

are thus only interacting weakly, having an average spacing $\tilde{a} \sim \xi^{1/3}$ much greater than their pair interaction range ξ. The mimic particles are supposed to respond to the $\tilde{\phi}_R$ with the same distribution as that of the counterions, which means that the mimic particles are also in a very dilute and weakly interacting state. The ideal gas approximation for the mimic particles' singlet density

$$\tilde{n}(\tilde{z}) = \tilde{n}_0(\tilde{z}) \approx Ae^{-\tilde{\phi}_R(\tilde{z})} \tag{6.31}$$

should thus suffice. Because $\tilde{n}(\tilde{z})$ is the charge density, the constant A in Eq.(6.31) absorbs the fugacity. The approximation of Eq.(6.31) states that only the external field $\tilde{\phi}_R(\tilde{z})$ is responsible for the spatial variation of the $\tilde{n}(\tilde{z})$ and the A determines the total surface particle density of both the full and the mimic system. $\tilde{n}(z)$ can then be obtained by solving Eq.(6.31) and Eq.(6.18) self-consistently , with A determined by the neutrality condition Eq.(6.16).

If $\tilde{\sigma} \ll 1$, Eq.(6.31) with the LMF equation reproduces the PB approximation, which is exact as $\xi \to 0$ [2], and the $\tilde{n}(\tilde{z})$ decays algebraically

$$\lim_{\xi \to 0} \tilde{n}(\tilde{z}) = \tilde{n}_{PB}(\tilde{z}) = \frac{1}{(\tilde{z}+1)^2}. \tag{6.32}$$

Eq.(6.32) corresponds to

$$\tilde{\phi}_R(\tilde{z}) \to \tilde{\phi}_{PB}(\tilde{z}) = 2\log(\tilde{z}+1). \tag{6.33}$$

Note that although $\tilde{\phi}_{PB}(\tilde{z})$ diverges as $\tilde{z} \to \infty$, the attractive force from the wall $-\frac{d\tilde{\phi}_{PB}(\tilde{z})}{d\tilde{z}} = \frac{-2}{(\tilde{z}+1)}$ decays to zero at large $\tilde{z}$, in contrast to the *constant* attraction

from the wall when there is only one counterion present. Seen far enough from the wall, the charged wall would appear *screened* by the counterions. However, it still takes an infinite amount of work for a counterion to escape from the wall, though the work is "much reduced", and this agrees with the fact that eventually all the counterions are bound to the wall such that they constitute a finite surface charge density which neutralizes the wall charges. The screening of the wall-counterion interaction appears to be weaker than that of the ion-ion interaction in a bulk electrolyte fluid because in this model there are only counterions. Although the wall charges can be screened by the oppositely charged counterions, there are no co-ions to screen a counterion, so the counterions can not form a bulk phase far away from the charged wall. The profile $\tilde{n}(\tilde{z})$ and a schematic presentation of how the the counterions are distributed within the wall's confining potential well is shown in the $\xi = 0.1$ case of Fig.(6.2).

In the opposite limit, when $\xi \gg 1$, the $\tilde{\sigma}$ should be chosen to be at least $\tilde{\sigma} \approx \tilde{a}_{\|} \sim \xi^{1/2}$. This means that $\tilde{\sigma} \gg 1$, i.e., $\tilde{\sigma}$ is much greater than the Gouy-Chapman length. Because the $u_1(\tilde{z}_1; \tilde{z}_2)$ is small for $\tilde{z}_1, \tilde{z}_2 < \tilde{\sigma}$, it thus remains very small in essentially all of the $\tilde{z}$ space. The onset of the linear behavior of the $\tilde{G}(\tilde{z}_1; \tilde{z}_2)$ is delayed to increasingly large distances as $\xi \to \infty$. In such a limit, the integration of the $\tilde{G}(\tilde{z}_1, \tilde{z}_2)$ has no contribution for any finite separation from the wall, so the molecular field reduces to the bare electric potential energy between the

wall and a single counterion, i.e.,

$$\tilde{\phi}_R(\tilde{z}) \;=\; \tilde{z},\ \forall \tilde{z} > 0. \tag{6.34}$$

The mimic particles' core size is about $\tilde{\sigma}$, which becomes much bigger than the width of the attractive potential well $\tilde{\phi}_R(\tilde{z})$'s width, which is unity. For the mimic particles, this is actually a very *confining* potential well, and is similar to the "narrow slit" case discussed in chapter **2**. When the potential well appears to be so narrow that it essentially could accommodate only a single 2D layer of mimic particles and allows little position fluctuation perpendicular to the wall, a mimic particle feels forces from its neighbors mostly along the lateral direction, resulting in little net force perpendicular to the wall. In the strong coupling limit, only the external field $\tilde{\phi}_R$ contributes to the $\tilde{z}$-component of the mean force felt by the mimic particles. Perpendicular to the wall, the mimic particles appear to be non-interacting, so the probability of finding a mimic particle is only proportional to $e^{-\tilde{\phi}_R(\tilde{z})}$. This agrees with the results reported earlier for the "narrow slit" limit, at which the fluid appears ideal gas like and the contribution from the $C^{(1)}(\mathbf{r})$ vanishes from the sum rule Eq.(13.1).

This means that, the approximation in Eq.(6.31), which is justified for a weak coupling state, should also apply in the strong coupling limit, though for a very different reason! Using this approximation and the fact that in the strong coupling limit, the $\tilde{\phi}_R(\tilde{z})$ is given by the bare wall potential (Eq.(6.34)), the LMF equation

clearly reduces to

$$\lim_{\xi\to\infty} \tilde{n}(\tilde{z}) = e^{-\tilde{z}}, \tag{6.35}$$

where the constant A is fixed by the neutrality condition. This is in fact an exact result in the limit $\xi \to \infty$, as has been discussed previously by other authors [54]. The PB approximation, though exact in the weak coupling limit, fails to capture the qualitative behavior of the counterions in this opposite regime. In fact, the argument above for the density response of the mimic particles also applies to the counterions directly, since for the counterions the $\tilde{\phi}(\tilde{z})$ is also a very confining "narrow slit". By the same token the counterion response can be deduced to be that of Eq.(6.35) as well, consistent with the result from the LMF theory. Contrary to the weak coupling limit, when $\xi \gg 1$, $\tilde{\phi}_R(\tilde{z}) \approx \tilde{\phi}(\tilde{z}) = \tilde{z}$ recovers the bare potential of the charged wall, so the charged wall is hardly screened. This has to do with the huge repulsive cores that the counterions must force upon each other. Because of the strong repulsive cores, the counterions cannot arrange themselves perpendicular to the wall and still stay in the narrow well. The PB approximation completely ignores such short-range repulsions between the counterions. In fact, the PB in the context of the LMF equation is equivalent to choosing an ideal gas mimic system. As a result, the PB can not cope with a regime where such counterion correlation plays a major role. But the lowest order Boltzmann factor in Eq.(6.31) can readily take into account of such "size" induced correlations in the mimic system. The profile $\tilde{n}(\tilde{z})$ and a schematic presentation of how the the counterions are distributed within

the wall's confining potential well is shown in the $\xi = 1000$ case of Fig.(6.2).

Though arising from different physical reasons, the Boltzmann factor approximation Eq.(6.31) turns out to be very accurate (in fact exact) for both the weak and strong coupling limits. Thus it may well be a reasonable approximation for the mimic system for all ξ's and to naturally bridge the very different regimes of ξ. The combined use of Eq.(6.35) with the LMF equation Eq.(6.18) is the *Mimic Poisson Boltzmann* (MPB) approximation used for low density OCP and OCCHS in Chapter 4.

6.1.6 The Asymptotic Solution of MPB and the Absorption Layer

At large $\tilde{z}$'s, where both $\tilde{n}(\tilde{z})$ and $\dot{\tilde{n}}(\tilde{z})$ are approaching zero, then $\tilde{n}^*(\tilde{z}) \approx \tilde{n}(\tilde{z})$ ($\tilde{n}^*(\tilde{z})$ defined in Eq.(6.24)). Suppose this approximation starts being valid from $\tilde{z} = \tilde{z}^*$, then Poisson's equation Eq.(6.23) reduces to the PB form

$$\ddot{\tilde{\phi}}_R(\tilde{z}) \approx -2\tilde{n}(\tilde{z}) \tag{6.36}$$

$$\approx -2Ae^{-\tilde{\phi}_R(\tilde{z})}, \forall \tilde{z} > \tilde{z}^*. \tag{6.37}$$

After multiply both sides of Eq.(6.37) by $\dot{\tilde{\phi}}_R(\tilde{z})$, the equation can be integrated to yield

$$\frac{1}{2}(\dot{\tilde{\phi}}_R)^2 = 2Ae^{-\tilde{\phi}_R(\tilde{z})} + C_1, \tag{6.38}$$

where C_1 is the constant of integration, but $C_1 = 0$ since charge neutrality of the whole system requires that $\dot{\tilde{\phi}}_R(\infty) = 0$. Eq.(6.38) can be integrated again to give

$$\frac{1}{\sqrt{A}} e^{\frac{1}{2}\tilde{\phi}_R(\tilde{z})} = \tilde{z} + C_2. \tag{6.39}$$

Since $\tilde{n}(\tilde{z}) = Ae^{-\tilde{\phi}_R(\tilde{z})}$, Eq.(6.39) predicts an asymptotic algebraic decay of the MPB approximation

$$\tilde{n}(\tilde{z}) \approx \frac{1}{(\tilde{z} + C_2)^2}, \; \forall \tilde{z} > \tilde{z}^*. \tag{6.40}$$

Eq.(6.40) has a form to the PB solution but with a different decay constant C_2 usually greater than unity for finite ξ's. The exact asymptotic decay of $\tilde{n}(\tilde{z})$ is believed to be the form of Eq.(6.40) [6]. This analysis is equally valid in general for the LMF, as long as the theory for the response of the mimic system to the $\tilde{\phi}_R$ eventually goes as $e^{-\tilde{\phi}_R}$ for large $\tilde{z}$'s, where the $\tilde{\phi}_R$ becomes very large and the density of the counterions or the mimic particles is very small. $\tilde{z}^*$ thus divides the space into two regions of different nature. For $\tilde{z} < \tilde{z}^*$ the counterions are tightly confined to the wall and appear as an *absorption layer* which effectively reduces the surface charge density of the wall. For $\tilde{z} > \tilde{z}^*$, counterions see an effective wall with reduced surface density. The counterions that escape to $\tilde{z} > \tilde{z}^*$ are only weakly bound to the wall and are far apart from each other, so the PB approximation eventually becomes legitimate at large $\tilde{z}$'s. In the absorption layer, the repulsive cores sizes of the counterions appear to be much bigger than the potential well near the wall. Most of the counterions are forced to distance themselves from each other along the lateral

direction and near the wall. The counterion behavior inside the absorption layer is thus very different from the asymptotic region, and the counterion correlation due to their strong cores is most important when describing the counterion distribution near the wall. The LMF approximation fixes the core correlation of the counterions in the mimic system by an appropriate choice of $\tilde{\sigma}$ while the subsequent long-ranged perturbation of $\tilde{u}_1(\tilde{\mathbf{r}})$ causes little change on short-range structure of the mimic system. The larger the ξ is, the more counterions are tightly absorbed to the wall, as shown in the strong coupling case of Fig.(6.2), and the "loosely bound region" is delayed further from the wall, corresponding to increasingly larger $\tilde{z}^*$'s. Thus in the $\xi \to 0$ limit, all the counterions are loosely bound, such that $\tilde{z}^* = 0$ and PB solution $\tilde{n}(\tilde{z}) = 1/(\tilde{z}+1)^2$ is recovered for all $\tilde{z}$'s. In the opposite limit of $\xi \to \infty$, the $\tilde{n}(\tilde{z})$ is dominated by the confinement of the mimic particles in the bare field $\tilde{n}(\tilde{z}) \to e^{-\tilde{z}}$ for all $\tilde{z}$'s and the "loosely bound region" is pushed to infinitely far away.

6.1.7 The Chemical Potential of the Mimic System

In principle, the chemical potential of the mimic system should be solved along with the LMF equation, and the converged solution for the counterion density is $\tilde{\rho}(\tilde{z}; \mu(\xi), [\tilde{\phi}]) = \tilde{\rho}_0(\tilde{z}; \mu_0, [\tilde{\phi}_R])$ [74]. However, for strong coupling states, the correction from $\tilde{\phi}_{R1}(\tilde{z})$ to $\tilde{\rho}_0(\tilde{z}; \mu_0, [\tilde{\phi}_0])$ causes little modification within a distance $\tilde{\sigma}$ from the wall. The counterion density near the wall thus can be often estimated by $\tilde{n}(\tilde{z}) \approx \tilde{n}_0(\tilde{z}; \mu_0, [\tilde{\phi}_0])$. Because the $\tilde{\phi}_R(\tilde{z})$ eventually becomes infinite, $\tilde{\rho}_0(\tilde{z}; \mu_0, [\tilde{\phi}_R]) \to 0$ as $\tilde{z} \to \infty$ such that the integration of $\tilde{\rho}_0(\tilde{z}; \mu_0; [\tilde{\phi}_R])$ gives rise to

a finite surface charged density and maintains the neutrality of the system. However, as shown in Fig.(6.1) $\tilde{\phi}_0(\tilde{z})$ eventually approaches a plateau. This means that the confinement of the mimic particles by $\tilde{\phi}_0(\tilde{z})$ is only local, and eventually the particles are able to escape the near-wall well and form a bulk state with nonzero density far away enough from the wall, although the bulk density would be very low for $\xi \gg 1$. $\tilde{\rho}_0(\tilde{z}; \mu_0, [\tilde{\phi}_0])$ is thus inevitably unnormalizable, and as a result it is impossible to determine the μ_0 by imposing the neutrality condition. This simply reflects the fact that although the mimic system could have a local structure near the wall very similar to that of the full system, it asymptotically has to deviate from that of the full system, if no correction of $\tilde{\phi}_{R1}(\tilde{z})$ is considered. However, because $\tilde{n}(\tilde{z}) \approx \tilde{n}_0(\tilde{z}; \mu_0, [\tilde{\phi}_0])$ should be only expected to hold for finite $\tilde{z}$'s anyway, the μ_0 does *not* have to take care of the asymptotic behavior of $\tilde{n}_0$. A μ_0 that best helps mimic $\tilde{n}(\tilde{z})$ near the wall is a more desirable (and possible!) choice. Fortunately, for this system of one charged wall, there is an exact *contact theorem* [8, 21, 22]

$$\tilde{n}(0_+) = 1 \tag{6.41}$$

that in fact serves as a perfect constraint for the μ_0 to ensure that the $\tilde{n}_0(\tilde{z}; \mu_0, [\tilde{\phi}_0])$ is similar to the exact $\tilde{n}(\tilde{z})$ near the wall. So as a zeroth order approximation if $\tilde{\phi}_{R1}(\tilde{z})$ is not yet solved from the LMF equation, the μ_0 of the mimic system can be determined by requiring $\tilde{n}_0(0_+; \mu_0, [\tilde{\phi}_0]) = 1$. The value of μ_0 will depend on how the mimic system is described, and will be in general different from that determined self-consistently from the LMF equation.

It is shown in Appendix E that the PB approximation and the converged solution of the LMF (thus including MPB) satisfy the contact theorem. Derivations of this are in the appendix E. Not all theories will be able to satisfy the contact theorem. In particular, the recently developed pair level PB theory [6], *Test Charge Mean Field* theory (TCMF), that also gives the exact SC limit in general does not satisfy the contact theorem for finite ξ values, and further more, predicts an incorrect asymptotic decay of $c(\xi)/(\tilde{z}+1)^2$.

6.2 Two Walls with Counterions

While the system of one charged wall with counterions studied above models the macroion-counterion distribution when macroions are all very far apart, now we discuss a system which models explicitly how two macroions, separated by a finite distance, experience an effective interaction mediated by the counterions. experience the counterion meditated interaction. Consider two parallel charged planar walls facing parallel to each other, with single component counterions in between the walls. Each of the walls is charged with a surface density λe_0 and each counterion carries a point charge qe_0. The two walls are separated by a distance d. The following discussion will use same reduced unit convention as in the discussion of the one wall case, and we let

$$\tilde{d} \equiv d/l_G. \tag{6.42}$$

The whole system is neutral, therefore, the counterions should form a slab of charges where the total charge confined per unit area of the wall neutralizes that of the two walls. The one wall system is just the limit that $\tilde{d} \to \infty$.

The net electric field between the walls is zero, since the constant electric fields from both walls are equal in their magnitudes but opposite in direction in between the walls. Thus the net electric potential in between the walls is a constant, and will be set to be zero. The zero of potential in general will be set at $\tilde{z} = \tilde{d}/2$ for the sake of the reflection symmetry. The LMF solution will not depend on the choice of the zero of potential. The LMF equation for this system now is

$$\tilde{\phi}_R(\tilde{z}) = \begin{cases} \int_0^{\tilde{d}} d\tilde{z}_0 \tilde{n}(\tilde{z}_0)\tilde{G}(\tilde{z}_0, \tilde{z}), \ \forall \tilde{z} \in [0, \tilde{d}] \\ \infty, \text{ otherwise,} \end{cases} \tag{6.43}$$

and $\tilde{G}(\tilde{z}_0, \tilde{z})$ is defined as in Eq.(6.21). Here the electronic part of the molecular field only comes from the *nonuniformity of the counterions*. The nonuniform mimic system is then the mimic particles with an appropriate $\tilde{\sigma}$ in the presence of the external field $\tilde{\phi}_0$ where

$$\tilde{\phi}_0(\tilde{z}) = \begin{cases} |\tilde{z}|\text{erfc}(\frac{|\tilde{z}|}{\tilde{\sigma}}) + |\tilde{z} - \tilde{d}|\text{erfc}(\frac{|\tilde{z}-\tilde{d}|}{\tilde{\sigma}}) - \tilde{d}\text{erfc}(\frac{\tilde{d}}{2\tilde{\sigma}}) \\ -\frac{\tilde{\sigma}}{\sqrt{\pi}}(e^{-(\frac{\tilde{z}}{\tilde{\sigma}})^2} + e^{-(\frac{\tilde{z}-\tilde{d}}{\tilde{\sigma}})^2} - 2e^{-(\frac{\tilde{d}}{2\tilde{\sigma}})^2}), \ \forall \tilde{z} \in [0, \tilde{d}] \\ \infty, \text{ otherwise.} \end{cases} \tag{6.44}$$

The left most graph of Fig.(6.3) shows how the $\tilde{\phi}_0(\tilde{z})$ of a two-wall system is simply given by the summation of the single-wall fields $\tilde{\phi}_0^{1w}(\tilde{z})$ from the walls at $\tilde{z} = 0, \tilde{d}$.

The LMF's correction to the $\tilde{\phi}_0(\tilde{z})$ is then

$$\tilde{\phi}_{R1}(\tilde{z}) = \int_0^{\tilde{d}} d\tilde{z}_0[-\delta(\tilde{z}_0) - \delta(\tilde{z}_0 - \tilde{d}) + \tilde{n}(\tilde{z}_0)]\tilde{G}(\tilde{z}_0, \tilde{z}). \tag{6.45}$$

The $\tilde{\phi}_{R1}(\tilde{z})$ of Eq.(6.45) integrates over the mean electric potential energy contributed by the surface charges of both walls and the counterions. A counterion near one of the walls would feel the rest of the counterions' repulsion pushing it against the wall, while near the middle of the two walls ($\tilde{z} = \tilde{d}/2$), because of the symmetry of the system, there are about equal number of counterions pushing from both sizes, so the net force on a counterion near the middle should be small. This as a result causes the counterions to accumulate near the two walls. The electronic interaction from the walls has no direct effect on the *counterion distribution* except implicitly through determining how many counterions per unit area have to be present. However, without the wall surface charges, it would take infinite energy per unit area to assemble the counterions in between the walls at finite separations and the pressure between the walls certainly would be different, too. Because there are two charged walls, the neutrality condition for this system is now $\int d\tilde{z}\tilde{n}(\tilde{z}) = 2$.

For two walls, the average lateral spacing $\tilde{a}_{\parallel}$ of the counterions is still determined as before by $\tilde{a}_{\parallel} \sim \xi^{1/2}$, while the $\tilde{a}_{3D}$ now involves the interplay between the Gouy-Chapman length and the wall separation $\tilde{d}$. When counterions *spread* rather uniformly from one wall to the other, $\tilde{a}_{3D}$ can be roughly estimated by $\tilde{d}/\tilde{a}_{3D}^3 \sim q/2\pi\xi$, using the surface charge density $q/2\pi\xi$ of the wall and the integration range $\tilde{d}$ of the counterion distribution, so $\tilde{a}_{3D} \sim (\tilde{d}\xi)^{1/3}$. On the other hand,

especially at strong coupling and when the walls are "well separated" from one another, the counterions tend to be tightly bound next to the walls, and the width of attractive wells near the walls are more characterized by the Gouy-Chapman length l_G, which is order of unity in the reduced units. In this later case, as for the one wall system previously discussed, the $\tilde{a}_{3D} \sim \xi^{1/3}$. To consistently use the LMF equation, as with the case of one wall, $\tilde{\sigma}$ in general has to be chosen such that $\tilde{\sigma} \geq \tilde{a} \sim \xi^{1/2}$ for strongly confined counterions, since the counterions' spacing is characterized by their lateral distance. However, $\tilde{\sigma_{min}} \sim \xi$ when counterions' spacing is greater than counterions' interaction range ξ (that is, dilute counterions). The following will analyze in more details the LMF' and the MPB solutions for several limiting regimes.

6.2.1 Weak Coupling $\xi \ll 1$

For this system at this limit of $\xi \ll 1$, the hard wall potential and the single wall attractive well ($\sim \tilde{z}$) compete as two sources of confinement on the counterions. The width of single wall potential well is measured by the Gouy-Chapman length and is unity in reduced units. When $\tilde{d} > 1$, the single wall potential well is effective and localizes the counterions next to each wall within the Gouy-Chapman length, so the $\tilde{a}_{3D} \sim \xi^{1/3}$ just as was estimated for the one wall system. On the other hand, when $\tilde{d} < 1$, the single wall potential well becomes shallow in between the hard walls and the counterions do not localize near each wall but are spread rather uniformly across the slit width. It is then the hard wall potential that is responsible for the

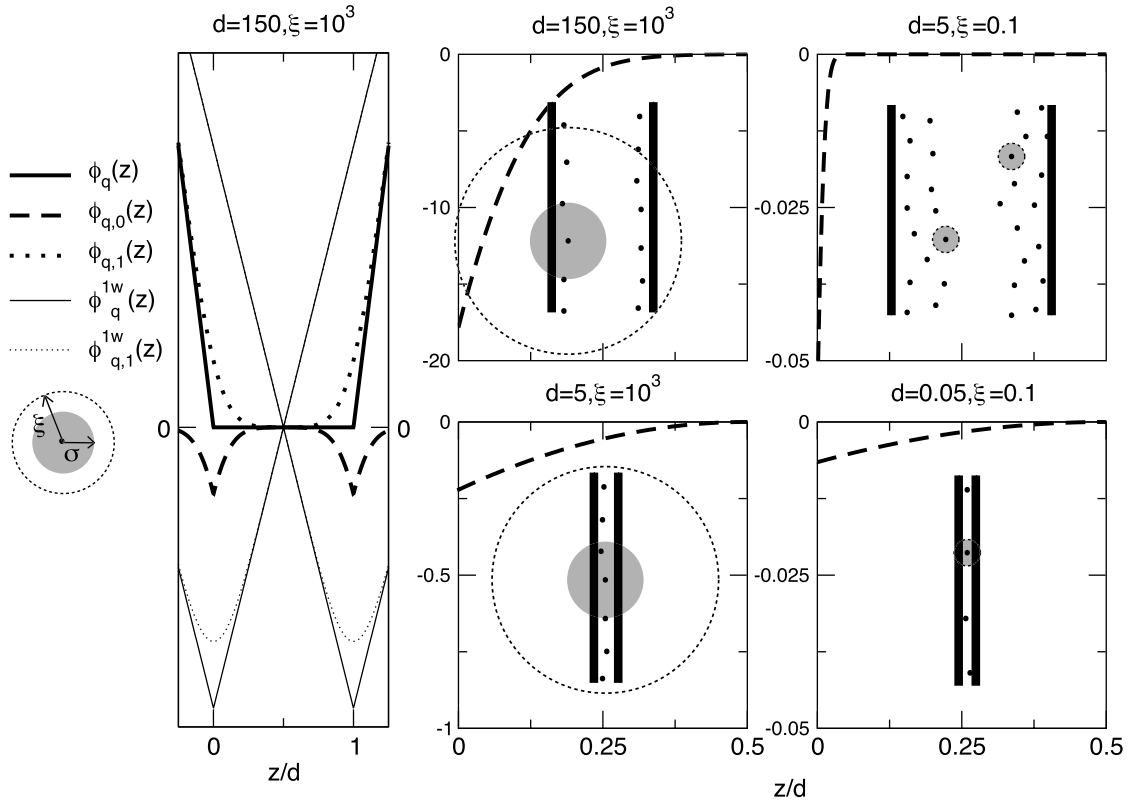

Figure 6.3: The left most graph represents the separation of electric potential $\tilde{\phi}_q(\tilde{z})$ of a two-wall system. The $\tilde{\phi}_{q,0}(\tilde{z})$ and $\tilde{\phi}_{q,1}(\tilde{z})$ (thus excluding the potential of the hard walls) of a two-wall system are the summation of those from two single walls positioned at both $\tilde{z} = 0$ and $\tilde{z} = \tilde{d}$. The one-wall potentials are denoted by a superscript "1w". The $\tilde{\phi}_{q,0}(\tilde{z})$ is subsequently plotted for two strong coupling and two weak coupling states, so is the corresponding schematic representation of counterion distribution.

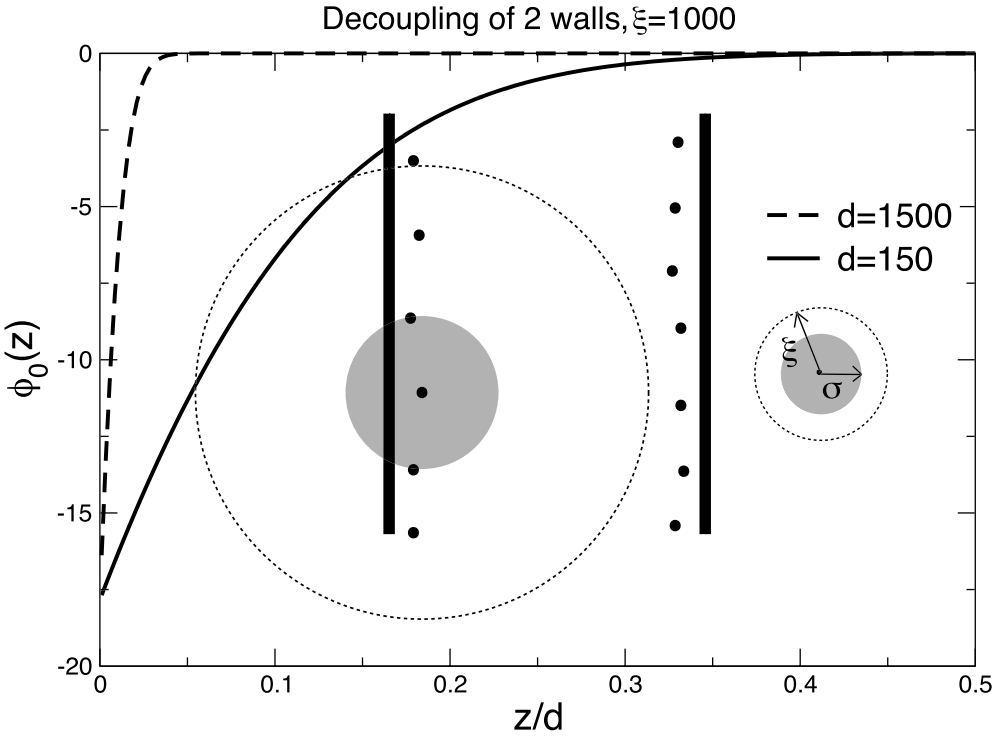

Figure 6.4: The $\tilde{\phi}_0(\tilde{z})$'s of two-wall systems, both of the same strong coupling state $\xi = 1000$ as that in Fig.(6.3), but at two different wall separations $\tilde{d} = 150$ and $\tilde{d} = 1500$. For $\tilde{d} = 1500$ the two-wall system enters the decoupling regimes $\tilde{d} > \xi$, while for $\tilde{d} = 150$ the counterions are localized to the walls but not fully decoupled.

counterion confinement. In this later case the $\tilde{a}_{3D}$ should be instead estimated by $\tilde{d}/\tilde{a}_{3D}^3 \sim q/2\pi\xi$, so $\tilde{a}_{3D} \sim (\tilde{d}\xi)^{1/3}$. The lateral spacing of the counterions does not depend on $\tilde{d}$ and is estimated by $\tilde{a}_{\|} \sim \xi^{1/2}$ as before.

$\tilde{d} > \xi$, PB Like

For $\tilde{d} > 1$, $\tilde{a}_{3D} > \tilde{a}_{\|}$ so $\tilde{a} \sim \tilde{a}_{3D} \sim \xi^{1/3}$. $\tilde{a}$ thus is much greater than counterions' Bjerrum length ξ. This implies that the counterions appear to be only loosely bound by the single wall potential well. The $\tilde{\sigma}_{min}$ should be chosen to be $\tilde{\sigma}_{min} \sim \xi$, so $\tilde{\sigma}_{min} \ll 1$. A mimic system with $\tilde{\sigma} \sim \xi$ is thus very dilute with respect to either $\tilde{d}$ or $\tilde{l}_G$, so the MPB approximation should suffice. In the limit that $\tilde{\sigma} \to 0$, $\tilde{G}(\tilde{z}_0, \tilde{z}) \to -|\tilde{z}_0 - \tilde{z}| + |\tilde{z}_0|$, and the LMF equation reduces to the integral form of Poisson's equation, as $\tilde{n}^*(\tilde{z}) \to \tilde{n}(\tilde{z})$ in Eq.(6.22,6.24), so LMF simply reduces to the PB approximation [2]

$$\tilde{n}_{PB}(\tilde{z}) \;=\; A/\cos^2(A^{1/2}[\tilde{z} - \tilde{d}/2]), \tag{6.46}$$

A is determined by the neutrality condition. However, $\tilde{n}_0(\tilde{z}; \mu_0, [\tilde{\phi}_R])$ can not be accurately estimated by the density of the nonuniform mimic system $\tilde{n}_0(\tilde{z}; \mu_0, [\tilde{\phi}_0])$ since the LMF correction from $\tilde{\phi}_R(\tilde{z})$ quickly arises away from each wall, and the full LMF (or MPB) solution should always be used.

As long as ξ remains small with respect to $\tilde{a}$ and $\tilde{d}$, the LMF can be well approximated by the MPB and gives solutions close to that of the PB. However, because for $\tilde{d} < 1$, $\tilde{a}_{3D} \sim (\tilde{d}\xi)^{1/3}$, for sufficiently small $\tilde{d}$ such that $\tilde{d} < \xi^{1/2}$, the 3D

spacing $\tilde{a}_{3D} \sim (\tilde{d}\xi)^{1/3}$ can actually become smaller than $\tilde{a}_{\|} \sim \xi^{1/2}$. So for $\tilde{d} < \xi^{1/2}$, the typical counterion spacing should instead be $\tilde{a} \sim \tilde{a}_{\|} \sim \xi^{1/2}$. At such wall separations, the perpendicular fluctuation of the counterions is much suppressed compared with their lateral fluctuation. However, if $\xi < \tilde{d} < \xi^{1/2}$, the slit would still appear wide to the counterions, and some counterions can move next to each other perpendicular to the walls without feeling much of their short range repulsion. So until $\tilde{d} < \xi$, the PB approximation could still remain valid and and give results very similar to the MPB approximation, since $\tilde{\sigma} \sim \xi \ll 1$ still is much smaller than the slit width. When $\tilde{d} < \xi$, the slit width is finally smaller than the counterions' core size, and the core repulsion of the counterions would prevent any counterion from ever aligning perpendicularly to another counterion. So the counterions in this limiting wall separation become a 2D, single-layer thin film, and a counterion feels from the others almost no net mean force along the $\tilde{z}$ direction. This regime corresponds to the $\xi = 0.1, \tilde{d} = 5$ graph in Fig.(6.3) and the "WC2" region labeled in the phase diagram Fig.(6.5).

$\tilde{d} < \xi$, "Narrow Slit" Like, Counterions Weakly Interacting in a 2D Layer

For $\tilde{d} < \xi \ll 1$, $\tilde{a} \sim \xi^{1/2} \gg \xi$, the counterions are only *weakly* interacting and have little overlap of their short-ranged core potentials on the lateral plane. The $\tilde{\sigma}_{min}$ thus is still $\tilde{\sigma}_{min} \sim \xi \gg \tilde{d}$. So for $\tilde{\sigma} \sim \xi$, the LMF should be reduced to the MPB because this again is a "narrow slit" limit as the strong coupling limit of the one wall system, and the $\tilde{\phi}_{R1}$ provides little modification on the $\tilde{\phi}_0$. The LMF then predicts

in this limit that $\tilde{\phi}_R(\tilde{z}) \approx 0$, $\forall \tilde{z} \in [0, \tilde{d}]$ and the counterion density $\tilde{n}(\tilde{z})$ approaches a constant that is determined by the neutrality condition

$$\tilde{n}(\tilde{z}) = \begin{cases} \frac{2}{\tilde{d}}, \forall \tilde{z} \in [0, \tilde{d}] \\ 0, \text{ otherwise} \end{cases} . \tag{6.47}$$

Eq.(6.47) is consistent with the picture that the counterions form a thin 2D layer and is the exact solution for $\tilde{n}(\tilde{z})$ as $\tilde{d} \to 0$. It is the repulsion between the counterion cores whose size is much greater than the slit width that forces them into a 2D layer. Although the PB gives solutions close to that of the MPB for weak coupling and wider walls' separations, because the PB completely ignores the correlation of the counterions when computing the potential of mean force, the PB can not distinguish the difference of this $\tilde{\sigma}_{min}$ regime from the other regimes in which the wall separation is wider than ξ. On the other hand for the LMF (and thus MPB in this limit), the finite value of $\tilde{\sigma}_{min} \sim \xi$ eventually exposes this regime where the PB should fail. In fact, the neutrality condition imposes on the PB solution that

$$\sqrt{A} \tan(\sqrt{A}\frac{\tilde{d}}{2}) = 1, \tag{6.48}$$

which can then be used to show that

$$\tilde{n}_{PB}(\frac{\tilde{d}}{2}) - \tilde{n}_{PB}(0) = 1. \tag{6.49}$$

Eq.(6.49) implies that the $\tilde{n}(\tilde{z})$ given by PB always varies along $\tilde{z}$, no matter how small $\tilde{d}$ is, and the difference of the contact density and the middle density of the $\tilde{n}_{PB}(\tilde{z})$ is exactly unity for all separations. This also proves that the PB solution

can never reduce to the constant density result of Eq.(6.47).This regime corresponds to the $\xi = 0.1, \tilde{d} = 0.05$ graph in Fig.(6.3) and the "WC1" region labeled in the phase diagram Fig.(6.5).

Summary

For weak coupling $\xi \ll 1$, $\tilde{a} \gg \xi$ and $\tilde{\sigma}_{min} \sim \xi$ suffices. The LMF reduces to PB as $\xi \to 0$. For $\tilde{d} > \xi^{1/2}$, the LMF reduces to the MPB and gives solutions close to that of the PB. But the LMF theory is also exact in the narrow slit limit $\tilde{d} \ll \xi^{1/2}$, which the PB fails to predict.

6.2.2 Strong Coupling, $\xi \gg 1$

At this limit, similar to the weak coupling limit of the last section, the lateral spacing is still estimated by $\tilde{a}_{\parallel} \sim \xi^{1/2}$, but the $\tilde{a}_{3D}$ needs to be analyzed depending on the walls' separation. Because of the huge "size" of the counterions, only when $\tilde{d} > \xi$ can the walls possibly be decoupled, since a counterion near one wall would feel little force from the counterions on the other half of the space. For such a widely separated case counterions are localized within a distance of Gouy-Chapman length from the wall like the single wall system and $\tilde{a}_{3D} \sim \xi^{1/3}$.

For smaller $\tilde{d}$'s, the counterions near one wall significantly interfere with those near the other wall at the same vertical level, and the counterions are more spread across the $\tilde{z}$ space, so $\tilde{d}$ characterizes the range of the counterion distribution, leading

to $\tilde{a}_{3D} \sim (\tilde{d}\xi)^{1/3}$. The behavior of the counterion distribution can be categorized into three regions and are discussed in below. The PB approximation can not describe any of the following strong coupling regimes categorized by different wall separations.

$\tilde{d} < \xi^{1/2}$, "Tiny Slit" Like, Counterions Strongly Correlated in a 2D Layer

Because $\tilde{d} \ll \xi^{1/2} \ll \xi$, there could hardly be more than one counterion aligned perpendicular to the wall, the system enters this "narrow slit", 2D-like regime for a similar reason as that of the weak coupling case. It can be estimated that $\tilde{a}_{3D} \sim (\tilde{d}\xi)^{1/3}$, so the lateral spacing $\tilde{a}_{\|} \sim \xi^{1/2}$ is much greater than $\tilde{a}_{3D}$, which agrees with that the counterions appear to be 2D like. The typical spacing is thus characterized by $\tilde{a} \sim \tilde{a}_{\|} \sim \xi^{1/2}$. However, for $\xi \gg 1$, $\xi \gg \tilde{a}$, so unlike the weak coupling limit's "tiny slit" regime, the counterions interact with strong repulsive cores and are highly correlated laterally. In other words, the counterions are very crowded on the x-y plane and much cancellation of their long-range forces can be expected. Thus $\tilde{\sigma}_{min} \sim \tilde{a} > \tilde{d}$ should be chosen for the mimic system in this regime. in this regime, so $\tilde{\phi}_R(\tilde{z}) \approx \tilde{\phi}_0(\tilde{z}) \approx 0, \forall \tilde{z} \in [0, \tilde{d}/2]$. The mimic system also appears to be "narrow slit" like and so the LMF again predicts also a constant counterion density profile like that in Eq.(6.47). This regime is illustrated by the $\xi = 1000, \tilde{d} = 5$ graph in Fig.(6.3) and the "SC1" region labeled in the phase diagram Fig.(6.5). This limit had been previously examined by Netz [53, 54], particularly for explaining the origin of effective attractions between the walls at strong coupling states. However, the

connection between the narrow slit limit of both a weak and a strong coupling state had not been noted before.

$\xi^{1/2} < \tilde{d} < \xi$, Counterions Localized next to the Two Walls, the Walls not yet Decoupled

In this regime, the interaction of counterions of a counterion near one wall with others on the same side is significantly stronger than it is with others directly across on the other wall. As a result it is possible to occasionally find more than one counterion perpendicular to the wall since this can be favorable compared with being forced to align laterally at a smaller spacing $\tilde{a}_{\|} \sim \xi^{1/2}$. Because of the counterions' strong repulsion in the $\xi \gg 1$ limit, most counterions are tightly pushed against the wall and concentrated within a distance of Gouy-Chapman length from the wall. So $\tilde{a}_{3D} \sim \xi^{1/3}$, which for this regime implies $\xi > \tilde{a}_{\|} > \tilde{a}_{3D}$, thus the typical spacing is still $\tilde{a} \sim \tilde{a}_{\|} \sim \xi^{1/2}$. However, since $\tilde{d} < \xi$ still, the counterions on each side still significantly influence the other, so only $\tilde{d} > \xi^{1/2}$ is not sufficient to ensure that the walls have completely decoupled.

Since $\tilde{a} \ll \xi$, the mimic system should be chosen that $\tilde{\sigma}_{min} \sim \tilde{a} \sim \xi^{1/2}$. $\tilde{\phi}_0(\tilde{z})$ forms a potential well ($\sim \tilde{z}$) near each wall that turns to a plateau value only until about a $\tilde{\sigma}$ distance away from the wall. Since $\xi \gg 1$, $\tilde{\sigma}_{min} \gg 1$, the potential wells can be very deep, thus very effective in trapping most counterions near the walls and forcing them into two 2D like layers near the walls. The $\tilde{\phi}_{R1}(\tilde{z})$ can only modify $\tilde{\phi}_0(\tilde{z})$ for $\tilde{z} > \tilde{\sigma}$ or $\tilde{d} - \tilde{z} > \tilde{\sigma}$, i.e., where $\tilde{\phi}_0(\tilde{z})$ turns to a constant as Fig.(6.4)

shows. However, in this regime there is not enough space between the walls for the rise of the $\tilde{\phi}_{R1}(\tilde{z})$ to suppress the $\tilde{n}(\tilde{z})$ to the asymptotic decay of a single wall solution, although $\tilde{n}(\tilde{d}/2)$ can already be very small. Near the walls, the mimic system's charge density $\tilde{n}_0(\tilde{z}; \mu_0, [\tilde{\phi}_0])$ can be very similar to that of the full solution of the LMF and agree qualitatively with what's expected for the full system. This regime corresponds to the $\xi = 1000, \tilde{d} = 150$ graph in Fig.(6.3) and the "SC2" region labeled in the phase diagram Fig.(6.5). Although the walls can still exhibit effective attractions in this regime, the strong coupling field theory of Netz [54] can no longer apply.

$\tilde{d} > \xi$, the Walls Decoupled, Recovering Single Wall, Strong Coupling Solution

For $\tilde{d} > \xi$, the counterions localized near each wall hardly feel the strong core repulsion from the others, so the two halves become uncorrelated, and the walls essentially decouple. The counterion distribution would be expected to recover that of the single wall solution in this regime when $\tilde{d} \to \infty$.

In this regime the $\tilde{\phi}_{R1}(\tilde{z})$ becomes important and eventually asymptotically infinite near $\tilde{z} = \tilde{d}/2$, as $\tilde{d} \to \infty$. Without the correction of $\tilde{\phi}_{R1}$, the mimic system alone with $\tilde{\phi}_0$ results in a bulk phase with a finite density in between the walls. For the LMF, since most of the counterions are absorbed near the walls, the few left that make it further towards the middle region view the walls with surface charges that are much reduced by the strongly bound counterions. As already shown in the

study of the single charged wall system, for finite ξ's, the LMF predicts an algebraic decay $1/(\tilde{z}+b)^2$ as Eq.(6.40). The b value is the much *lengthened* effective Gouy-Chapman arising from the remaining small effective surface charge of the wall. In the asymptotic region the counterions appear to be dilute so that $b > \xi$. For strong coupling although $\tilde{l}_G = 1 \ll \xi$, by absorbing most counterions near the wall, the remaining ones are effectively weak coupling. So for the LMF solution for the two wall system to reduce to that of two decoupled single walls, at least $\tilde{d} > \xi$ is needed to provide the asymptotic region for the algebraic decay region of the single wall counterion distribution. This regime corresponds to the $\xi = 1000, \tilde{d} = 1500$ graph in Fig.(6.4) and the "SC3" region labeled in the phase diagram Fig.(6.5).

It had also previously been suggested that for $\tilde{d} > \xi$ (up to a logarithmic correction), the system *re-enters* a "PB" regime [54]. Such a criterion was proposed based on the loop-expansion analysis of the PB limit from a field theory context. However it was by no means clear how such change of regimes could occur based on the field theory analysis, since eventually the two wall system of a strong coupling state must decouple and recover the solution for the one wall system of the same surface charge density. And it is been known that for a strong coupling state of a single wall system, the $\tilde{n}(\tilde{z})$ for finite $\tilde{z}$'s is quite different from the profile the PB would describe. The LMF, on the contrary, bridges the different strong coupling regimes very naturally, from small $\tilde{d}$ to the eventual decoupling of the two walls. In fact, such arguments about the asymptotic "PB" state at large $\tilde{d}$'s can at best

describe only the asymptotic $\tilde{n}(\tilde{z}) \sim 1/\tilde{z}^2$ behavior at large $\tilde{z}$'s , all other vital information, including the right algebraic decay constant, and mostly important, the $\tilde{n}(\tilde{z}) \sim e^{-\tilde{z}}$ profile near the walls (most crucial for recovering the strong coupling, single wall solution) is completely *lost.* The previous inability of theoretical studies to consistently treat strong coupling states for all wall separations thus left the physical interpretation of the decoupling of strongly charged walls rather unclear.

Summary

For strong coupling states, for all wall separations, $\tilde{\sigma}_{min} \sim \tilde{a} \sim \xi^{1/2}$. The counterion distribution $\tilde{n}(\tilde{z})$ near the walls can be approximated by the nonuniform mimic system's distribution $\tilde{n}_0(\tilde{z}; \mu_0, [\tilde{\phi}_0])$ for moderate separations $\xi^{1/2} < \tilde{d} < \xi$. For $\tilde{d} > \xi$, the LMF correction of $\tilde{\phi}_{R1}(\tilde{z})$ becomes important in correcting the asymptotic decay of the $\tilde{n}(\tilde{z})$ decays into the middle region. Subtleties about how μ_0 could be chosen with $\tilde{\phi}_0$ for an appropriate mimic system will be addressed in section 6.2.4. Once $\tilde{d} > \xi^{1/2}$, the counterions start being localized in a 2D layer near the walls, and the $\tilde{\phi}_0(\tilde{z})$ gives rise to deep attractive wells near the walls when $\xi \to \infty$. In this case, the $\tilde{n}(\tilde{z})$ can be roughly estimated by the superposition of two single-wall exponential profiles,

$$\tilde{n}(\tilde{z}) \sim \frac{e^{-\tilde{z}} + e^{-(\tilde{d}-\tilde{z})}}{1 - e^{-\tilde{d}}} \tag{6.50}$$

where the neutrality condition determines the overall prefactor. This estimate Eq.(6.50) is what Netz [53, 54] had proposed for strong coupling but larger $\tilde{d}$'s. However, this estimate was purely an "observation" of what would be expected to

make connection with the single wall solution when $\tilde{d} \to \infty$. Conceptually it is rather ad hoc, since it cannot be obtained directly from the field theory expansion for two wall system devised by these authors, and it hardly conveys how the subsequent re-entrance into the "PB" regime [54] that these authors had argued takes place.

6.2.3 Effective Interaction between the Two Walls

Here the pressure in between the two walls,

$$\tilde{P} \equiv P/2\pi l_G \lambda^2 \tag{6.51}$$

in reduced unit is introduced. For this two charged wall system, the contact density of $\tilde{n}(\tilde{z})$ is no longer unity except at the limit that $\tilde{d} \to \infty$. Instead, the contact density is related exactly to the pressure between the walls by [8, 21, 22]

$$\tilde{P} = -1 + \tilde{n}(0_+). \tag{6.52}$$

The wall at $\tilde{z} = 0$, supposedly carrying a surface charge 1, feels a constant attraction from a net surface charge "-1" from the positive charge $(+1)$ on the other wall and the negative charge (-2) form the counterions. This net electric attraction contributes to the "-1" term in Eq.(6.52). However, the counterions are not a static, uniform film of charges, but rather have microscopic correlations. The counterions also fight with the walls' confinement through their contact collisions to the walls, and this gives rise to an effective repulsion between the walls that favors a wider wall

separation. Whether or not the walls in effect attract depends on the competition of the constant electric attraction and the entropic repulsion due to counterion confinement. When the two walls decouple, the interaction between them is completely screened to zero so $\tilde{P} = 0$, and Eq.(6.52) requires $\tilde{n}(0_+) = 1$. The contact theorem for one wall thus is a limiting case of Eq.(6.52).

It has been observed that like-charge macroions can exhibit effective attraction to each other, especially for highly charged macroions or at low temperature states. As several authors have pointed out [23, 54], such effective interaction is counterion mediated and can be seen its onset at the strong coupling limit. We will first reiterate how such effective attraction can be derived and will also demonstrate how all the regimes in the $\tilde{d} - \xi$ phase diagram in Fig.(6.5), obtained by Moreira and Netz [53] using computer simulations, can be at least qualitatively understood and reproduced using the unified framework of the LMF theory and the mimic system.

$\tilde{d} - \xi$ Phase Diagram

Strong Coupling States, $\xi \gg 1$ For small separations $\tilde{d} < \xi^{1/2}$, the $\tilde{n}(\tilde{z})$ is roughly given by the constant profile of Eq.(6.47), so

$$\tilde{P} \approx -1 + \frac{2}{\tilde{d}}. \tag{6.53}$$

The $\tilde{P}$ of the result of Eq.(6.53) is repulsive for smaller separations, *yet may become attractive* when $\tilde{d}$ is increased. Thus $\tilde{d}^* = 2$ is the equilibrium separation in this regime, and the position of the walls is stable to the variation of $\tilde{d}$ near $\tilde{d}^*$. This

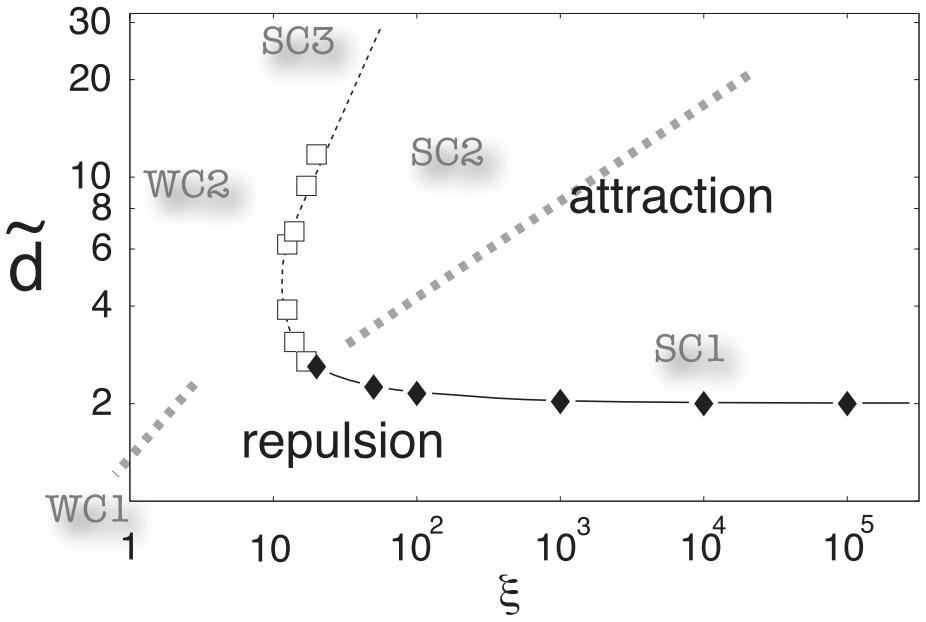

Figure 6.5: The $\tilde{d}-\xi$ phase diagram of a two-wall system as obtained by Moreira and Netz using computer simulations [53]. The labels "SC1", "SC2", "SC3", "WC1", "WC2" were later added by Y.-G. Chen for discussing different $\tilde{d}-\xi$ regimes. SC1: $\tilde{d} < \xi^{1/2}$, SC2: $\xi^{1/2} < \tilde{d} < \xi$, SC3: $\tilde{d} > \xi$, WC1: $\tilde{d} < \xi$, WC2: $\tilde{d} > \xi$.

regime demonstrates how an effective attraction between like-charged walls could ever exist through the counterions' mediating attraction to the both walls. This result has been well understood by Netz et al [53, 54], and is also reproduced by the LMF.

For larger $\tilde{d}$'s, when $\xi^{1/2} < \tilde{d} < \xi$, the approximation of Eq.(6.47) is no longer valid and the counterions start being localized next to the walls. The $\tilde{\phi}_0(\tilde{z})$ of the mimic system can form deep attractive wells near the walls and turn into a plateau in the middle region. The LMF's correction of $\tilde{\phi}_{R1}(\tilde{z})$ will further add the remaining counterion repulsion from the $\tilde{u}_1$ to create a higher barrier towards the middle region and suppress the counterion density there. However, because in this regime there is not enough space for the full onset of the $\tilde{\phi}_{R1}(\tilde{z})$, the $\tilde{\phi}_R(\tilde{z})$ is not sufficiently big to stop the counterions from escaping the $\tilde{\phi}_0(\tilde{z})$ potential wells. This implies that $\tilde{n}(0_+)$ may be still lower than its asymptotic value $\tilde{n}(0_+) \to 1, \tilde{d} \to \infty$, thus still resulting in a net attraction which persists from $\tilde{d} \geq 2$, but this attraction is increasingly weakened by bigger $\tilde{d}$'s.

For $\tilde{d} > \xi$, $\tilde{\phi}_{R1}(\tilde{z})$ eventually builds a robust barrier in the plateau region of the bare $\tilde{\phi}_0(\tilde{z})$ that prevents the counterions from escaping the walls and forming a finite bulk density. At $\tilde{d} \to \infty$, the $\tilde{n}(\tilde{z})$ and $\tilde{\phi}_R(\tilde{z})$ recover those of the LMF's single wall solution. As $\tilde{d}$ is decreased to a very big but finite value, the $\tilde{\phi}_R(\tilde{z})$'s logarithmic increase towards $\tilde{z} \to \tilde{d}/2$ remains almost equally formidable for the counterions, but the now reduced space requires them to return to and concentrate

near the walls more. So for most of the $\tilde{d}$'s in this regime, the $\tilde{n}(0_+)$ would be slightly higher than unity and result in a net repulsion between the walls. This repulsion can be also understood from the fact that if $\tilde{n}(\tilde{z})$ is already close to its asymptotic form of $\tilde{d} \to \infty$, the neutrality condition should require an overall increase of $\tilde{n}(\tilde{z})$ upon the decrease of the $\tilde{d}$. The $\tilde{n}(\tilde{z})$ thus should approach unity from above.

Note that in going from $\tilde{d} < \xi$ to $\tilde{d} > \xi$, the trend that the attraction between the walls weakens upon increasing $\tilde{d}$ must transit to the other trend that the walls' effective interaction turns repulsive and weakens as $\tilde{d}$ keeps increasing. The attractive regime for smaller $\tilde{d}$'s corresponds to $\tilde{n}(0_+) < 1$ while $\tilde{n}(0_+) > 1$ for the repulsive regime at even large $\tilde{d}$'s. This implies a meta stable equilibrium position for strong coupling states at large $\tilde{d}$'s and is the re-entrant of repulsion that Netz et al have previously conjectured and shown by computer simulations [54].

Weak Coupling, $\xi < 1$ For exceptionally small wall separation $\tilde{d} < \xi$, it is possible for the walls themselves to squeeze the counterions into a constant distribution as seen in Eq.(6.50). However, for this profile to hold, it *must* be that $\tilde{d} \ll 1$, implying that $\tilde{P} > 0$ should be very repulsive. Well before $\tilde{d}$ approaches 2, the system has already entered the regimes where the PB approximation is valid and it always predicts repulsion between the walls. The walls thus exhibit no effective attraction at weak coupling states.

Decouple of the Two Walls

Although the bare external field $\tilde{\phi}(\tilde{z})$ seen by the counterions is a constant between the walls, the $\tilde{\phi}_0(\tilde{z})$ reveals the potential wells near the walls that are particularly effective in trapping and localizing the mimic particles in strong coupling states. This provides an important perspective for understanding very simply how the two walls could decouple, and how the solution could approach asymptotically the single-wall solution as $\tilde{d} \to \infty$. On the other hand, the seemingly mysterious decouple of the two walls can be also understood from the full system without considering the mimic system.

Because of the reflection symmetry, there must be equal number of counterions in both $\tilde{z} \in [0, \tilde{d}/2]$ and $\tilde{z} \in [\tilde{d}/2, 0]$, and the mean force felt by a counterion must vanish at $\tilde{z} = \tilde{d}/2$. For weak coupling, when particles are on average far away from each other and very weakly correlated, the counterions on one half of the space appear to be a uniform slab of charges. From Gauss's theorem this slab of charges cause a constant repulsive electric field (thus linear in potential) to the other half of the counterions. For counterions within $\tilde{z} \in [0, \tilde{d}/2]$, the effect of this repulsive field is equivalent to adding to the hard wall at $\tilde{z} = 0$ a linear attractive well to "trap" the counterions near the wall.

However, for strong coupling, the counterions on both sides of the slit keep being correlated even for very large $\tilde{d}$'s, until finally $\tilde{d} > \xi \gg 1$. For $\tilde{d} \gg \xi$, the fluctuation of the counterions on each side still hardly alters the lateral uniformity

of their charge distribution and the estimate for the mutual repulsion of the two sides is similar to what's already argued above for weak coupling walls. The system thus can be solved as if there is only a *single strong coupling* wall. Moreover, as the $\tilde{d}$ is further decreased, the counterions from each side would be more strongly correlated. If $\tilde{d} < \xi$, any counterion fixed on one side would significantly "dent" the lateral uniformity of the counterion distribution on the other side. The forces from the counterions on the other side and act on the held counterion thus are often "skewed" in the lateral direction and subsequently results in a reduction of the net mean force along the $\tilde{z}$ direction. This weakening of the single-wall confinement and counterion localization to the walls explains how for $\tilde{d} < \xi$, $\tilde{n}(0_+)$ could be lowered as the spacing $\tilde{d}$ decreases and a net attraction between the walls *could* be induced.

As to the LMF equation Eq.(6.43), it can be decomposed into two parts

$$\tilde{\phi}_R(\tilde{z}) = \int_0^{\frac{\tilde{d}}{2}} d\tilde{z}_0 \tilde{n}(\tilde{z}_0, \tilde{z}) \tilde{G}(\tilde{z}_0, \tilde{z}) + \int_{\frac{\tilde{d}}{2}}^{\tilde{d}} d\tilde{z}_0 \tilde{n}(\tilde{z}_0, \tilde{z}) \tilde{G}(\tilde{z}_0, \tilde{z}). \tag{6.54}$$

Because the $\tilde{G}(\tilde{z}_0, \tilde{z})$ approaches $-|\tilde{z} - \tilde{z}_0| + Const.$ when $|\tilde{z} - \tilde{z}_0| \gg \tilde{\sigma}$ (as shown in Fig.(6.1)), the $\tilde{z} > \tilde{d}/2$ integral of the Eq.(6.54) should produce a linear potential $\tilde{z} - \tilde{z} + Const.$ for $\tilde{z} < \tilde{d}/2$, if $\tilde{d} \gg \tilde{\sigma}$. So at the limit of $\tilde{d} \to \infty$, Eq.(6.54) becomes

$$\tilde{\phi}_R(\tilde{z}) \quad \to \quad \tilde{z} + \int_0^{\frac{\tilde{d}}{2}} d\tilde{z}_0 \tilde{n}(\tilde{z}_0, \tilde{z}) \tilde{G}(\tilde{z}_0, \tilde{z}), \forall \tilde{z} < \frac{\tilde{d}}{2}, \tag{6.55}$$

which is the LMF equation of a single wall system. So the LMF solution for a two-wall system reduces to two single-wall solutions at the limit of infinite wall separation. Note that the linear potential in Eq.(6.55) is in fact only given by the

counterion repulsion from the other half space with $\tilde{z} \in [\tilde{d}/2, \tilde{d}]$. The PB approximation decouples to single wall solutions similarly, since it is just the limit of the LMF at $\tilde{\sigma} \to 0$. The $\tilde{\phi}_0(\tilde{z})$ approaches $\tilde{\phi}_0(\tilde{z}) \to \tilde{\phi}_0^{1w}(0, \tilde{z})$, for $\tilde{z} < \tilde{d}/2$, when $\tilde{d} \to \infty$ (the first argument of $\tilde{\phi}_0^{1w}(0, \tilde{z})$ indicates the position of the single wall). The $\tilde{\phi}_{R1}(\tilde{z})$ correction

$$\begin{aligned}
\tilde{\phi}_{R1}(\tilde{z}) &= \int_0^{\frac{\tilde{d}}{2}} d\tilde{z}_0[-\delta(\tilde{z}) + \tilde{n}(\tilde{z}_0, \tilde{z})]\tilde{G}(\tilde{z}_0, \tilde{z}) \\
&\quad + \int_{\frac{\tilde{d}}{2}}^{\tilde{d}} d\tilde{z}_0[-\delta(\tilde{z}_0 - \tilde{d}) + \tilde{n}(\tilde{z}_0, \tilde{z})]\tilde{G}(\tilde{z}_0, \tilde{z}) \qquad (6.56) \\
&\to \int_0^{\frac{\tilde{d}}{2}} d\tilde{z}_0[-\delta(\tilde{z}) + \tilde{n}(\tilde{z}_0, \tilde{z})]\tilde{G}(\tilde{z}_0, \tilde{z}),\ \tilde{d} \to \infty, \qquad (6.57)
\end{aligned}$$

because the neutrality of $[-\delta(\tilde{z}) + \tilde{n}(\tilde{z}_0, \tilde{z})]$ ensures that asymptotically it gives a screened potential. The second integral of Eq.(6.56) actually gives a logarithmic divergence, if measured from $\tilde{z} = \tilde{d}$. However, since the derivative of this logarithm term vanishes when $\tilde{d} - \tilde{z} \gg 1$, it appears as a constant for $\tilde{z} < \tilde{d}/2$, and in fact is made to be zero by the choice of zero of potential. So Eq.(6.57) is consistent with the decoupling of the LMF equation already observed.

However, for strong coupling states where $\tilde{\sigma}$ can be very big, the $\tilde{\phi}_0(\tilde{z}) \approx \tilde{\phi}_0^{1w}(0, \tilde{z})$ is no longer true for $\tilde{z} < \tilde{d}/2$, if $\tilde{d}$ becomes small enough. The $\tilde{\phi}_0(\tilde{z})$ can then become shallower when the contribution of $\tilde{\phi}^{1w}(\tilde{d}, \tilde{z})$ becomes more important, as can be seen in the strong coupling states of Fig.(6.3). This weakening of the single-wall confinement of the counterions correspond to the situation where the counterions from both sides start being significantly correlated, resulting in reduced

mutual repulsion. Because the PB approximation corresponds to $\tilde{\sigma} = 0$, it can not describe this weakening of the confinement, and always assumes a linear confining potential from the other half of the counterions.

6.2.4 The Chemical Potential of the Mimic System

Unlike the case for the one wall system, the special case of the contact theorem, Eq.(6.41), does not apply. The μ_0 thus can not be determined for $\tilde{n}_0(\tilde{z}; \mu_0, [\tilde{\phi}_0])$ from the contact density, if the full LMF is not solved. However, for strong coupling states at small to moderate separation $\tilde{d}$'s, when the correction of the $\tilde{\phi}_{R1}(\tilde{z})$ is unimportant, the μ_0 can be instead determined by the neutrality condition $\int d\tilde{z}\tilde{n}_0(\tilde{z}; \mu_0, [\tilde{\phi}_0]) = 2$. In fact, this can readily give the "narrow slit" limit profile $\tilde{n}(\tilde{z}) = 2/\tilde{d}, \forall \tilde{z} \in [0, \tilde{d}]$. However, when the $\tilde{\phi}_{R1}(\tilde{z})$ is important in correcting how the $\tilde{n}(\tilde{z})$ behaves asymptotically towards the middle region, the neutrality condition could not be used since $\tilde{n}(\tilde{z}; \mu_0, [\tilde{\phi}_0])$'s plateau bulk region of finite density eventually makes the normalization impossible, just is the case with the single wall system. Thus to accurately determine the effective interaction between the walls at large $\tilde{d}$, where $\tilde{P}$ is very small (whether repulsive or attractive), the LMF equation should be always solved in full for this subtle information. Nonetheless, for $\xi \gg 1$, the $\tilde{n}(\tilde{z})$'s variation near the walls should be still of the form $Ae^{-\tilde{z}}$, A is a constant in $\tilde{z}$. This can seen in the mimic system $\tilde{n}_0(\tilde{z}; \mu_0, [\tilde{\phi}_0])$ as well, and is insensitive to how the μ_0 is chosen (though A's value could change).

6.3 Conclusion

In this chapter, a qualitative investigation of model charged wall systems is carried out based on the LMF theory. Although many of the important phenomena such as the effective attraction between like-charged walls and the re-entrant behavior of the walls' repulsion have previously been addressed by various authors [53, 54], a consistent theoretical framework to provide physical interpretations and successfully bridge the very different coupling regimes can not be obtained in these works. In contrast to previous theoretical studies, it has been argued above that the LMF is able to connect and reproduce very naturally all the regimes. In fact, while the field theory treatment proposed by Netz et al to a great extent takes advantage of the special form of the counterion interaction, the LMF can be straightforwardly generalized to different counterion core interactions (such as embedded hard cores) and more realistic macroion modeling. Moreover, in most cases the LMF can be reduced to the MPB, especially for the systems discussed in this chapter, and the numerical computation of the MPB is straightforward and no more difficult than using the PB approximation. This also compares very favorably with the *Test-Charge Mean Field Theory* (TCMF) [6], a pair level PB approximation, developed very recently by Burak et al, which is able to recover the strong coupling limit of the one wall system, but is computationally much more demanding. Even with its much greater computational cost, the TCMF still predicts an incorrect asymptotic decay of $\tilde{n}(\tilde{z})$ and fails to satisfy the contact theorem for its one wall solution. In

previous chapters, the LMF has been applied to the correlation functions of uniform fluids. Here its application to an explicitly nonuniform system again demonstrates its versatility for the theoretical understanding of general ionic fluids.

Chapter 7

Summary and Outlook

In this dissertation, we have (hopefully!) developed physically motivated theoretical frameworks for understanding equilibrium fluid structure. The scope of the research ranges from simple liquids whose constituents interact with regular short-range intermolecular potential, to ionic systems whose very long-ranged Coulomb interaction has cast many unique challenges for theoretical statistical mechanics. What contrasts our approach to others is often a closer look into theories that originate from physical approximations but fail to gain success in a wider range of general applications. Instead of engaging in technical and ad hoc modifications whose physical justification is unclear, we have striven to gain new insights into the success of "the old theories", e.g., the PY approximation[60] for hard sphere fluids, and the mean field approximations[2, 50] for ionic systems. Such efforts have rewarded us with new and exciting theoretical methods whose range of validity extends well beyond the conventional theories. Nonetheless, many more possible applications and further refinement and generalization of these theoretical developments are still worth pursuing. We believe such research will continue to generate exciting contributions

to relevant fields of research.

7.1 Future Directions

With proper choice of the reference density $\tilde{\rho}^{\mathbf{r}}$ for a nonuniform fluid, the *shifted linear response* (SLR) equation can serve as a versatile framework for bridging several important limits. The *insensitivity criterion* (IC) has been proposed for determining the $\tilde{\rho}^{\mathbf{r}}$. Although the IC has been shown to accurately predict the singlet density response of hard sphere fluids to a variety of external fields, in particular those where the *hydrostatic linear response* (HLR) equation has failed qualitatively, it is by no means the optimal or only possible choice for determining the reference density. In particular, despite the IC's success in tiny fields and confining fields, it is significantly less accurate for hard wall or rigid cavity potentials. It seems that other recipes that could also work well for hard walls might be devised for the reference density used with the SLR equation.

The solution of the *local molecular field* (LMF) equation also requires the treatment of the mimic system's response to general external fields. For general and especially more realistic systems, molecules can have all kinds of effective repulsive cores, so it is essentially hopeless to devise a theory that can apply satisfactorily to all possible short-range interactions. However, primitive models are of particular importance for understanding the essential physics involving Coulomb interactions and are also superb test grounds for new theories. In the applications of the LMF

to model ionic systems, the mimic systems' molecular potentials $u_{0,ij}(r)$ are all of the form of a hard core plus a potential of the form $w_{q0,ij}(r) = q_i q_j \mathrm{erfc}(r/\sigma)/\epsilon r$, which decays rapidly in r-space. However, so far we have only employed computer simulations and a simple Boltzmann approximation at low densities (*mimic Poisson Boltzmann*) for the mimic system. It should further facilitate the LMF's application to these models if well controlled theoretical approximations can be provided for these mimic systems.

The systems that have been considered so far all have a constant static dielectric constant throughout all space. This assumption, though simplifying, excludes the interesting and possibly more challenging situations where image charges can be also induced due to a discontinuity of the dielectric constant in space. Systems with conducting boundaries and polarizable charge carriers pose questions as to how the concept of a mimic system can be generalized to such systems, and might even highlight the limitations of the LMF picture itself. Thus more thorough study of such boundary conditions is thus also highly desirable. The potential separation for general charge distributions has been derived in this dissertation. It then becomes straightforward to apply the LMF to systems involving molecules carrying net dipoles rather than net charges. The mimic systems suitable for these dipolar molecules can be readily defined. Explicit applications of the LMF to dipolar systems will be continued with co-workers. Hopefully such applications will also prove useful for the study of water, which is a subject of intense research interest for many

years.

The LMF has close connections to computer simulation methods which are indispensable for treating Coulomb interactions[16, 1]. A more detailed investigation of these connections may benefit both simulation development and the understanding of the LMF. In particular, as mentioned before, because ionic systems represent such a broad category that can embed any kind of short-ranged cores, it eventually becomes more practical and useful to develop effective simulations of the mimic system but with LMF corrections from the long ranged forces effectively taken into account "on the fly" as the simulation proceeds. Some preliminary thought has been given to such developments but much more work along such directions remains to be pursued.

So far our study has focused on equilibrium properties of ionic systems. However, in biological systems, life sustaining processes are hardly in equilibrium. Transport properties of charged molecules in highly nonuniform geometry are often most crucial and interesting in such processes, as occurs in ion channels. What our theory implies for the dynamic properties of ionic systems thus is definitely worth further research work and should enable more relevant theoretical exploration into biological systems.

Appendix A

Surface Tension of a Hard Sphere Fluid Next to an Infinite Spherical Cavity – the "Wall" Limit

In the "wall" limit where $R_v \to \infty$, the surface tension given by the compressibility route is determined from

$$\gamma_\infty = -\int_0^{\rho^B} d\rho \frac{\partial \mu}{\partial \rho} \int_0^\infty dz[\rho_w(z) - \rho], \tag{A.1}$$

with $\rho_w(z) \equiv \rho(z + R_v)$. The virial route gives

$$\gamma_\infty = k_B T \rho^B \int_0^\infty dR[G(R) - G(\infty)], \tag{A.2}$$

Here $\rho^B G(R)$ is the contact value of the density response to a cavity of size R. In the case considered in Chapter 2, the γ_∞ from both the compressibility and the virial routes can be determined analytically. In general, when no analytical expressions are available, one may need to carry out these integrations numerically.

There also exists the exact virial sum rule $\rho^B G(\infty) = \beta p^B$ for a planar wall immersed in the hard sphere fluid [32]. However, this focuses on the structure at contact for the planar wall, which is the region where the HLR equation is least

accurate. Thus this thermodynamic pathway for the bulk pressure gives relatively poor results.

Appendix B

Exact Density Response to "Tiny" Fields

While the derivation given above for the exact density response of a hard sphere fluid to a tiny fields is quite simple, more work is required to prove that the PY approximation, i.e., Eq.(3.12) with the choice $\tilde{\rho}^{\mathbf{r}} = \rho^B$, is exact in this limit as well. Suppose that the external field $\phi(\mathbf{r})$ is the following general tiny field

$$\begin{aligned} \phi(\mathbf{r}) &\neq 0, \forall \mathbf{r} \in V^\phi \\ &= 0, \forall \mathbf{r} \notin V^\phi, \end{aligned} \tag{B.1}$$

where V^ϕ can accommodate no more than one fluid particle simultaneously. The following derivation will be based on this division of $\mathbf{r}$-space into two regions, V^ϕ where $\phi(\mathbf{r})$ can be nonzero, and its complement, with zero external field.

First we introduce several identities related to the linear response and inverse linear response functions of the bulk hard sphere fluid:

$$\chi(\mathbf{r}_1, \mathbf{r}_2; \rho) = \rho\delta(r_{12}) + \rho^2 h^{(2)}(r_{12}; \rho), \tag{B.2}$$

$$\chi^{-1}(\mathbf{r}_1, \mathbf{r}_2; \rho) = \frac{1}{\rho}\delta(r_{12}) - c^{(2)}(r_{12}; \rho). \tag{B.3}$$

$\chi(\mathbf{r}_1, \mathbf{r}_2; \rho)$ and $\chi^{-1}(\mathbf{r}_1, \mathbf{r}_2; \rho)$ are functional matrix inverses of each other, i.e.,

$$\int d\mathbf{r}_3 \chi(\mathbf{r}_1, \mathbf{r}_3; \rho)\chi^{-1}(\mathbf{r}_3, \mathbf{r}_2; \rho) = \delta(\mathbf{r}_1 - \mathbf{r}_2). \tag{B.4}$$

We may divide these matrices into four blocks based on whether the coordinates $\mathbf{r}_1$ and $\mathbf{r}_2$ are inside or outside the volume V^ϕ:

$$\chi = \begin{pmatrix} \chi_{11} & \chi_{12} \\ \chi_{21} & \chi_{22} \end{pmatrix} \ , \ \chi^{-1} = \begin{pmatrix} \chi^*_{11} & \chi^*_{12} \\ \chi^*_{21} & \chi^*_{22} \end{pmatrix}. \tag{B.5}$$

The i label of $\chi_{ij}(\mathbf{r}_1, \mathbf{r}_2)$ refers to the first argument $\mathbf{r}_1$, so $i = 1$ indicates that all $\mathbf{r}_1 \in V^\phi$ and $i = 2$ otherwise. The j label similarly refers to the second argument $\mathbf{r}_2$. Consider matrices χ_{out} and χ^{-1}_{in} defined by

$$\chi_{out} \equiv \begin{pmatrix} 0 & 0 \\ 0 & (\chi^*_{22})^{-1} \end{pmatrix}, \ \chi^{-1}_{in} \equiv \begin{pmatrix} \chi^{-1}_{11} & 0 \\ 0 & 0 \end{pmatrix}. \tag{B.6}$$

Since $\chi_{out}\chi^{-1}_{in} = 0$ (zero matrix), $\chi_{out}\chi^{-1}\chi\chi^{-1}_{in} = 0$ and $\chi^{-1}_{in}\chi\chi^{-1}\chi_{out} = 0$ give rise to the identities:

$$\chi^*_{12}(\chi_{22})^{-1} + \chi^{-1}_{11}\chi_{12} = 0, \tag{B.7}$$

$$(\chi^*_{22})^{-1}\chi^*_{21} + \chi_{21}\chi^{-1}_{11} = 0. \tag{B.8}$$

In addition, a Mayer f-function matrix $\mathbf{F}$ for the external field is defined by

$$\mathbf{F} \equiv \begin{pmatrix} \mathbf{F}_{11} & 0 \\ 0 & 0 \end{pmatrix}, \ \mathbf{F}_{11}(\mathbf{r}_1, \mathbf{r}_2) \equiv f^{\phi}(\mathbf{r}_1)\delta(\mathbf{r}_1, \mathbf{r}_2), \tag{B.9}$$

$$\mathbf{E} \equiv \mathbf{U} + \mathbf{F} \tag{B.10}$$

$$f^{\phi}(\mathbf{r}_1) \equiv e^{-\beta\phi(\mathbf{r}_1)} - 1, \tag{B.11}$$

$$a \equiv \int d\mathbf{r}_1 f^{\phi}(\mathbf{r}_1), \tag{B.12}$$

$$v \equiv \int_{V^{\phi}} d\mathbf{r}_1 1, \tag{B.13}$$

where $\mathbf{U} = \delta(\mathbf{r}_1, \mathbf{r}_2)$ is the identity matrix.

The PY approximation Eq.(3.7) can be re-written as

$$(1+f^{\phi}(\mathbf{r}_1))\rho^B \int d\mathbf{r}_2 \chi^{-1}(\mathbf{r}_1, \mathbf{r}_2)\rho(\mathbf{r}_2) - f^{\phi}(\mathbf{r}_1)\rho(\mathbf{r}_1) = \rho^B(1+f^{\phi}(\mathbf{r}_1)) \int d\mathbf{r}_2 \chi^{-1}(\mathbf{r}_1, \mathbf{r}_2)\rho^B \tag{B.14}$$

which can be cast using matrix multiplication as

$$\rho^B \mathbf{E}\chi^{-1}\hat{\rho} - \mathbf{F}\hat{\rho} = \rho^B \mathbf{E}\chi^{-1}\rho^B \hat{\mathbf{I}}, \tag{B.15}$$

where $\hat{\rho} = \rho(\mathbf{r})$ is a Hilbert space vector on which the matrices operate, $\hat{\mathbf{I}}$ is a constant vector, i.e., $\hat{\mathbf{I}} = 1$, $\forall \mathbf{r}$. Now Eq.(B.15) can be split into two equations in terms of the i, j block labels as

$$\rho^B \mathbf{E}_{11}(\chi^*_{11}\hat{\rho}_1 + \chi^*_{12}\hat{\rho}_2) - \mathbf{F}_{11}\hat{\rho}_1 = \rho^B\rho^B \mathbf{E}_{11}(\chi^*_{11}\hat{\mathbf{I}}_1 + \chi^*_{12}\hat{\mathbf{I}}_2), \tag{B.16}$$

$$\rho^B(\chi^*_{21}\hat{\rho}_1 + \chi^*_{22}\hat{\rho}_2) = \rho^B\rho^B(\chi^*_{21}\hat{\mathbf{I}}_1 + \chi^*_{22}\hat{\mathbf{I}}_2). \tag{B.17}$$

$\hat{\rho}_1$ refers to $\rho(\mathbf{r})$ when $\mathbf{r}$ is inside V^ϕ while $\hat{\rho}_2$ describes $\mathbf{r}$ outside V^ϕ. Using the identities Eq.(B.7,B.8), $\hat{\rho}_1$ can be expressed in terms of χ_{11} and χ_{11}^* only, as

$$\hat{\rho}_1 = (\rho^B \mathbf{E}_{11}\chi_{11}^{-1} - \mathbf{F}_{11})^{-1}\rho^B \mathbf{E}_{11}\chi_{11}^{-1}\rho^B \hat{\mathbf{I}}_1. \tag{B.18}$$

Since the volume V^ϕ can not accommodate more than one fluid particle, χ_{11} is simply

$$\chi_{11}(\mathbf{r}_1, \mathbf{r}_2) = \rho^B \delta(\mathbf{r}_1, \mathbf{r}_2) - (\rho^B)^2, \forall \mathbf{r}_1, \mathbf{r}_2 \in V^\phi, \tag{B.19}$$

whose inverse $\chi_{11}^{-1}(\mathbf{r}_1, \mathbf{r}_2)$ can be easily found as

$$\chi_{11}^{-1}(\mathbf{r}_1, \mathbf{r}_2) = \frac{1}{\rho^B}\delta(\mathbf{r}_1, \mathbf{r}_2) + \frac{1}{1-\rho^B v}. \tag{B.20}$$

Then $(\rho^B \mathbf{E}_{11}\chi_{11}^{-1} - \mathbf{F}_{11})$ can be expressed in terms of the coordinate indices as

$$\left(\rho^B \mathbf{E}_{11}\chi_{11}^{-1} - \mathbf{F}_{11}\right)(\mathbf{r}_1, \mathbf{r}_2) = \delta(\mathbf{r}_1 - \mathbf{r}_2) + \rho^B \frac{1 + f^\phi(\mathbf{r}_1)}{1-\rho^B v}. \tag{B.21}$$

To find the inverse of Eq.(B.21), one can take advantage of the fact that the off diagonal elements depend only on one coordinate, so that one has

$$\int d\mathbf{r}_2 \int d\mathbf{r}_3 \left(\rho^B \mathbf{E}_{11}\chi_{11}^{-1} - \mathbf{F}_{11}\right)^{-1}(\mathbf{r}_1, \mathbf{r}_2)\left(\rho^B \mathbf{E}_{11}\chi_{11}^{-1} - \mathbf{F}_{11}\right)(\mathbf{r}_2, \mathbf{r}_3) = \int d\mathbf{r}_2 \delta(\mathbf{r}_1, \mathbf{r}_2) \tag{B.22}$$

Integrating $\mathbf{r}_3$ on the left hand side using the expression of Eq.(B.21) yields

$$\begin{aligned} \int d\mathbf{r}_2 \left(\rho^B \mathbf{E}_{11}\chi_{11}^{-1} - \mathbf{F}_{11}\right)^{-1}(\mathbf{r}_1, \mathbf{r}_2) &= 1 - \frac{\rho^B(v+a)}{1+\rho^B a} \\ &= \int d\mathbf{r}_1 \left(\delta(\mathbf{r}_1, \mathbf{r}_2) - \frac{\rho^B(1+f^\phi(\mathbf{r}_1))}{1+\rho^B a}\right) \end{aligned} \tag{B.23}$$

which is obtained by rearrangement. From this result in Eq.(B.23) one can easily verify that

$$(\rho^B \mathbf{E}_{11}\chi_{11}^{-1} - \mathbf{F}_{11})^{-1} = \delta(\mathbf{r}_1, \mathbf{r}_2) - \frac{\rho^B(1 + f^\phi(\mathbf{r}_1))}{1 + \rho^B a}. \tag{B.24}$$

The value of χ_{11}^{-1} can be also determined in a similar way. With Eq.(B.24), Eq.(B.18) gives $\hat{\rho}_1$ as

$$\rho(\mathbf{r}) = \frac{\rho^B e^{-\beta\phi(\mathbf{r})}}{1 + \rho^B a}, \; \forall \mathbf{r} \in V^\phi \tag{B.25}$$

and $\hat{\rho}_2$ can be determined from either Eq.(B.16) or (B.17) as

$$\begin{aligned} \hat{\rho}_2 &= \rho^B \hat{\mathbf{I}}_2 + (\chi_{22}^*)^{-1}\chi_{21}^*(\rho^B \hat{\mathbf{I}}_1 - \hat{\rho}_1) \\ &= \rho^B \hat{\mathbf{I}}_2 - \chi_{21}\chi_{11}^{-1}(\rho^B \hat{\mathbf{I}}_1 - \hat{\rho}_1). \end{aligned} \tag{B.26}$$

Thus for $\mathbf{r} \notin V^\phi$ we have

$$\rho(\mathbf{r}) = \rho^B \frac{1 + \int_v d\mathbf{r}' \rho^B g(|\mathbf{r} - \mathbf{r}'|; \rho^B) f^\phi(\mathbf{r}')}{1 + \rho^B \int d\mathbf{r}' f^\phi(\mathbf{r}')}. \tag{B.27}$$

Equations (B.25) and (B.27) together give the PY predictions for $\rho(\mathbf{r})$ for tiny fields, and they agree with the exact result in Eq.(3.21). Thus the PY approximation is indeed exact for tiny fields. In particular, the PY approximation gives the exact density values inside V^ϕas long as the bulk direct correlation function $c^{(2)}(|\mathbf{r}-\mathbf{r}'|; \rho^B)$ used is consistent with a $g(\mathbf{r}-\mathbf{r}'|; \rho^B)$ that vanishes when $|\mathbf{r}-\mathbf{r}'|$ is smaller than the hard core diameter. However, to obtain the density *outside* V^ϕ exactly, the exact $c^{(2)}(|\mathbf{r} - \mathbf{r}'|; \rho^B)$ has to be used. Note that the fluid particles' interaction does not have to be only hard cores; Eq.(B.25) and Eq.(B.27) will still hold even when there are additional softer tails in the molecular interaction if the exact bulk g is used.

Appendix C

Insensitivity Criterion (IC) for the SLR Equation

After carrying out the functional derivative $\delta\rho(\mathbf{r}_1)/\delta\tilde{\rho}^{\mathbf{r}_2}$ in Eq.(3.28) on the $\rho(\mathbf{r}_1)$ given by the SLR equation, one can rewrite the resulting equation as

$$\begin{aligned}
&\int d\mathbf{r}_3 \left[\delta(\mathbf{r}_1,\mathbf{r}_3) - \tilde{\rho}^{\mathbf{r}_1} e^{-\beta\tilde{\phi}^{\mathbf{r}_1}(\mathbf{r}_1)} c^{(2)}(|\mathbf{r}_1-\mathbf{r}_3|;\tilde{\rho}^{\mathbf{r}_1})\right] \frac{\delta\rho(\mathbf{r}_3)}{\delta\tilde{\rho}^{\mathbf{r}_2}} \\
= \;& \delta(\mathbf{r}_1,\mathbf{r}_2) e^{\beta(\mu-\phi(\mathbf{r}_1))}/\Lambda^3 e^{C^{(1)}(\tilde{\rho}^{\mathbf{r}_1})} \{\dot{c}^{(1)}(\tilde{\rho}^{\mathbf{r}_1}) - \int d\mathbf{r}_3 c^{(2)}(|\mathbf{r}_1-\mathbf{r}_3|;\tilde{\rho}^{\mathbf{r}_1}) \\
&+ \int d\mathbf{r}_3 [\dot{c}^{(1)}(\tilde{\rho}^{\mathbf{r}_1}) c^{(2)}(|\mathbf{r}_1-\mathbf{r}_3|;\tilde{\rho}^{\mathbf{r}_1}) \qquad \text{(C.1)} \\
&+ \dot{c}^{(2)}(|\mathbf{r}_1-\mathbf{r}_3|;\tilde{\rho}^{\mathbf{r}_1})(\rho(\mathbf{r}_3)-\tilde{\rho}^{\mathbf{r}_1})]\} \qquad \text{(C.2)}
\end{aligned}$$

A special case of Eq.(3.4) relating the $n-1$ and nth order direct correlation functions can be written as[15]

$$\dot{c}^{(n-1)}(\mathbf{r}_1,\mathbf{r}_2,...,\mathbf{r}_{n-1};\rho) = \int d\mathbf{r}_n c^{(n)}(\mathbf{r}_1,\mathbf{r}_2,...,\mathbf{r}_{n-1},\mathbf{r}_n;\rho). \qquad \text{(C.3)}$$

Using this on the right hand side of Eq.(C.1), we are left with only the integral terms in the third line in the curly brackets. Thus, the condition Eq.(3.28) requires that

$$\int d\mathbf{r}_3 \left[\dot{c}^{(1)}(\tilde{\rho}^{\mathbf{r}_1}) c^{(2)}(|\mathbf{r}_1-\mathbf{r}_3|;\tilde{\rho}^{\mathbf{r}_1}) + \dot{c}^{(2)}(|\mathbf{r}_1-\mathbf{r}_3|;\tilde{\rho}^{\mathbf{r}_1})(\rho(\mathbf{r}_3)-\tilde{\rho}^{\mathbf{r}_1})\right] = 0, \qquad \text{(C.4)}$$

which implies the result in Eq.(3.29). Note that by using Eq.(C.3), the equation above can be written as

$$\int d\mathbf{r}_2 \int d\mathbf{r}_3 c^{(2)}(|\mathbf{r}_1 - \mathbf{r}_2|\tilde{\rho}^{\mathbf{r}_1}) c^{(2)}(|\mathbf{r}_1 - \mathbf{r}_3|; \tilde{\rho}^{\mathbf{r}_1}) + c^{(3)}(\mathbf{r}_1, \mathbf{r}_2, \mathbf{r}_3; \tilde{\rho}^{\mathbf{r}_1})(\rho(\mathbf{r}_3) - \tilde{\rho}^{\mathbf{r}_1}) = 0. \quad \text{(C.5)}$$

This could also be derived by making the following approximation for $\mathbf{Q}(\mathbf{r})$ in Eq.(3.27):

$$\mathbf{Q}(\mathbf{r}_1) \approx (\rho(\mathbf{r}_1) - \tilde{\rho}^{\mathbf{r}_1}) \int d\mathbf{r}_2 \int d\mathbf{r}_3 c^{(2)}(r_{12}; \tilde{\rho}^{\mathbf{r}_1}) c^{(2)}(r_{13}; \tilde{\rho}^{\mathbf{r}_1}) + c^{(3)}(\mathbf{r}_1, \mathbf{r}_2, \mathbf{r}_3; \tilde{\rho}^{\mathbf{r}_1}))(\rho(\mathbf{r}_3) - \tilde{\rho}^{\mathbf{r}_1}), \quad \text{(C.6)}$$

i.e., by assuming that $\rho(\mathbf{r}_2)$ differs little from $\rho(\mathbf{r}_1)$ in the region of integration near $\mathbf{r}_1$ in the definition for $\mathbf{Q}$, and setting the result to zero.

Appendix D

Numerically Stable Version of LMF Equation

The LMF equation 4.28 will produce the desired short ranged $\phi_{R1}(r)$ with a finite value of $\hat{\phi}_{R1}(0)$ only if $S_R(k)$ rigorously vanishes at $k = 0$ as in Eq.(4.30), which of course is the exact result. However, such self consistent equations are usually solved by iteration and any small errors in an intermediate approximation to $S_R(k)$ at small k are greatly amplified. This can lead to numerical instabilities. The following rewriting of Eq.(4.28) can alleviate this problem. We can remove the sensitivity at small k by multiplying both sides of Eq.(4.28) by k^2, giving

$$k^2\beta\rho^B\hat{\phi}_{R1}(k) = \alpha k_D^2 \exp[-\tfrac{1}{4}(k\sigma)^2]S_R(k). \tag{D.1}$$

This equation suffices to determine $\hat{\phi}_{R1}(k)$ everywhere except near $k = 0$, where $\hat{\phi}_{R1}$ is assumed to be regular. We next formally write an identity involving $\hat{\phi}_{R1}(k)$ that remains finite as $k \to 0$, namely,

$$K^2\beta\rho^B\hat{\phi}_{R1}(k) = K^2\beta\rho^B\hat{\phi}_{R1}(k), \tag{D.2}$$

where K is a (real) *constant* wavevector. (More generally, we can multiply both sides by a known real function of k that does not vanish as $k \to 0$.) We now add

these two equations as written and divide by $k^2 + K^2$, which yields our final result

$$\begin{aligned} \beta\rho^B\hat{\phi}_{R1}(k) &= \frac{\alpha k_D^2}{k^2+K^2}\exp[-\tfrac{1}{4}(k\sigma)^2]S_R(k) \\ &\quad + \frac{K^2}{k^2+K^2}\beta\rho^B\hat{\phi}_{R1}(k). \end{aligned} \tag{D.3}$$

This equation has no divergences at small k and is stable when iterated, with a choice of K of order k_D. A converged solution will produce a $S_R(k)$ that vanishes identically at $k = 0$ with $\beta\rho^B\hat{\phi}_{R1}(0)$ finite. From Eq.(4.31) this quantity is in fact of order unity when the second moment condition is satisfied. This way of rewriting equations of this kind was suggested by Kirill Katsov [39].

Appendix E

Demonstration that the PB and LMF Theories Satisfy the Contact Theorem for One Charged Wall

A neutral system consisting of a single charged planar wall and one species of counterions is considered. The "contact theorem"[8, 21, 22] imposes a constraint on the counterion density at contact with the wall,namely,

$$\tilde{n}(0) = 1. \tag{E.1}$$

The PB approximation satisfies this condition. The following discussion will start from a derivation of how the PB approximation satisfies the contact condition and then generalize it to show that the LMF theory also does.

E.1 PB

The Poisson-Boltzmann approximation for this system is

$$\frac{\mathrm{d}^2\tilde{\phi}_R(\tilde{z})}{\mathrm{d}\tilde{z}^2} = -2\tilde{n}(\tilde{z}), \tag{E.2}$$

while $\tilde{n}(\tilde{z})$ is approximated by Eq.(6.31). From Eq.(6.31), one can relate the $\dot{\tilde{n}}(\tilde{z})$ with $\dot{\tilde{\phi}}_R(\tilde{z})$

$$\dot{\tilde{n}}(\tilde{z}) = -\tilde{n}(\tilde{z})\dot{\tilde{\phi}}_R(\tilde{z}). \tag{E.3}$$

Integrating Eq.(E.3) from $\tilde{z} = 0$ to ∞, we have

$$\tilde{n}(\infty) - \tilde{n}(0_+) \;=\; -\int_{0_+}^{\infty} d\tilde{z}\tilde{n}(\tilde{z})\dot{\tilde{\phi}}_R(\tilde{z}). \tag{E.4}$$

With the boundary conditions that $\tilde{n}(\infty) = 0$ and $\dot{\tilde{\phi}}_R(\infty) = 0$, using Eq.(E.2), Eq.(E.4) gives

$$\begin{aligned}
\tilde{n}(0_+) &= -\frac{1}{2}\int_{0_+}^{\infty} d\tilde{z}\ddot{\tilde{\phi}}_R(\tilde{z})\dot{\tilde{\phi}}_R(\tilde{z}) \\
&= -\frac{1}{4}(\dot{\tilde{\phi}}_R(\infty))^2 + \frac{1}{4}(\dot{\tilde{\phi}}_R(0))^2 \\
&= \frac{1}{4}(\dot{\tilde{\phi}}_R(0_+))^2,
\end{aligned} \tag{E.5}$$

Due to the surface charge density (which is normalized to $\delta(\tilde{z})$) on the wall, $\dot{\tilde{\phi}}(\tilde{z})$ has a discontinuity across $\tilde{z} = 0$, i.e.,

$$\dot{\tilde{\phi}}_R(0_+) - \dot{\tilde{\phi}}_R(0_-) = -2. \tag{E.6}$$

Also, because of the neutrality of the whole system and the boundary condition that $\dot{\tilde{\phi}}_R(\infty) = 0$, one has

$$\dot{\tilde{\phi}}_R(\infty) - \dot{\tilde{\phi}}_R(0_-) \;=\; 0, \text{ which implies} \tag{E.7}$$

$$\dot{\tilde{\phi}}_R(0_-) \;=\; 0. \tag{E.8}$$

The results of Eq.(E.6) and Eq.(E.7) are just the consequence of Gauss's law and together they result in $\dot{\tilde{\phi}}_R(0_+) = -2$. So Eq.(E.5) now yields the contact theorem

that states $\tilde{n}(0_+) = 1$.

E.2 LMF

E.2.1 MPB

The MPB approximation satisfies Eq.(6.23) instead of Eq.(E.2). Because $\tilde{n}^*(\tilde{z})$ is the convolution of $\tilde{n}(\tilde{z})$ with a Gaussian function, $\tilde{n}^*(\tilde{z})$ does not have a sharp discontinuity from a finite contact value to zero behind the walls. To facilitate a derivation similar to that above, define another mean potential function $\tilde{\psi}(\tilde{z})$ by

$$\frac{\mathrm{d}^2\tilde{\psi}(\tilde{z})}{\mathrm{d}\tilde{z}^2} \equiv -2\tilde{n}(\tilde{z}), \text{ i.e.,} \tag{E.9}$$

$$\Rightarrow \tilde{\psi}(\tilde{z}) = \tilde{z} + \int_0^\infty d\tilde{z}_0 \tilde{n}(\tilde{z}_0)(-|\tilde{z} - \tilde{z}_0| + |\tilde{z}_0|). \tag{E.10}$$

The $\tilde{\psi}(\tilde{z})$ differs from $\tilde{\phi}_R(\tilde{z})$ by $\Delta(\tilde{z})$

$$\Delta(\tilde{z}) \equiv \tilde{\psi}(\tilde{z}) - \tilde{\phi}_R(\tilde{z}) = \int_0^\infty d\tilde{z}_0 \tilde{n}(\tilde{z}_0)\tilde{H}(\tilde{z}_0, \tilde{z}) \tag{E.11}$$

$$\tilde{H}(\tilde{z}_0, \tilde{z}) = -|\tilde{z} - \tilde{z}_0|\mathrm{erfc}(\frac{|\tilde{z} - \tilde{z}_0|}{\tilde{\sigma}}) + \frac{\tilde{\sigma}}{\sqrt{\pi}} e^{-(\frac{\tilde{z}-\tilde{z}_0}{\tilde{\sigma}})^2} + |\tilde{z}_0|\mathrm{erfc}(\frac{|\tilde{z}_0|}{\tilde{\sigma}}) - \frac{\tilde{\sigma}}{\sqrt{\pi}} e^{-(\frac{\tilde{z}_0}{\tilde{\sigma}})^2}. \tag{E.12}$$

$\tilde{H}(\tilde{z}_0, \tilde{z})$ is just the $u_0(\mathbf{r}_1, \mathbf{r}_2)$ of the mimic particles integrated over the planar degrees of freedom (though stripped of the charge strength ξ and in reduced units). With

Eq.(E.9,E.11), we can re-write Eq.(E.4) as

$$\begin{aligned}
\tilde{n}(\infty) - \tilde{n}(0_+) &= -\int_{0_+}^{\infty} d\tilde{z}\tilde{n}(\tilde{z})(\dot{\tilde{\psi}}(\tilde{z}) - \dot{\Delta}(\tilde{z})) && \text{(E.13)} \\
&= \frac{1}{2}\int_{0+}^{\infty} d\tilde{z}\ddot{\tilde{\psi}}(\tilde{z})\dot{\tilde{\psi}}(\tilde{z}) \\
&\quad + \int_{0_+}^{\infty} d\tilde{z}\int_{0_+}^{\infty} d\tilde{z}_0\tilde{n}(\tilde{z})\tilde{n}(\tilde{z}_0)\frac{\mathrm{d}}{\mathrm{d}\tilde{z}}\tilde{H}(\tilde{z}_0,\tilde{z}) && \text{(E.14)} \\
&= \frac{1}{4}(\dot{\tilde{\psi}}(\tilde{z}))^2|_{0_+}^{\infty} + \int_{0_+}^{\infty} d\tilde{z}\int_{0_+}^{\infty} d\tilde{z}_0\tilde{n}(\tilde{z})\tilde{n}(\tilde{z}_0)\frac{\mathrm{d}}{\mathrm{d}\tilde{z}}\tilde{H}(\tilde{z}_0,\tilde{z}) && \text{(E.15)}
\end{aligned}$$

Note that $\frac{\mathrm{d}}{\mathrm{d}\tilde{z}}\tilde{H}(\tilde{z}_0,\tilde{z})$ is the force from a particle at $\tilde{z}_0$ acting on another one at $\tilde{z}$, and the force should be of the same magnitude but in the opposite direction if it is from $\tilde{z}$ to $\tilde{z}_0$, i.e., $\frac{\mathrm{d}}{\mathrm{d}\tilde{z}}\tilde{H}(\tilde{z}_0,\tilde{z}) = -\frac{\mathrm{d}}{\mathrm{d}\tilde{z}_0}\tilde{H}(\tilde{z},\tilde{z}_0)$, as should be required by Newton's third law. The second term of the Eq.(E.15) thus should *vanish*. So again we have from the Eq.(E.13) that

$$\begin{aligned}
\tilde{n}(\infty) - \tilde{n}(0_+) &= \frac{1}{4}(\dot{\tilde{\psi}}(\tilde{z}))^2|_{0_+}^{\infty} && \text{(E.16)} \\
\tilde{n}(0_+) &= 1,
\end{aligned}$$

following the similar argument of Eq.(E.6-E.8) for the $\tilde{\psi}(\tilde{z})$. So the MPB also satisfies the contact theorem condition.

E.2.2 General Treatment for the Reference System's Response to ϕ_R

An accurate and different treatment for the density response of the mimic system can be also used with the LMF equation. So can this approach also satisfy the contact theorem? The exact density response of the mimic system to the molecular

field $\tilde{\phi}_R(\tilde{z})$ should be of the form

$$\tilde{n}(\tilde{z}) = Ae^{-\tilde{\phi}_R(\tilde{z})+\tilde{V}(\tilde{z})}, \tag{E.17}$$

where the $\tilde{V}(\tilde{z})$ simply accounts for the potential of mean force of the rest of the mimic particles. In addition to the Boltzmann factor of the molecular field, in general the potential of mean force $\tilde{V}(\tilde{z})$ from the other particles should be also taken into account. $\dot{\tilde{V}}(\tilde{z})$ is the mean force and is of the following form

$$\dot{\tilde{V}}(\tilde{z}) = \int_{-\infty}^{\infty} d\tilde{x}'d\tilde{y}' \int_{0_+}^{\infty} d\tilde{z}'\tilde{\rho}(\tilde{z}')g_0(\tilde{\mathbf{r}}', \tilde{\mathbf{r}})\frac{\partial}{\partial\tilde{z}}\tilde{u}_0(|\tilde{\mathbf{r}} - \tilde{\mathbf{r}}'|). \tag{E.18}$$

Note that the subscript "0" of $g_0(\tilde{\mathbf{r}}', \tilde{\mathbf{r}})$ denotes that it is the pair correlation function of the mimic system. As long as $g_0(\tilde{\mathbf{r}}', \tilde{\mathbf{r}})$ has permutation symmetry in the treatment of the mimic system,

$$\int_{0_+}^{\infty} d\tilde{z}\tilde{n}(\tilde{z})\dot{\tilde{V}}(\tilde{z}) \;=\; 2\pi\xi \int_{-\infty}^{\infty} d\tilde{x}'d\tilde{y}' \int_{0_+}^{\infty} d\tilde{z} \int_{0_+}^{\infty} d\tilde{z}'\tilde{\rho}(\tilde{z})\tilde{\rho}(\tilde{z}')g_0(\tilde{\mathbf{r}}', \tilde{\mathbf{r}})\frac{\partial}{\partial\tilde{z}}\tilde{u}_0(|\tilde{\mathbf{r}} - \tilde{\mathbf{r}}'|) \tag{E.19}$$

vanishes also owing to Newton's third law that $\frac{\partial}{\partial\tilde{z}}\tilde{u}_0(|\tilde{\mathbf{r}} - \tilde{\mathbf{r}}'|) = -\frac{\partial}{\partial\tilde{z}'}\tilde{u}_0(|\mathbf{r} - \mathbf{r}'|)$, since Eq.(E.19) is the *net internal force* per unit area of the particles along the $\tilde{z}$ direction. With Eq.(E.17), the Eq.(E.13) of the MPB gains an additional term and become

$$\tilde{n}(\infty) - \tilde{n}(0_+) = -\int_{0_+}^{\infty} d\tilde{z}\tilde{n}(\tilde{z})(\dot{\tilde{\psi}}(\tilde{z}) - \dot{\Delta}(\tilde{z}) + \dot{\tilde{V}}(\tilde{z})). \tag{E.20}$$

Since the integration with the $\dot{\Delta}(\tilde{z})$ and $\dot{\tilde{V}}(\tilde{z})$ vanishes, by going through the similar argument as that has been presented for the PB and MPB, it can be also proved that

the contact condition $\tilde{n}(0_+) = 1$ can be also satisfied by more general treatments of the mimic system with the LMF equation.

GLOSSARY

1. **DFT:** Density Functional Theory
2. **DH:** Debye-Huckel
3. **FMM:** Fast Multipole Method
4. **GDH:** Generalized Debye-Huckel
5. **GFM:** Gaussian Field Model
6. **GMSA:** Generalized Mean Spherical Approximation
7. **HLR:** Hydrostatic Linear Response
8. **HNC:** Hyper-Netted Chain
9. **LMF:** Local Molecular Field
10. **MPB:** Mimic Poisson Boltzmann
11. **OCCHS:** One Component Charged Hard Spheres
12. **OCP:** One Component Plasma
13. **SAPM:** Size Asymmetric Primitive Model

14. **SL:** Stillinger-Lovett

15. **SLR:** Shifted Linear Response

16. **TCMF:** Test-Charge Mean Field

17. **PB:** Poisson-Boltzmann

18. **PY:** Percus-Yevick

19. **WL:** Weis and Levesque

20. **YBG:** Yvon-Born-Green

BIBLIOGRAPHY

[1] M. P. Allen and D. J. Tildesley. *Computer Simulation of Liquids*. Clarendon Press; Oxford University Press, Oxford England, New York, 1989.

[2] D. Andelman. *Handbook of Biological Physics*, volume 1. Elsevier, Amsterdam; New York, 1995.

[3] J. Barnes and P. Hut. A Hierarchical O(N-Log-N) Force-Calculation Algorithm. *Nature*, 324:446, 1986.

[4] A. Bellemans. Statistical Mechanics of Surface Phenomena. 1. A Cluster Expansion for Surface Tension. *Physica*, 28(5):493, 1962.

[5] K. Binder and P. C. Hohenberg. Phase-Transitions and Static Spin Correlations in Ising Models with Free Surfaces. *Physical Review B*, 6(9):3461, 1972.

[6] Y. Burak, D. Andelman, and H. Orland. Test-Charge Theory for the Electric Double Layer. *Physical Review E*, 70(1):016102, 2004.

[7] N. F. Carnahan and K. E. Starling. Equation of State for Nonattracting Rigid Spheres. *Journal of Chemical Physics*, 51(2):635, 1969.

[8] S. L. Carnie and D. Y. C. Chan. The Statistical-Mechanics of the Electrical Double-Layer - Stress Tensor and Contact Conditions. *Journal of Chemical Physics*, 74(2):1293, 1981.

[9] S. L. Carnie and D. Y. C. Chan. The Stillinger-Lovett Condition for Nonuniform Electrolytes. *Chemical Physics Letters*, 77(3):437, 1981.

[10] D. M. Ceperley and G. V. Chester. Perturbation Approach to Classical One-Component Plasma. *Physical Review A*, 15(2):756, 1977.

[11] D. Chandler. Gaussian Field Model of Fluids with an Application to Polymeric Fluids. *Physical Review E*, 48(4):2898, 1993.

[12] D. Chandler and J. D. Weeks. Equilibrium Structure of Simple Liquids. *Physical Review Letters*, 25(3):149, 1970.

[13] G. E. Crooks and D. Chandler. Gaussian Statistics of the Hard-Sphere Fluid. *Physical Review E*, 56(4):4217, 1997.

[14] R. J. F. L. DeCarvalho and R. Evans. The Screened Coulomb (Yukawa) Charged Hard Sphere Binary Fluid. *Molecular Physics*, 92(2):211, 1997.

[15] R. Evans. Density Functionals in the Theory of Nonuniform Fluids. In D. Henderson, editor, *Fundamentals of Inhomogeneous Fluids*. Dekker, New York, 1992.

[16] D. Frenkel and B. Smit. *Understanding Molecular Simulations*. Academic Press, San Diego, 2002.

[17] S. Galam and J.-P. Hansen. Statistical-Mechanics of Dense Ionized Matter. 6. Electron Screening Corrections to Thermodynamic Properties of One-Component Plasma. *Physical Review A*, 14(2):816, 1976.

[18] L. Greengard and V. Rokhlin. A Fast Algorithm for Particle Simulations. *Journal of Computational Physics*, 73(2):325, 1987.

[19] N. Gronbech-Jensen, R. J. Mashl, R. F. Bruinsma, and W. M. Gelbart. Counterion-Induced Attraction between Rigid Polyelectrolytes. *Physical Review Letters*, 78(12):2477, 1997.

[20] A. Y. Grosberg, T. T. Nguyen, and B. I. Shklovskii. Colloquium: The Physics of Charge Inversion in Chemical and Biological Systems. *Reviews of Modern Physics*, 74(2):329, 2002.

[21] L. Guldbrand, B. Jonsson, H. Wennerstrom, and P. Linse. Electrical Double-Layer Forces - A Monte-Carlo Study. *Journal of Chemical Physics*, 80(5):2221, 1984.

[22] L. Guldbrand, L. G. Nilsson, and L. Nordenskiold. A Monte-Carlo Simulation Study of Electrostatic Forces between Hexagonally Packed DNA Double Helices. *Journal of Chemical Physics*, 85(11):6686, 1986.

[23] B. Y. Ha and A. J. Liu. Counterion-Mediated Attraction between Two Like-Charged Rods. *Physical Review Letters*, 79(7):1289, 1997.

[24] J.-P. Hansen and I. R. McDonald. *Theory of Simple Liquids*. Academic Press, London, 1986.

[25] J.-P. Hansen and J. J. Weis. Charged Hard Spheres in a Uniform Neutralizing Background - Comparison of Monte-Carlo Results With Perturbation Theories. *Molecular Physics*, 33(5):1379, 1977.

[26] E. Helfand, H. Reiss, H. L. Frisch, and J. L. Lebowitz. Scaled Particle Theory of Fluids. *Journal of Chemical Physics*, 33(5):1379, 1960.

[27] D. Henderson, F. F. Abraham, and J. A. Barker. The Ornstein-Zernike Equation for a Fluid in Contact with a Surface. *Molecular Physics*, 31(4):1291, 1976.

[28] D. Henderson and M. Plischke. Calculation of the Density Profile of a System of Hard-Spheres near a Hard-Wall Using the Henderson-Plischke and Related Approximations. *Proceedings of the Indian Academy of Sciences-Chemical Sciences*, 97(3-4):297, 1986.

[29] D. Henderson, S. Sokolowski, and D. T. Wasan. Simple Integral Equation and Density Functional Study of a Hard Sphere Fluid in a Pore Formed by Two Hard Walls. *Journal of Physical Chemistry B*, 102(16):3009, 1998.

[30] J. R. Henderson. Statistical Mechanics of Fluids at Spherical Structureless Walls. *Molecular Physics*, 50(4):741, 1983.

[31] J. R. Henderson. Compressibility Route to Solvation Structure. *Molecular Physics*, 59(1):89, 1986.

[32] J. R. Henderson. Statistical Mechanical Sum Rules. In D. Henderson, editor, *Fundamentals of Inhomogeneous Fluids*. Dekker, New York, 1992.

[33] J. R. Henderson. Solvation of a Solvophobic Sphere. *Journal of Chemical Physics*, 116(12):5039, 2002.

[34] J. R. Henderson and F. van Swol. On the Interface Between a Fluid and a Planar Wall. Theory and Simulations of a Hard Sphere Fluid at a Hard Wall. *Molecular Physics*, 51(4):991, 1984.

[35] G. Hummer, S. Garde, A. E. Garcia, A. Pohorille, and L. R. Pratt. An Information Theory Model of Hydrophobic Interactions. *Proceedings of the National Academy of Sciences of the United States of America*, 93(17):8951, 1996.

[36] G. Hummer, D. M. Soumpasis, and M. Neumann. Pair Correlations in an NaCl-SPC Water Model - Simulations Versus Extended Rism Computations. *Molecular Physics*, 77(4):769, 1992.

[37] G. Hummer, D. M. Soumpasis, and M. Neumann. Computer-Simulation of Aqueous Na-Cl Electrolytes. *Journal of Physics-Condensed Matter*, 6(23A):A141, 1994.

[38] J. D. Jackson. *Classical Electrodynamics*. Wiley, New York, 1999.

[39] K. Katsov. Private Communication.

[40] K. Katsov and J. D. Weeks. Density Fluctuations and the Structure of a Nonuniform Hard Sphere Fluid. *Physical Review Letters*, 86(3):440, 2001.

[41] K. Katsov and J. D. Weeks. On the Mean Field Treatment of Attractive Interactions in Nonuniform Simple Fluids. *Journal of Physical Chemistry B*, 105(28):6738, 2001.

[42] K. Katsov and J. D. Weeks. Incorporating Molecular Scale Structure into the Van der Waals Theory of the Liquid-Vapor Interface. *Journal of Physical Chemistry B*, 106(33):8429, 2002.

[43] K. Katsov and J. D. Weeks. Incorporating Molecular Scale Structure into the Van der Waals Theory of the Liquid-Vapor Interface. *Journal of Physical Chemistry B*, 106(33):8429, 2002.

[44] C. Kaur, Y.-G. Chen, and J. D. Weeks. (unpublished).

[45] J. L. Lebowitz. Exact Solution of Generalized Percus-Yevick Equation for Mixture of Hard Spheres. *Physical Review A*, 133(4A):A895, 1964.

[46] J. L. Lebowitz, G. Stell, and S. J. Baer. Separation of Interaction Potential into 2 Parts in Treating Many-Body Systems. I. General Theory and Applications to Simple Liquids with Short-Range and Long-Range Forces. *Journal of Mathematical Physics*, 6(8):1282, 1965.

[47] Y. Levin and M. E. Fisher. Criticality in the Hard-Sphere Ionic Fluid. *Physica A*, 225(2):164, 1996.

[48] P. Linse and V. Lobaskin. Electrostatic Attraction and Phase Separation in Solutions of Like-Charged Colloidal Particles. *Journal of Chemical Physics*, 112(8):3917, 2000.

[49] K. Lum, D. Chandler, and J.D. Weeks. Hydrophobicity at Small and Large Length Scales. *Journal of Physical Chemistry B*, 103(22):4570, 1999.

[50] D. A. McQuarrie. *Statistical Thermodynamics*. University Science Books, Mill Valley, California, 1973.

[51] T. F. Meister and D. M. Kroll. Density-Functional Theory for Inhomogeneous Fluids - Application to Wetting. *Physical Review A*, 31(6):4055, 1985.

[52] A. G. Moreira and R. R. Netz. Strong-Coupling Theory for Counter-Ion Distributions. *Europhysics Letters*, 52(6):705, 2000.

[53] A. G. Moreira and R. R. Netz. Binding of Similarly Charged Plates with Counterions Only. *Physical Review Letters*, 8707(7):078301, 2001.

[54] R. R. Netz. Electrostatistics of Counter-Ions at and between Planar Charged Walls: From Poisson-Boltzmann to the Strong-Coupling Theory. *European Physical Journal E*, 5(5):557, 2001.

[55] C. W. Outhwaite. Comment on the Second Moment Condition of Stillinger and Lovett. *Chemical Physics Letters*, 24(1):73, 1974.

[56] R. G. Palmer and J. D. Weeks. Exact Solution of the Mean Spherical Model for Charged Hard Spheres in a Uniform Neutralizing Background. *Journal of Chemical Physics*, 58(10):4171, 1973.

[57] R. Penfold and S. Nordholm. A Simple Analysis of the Classical Hard-Sphere One-Component Plasma. 2. Density Functional Theory. *Journal of Chemical Physics*, 96(4):3102, 1992.

[58] J. K. Percus. Approximation Methods in Classical Statistical Mechanics. *Physical Review Letters*, 8(11):462, 1962.

[59] J. K. Percus. The Pair Correlation Function in Classical Statistical Mechanics. In H. L. Frisch and J. L. Lebowitz, editors, *The Equilibrium Theory of Classical Fluids*. W.A. Benjamin, New York, 1964.

[60] J. K. Percus and G. J. Yevick. Analysis of Classical Statistical Mechanics by Means of Collective Coordinates. *Physical Review*, 110(1):1, 1958.

[61] R. Podgornik and V. A. Parsegian. Charge-Fluctuation Forces between Rodlike Polyelectrolytes: Pairwise Summability Reexamined. *Physical Review Letters*, 80(7):1560, 1998.

[62] L. R. Pratt and H. S. Ashbaugh. Self-Consistent Molecular Field Theory for Packing in Classical Liquids. *Physical Review E*, 68(2):021505, 2003.

[63] L. R. Pratt, G. G. Hoffman, and R. A. Harris. Statistical-Theory of Electron-Densities. *Journal of Chemical Physics*, 88(3):1818, 1988.

[64] H. Reiss and R. V. Casberg. Radial Distribution Function for Hard Spheres from Scaled Particle Theory, and an Improved Equation of State. *Journal of Chemical Physics*, 61(3):1107, 1974.

[65] H Reiss, H. L. Frisch, and J. L. Lebowitz. Statistical Mechanics of Rigid Spheres. *Journal of Chemical Physics*, 31(2):369, 1959.

[66] J. M. Romero-Enrique, G. Orkoulas, A. Z. Panagiotopoulos, and M. E. Fisher. Coexistence and Criticality in Size-Asymmetric Hard-Core Electrolytes. *Physical Review Letters*, 85(21):4558, 2000.

[67] J. M. Romero-Enrique, L. F. Rull, and A. Z. Panagiotopoulos. Dipolar Origin of the Gas-Liquid Coexistence of the Hard-Core 1 : 1 Electrolyte Model. *Physical Review E*, 66(4):041204, 2002.

[68] W. L. Slattery, G. D. Doolen, and H. E. Dewitt. N-Dependence in the Classical One-Component Plasma Monte-Carlo Calculations. *Physical Review A*, 21(6):2087, 1980.

[69] F. H. Stillinger and R. Lovett. General Restriction on the Distribution of Ions in Electrolytes. *Journal of Chemical Physics*, 49(5):1991, 1968.

[70] M. N. Tamashiro, Y. Levin, and M. C. Barbosa. The One-Component Plasma: A Conceptual Approach. *Physica A*, 268(1-2):24, 1999.

[71] J. P. Valleau, R. Ivkov, and G. M. Torrie. Colloid Stability - The Forces between Charged Surfaces in an Electrolyte. *Journal of Chemical Physics*, 95(1):520, 1991.

[72] K. Vollmayr, K. Katsov, and J. D. Weeks. Using Mean Field Theory to Determine the Structure of Uniform Fluids. *Journal of Chemical Physics*, 114(1):416, 2001.

[73] E. Waisman. The Radial Distribution Function for a Fluid of Hard Spheres at High Densities. Mean Spherical Integral Equation Approach. *Molecular Physics*, 25(1):45, 1973.

[74] J. D. Weeks. Connecting Local Structure to Interface Formation: A Molecular Scale Van der Waals theory of Nonuniform Liquids. *Annual Reviews of Physical Chemistry*, 53:533, 2002.

[75] J. D. Weeks, D. Chandler, and H. C. Andersen. Perturbation Theory of the Thermodynamic Properties of Simple Liquids. *Journal of Chemical Physics*, 55(11):5422, 1971.

[76] J. D. Weeks, D. Chandler, and H. C. Andersen. Role of Repulsive Forces in Determining the Equilibrium Structure of Simple Liquids. *Journal of Chemical Physics*, 54(12):5237, 1971.

[77] J. D. Weeks and G. H. Gilmer. Pair Approximation Equations for Interfaces and Free Surfaces in the Ising Model. *Journal of Chemical Physics*, 63(7):3136, 1975.

[78] J. D. Weeks, K. Katsov, and K. Vollmayr. Roles of Repulsive and Attractive Forces in Determining the Structure of Nonuniform Liquids: Generalized Mean Field Theory. *Physical Review Letters*, 81(20):4400, 1998.

[79] J. D. Weeks, R. L. B. Selinger, and J. Q. Broughton. Self-Consistent Treatment of Repulsive and Attractive Forces in Nonuniform Liquids. *Physical Review Letters*, 75(14):2694, 1995.

[80] J. D. Weeks, K. Vollmayr, and K. Katsov. Intermolecular Forces and the Structure of Uniform and Nonuniform Fluids. *Physica A*, 244(1-4):461, 1997.

[81] J. J. Weis and D. Levesque. Thermodynamic and Structural Properties of Size-Asymmetric Charged Hard Spheres. *Chemical Physics Letters*, 336(5-6):523, 2001.

[82] B. Widom. Some Topics in the Theory of Fluids. *Journal of Chemical Physics*, 39(11):2808, 1963.

[83] B. Widom. Intermolecular Forces and Nature of Liquid State. *Science*, 157:375, 1967.